Development of an Automated Structural Health Monitoring System based on Wireless Sensor Network for Civil Structures

Niusha Navabian

A thesis submitted to
Auckland University of Technology in fulfilment of the
requirements for the degree of

Doctor of Philosophy (PhD)

Supervisor:

Dr Sherif Beskhyroun

August 2020

School of Future Environments, Department of Built Environment Engineering

Auckland University of Technology (AUT), New Zealand

Abstract

Structural Health Monitoring (SHM) is used to assess and identify damage and deterioration in civil infrastructures during their regular lifetime as well as after extreme events, such as earthquakes. A complete SHM system incorporates sensing system, signal processing, data management, data transmission, and data analysis for reliable and fast decision-making purposes. This research has been scheduled after a comprehensive literature review on different components of a SHM system. The main objective of this research was to develop a state-of-the-art vibration-based SHM system for condition assessment of large-scale civil structures. Another purpose of developing the new SHM system was to enhance the performance and reduce the costs associated with the existing traditional SHM systems. This structural health monitoring system consists of three significant components; a new wireless smart sensor network, a compatible MATLAB-based data management and data analysis platform with the sensor network, and a new vibration-based nonlinearity identification technique for early damage identification purposes.

The wireless smart sensor network has been designed to meet the requirements for low-amplitude ambient vibration measurements and sudden event monitoring of civil structures. This wireless smart network can record both ambient and earthquake-induced vibrations from structures using two periodic and event-triggered sampling modes. One of the main goals of the sensor design was to achieve higher performance and efficiency, improve the power consumption, and lower the cost compared to the existing wired and wireless sensor system. Also, making a great trade-off between these important features of a wireless sensor network was another goal that was considered in hardware and software design of the system. Another goal was the ability to control the hardware part of the system to be applicable for different SHM applications. The hardware of the smart sensor nodes was designed to provide high resolution and sensitivity, low noise, low power consumption, and capability to measure

structural vibration in ultralow-power consumption mode to record sudden events. Also, the software architecture of the smart sensor nodes was implemented to provide accurate time synchronisation and event-triggered sensing with high resolution. To test the various features of the sensor system, a series of experimental tests was conducted on a small-scale steel bridge model. The wireless smart sensor network performance was investigated in terms of sensitivity, event-triggered sampling mode, and time synchronisation. In addition, the wireless-based structural health monitoring system has been installed on one span of a full-scale bridge in Auckland, New Zealand. The main goals of this instrumentation were to evaluate the performance of the wireless smart sensor network in an outdoor environment and to assess dynamic performance of the superstructure using its modal characteristics after several years in operation.

The second part of the research is to develop a data management and data analysis toolbox for the integrated SHM system. MATLAB Graphical User Interface (GUI) Layout Toolbox was utilised to design the new management and analysis toolbox that has been connected to the developed wireless smart sensor network. The original feature of this toolbox is its compatibility with the developed wireless smart sensor network. The recorded data files can be downloaded, managed and synchronised using the first tab of the toolbox. Then, the managed data files can be analysed using different data analysis techniques to extract useful information from raw vibration measurements. Various time-domain and frequency-domain system identification techniques were implemented into the data analysis platform to extract modal parameters from vibration measurements. The results obtained using these techniques can be compared to each other to estimate computational precision of the dynamic characteristics of target structures. Extracting maximum useful information from raw measurements for condition assessment, avoiding human errors in processing large sets of

monitoring data, and having an integrated platform for the developed sensor system were among the mains goals of developing this toolbox.

In addition, the third component of the system is a technique to identify nonlinearities in structural systems using vibration measurements, which are collected using the developed wireless smart sensor system. This technique combines vibration data sets with time series autoregressive modelling and fuzzy clustering technique to identify nonlinearity in a dynamic system. The technique is able to categorise the linear and nonlinear behaviour of a structure, when it is subjected to various levels of excitation source. In order to verify the performance of the method, a series of shaking table tests was conducted on a small-scale steel truss bridge model in the laboratory environment. The vibration data recorded using high performance accelerometers from the bridge model under different ground motions have been used for data analysis.

A research paper presenting the results obtained on structural health monitoring of a large-scale bridge located in Wellington, New Zealand has been also provided to show the efficiency of vibration-based SHM systems for large-scale structures. This bridge was subjected to two large-amplitude earthquakes and several aftershocks. The vibration data sets recorded using several accelerometer sensors were utilised to assess the bridge condition. The bridge performance has been assessed using non-parametric and parametric analysis techniques to obtain the vibration intensity parameters and dynamic characteristics of the bridge. In addition to the results obtained on dynamic performance of the structure, the results of this research paper confirm the efficiency and reliability of vibration-based structural health monitoring techniques and MATLAB-based data analysis toolbox for condition assessment of large-scale civil structures.

Attestation of Authorship

I hereby declare that this submission is my own work and that, to the best of my knowledge and belief, it contains no material previously published or written by another person (expect where explicitly defined in the acknowledgements), nor material which to a substantial extent has been submitted for the award of any other degree or diploma of a university or other institutions of higher learning.

Signature:

Niusha Navabian

Date: 22 August 2020

Acknowledgement

First and foremost, I would like to express my thanks and deepest gratitude to my supervisor, Dr Sherif Beskhyroun, for providing consistent technical and spiritual supports throughout this study. He has made this whole journey possible, pleasant, and enjoyable. None of this would have been possible without his great mentorship and support. I sincerely appreciate for all the lessons that I have learn from him regarding my professional and personal life. Words cannot express my deep gratitude, but I will be grateful to him for the rest of my life. Also, I would like to thank Professor John Tookey for his supports throughout this thesis.

I would like to thank Earthquake Commission (EQC) for their financial supports for this study. Without their helps, I could not perform all these valuable experimental tests. In addition, many thanks to New Zealand Transport Agency (NZTA) for supporting us regarding instrumentation of one of the most important civil structures in New Zealand, Newmarket Viaduct.

I would like to express my gratitude to all the professional technicians and mentors in the Engineering department of Auckland University of Technology, Justin Matulich, Dave Crofts, Andrew Virtue, Allan Dixon, who have been one the biggest supports during the most difficult times of this study. In addition, special thanks to Hui Zhang, for all her times and helps during the experimental tests on the Newmarket Viaduct.

I would like to express my deepest love and gratitude to my father, my mother, and my sister for their infinite love, emotional support and encouragement that I received from them throughout my life. Thank you for giving me strength to reach for the stars and chase my dreams. Also, my wholehearted thanks to my grandmother and my brother-in-law for all their love and supports. Last but not least, I would like to appreciate my best friend and my love, Dr Farhad Mohammadi Darani, for all his love, support and understanding during my journey. I would not have been able to finish this work without his support.

Dedication

This thesis is honourably dedicated to:

My dearest parents

for all I have from them, for their infinite love and endless sacrifice and compassion,
Thank you for always giving me the courage and confidence to pursue my dreams.

My lovely sister

For all her infinite love, supports, and kindness,
Thank you for always being by my side and for helping me in infinite ways.

My wonderful husband

For all his endless love and supports,
Thank you for always making me feel like the happiest woman in the world.

Iran & New Zealand

For all the love and supports given to me.

Related Research Outputs

Journal Papers:

1. **Navabian, N.**, & Beskhyroun, S. (2019). Investigation on dynamic behaviour of a full-scale reinforced concrete bridge subjected to strong earthquakes using an automated analysis platform. Structure and Infrastructure Engineering, 15(4), 504-523.
2. Beskhyroun, S., **Navabian, N.**, Wotherspoon, L., & Ma, Q., (2020). Dynamic Behaviour of a 13-Story Reinforced Concrete Building under Ambient Vibration, Forced Vibration, and Earthquake Excitation. Journal of Building Engineering 28, 101066.

Conference Papers:

1. **Navabian. N.**, Beskhyroun. S., (2020), "An automated wireless-based system for real-time health monitoring of civil infrastructures", New Zealand Society for Earthquake Engineering (NZSEE) conference, Auckland, New Zealand.
2. **Navabian. N.**, Beskhyroun. S., (2020), "Development of an integrated structural health monitoring system using wireless sensor network", 17th World Conference on Earthquake Engineering, Sendai, Japan.
3. **Navabian. N.**, Beskhyroun. S., (2019), "Development of a wireless sensory system for long-term monitoring of large-scale civil structures", 11th Pacific Conference on Earthquake Engineering (PCEE), Auckland, New Zealand.
4. **Navabian. N.**, Beskhyroun. S., (2019), "Structural Health Monitoring of a post-tensioned concrete bridge using wireless sensory system: deployment and evaluation", 5th International Conference on Smart Monitoring, Assessment and Rehabilitation of Civil Structures (SMAR), Potsdam, Germany.
5. **Navabian. N.**, Beskhyroun. S., (2018), "Low-cost and high-performance wireless sensor nodes for structural health evaluation", 9th European Workshop on Structural Health Monitoring (EWSHM) conference, Manchester, United Kingdom.
6. **Navabian. N.**, Beskhyroun. S., (2017), "Condition Monitoring of a Concrete Bridge in Wellington, New Zealand", New Zealand Society for Earthquake Engineering (NZSEE) conference, Auckland, New Zealand.

Table of Contents

List of Figures

List of Tables

Chapter 1: Introduction

1.1 Structural Health Monitoring (SHM)

Our daily life heavily relies on various types of civil infrastructures, such as high-rise buildings, long-span bridges, offshore platforms, and tunnels, in which the industrialised nations and governments have invested huge amount of money. Several of these important civil infrastructures are being utilised around the world despite their age and the possible risk of damage accumulation. Any structural malfunctioning and collapse can result in massive economic loss and more importantly threaten human lives. Therefore, monitoring safety and integrity of these important structures is crucially significant from both life-safety and economic points of view to ensure an adequate level of safety and reliability, hence preventing catastrophic failures and prolonging their service lives.

Structural Health Monitoring (SHM) is an engineering implement and a research area that assesses, controls, and informs about the current status or any changes in the condition of civil infrastructures. This engineering technology plays a significant role to continuously monitor the integrity of civil infrastructures in real-time. Early detection of dangerous structural behaviours using SHM systems could also provide the asset owners with a warning for removing the structure from service, resulting in an efficient management and decision-making procedure in emergency cases. In addition, an accurate and quick structural condition assessment is essentially important after destructive environmental events, such as strong earthquakes, which can prevent significant economic losses and enhance the reconstruction speed of the affected earthquake regions. The structure might be in danger of total collapse after earthquakes; therefore, such monitoring systems could recognize the existence of possible damages for building evacuation during aftershocks. As mentioned, the main objective of SHM systems is to guarantee an adequate level of safety for the important civil infrastructures [1].

Although the earliest application of SHM discipline was for aerospace structures, it has become very popular as an efficient tool in mechanical and civil applications in the last few decades. Specifically, in structural engineering, SHM applications have gained momentum in the last decade as the number of aging large-scale and important civil infrastructures is increasing around the world. Emerging of new construction solutions and materials, increasing the traffic loading on bridges, construction of high-rise and slender buildings, shortened construction periods, timesaving and cost reduction needs for construction projects, etc. are among the important factors that need efficient assessment and control, which make SHM an important tool to enhance the safety of civil structures.

In overall, Structural Health Monitoring is an interdisciplinary area that includes various technologies. Among these technologies, experimental testing of structures, different sensing technologies, data acquisition and management, digital signal processing, system identification, feature extraction and statistical analysis are most essential components of a SHM system. The first step of implementing a SHM system is data sensing and acquisition. The properties of sensor network and data acquisition system, including the number and type of the sensors, depend on the SHM application. The measurements from a structure using various sensor categories can reflect structural responses at different locations and provide information on its environmental and operational condition. These measurements may include acceleration, rotation, displacement, strain, temperature, humidity, and etc. Utilisation of a sensor network system integrated within a structure itself can greatly enhance the inspection process through rapid in-situ data collection and processing. However, these sensor networks typically produce large and complex sets of data that it becomes difficult to process using on-hand database management tools or traditional data processing applications. The challenges include capture, storage, search, sharing, transfer, analysis and visualization. Therefore, the step after data collection is data management to avoid overwhelming situation for data analysis

and missing critical information. The managed structural measurements are then analysed using various methodologies to provide useful information about condition and performance of the structure. In some cases, data analysis requires numerical modelling and simulation of the structure to compare with experimental results. The last step of SHM implementation is to utilise the information obtained from the analysis for a reliable maintenance and decision-making. To sum up, all these steps, including the data sensing, data management, and data analysis should properly work together to provide a reliable and efficient integrated structural health monitoring system.

1.2 Classification of monitoring in literature

According to application and the desired structural parameters, Structural Health Monitoring can be divided into different categories, including static monitoring and dynamic monitoring. Static monitoring is usually referred to structural long-term testing or monitoring and dynamic monitoring is usually referred to periodic short-term testing or event triggered monitoring [2]. These categories of monitoring can be applied to various types of structure, substructures, and materials. In the literature, there are several classifications for structural monitoring techniques. Here, a classification carried out by [3] for monitoring techniques is shown in Figure 1.1.

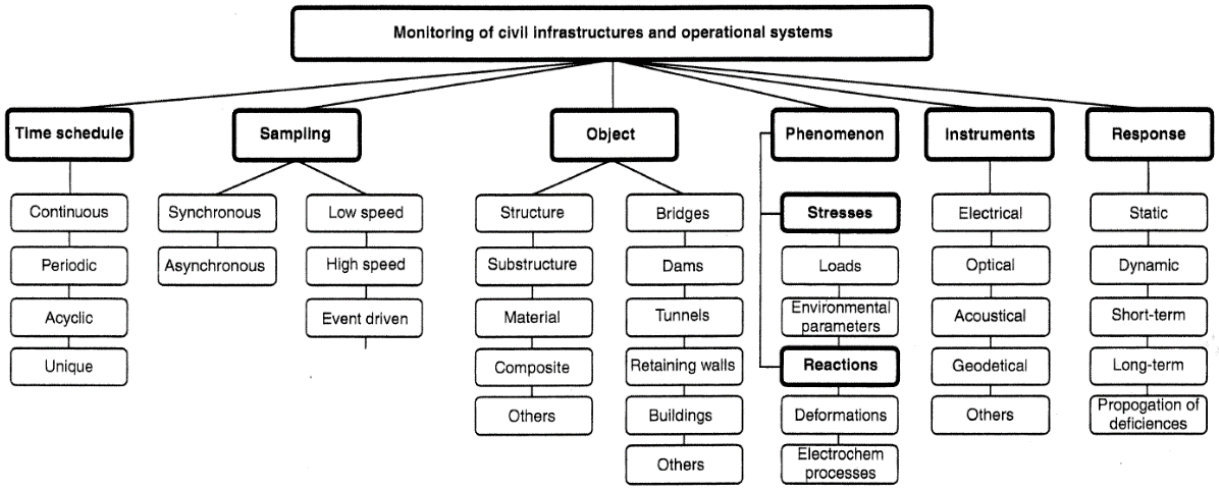

Figure 1.1. Classification of monitoring techniques according to Bergmeister & Santa [3].

The static parameters of a structural system and changes in these parameters can be obtained during a static global monitoring. This procedure can last for a few hours to years or decades. This category of structural health monitoring can be temporary, continuous, periodic, and acyclic or a combination of these different time schedules. It should be mentioned that continuous SHM system is usually applied for structures with high importance, which are usually subjected to extreme sudden events, such as earthquakes and severe winds. On the other hands, dynamic global monitoring techniques are used to obtain dynamic parameters of a structure, such as natural frequencies, mode shapes, and modal damping ratios. In the next chapter, more details on the applications of dynamic testing for damage identification of civil structures will be provided.

SHM of civil structures can be divided into two general categories, including short-term and long-term monitoring. Long-term monitoring usually includes recording structural responses due to ambient factors, such as vibration, and environmental data, such as temperature and humidity to assess the condition of structures over long periods of time. On the other hand, short-term monitoring usually refers to live-load and one-off dynamic testing on structures. These measurements are utilised to evaluate the structural performance, such as stress/strain levels, force distributions, and vibration signature of structures. Such information can be also used to improve the future design criteria and updating the numerical models.

1.3 Monitoring benefits and disadvantages

An advanced and reliable structural health monitoring system can provide the engineers and the asset owners with several benefits. Some of these profits are mentioned in the following:

1. Quick and immediate warning in case of occurrence of damage after earthquakes or other natural disasters, hence avoiding any catastrophic loss of life,
2. Providing quick evaluation of structures integrity after earthquakes or other natural disasters,

3. Proving detection of damage and deterioration of structural components and hence avoiding any global collapse
4. Providing important information related to durability, design criteria, and long-term response of structures,
5. Providing a whole maintenance cost reduction by reducing visual inspection costs,
6. Providing an efficient system for managing and processing large sets of monitoring data,
7. Providing a reliable tool for seismic assessment of civil structures [4-6].

Although monitoring of a structure provides lots of advantages for engineering community, it might cause some disadvantages and drawbacks. For an instance, utilisation of traditional wired monitoring systems is usually associated with high installation time and cost for condition assessment of large-scale structures. Also, condition assessment of a structure under construction can disturb and affect the efficiency of the construction work.

1.4 Use of SHM for damage identification

In some references in the literature, SHM term is considered the same meaning as damage identification for civil structures. However, structural health monitoring term refers to a broader technology and research area, which is utilised for various purposes, such as real-time and long-term monitoring of structures, calibration of structural numerical models, structural control, etc. There is a general review in [7] on SHM applications for civil infrastructures. Damage identification of civil engineering structures is one of the significant components of structural health monitoring. In overall, structural damage refers to any changes in structural elements and/or materials that affect the performance and behaviour of the structure and cause a reduction in its effective serviceability and overall lifetime. There are various types of structural damage in different types of civil structures, such as cracks and fractures in concrete and steel structural elements, changing in boundary conditions, bolt looseness in steel truss

structures, fatigue or corrosion in offshore platforms, etc. Identification of damage presence in structures is usually considered as the first step to understand causes of the change in structural behaviour. Rytter [8] introduced a widely acceptable definition on various levels of damage identification in civil engineering structures. Based on this definition, there are four steps for a complete and efficient damage identification, which are: (1) identification of the presence of damage in structures, (2) damage localization, (3) evaluation of severity of the damage, and (4) estimation of remaining operational life of structures and decision-making. It should be mentioned that all of the mentioned steps include some challenges especially for large-scale structures. For an instance, the real-world structures are usually subjected to operational or environmental condition changes, which impose some difficulties in detecting and identifying structural damages. Such variations usually affect the stiffness or mass of a structure in a linear manner, which is different from real structural damage that has a significant effect on the structural integrity. In addition, there are also some challenges to distinguish between the linear and nonlinear types of structural damage and between nonlinear damage and intrinsic types of nonlinearities in an undamaged structural system. In other word, the nonlinear behaviour of structure's elements and boundary condition cannot be considered as structural damage. For example, in a study carried out by Navabian and Beskhyroun [9], the condition of a full-scale concrete bridge was assessed using the vibration data collected from the structure during two large amplitude earthquakes. Based on analysis results, it was observed that there are some minor but permanent changes in dynamic characteristics of the bridge and possible nonlinearity in the bridge behaviour due to the subjected strong ground motions. However, more investigations need to be done to determine the type of nonlinearity (intrinsic nonlinearity and/or nonlinear damage) and location and severity of any possible structural damage throughout the bridge due to the subjected earthquakes. Therefore, it is of paramount

importance to categorise the types of damage in structures to provide an accurate damage identification for a reliable condition assessment of civil structures [10].

1.5 Thesis structure

This thesis consists of 8 chapters, which are structured in the following way:

Chapter 2: This chapter reviews the background and current literature on different components of a vibration-based structural health monitoring system. This literature review is mainly discussed on the wireless sensor network, data management and analysis systems, and damage identification techniques developed during the last decade for vibration-based condition assessment of civil structures. This chapter also investigates the New Zealand need for a state-of-the-art structural health monitoring system for its important civil infrastructures through a real scenario structural collapse due to a large-amplitude earthquake. At the end of this chapter, the research questions and gaps in the current knowledge are identified and presented using the conducted comprehensive literature review on different components of a SHM system. In addition, the research goals and contributions to fill out the research gaps are discussed.

Chapter 3: In chapter 3, the development process of the wireless smart sensor network is introduced. It includes the hardware design and software architecture of the new wireless smart sensor network developed in this research. This chapter begins with an initial hardware design of the wireless smart sensor nodes following with preliminary experimental tests on a footbridge and two office buildings. Then, the final hardware design of the last version of wireless smart sensor node is presented. The components of the wireless smart sensor node will be compared with most recent developed high-performance wireless sensor nodes. Then, the software workflow of wireless smart sensor network is discussed. This chapter ends with a summary of various features of the new wireless smart sensor network developed for vibration-based SHM system in this research.

Chapter 4: This chapter introduces a new data management and data analysis toolbox that is integrated into the wireless smart sensor system. It consists of a detailed description of a data management toolkit (DMT) and a data analysis toolkit (DAT), including several preliminary data manipulation and analysis techniques and various time-domain and frequency-domain system identification techniques. In the last part, a new vibration-based nonlinearity identification method is introduced based on residual error and coefficients of autoregressive time series models to determine a specific range that a dynamic system starts to behave nonlinearly. This chapter ends with a summary of various features of the developed data management and analysis toolkit and the new nonlinearity identification technique.

Chapter 5: In chapter 5, experimental verifications of the wireless smart sensors and the new nonlinearity identification technique are presented using a series of shaking table tests on a steel truss bridge model. First, the details of experimental test setup, including description of the bridge model, instrumentation, and data acquisition system are provided. Then, several experimental results related to sensitivity and resolution, event detection feature, and time synchronisation protocols of the wireless smart sensor network are discussed. In addition, the analysis results obtained for the new vibration-based nonlinearity identification technique are presented and performance of the technique is experimentally verified.

Chapter 6: In chapter 6, a case study research paper conducted by Navabian et al. [9] is presented to provide the results obtained on structural health monitoring of a large-scale bridge located in Wellington, New Zealand. This bridge was subjected to two large-amplitude earthquakes and several aftershocks. The vibration data sets recorded using several accelerometer sensors have been utilised to assess the bridge condition. The bridge performance has been assessed using non-parametric and parametric analysis techniques to obtain the vibration intensity parameters and dynamic characteristics of the bridge. A dynamic performance index based on Autoregressive Moving Average with eXogenous excitation

(ARMAX) models is utilised to assess the dynamic behaviour of the superstructure under different amplitudes of ground motions. The results of this research paper have been utilised to confirm the efficiency of vibration-based structural health monitoring systems and MATLAB-based data analysis toolbox for condition assessment of large-scale civil structures.

Chapter 7: In the last chapter, the wireless-based structural health monitoring system is utilised for a full-scale bridge health monitoring project in Auckland, New Zealand. The testbed structure is the Newmarket Viaduct, which is one of the most important civil infrastructures in New Zealand. The main goals of this instrumentation were to evaluate the performance of the developed wireless smart sensor network in an outdoor environment and to assess dynamic performance of the superstructure using its modal characteristics after several years in operation. It should be mentioned that the instrumentation was conducted during two phases of field testing. The hardware and software considerations of initial deployment of wireless SHM system on the Newmarket Viaduct are presented first following with some results related to the system performance. Then, the second phase of bridge instrumentation is presented using the final version of wireless smart sensor nodes. At the end, the dynamic performance of the structure is investigated by comparing the bridge modal parameters with their counterparts measured during previous ambient vibration tests.

Chapter 8: The final chapter concludes the key original findings of this thesis and presents possible future developments and applications of this research.

Chapter 2: Background

2.1 Full-scale structural health monitoring applications

In this part, the importance of SHM of civil infrastructures is investigated in New Zealand, where there has virtually been no local activity in this internationally recognized strategic research field. This investigation is carried out using a real-scenario total structural collapse in Christchurch, New Zealand after the Christchurch earthquake. This large-amplitude earthquake occurred in Christchurch on 22 February 2011 with a great magnitude of 6.3 causing 185 people death and considered as the New Zealand fifth-deadliest disaster. Among 185 deaths, 115 people died in Christchurch Television Building (CTV). Figure 2.1 shows the CTV building before and after the collapse as a result of the earthquake.

(a) **(b)**

Figure 2.1. CTV Building; (a) before, and (b) after Christchurch Earthquake.

Another large-amplitude earthquake, called Darfield earthquake, struck South Island of the New Zealand on 4 September 2010 with a great magnitude of 7.1, one year before the Christchurch earthquake. After the Darfield earthquake, the CTV building was visually

inspected by engineers to investigate integrity of the structure. The building was declared safe and the local authority permitted the building to be re-occupied by residents.

After the Christchurch earthquake and structural collapse, the building was assessed during several investigations carried out by engineers to find out the causes of structural collapse. According to investigations carried out by Professor Mander, it was reported that the building had been already weakened and considerably damaged by the Darfield Earthquake (the first large-amplitude earthquake). As observed, the CTV building must have also hidden (unobserved and/or unobservable) damage in specific structural components, because the level of ground motion sustained by the building was close to the level that the design code NZS4203 called for. In addition, eyewitnesses reported that the CVT building was uncomfortably lively on several occasions and these issues should be considered as a signal for Red Sticker on the building. This example of structural collapse emphasizes the fact that real-time and reliable monitoring of structural integrity after events are crucially important using a reliable SHM system, especially in an earthquake-prone country, such as New Zealand.

In addition, New Zealand Officer of the Auditor General (NZOAG) presented a series of reports for road infrastructure asset management between 2002 and 2010. According to these reports, it was shown that although the local authorities have access to primary information about their road infrastructure and some management plans for immediate actions, the existing methods are relatively insufficient for a proper management plan [11]. Based on these reports, there are few authorities in New Zealand received an advanced asset management. Specifically, in an NZOAG audit in 2010, the necessity for particular improvements of bridge asset management was further investigated. This survey mentions that:

1. There is no efficient system to monitor bridge condition deterioration,
2. There is a high risk of losing knowledge, which is crucially significant for long-term monitoring and management,

3. With a comparison between bridge asset management and road asset management, it was found that the former does not have an advanced management system [11].

Bridge infrastructures are important and expensive components in the transportation network. They provide necessary services and interconnections within the various road networks that support the community life. However, they are exposed to different natural events, such as earthquake and sever wind, in New Zealand. Therefore, their condition needs to be continuously monitored using an advanced monitoring system [12]. The results of asset management would considerably be improved if proper structural data sets are collected and connected to an advanced decision-making system. However, based on NZOAG audits, there are some gaps in existing asset monitoring and management methods, which have prevented a reliable and efficient structural condition assessment [11]. Therefore, development of a reliable monitoring system for bridges is of paramount importance to make an adequate level of safety for local community in New Zealand.

Most of bridge structures in New Zealand are old and need to be assessed using a reliable system to prevent any possible catastrophic events. Based on a risk and critically analyses carried out by Omenzetter et al. [11], the Auckland Harbour Bridge and the replacement Newmarket Viaduct are between critical and high risk bridges in Auckland. These bridges need to be monitored continuously due to their high importance and critical situation. To this end, the target bridge in this research is considered to be Newmarket Viaduct that is a post-tensioned concrete box highway bridge in Auckland. Due to the fact that the target structure in this research is a full-scale bridge, the literature review will be mostly performed on application of structural health monitoring systems for full-scale bridge structures.

During the past decade, instrumentation of SHM systems on full-scale bridges have significantly become acceptable by engineering community to assess their operational and structural conditions. Perhaps, earliest bridge health monitoring applications based on

structural engineering knowledge are the Golden Gate Bridge and the Bay Bridge in San Francisco [13]. Compared to the 1930s when these tests were performed, technology for data measurement and interpretation for SHM applications have been significantly enhanced in the last few decades. In this section, a review of bridge SHM projects performed by Inaudi [14] are presented. This review paper is an overview of 40 bridge monitoring projects carried out between 1995 to 2010 in 13 different countries.

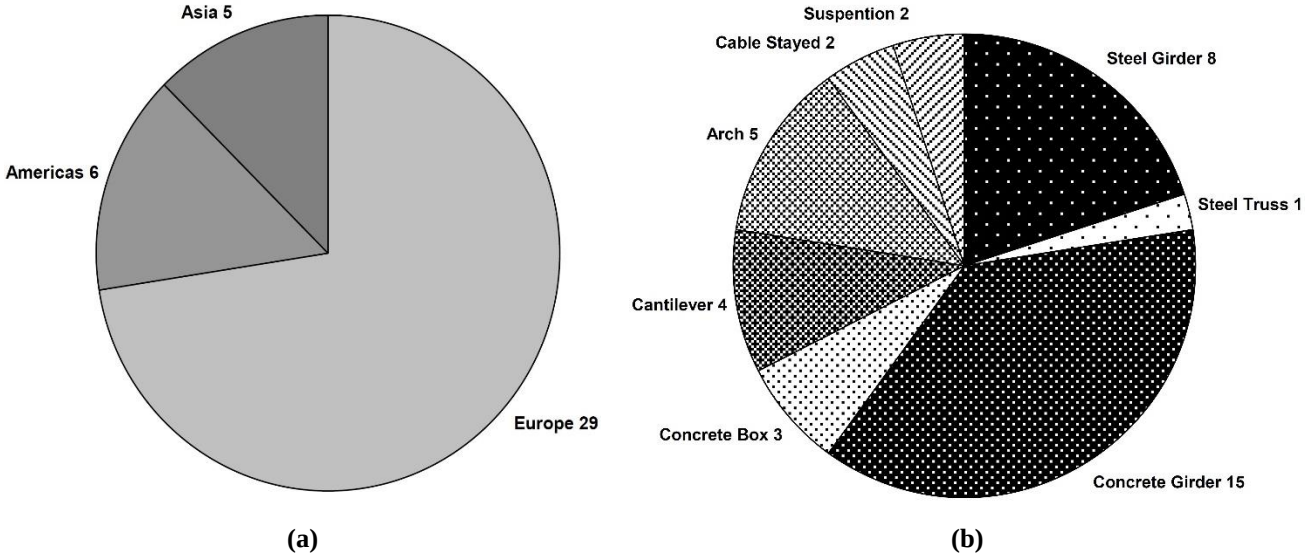

Figure 2.2. Bridge population by: a) continent, b) structural type [14].

Bridge location and type: According to this review, the location of full-scale bridges instrumented by SHM systems are in Austria, Belgium, Canada, Croatia, France, Germany, Italy, Japan, Luxembourg, Russia, Sweden, Switzerland, Taiwan, and USA. The bridges' population by continent and type are depicted in Figure 2.2. As is obvious, most of these bridges are concrete girder bridges, which are the most dominant types of bridges throughout the world. This diversity shows that the application of structural health monitoring systems for bridge structures is a popular topic around the world and can be successfully implemented on any type of bridge structures.

Lifetime phase: Bridge condition monitoring can be performed at different phases of the bridge lifetime. According to this review, this diversity for the under-study bridges was demonstrated:

- Installation during construction phase: 18
- Installation on an existing bridge: 13
- Installation during bridge refurbishment: 9

As can be understood from this category, the number of structures instrumented by SHM systems is approximately equal for existing and under construction bridges. It shows the high importance of structural condition assessment during different phases of its lifetime.

Customer: A project of bridge health monitoring can be financially supported and commenced by various institutes. For the under-review bridges, the customers are categorized as:

- Bridge owners: 23
- Universities through research funds:13
- Engineering company: 4

This category indicates the interest of owners to increase the safety of their assets using advanced monitoring systems. In addition, it is obvious that bridge health monitoring projects are still a significant research topic for many academic institutes, such as universities.

Installation: Instrumentation of SHM systems on the bridges was conducted by:

- Bridge Owner: 1
- Universities: 15
- Instrumentation Company: 24

As is clear, in many cases the implementation of monitoring systems was carried out by professional instrumentation companies or universities. Only one bridge among the 40 bridges was directly instrumented by the owner.

Budget: The cost distribution of monitoring systems installed on the bridges is shown in Figure 2.3. The cost only includes the hardware and installation costs without considering the costs of data analysis and system maintenance. As is clear, most of the SHM system budget is under $50k. These projects are generally among short-term monitoring with reduced number of

sensor nodes. More expensive group of instrumentation, including the projects with cost of $100-500k, was typically performed for long-term monitoring applications. Among the 40 monitoring projects, only the cost of one project exceeded $500k.

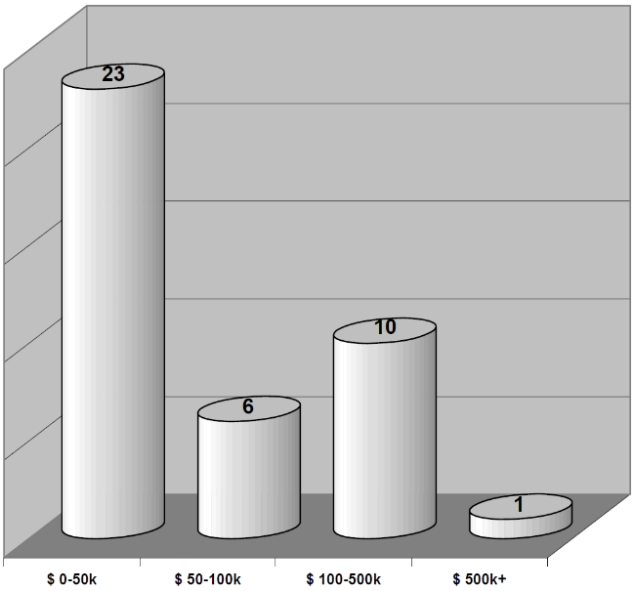

Figure 2.3. Monitoring system budget [14].

Sensors: Based on this review, the number of sensors installed for each bridge monitoring project is categorized as below. As is obvious, the small and short-term monitoring projects with 20 sensors or less are dominant.

- 1-10: 19
- 11-25: 8
- 66-50: 5
- 51-100: 5
- 100+: 3

Sensor location: The sensor location depends on the bridge type and can be installed on various parts of the structure. Based on this review, the most important parts of these bridges for instrumentation are:

- Deck: 9
- Load-carrying elements (beams, arch, cables): 31
- Piers: 4
- Foundations: 2

From this category, it can be concluded that the dominant concern of structural condition for bridges, as expected, is related to load-carrying elements, such as beams, arch and cables.

Frequency: A monitoring system can be implemented on bridge structures for different times and frequencies. The monitoring frequency for the reviewed bridges is categorised as:

- Short-term (less than 12 months): 17
- Long-term (more than 12 months, but not continuous): 12
- Permanent (continuous monitoring): 11

It is observed that the short-term monitoring projects with duration less than 12 months are dominant. This kind of projects are generally in construction phase and the monitoring systems are dropped once the application questions are answered [14]. In addition, the numbers of long-term and permanent monitoring projects are also noticeable for bridge health monitoring.

The SHM system installed on Alamos Canyon Bridge is an example of short-term monitoring system. The main goal of the bridge instrumentation was to investigate the change in measured dynamic parameters of the bridge due to variation in environmental factors [15]. This short-term monitoring system consisted of 31 accelerometer channels and 5 temperature sensors. During this experimental test, the bridge was excited using 31 impact hammer over 24-hour time period and the structural responses were recorded after each impact. The data analysis procedure included the application of the Eigensystem Realization Algorithm (ERA) in conjunction with a statistical approach to determine the modal characteristics of the structure and their standard statistical limits. The test results showed that there is a 5 percent fluctuation in modal parameters of the bridge over a 24-hour period as the result of temperature changes. Long-term SHM systems have been also installed on various full-scale and in-service bridges around the world. One of the most famous and extensive example of long-term bridge monitoring system is Tsing Ma Bridge in Hong Kong. This bridge was instrumented by the Wind and Structural Health Monitoring System (WASHMS). The monitoring system consists

of various types of sensors, data acquisition, data processing, and structural condition assessment systems [16]. The sensor system on the structure is able to measure acceleration, displacement, strain, wind, temperature, and GPS measurements using a total of 326 sensor channels. The structural responses under various loading conditions are recorded and analysed. Any abnormal change in the bridge behaviour can be considered as a potential over-loading on the structure. The main goals of this extensive monitoring system were: (1) system identification and characterisation, (2) measuring loading sources, and (3) measuring the structural responses. The Bill Emerson Memorial Bridge in Cape Girardeau, Missouri was also instrumented using a long-term SHM system. The purpose of this instrumentation was to measure the bridge seismic response and gain knowledge for design of future cable stayed bridges [17, 18]. In total, 84 accelerometer channels were installed on the bridge to measure structural vibration under various loading conditions. Anemometers were also installed on the bridge to record wind velocities. This long-term monitoring system can provide real-time structural response through internet for wide dissemination. The main goals of this project included assessment of damage detection techniques, seismic response evaluation, and model updating techniques. The long-term monitoring systems are still in operation. In the following, the bridge health monitoring projects that have been recently designed and implemented on bridge structures are presented.

In [19], an innovative health monitoring system was designed and implemented on a complicated long-span arch bridge. The system included newly designed high-performance sensors, multiscale data management and condition evaluation algorithms, and reliable warning strategies as a complete SHM system. It should be mentioned that more than 300 different sensors were installed on the bridge structure to measure various structural responses and environmental parameters. In another study, the features of different SHM systems installed on several long-span bridges in Turkey were presented in [20]. In this study, the general

preferences of the SHM systems of the bridge are discussed based on the monitoring objectives and requirements. Based on the experimental results obtained during this research, some future studies and development were recommended to effectively design and implement new SHM systems on the under-study bridges. In [21], a new deflection monitoring system was designed based on the optical fiber sensing for long-span cantilever bridges. In order to validate the performance of the SHM system, it was installed on a cantilever bridge to evaluate the deflection changes of each construction segment. A review paper on recent development of smart SHM systems for long-span arch bridges is also presented in [22]. This study covers the recent progress of SHM technology for condition monitoring of long-span bridges and presents a case study about a SHM system of a long-span arch bridge located in China. The conclusions of this review paper showed the challenges and future requirements for development of condition monitoring systems for long-span bridges.

2.2 Existing inspection methods and challenges

In this part of the thesis, the existing structural monitoring techniques were categorised and briefly explained. The first two methods, including traditional inspection methods and SHM using wired sensor system, will be explained first and then a comprehensive literature review on SHM using wireless sensor network will be presented.

2.2.1 Traditional inspection methods

Visual inspection is one of the traditional and widely used inspection technique for condition assessment of bridge structures. The structural condition is visually assessed by skilled experts in the field. As an example, any cracks in the bridge components or deformations of bridge's desk can be visually observed and reported using this technique. However, this technique has several disadvantages. For example, their time-consuming nature and high cost have limited their frequent uses. In addition, the most drawback of this technique is that not enough

information within the structure can be provided, as only some observations on the external condition of structure can be obtained. Moreover, such methods are highly variable, lack resolution and fail to provide a precise damage identification. Therefore, they are not reliable method to assess the condition of large and complex civil infrastructures [23]. An example of this method is the biennial visual inspection of the Brooklyn Bridge in New York. The cost of this inspection was evaluated around $1 million [24]. Based on a general study on the accuracy and reliability of visual inspection methods, it was observed that there is not consistency in the results of inspection. Therefore, such methods could put the public at a high risk due to inability to properly find structural damages and abnormalities [25].

Another traditional method of structural condition assessment is the use of ASTM recommended standard practice by sounding method. This method can be utilised for measuring delamination in concrete bridge decks by dragging a chain across the concrete bridge deck with a listener to observe the sound coming from the dragging motion. Any change in the sound can be considered as a possible delamination area in the bridge deck. This method has some drawbacks to identifying the localized delamination areas, as they are harder to detect. In overall, due to the fact that this method relies on human's ears to identify the change in sounds, it cannot be reliably used for an accurate and robust condition assessment of bridge structures [26].

Another structural monitoring method is the use of ultrasonic inspection that needs to be carried out by experienced experts [27]. The engineer should have enough understanding of possible damage area to concentrate on the most possible region of damage. An example of this method is the Post-Northridge structural inspection. The inspection team found a severe fatigue cracking in steel frame connections. Due to this discovery, all steel moment frame connections in Los Angeles area were assessed by ultrasonic methods. The cost of this inspection was reported around $200 to $1000 for each welded connection [28].

2.2.2 Structural health monitoring using wired sensor system

Implementation of sensors within structures quickly gained more popularity than the traditional inspection techniques due to higher reliability and lower cost. For condition assessment of civil structures, a variety of sensors, including accelerometers, strain gauges, displacement sensors, and inclinometers, are usually used. These sensors are embedded inside the structural members during the construction period or installed on different locations of structures, when they are in service. The wired sensor systems are usually designed to record structural responses on a continuous basis and for a long period.

For example, the Parkview Bridge was monitored using wired monitoring system. In total, 184 vibrating-wire strain gauges, Model VCE-4200, with built-in thermocouples were installed on the bridge deck during construction period. The aim of this installation was to measure the strain and stress variations of the bridge deck over operational period of the structure and compare the results with standard levels [29]. In another attempt, Magalhaes et al. [30] performed a dynamic analysis on a long-span bridge in Portugal. During this test, 12 wired accelerometers were installed on the bridge deck to measure the structural vibration for modal parameter estimation. These measurements were then utilised to calibrate numerical models of the bridge to evaluate accuracy of vibration-based damage identification techniques. According to the nature of wired monitoring system, each sensor is connected to data acquisition system through long cables to transfer the measurements to monitoring centres and to connect to a power supply. Figure 2.4 shows the schematic of a wired monitoring system and an application of such systems for a real structure.

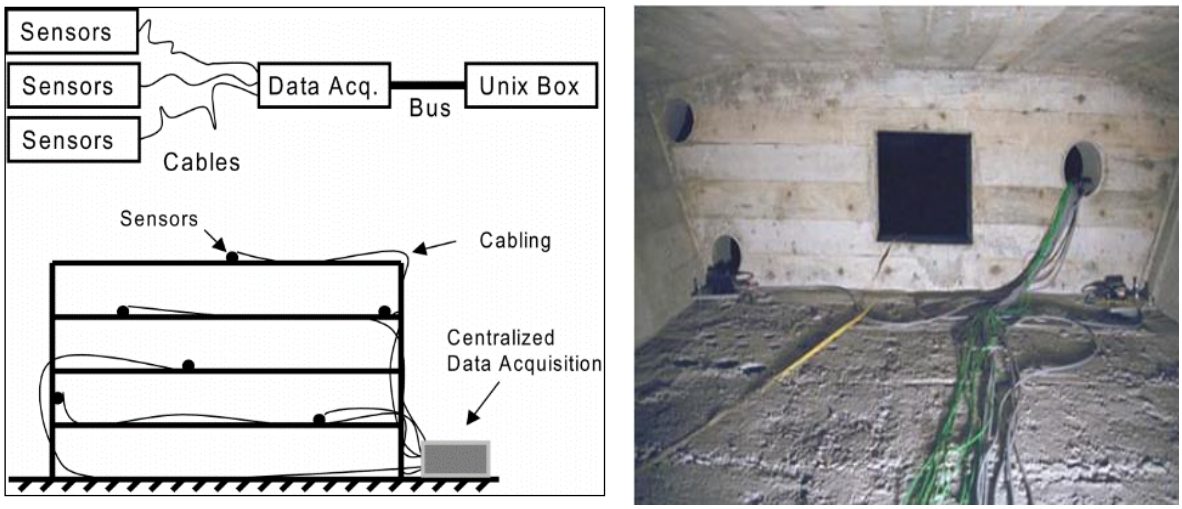

Figure 2.4. wired structural health monitoring system [31].

Due to the fact that the sensors are usually located far away from the base station unit, instrumentation of large-scale structures with wired SHM systems is costly and requires intensive cabling and high installation time. Therefore, the use of such system for large-scale structures is limited because of the following reasons [31].

1) Huge costs of cable and labours,
2) Huge installation time, cost and efforts and difficulties in maintaining wiring plant,
3) Vulnerability of cables to failures resulting in data loss,
4) Limited flexibility and scalability for instrumentation of large-scale structures,
5) Difficulties in management of large amount of data using manual management tools.

The monitoring system on Bill Emerson Memorial Bridge in Cape Girardeau, Missouri is an example that shows the high cost of wired SHM systems. The cost of this monitoring system was approximately evaluated around $1.3 million for 86 accelerometers, which makes the average installation cost around $15,000 per sensor. In another example, a wired monitoring system installed on the Tsing Ma suspension bridge in Hong Kong has a cost of $8 million ($27,000 per sensing channel) [32]. Moreover, it is mentioned in the literature that instrumentation cost of such system on high-rise buildings is more than $5,000 per sensing channel [33]. The high costs of wired SHM system totally depends on the cables utilised to

connect sensors to the centralized data acquisition. More than 75% of the installation time and up to 25% of the total cost of the system are related to lying of cables within structures and installation costs, respectively. Due to the aforementioned drawbacks, it can be concluded that wired SHM systems are not an efficient solution for monitoring large-scale civil infrastructures [34]. In response to the disadvantages of traditional inspection methods and wired SHM system, wireless sensor network (WSN) technology has emerged as a promising solution for monitoring the complex civil structures [35].

2.3 Structural health monitoring using wireless sensor network

In this part, the application of wireless sensor network for condition assessment of civil structures are presented. First, the features and components of a reliable wireless sensor network for health monitoring of civil structures are provided and then the existing wireless sensor platforms in the literature are presented. Also, a detailed literature review will be provided on most recent high-performance wireless accelerometer sensor nodes developed for SHM applications.

2.3.1 Features of a wireless sensor network

As mentioned, the limitations associated with traditional inspection methods and wired structural health monitoring systems can be significantly enhanced using wireless sensor network. In recent years, the improvements in Micro-Electro-Mechanical System (MEMS) provide engineers and researchers with great opportunities to develop wireless smart sensor network (WSSN) with sensing capabilities, wireless communication and data processing options for SHM applications [36]. Thanks to reduction in cost and physical dimension of MEMS sensors, many researchers have tried to instrument dense arrays of wireless sensors, hundreds or even thousands of nodes, throughout structures for a promising data collection resulting in an accurate condition assessment of structures. Due to the advantages of wireless

sensor nodes over the wired sensors, including portability, reusability, and lower cost, such advanced systems can provide more economical and efficient solutions for SHM applications comparing to the wired sensor systems.

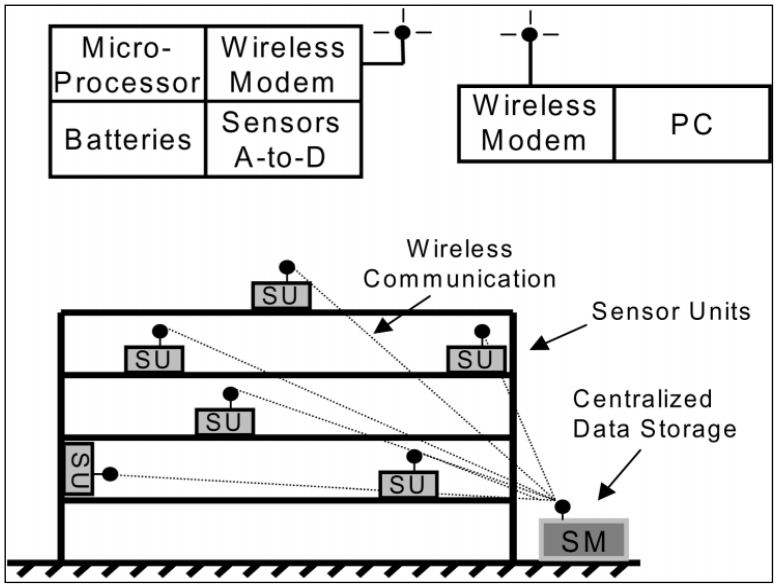

Figure 2.5. Wireless sensor network for structural health monitoring applications [37].

In the literature, there are several studies conducted on wireless sensor development concentrating on sensing devices [38, 39], wireless communication [40, 41], and data processing [42, 43]. Figure 2.5 shows a schematic diagram of wireless sensor network system installed on a building structure. As is clear, each wireless sensor node includes four main components, including sensing interface (sensors and data acquisition), computational core (Microprocessor), wireless transceiver (Wireless modem), and power supply (Batteries) [44]. A brief explanation about these components are presented in following parts.

Sensing interface: This part of a wireless sensor node is mostly responsible for sensing the physical parameters from structures and then to convert the recorded analogue signals to the corresponding digital signal for more data analysis. Also, it contains an interface through which sensing components can be connected to the whole board. The precision of the sensor interface depends on the conversion resolution (number of bits), sampling rate, and number of channels available on the Analogue-to-digital Convertor (ADC). A high-resolution ADC are usually

expensive in cost and power consumption. Therefore, it is desired to make a trade-off between resolution, cost and power consumption for an efficient assessment of structural condition.

Microprocessor: The microprocessor is programmed to control different operational modes of the wireless sensor node, such as sampling and transmission modes. The computational core store and process the recorded data from structures and prepare the data streams for wireless transmission. Microcontroller is also utilised as computational component to store the measurements in an on-board memory. The data bus size of microcontrollers is usually in the range of 8 to 16-32 bits that can determine the processing throughput. Larger data bus results in higher processing throughput and subsequently higher cost and power consumption, which need to be considered in the design of wireless sensor nodes [45].

Wireless transceiver: The wireless transceiver is an important component of the wireless sensor node to make communication between various sensor nodes and the gateway node. The wireless transceiver is responsible for broadcasting different commands related to various operational modes and to wirelessly transfer the measurements from sensor nodes to the gateway node. The radio frequency, which is usually used for the wireless sensor nodes, is unlicensed and operates on 900 MHz, 2.4 GHz, or 5 GHz. Due to the fact that Radiofrequency (RF) modules consume most power of a wireless sensor board, a proper RF component and a careful software architecture need to be implemented for the sensor board design.

Power component: while power in wired sensor system can be easily supplied through cable connections and the sensor network can continuously operate, power supply in wireless sensor network has become a serious issue. Most of the sensor nodes in a wireless network use various types of batteries for operation. Therefore, careful implementation of power management system is one the critical factors in development of wireless sensor network [46]. As mentioned, the power consumption of wireless sensor nodes mostly depends on RF module, microprocessor clock speed, and sensing components, which needs to be optimized for long-

term monitoring applications [47]. There are some other available options to save the power on the wireless sensor nodes. The use of time-triggered or periodic sampling mode is a promising way, which allows the network to sleep most of the time for energy-saving. Another possible way is to harvest energy from existing natural resources. Solar panels and wind turbines can be employed for civil structures to expand the lifetime of sensor network.

Another important feature of a wireless sensor node is its low cost. Most of the wireless sensor nodes are primarily made of MEMS and integrated circuits (IC) that have low cost as well as being small in size. In addition, there is very low cost for wireless sensor instrumentation throughout civil structures. These features enable dense array of wireless smart sensors to be installed over structures.

Besides the advantages associated with wireless sensor network for SHM applications, it should be mentioned that such systems have some limitations in resources. Some of these limitations, such as stable power source requirements and synchronised data sampling, are global for wireless sensor networks. The other issue is that most SHM applications need high resolution sensing of physical parameters, such as acceleration, strain, and displacement. However, there are several sources of measurement noises that could affect the resolution of data recording. All of the aforementioned issues should be addresses in hardware and software design of wireless sensor node for SHM applications [48]. Based on the comprehensive literature review and the lessons learned from them, some of the most important requirements for sensor board design and implementation techniques considered in this research are summarized in Table 2.1.

.

Table 2.1. Wireless sensor network features for SHM applications.

Features	Requirements	Implementation strategy
Sensor Types	Accelerometers, Environment sensors, etc.	Designing high-performance sensors to measure physical parameters from civil structures
Noise Density	Low-noise design and noise-reducing devices for a high-quality signal.	Using anti-aliasing analogue filter, low-pass and high-pass digital filters
High Resolution	Resolution of accelerometer < 1 mg	Using high performance digital output accelerometer with high resolution ADC
Sampling Rate	High sampling frequency (X00 time per second)	Based on the frequency range of the structure and Nyquist sampling theorem, sampling rate > 100 Hz
Data Volume	Raw measurement data at each sensor node: X000-X0000 bytes	Using high capacity external flash memory for storing vibrations data
Time Synchronisation	Synchronized sensing: - All the sensors should work simultaneously, - Synchronisation error < 1 mms	New time synchronisation protocols before and after data sensing
Transmission Speed	Trade-off between high-speed data transmission and power consumption (maximum of 250 kbps)	Using improved power consumption XBee RF module with robust wireless communication
Long-distance Transmission	Multi-hop routing for large wireless network desired for linear structures like bridges	Using multi-hop wireless communication protocol
Power Management	Implementation of careful power management strategy	1. Selection of low-power components, 2. Periodic and event-triggered sampling modes

The important requirements that need to be considered in designing wireless sensor network for structural health monitoring of large-scale civil structures are pointed out as follows:

1. The wireless sensor system network should be installed throughout structures for long-term periods. Therefore, implementation of a careful and reliable power management strategy using ultralow power consumption components and integrating time-triggered and event-triggered sampling modes are necessary.
2. Another important feature that needs consideration is to have an accurate time synchronisation between sensor nodes. The sensor measurements must be tightly

synchronized to perform accurate correlation analyses using the data measured by different sensor nodes for a highly precise damage identification.

3. The wireless network is required to support a seamless and reliable communication between sensor nodes and base station unit to disseminate commands and transfer measurements to gateway node without loss of information and data. In addition, due to the geometry of large-scale civil structures, such as bridges, multi-hop wireless communication is demanded to expand the communication range.
4. The wireless sensor board should have a low-noise design, high sampling rate, high resolution Analog-to-Digital converter (ADC), and noise-reducing features, such as analogue and digital filtering options, for high-quality sampling of structural vibrations with different amplitudes.
5. Vibration data induced by sudden events, such as earthquakes, are important to be analysed for condition assessment of civil structures. Therefore, the sensor nodes should be able to record event-induced vibrations using a reliable event-triggered sampling mode in addition to time-triggered sampling mode.

2.3.2 Comparisons of existing wireless smart sensor platforms

Due to the advantages of wireless sensor network for SHM applications, many researchers have made continuous attempts to design robust and reliable wireless sensor platforms. Although there are several wireless sensor nodes available for SHM applications, a limited number of full-scale structures has been instrumented due to several uncertainties in their hardware and software design [49]. Straser [34] developed some of the first wireless sensor platforms for structural condition monitoring. Following this development, many wireless smart sensor platforms have been designed and developed.

Table 2.2. Wireless MEMS-based sensor platforms developed between 2007 and 2017.

Study	Accelerometer	Noise Density	Sensitivity	Range	Bandwidth	ADC
Nagayama [50] (2007)	LIS3L02DQ	1.03	67.30	±2.00	0-56	N.A
Pakzad [36] (2008)	SD-1221	0.05	203.96	±2.00	0.1-25	16
Cho [51] (2008)	CXL02LF	1.37	101.98	±2.00	0-50	16
Rice [52] (2008)	LIS3L02AS4	0.49	67.30	±2.00	0-50	16
Whalen [53] (2009)	LIS2L02AL	0.29	67.30	±2.00	0-50	12
Meyer [31] (2009)	LIS2L06AL	0.88	22.43	±2.00	0-100	12
Swarts [54] (2010)	CXL01LF	0.69	203.96	±1.00	0.03-25	16
Park [55] (2010)	SD-1221	0.05	203.96	±2.00	0.1-100	16
Jo [56] (2010)	SD-1221	0.05	203.96	±2.00	0-15	16
Bocca [57] (2011)	LIS3LV02DQ	1.03	67.30	±2.00	0-56	N.A
Chae [58] (2012)	AC310-002	0.13	203.96	±2.00	0-300	16
Kohler [59] (2013)	SE1500	0.003	122.37	±3.00	0.1-1500	24
Sabato [60] (2014)	SF1600	0.003	122.37	±3.00	0-1500	24
Hu [61] (2015)	SD-1221	0.05	203.96	±1.00	0-50	12
Spencer [1] (2017)	LIS344ALH	0.5	660	±2.00	0-1800	16

An overview of wireless sensor development for SHM applications was provided by Lynch et al. [44] to show the eligibility of this technology for improvements in structural health monitoring. This review paper cites over 150 papers published for wireless sensor development and investigates 24 wireless sensor nodes that were developed for SHM. Based on this review, the developed platforms can be categorized into two groups: 1. academic prototypes, and 2. commercially available platforms. In the following, some of the academic and commercial wireless sensor nodes found in literature from 2007 to 2017 are presented.

Academic prototypes: this category of wireless sensor platforms was designed using commercial-off-the-shelf (COTS) components to address the hardware requirements for SHM applications. Most of these platforms utilised 8-bit or 16-bit microcontrollers with an integrated analogue-to-digital converter. A summary of these high-performance wireless MEMS-based sensor nodes is presented in order of time in Table 2.2. In this table, the accelerometer sensor features, including noise density ($\times 10^{-3}$ $m.s^2/Hz^{0.5}$), sensitivity ($mV/m.s^2$), range (g), bandwidth (Hz), and ADC resolution (bit) are given. Also, a brief description of experimental tests carried out using these sensors are also summarized in Table 2.3 [62].

Commercial prototypes: In addition to academic platforms, commercial wireless sensor nodes have also made considerable attentions among users. While most of these commercial platforms are proprietary, which means their hardware design and operation software are not subjected to users. This proprietary nature of commercial sensor platforms has prevented free development of their hardware and software for a specific SHM application [63]. As an example, a family of Berkeley wireless sensor nodes designed by researchers at University of California are presented in Table 2.4 with their hardware specifications.

Table 2.3. Experimental tests carried out using the developed wireless sensor nodes.

Study	Test type	Test results
Pakzad [64]	SHM of the Golden Gate bridge	Estimation of acceleration amplitude and modal characteristics
Cho [51]	SHM of a theatre balcony	Estimation of modal characteristics
Cho [51]	SHM of a balcony & a cable-stayed bridge	Estimation of modal characteristics and tension force
Swartz [54]	SHM of Wind turbines	Estimation of acceleration amplitude and modal characteristics
Park [55]	SHM of a lab-scaled concrete girder model	Estimation of modal characteristics and damage detection method
Rice [52]	Shake table tests	Estimation of acceleration amplitude and power spectrum
Rice [65]	SHM of the Stawamus Chief pedestrian bridge	Estimation of acceleration amplitude and modal characteristics
Rice [66]	SHM of the Jindo bridge	Estimation of acceleration amplitude and transmission protocol
Jo [67]	SHM of a steel truss structure	Estimation of acceleration amplitude and modal characteristics
Jo [68]	SHM of the Jindo bridge	Estimation of acceleration amplitude and modal characteristics
Whalen [69]	SHM of the Wright Road bridge	Estimation of acceleration amplitude and modal characteristics
Whalen [70]	SHM of the Big Sucker Brook bridge	Estimation of acceleration amplitude and modal characteristics
Meyer [31]	SHM of the Stork bridge	Estimation of modal characteristics
Bocca [57]	SHM of a wooden model bridge	Estimation of modal characteristics
Chae [58]	SHM of the Yongjong Grand bridge	Estimation of modal characteristics and cable tension
Hu [61]	SHM of the Zhengdian Highway bridge	Estimation of acceleration amplitude and modal characteristics
Sabato [71]	SHM of a real-size model of a stone pinnacle	Estimation of acceleration amplitude and modal characteristics
Sabato [72]	SHM of the Streicker bridge	Estimation of acceleration amplitude and modal characteristics
Sabato [73]	SHM of the Stone pinnacle	Estimation of acceleration amplitude and modal characteristics
Kohler [59]	SHM of high-rise buildings	Estimation of acceleration amplitude and modal characteristics
Kohler [59]	SHM of the Robert A. Millikan Library building	Estimation of acceleration amplitude and modal characteristics
Kohler [59]	SHM of the Wilshire Blvd. building	Estimation of modal characteristics

Commercial prototypes: In addition to academic platforms, commercial wireless sensor nodes have also made considerable attentions among users. While most of these commercial platforms are proprietary, which means their hardware design and operation software are not subjected to users. This proprietary nature of commercial sensor platforms has prevented free development of their hardware and software for a specific SHM application [63]. As an example, a family of Berkeley wireless sensor nodes designed by researchers at University of California are presented in Table 2.4 with their hardware specifications.

Table 2.4. Commercially available wireless sensor platforms for SHM applications.

Component	Mica2	Mica2Dot	MicaZ	Telos	Imote2
Processor	ATmega128L	ATmega128L	ATmega128L	TIMSP430	XScalePXA271
Bus Size (bits)	8	8	8	16	32
Processor Speed (MHz)	7.373	4	7.373	6.717	13-416
Program Flash (bytes)	128 K	128 K	128 K	48 K	32 M
EEPROM (bytes)	4 K	512 K	4 K	N.A	N.A
RAM (bytes)	4 K	4 K	4 K	10 K	256 K + 32 M
Radio Chip	CC1000	CC2420	CC2420	CC2420	CC2420
Radio frequency (MHz)	315/433/915	315/433/915	2400-2483.5	2400-2483.5	2400-2483.5
Data rate (kbps)	38.4	38.4	250	250	250
Outdoor range (m)	300/300/150	300/300/150	100	100	100
ADC channels	8	6	8	8	N.A
ADC resolution (bits)	10	10	10	12	N.A
Active Power (mW)	24	15	24	10	44@13 MHz 570@416 MHz
Sleep Power (µW)	75	75	75	8	100
Size (mm)	58×32×7	25×6	58×32×7	65×31×6	48×36×7

Acceleration is one of the most important structural responses that was employed in all the MEMS-based wireless sensor nodes for SHM applications. As was observed from the literature review, most of the reviewed wireless sensors are analogue-output and only two of them were designed with digital-output accelerometer. For the wireless sensor nodes developed with analogue-output accelerometers, an external analogue-to-digital converter (ADC) chip should be used to convert the recorded analogue signals to their digital counterparts. Higher power consumption, complexity in design, higher cost, and analogue noise challenges are disadvantages of such board designs [51, 54, 74]. In some of these wireless sensor designs, the internal ADC of the microcontroller was utilised for data conversion, which could cause jitter problem for the recorded vibration signals [75]. In general, such vibration measurements cannot be reliably used for damage identification in civil structures. In addition, as is obvious, these wireless sensor nodes employed high noise density accelerometer chips, which cannot provide adequate resolution to measure low-amplitude ambient vibrations from large-scale structures [76].

In a recent review research paper conducted by Sabato et al. [77], there are two high-resolution wireless accelerometer sensor nodes designed for SHM applications using analogue-output accelerometers. Kohler et al. [61] designed a wireless sensor node using the analogue-output SiFlex accelerometer manufactured by Colibrys. The sensor board employed three single-axis SiFlex 1500 accelerometers that operate at a supply voltage range from ±6 to ±15 V and provide a resolution of 1.4 μg for low-amplitude ambient vibration measurements. This accelerometer supports an acceleration range of ±3 g with a sensitivity and noise density of 1.2 V/g and 0.3 $\mu g/\sqrt{Hz}$, respectively. In another study conducted by Sabato et al. [78], a new wireless accelerometer board was developed using a low-noise SiFlex 1600 MEMS-based accelerometer providing an acceleration range of ±2.94 g and a resolution of 1.4 μg for vibration measurements. In the design of this sensor board, a low power Voltage to Frequency

(V/F) converter, AD650, was utilised to convert the analogue signals to the frequency counterparts, which could enhance the performance of the sensor for low-amplitude vibration measurements. Although the wireless accelerometer sensors developed in these studies could provide low noise floor for high-quality vibration measurements, they require high power consumption and a bipolar power supply of ±6V to ±15V, which is hard to supply with typical DC power sources [76].

In addition to efforts on development of analogue-output wireless sensors, a few researches were conducted in the literature to develop digital-output wireless accelerometer sensors for SHM applications. Bocca et al. [57] designed a synchronized wireless sensor board using a 3-axis digital-output accelerometer, LIS3LV02DQ manufactured by STMicroelectronics. This accelerometer can provide a selectable measurement range of ±2 g or ±6 g with a selectable 12-bit or 16-bit representation. The supply current for this accelerometer is 0.80 mA at 3.3 V supply voltage that is among the low power consumption accelerometers for SHM applications. However, this accelerometer has a noise density of 110 $\mu g/\sqrt{Hz}$ and sensitivity of 1024 LSB/g, which cannot be considered as a high-performance accelerometer for ambient vibration measurements. In a recent study, a wireless accelerometer sensor was developed using a low-noise tri-axial M-A351 accelerometer manufactured by Seiko Epson Corporation [76]. This high-performance digital-output accelerometer can provide a noise level of 0.5 $\mu g/\sqrt{Hz}$ and a measurement range of 0.06 μg/LSB that results in a high-quality measurement of low-amplitude vibrations. However, the power consumption of this accelerometer in measurement mode is 20 mA (60 mW) at a supply voltage of 3.3 V, which is considered high power consumption for SHM applications.

All the mentioned wireless sensors for SHM applications use time-triggered or periodic sampling mode to reduce the power consumption of the wireless sensor nodes for recording structural vibrations. Therefore, they are not able to detect and capture sudden events, such as

earthquakes, if they are in power-saving sleep mode when the event is subjected to the structure. For example, a catastrophic sudden collision was reported in [79] between barges and a piling of railroad bridge in Alabama in 1993. The bridge was damaged and totally collapsed 20 min later causing 47 people deaths. These deaths could have been presented if the bridge condition had been immediately assessed following the collision. Therefore, the wireless-based SHM system should be able to detect and capture such unpredictable events and record high-fidelity measurements for an immediate structural condition monitoring.

As is obvious from the provided literature review, there are some needs to develop and improve the performance of the existing wireless accelerometer sensor nodes using state-off-the-art technologies and to make a great trade-off between sensitivity, power consumption, and cost in the design of wireless sensor nodes for an efficient condition assessment of civil structures. In addition, due to the fact that most of the developed wireless sensor nodes used periodic or time-triggered sampling mode for ambient vibration measurements, the new wireless sensor node should be able to detect and capture high-fidelity measurements of unpredictable events.

2.4 Data management for SHM data

As mentioned in the previous sections, for an accurate and reliable structural health monitoring, a dense array of various types of sensor nodes should be installed throughout structures to collect enough structural responses for feature extraction. These sensor systems with high sampling rate usually create enormous amount of measurements during continuous and long-term monitoring. There are several accomplished and undergoing researches on development and improvement of sensor technologies for SHM applications. However, there are very few efforts have been conducted on the development of a reliable data management and data analysis platform for SHM data. The massive high-volume SHM data files are usually managed using traditional file-based approach [80, 81]. It was observed that utilisation of file-based management approaches makes the data digging hard and time-consuming because of massive

contents of monitoring data. They also cause some difficulties to extract maximum useful information from raw measurements and prevent the asset owners to gain advantages from SHM systems. Therefore, development of a data management and data analysis system for an efficient and user-friendly management, storage, query, visualisation, swap, and retrieval of monitoring data is a significant component of a SHM system [82].

Here, some of the conducted research on developing SHM data management techniques are presented. A MySQL database system was proposed by Koo et al. [83] to store and visualise structural response measurements. The system was utilised to interface with data processing and analysis techniques in order to extract information from SHM data. In another study, Smarsly et al. [84] developed an agent-based framework to store and analyse structural response data. In another study a self-managing software framework was designed and developed for managing the SHM data from a wind turbine structure. The system is able to manage the sensor data measurements, remotely access to the data, and perform data analysis on the raw measurements [85].

Another technique that has been used in developing management systems is cloud computing. It can provide a flexible and cost-effective solution for managing high volumes of monitoring data. In [86], the application of cloud computing has been investigated for monitoring of bridge infrastructures by developing a cloud-bases data management framework. Another considerable work in data management for SHM applications was conducted by Zarate et al. [87]. In this research, the authors developed a scalable cyber-environment data management platform for management and analysis of structural health monitoring data. In another research conducted by researchers at the University of Michigan, a scalable data infrastructure platform, named SenStore, was designed for managing sensor data and engineering information for bridge health monitoring applications [88].

In a specific research conducted by Beskhyroun [89], an automated data management and

analysis platform has been designed for SHM data. Graphical User Interface (GUI) of this platform has been created with MATLAB GUIDE. The automated analysis platform has been designed for structural modal identification, long-term dynamic monitoring, easy development of graphical interfaces, and providing powerful tools for data processing, which are important features in the context of continuous and long-term monitoring. The developed system consists of two independent toolkits: the modal parameters identification toolkit (MPIT) that is utilised for structural dynamic identification and the automated data analysis toolkit (ADAT) designed for data management and processing of large data sets. The former was developed for identification of dynamic characteristics of a structure such as natural frequencies, mode shapes, and damping ratios. The latter was designed for an automated dynamic monitoring without any user interaction. Using this toolkit, users can automatically manage and analyse large sets of data. This system has been utilised in a part of this research for condition assessment of a full-scale concrete bridge in Wellington, New Zealand. The results of this research paper will be presented in chapter 6 of this thesis. It was observed from the results published in [9] that MATLAB software can provide a powerful environment for data management, data storage, data integration, data visualization and other computing and information processing services that are essential for a SHM system.

Therefore, to enhance the performance of condition assessment of civil structures compared to the traditional file-based approaches, it was decided to utilise MATLAB Layout Toolbox environment in this research to design a new data management and analysis platform, which is compatible and connected to the new developed wireless sensor system.

2.5 Damage identification algorithms

As mentioned, damage identification and localisation in civil structures are important components of a SHM system. In the literature, numerous techniques have been presented for damage identification using SHM data. In general, these techniques can be categorised to two

major groups, including parametric and nonparametric methods. In parametric techniques, the mathematical model of the structure is known and the aim is to determine any changes in the structural parameters comparing to the baseline model to identify and localise structural damages. These parameters are usually referred to physical quantities of the structure, such as mass, damping, and stiffness. In non-parametric techniques, the relation between inputs and outputs of the system is constructed without any information and knowledge about the structural model. In the next step, the structural damage can be detected by finding any changes in the parameters of the created non-physical model. Therefore, it can be concluded that non-parametric methods cannot be utilised to localise structural damages unless a priori information from all potential damage states and the corresponding outputs of the system is available. In the following sections, the most common parametric and non-parametric techniques used for damage identification in civil structures are briefly explained.

2.5.1 Parametric damage detection methods

One of the most common parametric system identification techniques is modal parameter estimation, according to which the unknown physical parameters of the dynamic model, such as modal frequencies, modal damping ratios, mode shapes, and modal scaling, can be measured. Such methods utilise input-output or output-only datasets measured from the system using various types of sensors. One of the advantages of modal parameters for damage identification purposes is that they can efficiently interpret the physical characteristics of the system. In the literature, there are large numbers of research conducted to extract damage detection features using modal parameters for SHM. In a review paper published by Doebling et al. [90], a comprehensive literature review on various techniques based on modal characteristics have been discussed and summarized.

Dynamic testing is one of the most common and effective methods for modal parameter estimation. The measurements from these tests can provide information on global

characteristics as well as the local feature of the modal system. Dynamic testing on civil structures can be performed using two techniques depending on the availability of the input force. These testing methods are ambient vibration testing and forced vibration testing. In ambient vibration testing, the input excitations are unknown and coming from wind, traffic on the street, human and operational activities, etc. In forced vibration testing, the input excitations come from a known source at specific frequencies. The excitation force in forced vibration testing is usually provided using an exciter or shaker. Although, several forced vibration tests have been conducted on large-scale structure, such testing approaches are not generally practical and cost-effective for most of the large-scale civil structures. The datasets obtained during dynamic tests are analysed using input-output or output-only modal analysis techniques to estimate the modal parameters. Generally, modal parameter estimation techniques can be categorised into two groups including time domain techniques and frequency domain techniques that are explained in the following sections.

Time domain methods: Time domain analysis techniques directly extract the information from raw time series data sets. In general, such methods have been developed based on control theory concepts. Based on this theory, the time domain analysis methods are usually started from free response or pulse response of the system. However, most of them can be utilised with ambient vibration data after pre-processing of raw measurements to estimate the free decay time response data [91]. It should be mentioned that application of time domain methods for densely damped structural systems has some limitations and requires large sets of time domain data. Some of the widely used time domain analysis methods for modal parameter estimation are Complex Exponential Algorithm (CEA), Polyreference Time Domain (PTD), Eigensystem Realisation Algorithm (ERA), Eigensystem Realization Algorithm/Natural Excitation Technique (ERA/NExT), and Stochastic Subspace Identification (SSI). A comprehensive review on various time domain analysis methodologies is presented in the literature [92-95].

Frequency domain methods: Frequency domain techniques convert the time series measurements to frequency domain and then estimate modal parameters in the frequency domain. Such techniques utilise Frequency Response Functions (FRFs) to calculate the modal parameters. Frequency domain methods have some advantages and disadvantages over the time domain analysis methods. One of the main advantages is that less computational modes can be calculated using frequency domain methods compared to the time domain methods. One of the disadvantages of such methods is because of the limitations of Fast Fourier Transform (FFT).

There are several frequency domain analysis methods developed for modal parameter estimation. One of the simplest frequency-based techniques is Peal Picking (PP) method, according to which the modes are selected from the peaks of FRF values. The natural frequencies of the system can be obtained using FRF peaks if the structural system is not heavily damped and the models are well excited and separated. Analysis of output-only vibration data is also carried out by well-known Frequency Domain Decomposition (FDD) and Enhanced Frequency Domain Decomposition (EFDD) methods using Singular Value Decomposition (SVD) of the response spectrum matrix [96]. The frequency domain techniques mentioned here will be used in this study for modal parameter estimation.

Ambient vibration data analysis: Ambient vibration experiments are most common structural monitoring techniques, as they are economical, non-destructive, fast and easy to implement, and the test methodology does not affect the integrity and health of the structure [97]. However, as the input force is unknown in ambient vibration measurements, the output-only modal identification techniques must be applied to extract modal parameters. Additionally, as the input excitation in ambient vibration tests is usually weak, these tests are not effective in obtaining an accurate estimation of dynamic characteristics of the structure related to higher modes. In forced vibration testing, the input excitations come from a known source at specific frequencies. The excitation force in forced vibration testing is usually provided using an exciter

or shaker. During such tests, the structure is subjected to higher levels of excitation so that critical structural elements and boundaries can be properly activated and assessed. Forced vibration tests can overcome the issues associated with ambient vibration tests by providing higher input forces. However, they are substantially more expensive, time consuming to conduct, and often require special permissions as there are several potentials for damage to the structure.

In [97], the results of forced vibration tests on a 13-storey office building indicated that the amplitude of input force affects the dynamic characteristics of the structure. In this research, it was shown that the natural frequencies and the modal damping ratios respectively decreased and increased as the magnitude of input excitation force increased. In addition, a good agreement between the modal parameters of the building, including natural frequencies and modal damping ratios, was obtained from different sets of low-amplitude ambient vibrations induced by wind, traffic, and a M6.5 Earthquake. Therefore, it can be concluded that ambient vibration testing can be as effective as forced vibration tests to be used for condition assessment of such large-scale civil structures.

Identification of modal parameters using ambient vibration test data has become popular and there are many studies conducted in the literature [98-102]. The measurements from the ambient vibration tests can be analysed using various output-only methods to extract modal characteristics of structures. These methods are usually based on the methods mentioned in the previous sections in both time and frequency domains. For example, Frequency Domain Decomposition (FDD) methods has been widely used for ambient vibration analysis using Singular Value Decomposition (SVD) of the output spectrum matrix [96, 103]. In this study, several output-only analysis methods in time and frequency domains will be used for modal parameter estimation from ambient vibration data.

2.5.2 Non-parametric damage detection methods

In the last decades, the use of statistical pattern recognition techniques has gained attention to analyse large set of SHM data considering variations in them. Therefore, there are large number of studies are the literature focusing on development of new techniques based on statistical concepts. Most of these methods combine time series modelling with new statistical detection techniques such as outlier detection. It is noteworthy that the most important advantages of these methods is that they need data from undamaged system for training process. In addition, the premise of statistical pattern recognition approach is that the data from unknown condition of the system will likely be categorised as outliers in the data as the system is trained using the undamaged data sets. Sohn et al. [104] developed a damage sensitive feature based on statistical process control method. This method utilised coefficients of Auto-Regressive (AR) models to develop the damage identification feature. Various levels of damage were detected in a concrete column using this method. In another study, Worden et al. [105] and Sohn et al. [106] used an outlier detection based on Mahalanobis distance for damage identification in numerical models. In these studies, Worden utilised transmissibility function and Sohn used the coefficients of the AR models as damage sensitive features. Omenzetter and Brownjohn [107] analysed the static strain measurements recorded from a full-scale bridge using Auto-Regressive Integrated Moving Average (ARIMA) models. The strain data measured during construction phase and when the structure was in operation. Using this technique, the authors was able to identify structural changes in the structure. However, it should be noted that this method was not able to determine the nature, location, and extend of these changes. In another study, Carden and Brownjohn [108] proposed a damage indicator based on Auto-Regressive Moving Average (ARMA) models and a statistical pattern classifier. This method used the sum of squares of the residuals of the ARMA models. Based on the results, it was observed that the method was able to identify structural damages. However, as the authors mentioned, the

applications of this methods for ambient vibration measurements from structures should be investigated. As mentioned above, there are several damage identification methods using time series modeling and outlier detection to detect structural damages.

Another most common non-parametric SHM methods is Artificial Neural Networks (ANNs). A neural network consists of many layers with weight factors and a bias value. The outputs of one layer are multiplied by its weights and shifted by the layer's bias value. Then, these outputs are utilised as inputs to the next layer. During the training step, the weights and biases are modulated to minimise the error between the measured and predicted responses of the system. In the occurrence of any structural damage, the weights of the network change to compensate alterations in structural responses as a result of the damage. Generally, the application of ANNs for damage localisation and evaluation is difficult. Because, there is difficult to make relation between the changes in the weights and the location and severity of the damage using the non-uniqueness of the set of the network weights obtained for a specific type of structural damage [109]. An ANN-based technique has been proposed by Masri et al. [110, 111] to determine changes in the nonlinear dynamic behaviour of an unknown system. The method worked based on the output prediction when the responses measured from a damaged system are trained using the network to forecast the responses of an undamaged system. It should be noted that this technique is not practical for damage localisation and severity evaluation. In another study, Zang et al. [112] also proposed a technique to identify structural damage in a truss structure by combining the Independent Component Analysis (ICA) and ANN. The ICA method has been utilised to capture the necessary information from a large volume of vibration data sets measured from the structure to be trained by the ANN.

Discrete and Continuous Wavelet Analysis is also considered as one of the non-parametric method used for SHM applications. Kim and Melhem [113] carried out a comprehensive review on wavelet-based damage identification techniques. In a study conducted by Sun and

Chang [114], a statistical pattern classification method was developed based on Wavelet Packet Transform. In this study, the acceleration responses measured from a steel cantilever I-beam were used to identify damage in the beam. According to this technique, these structural responses are decomposed to wavelet packet components. Then, the dominant wavelet packet components are used as the Wavelet Packet Signature (WSP) to identify the damage in the beam. It is noteworthy that the time of the damage occurrence can be detected using the wavelet-based methods. An impulse in the wavelet decomposition plots of acceleration response data can show the damage and the time it occurs [115, 116].

2.5.3 Nonlinearity identification in structural dynamics

It is crucially important to detect structural damages at an early stage before irreversible consequences. However, despite the extensive literature summarising damage identification techniques for SHM applications over the last years, there are still some needs for further development of SHM systems, which can provide very early identification of any alterations in a dynamic system [117]. In most of the proposed damage identification techniques, civil infrastructures are assessed in their linear range and linear-based modelling method are used for dynamic analysis and condition assessment purposes. However, it should be mentioned that most of the real civil structures show nonlinear behaviour due to several reasons.

The nonlinear behaviour of a structure can be as a result of a local effect, such as friction in joints, joint and link flexibility, and nonlinear contact, or a global nonlinearity, such as geometric nonlinearities, boundary conditions, and nonlinear material behaviours. Existence of each of these nonlinearities in a system can alter its dynamic behaviour, thus the use of a linear-based approach is improper to model such dynamic systems. In such cases, a linear model is not able to model the structural system, as the basic principles of a linear system is not authentic for a nonlinear system anymore. It means that the superposition, the homogeneity and the

Maxwell reciprocity rules cannot be utilized for simulation of a nonlinear system. In addition, modal models are usually incorrect to simulate the behaviour of a nonlinear system [118].

A statistical pattern recognition paradigm is among the most effective approaches in development of SHM system. This paradigm consists of three main components, including data acquisition, feature extraction, and feature classification, which can be implemented for an automated SHM system. Several SHM feature extraction techniques are employed fitting linear models to measured system output before and after occurrence of damage. The damage indicators are then defined using any changes in these model parameters. More recently, the physic-based modelling approach was expanded to time series regression modelling, according to which the model parameters and residual errors are utilised as damage indicator [119, 120]. In addition, there are several methods proposed for identifying the presence of nonlinearities of a system in the literature [121, 122]. Some of these techniques utilized characteristics features of a nonlinear system, such as distortion of Frequency Response Function to detect the system nonlinearity. A few used the validity of principals of a linear system to identify nonlinearity in a dynamic system. However, most techniques are based on the comparison between the response of a linear system and an unknown system. Some of the researchers have suggested the use of higher order FRF's [123], while others consider spectral analysis and different Autoregressive Models, such as Nonlinear Autoregressive Moving Average with eXogenous inputs (NARMAX) models to detect the presence of nonlinearity in a dynamic system [121]. Based on the conducted literature review, it was observed that there is a need to develop an efficient approach based on vibration measurements to identify nonlinearities in a dynamic system at an early stage as an important part of an integrated SHM system.

2.6 Research gaps and contributions

A structural health monitoring system has strong potential to enhance the damage assessment process by providing information on structural performance and damage trends throughout structures, suggesting rehabilitation strategies with minimal life-cycle costs and optimal repairing timing, and distributing urgent alerts for immediate closure. It was shown in the first part of this chapter that there is a need in New Zealand to develop a SHM system and bring state-of-the-art technologies for condition assessment of civil infrastructures in this earthquake prone country. Therefore, the following research questions have been defined for this study based on the conducted literature review.

- How can asset owners enhance the accuracy and decrease the costs of structural health monitoring using state-of-the-art technologies, such as wireless sensor network?
- How can they manage large sets of measurement data and extract maximum useful information from raw measurements?
- How can they identify any change in the structural performance at its early stage to take an immediate action in emergency cases?

In answering the aforementioned questions, the main aim of this research is to develop a whole package of structural health monitoring system (SHMS) to provide owners and engineers a reliable and easy-to-use platform to monitor the integrity of civil structures. For achieving this goal, it was planned to develop an integrated vibration-based SHM system consisting of three important components, which are a new wireless smart sensor network, a new MATLAB-based data management and data analysis platform compatible with the wireless sensor system, and a new vibration-based nonlinearity identification technique for early damage identification purposes. The development of these components has been started after conducting a comprehensive literature review on each components of the system. The research gaps and the contributions of this research are summarised in the following.

Phase 1: Wireless smart sensor network development: In order to fill out the gaps found in existing wireless accelerometer sensor nodes, a new customized wireless sensor system is designed as the first component of the vibration-based SHM system. The wireless smart sensor network can record both ambient and earthquake-induced vibrations from structures using two periodic and event-triggered sampling modes. The wireless smart sensor network was designed to meet the requirements for high-quality measurements of low-amplitude ambient vibration and sudden events from civil structures. One of the main goals of the sensor design was to achieve higher performance, improve the power consumption, and lower the cost compared to the existing wireless sensor system designed for SHM applications. Also, making a great trade-off between these important features of a wireless sensor network was another goal that has been considered in hardware and software design of the wireless smart sensor network. Another goal of this development was the ability to control the hardware part of the system to be applicable for different SHM applications. The developed sensor platform consists of a high-sensitive sensing component for high-fidelity vibration measurements and a reliable event detection switch through a trigger accelerometer to detect and record sudden events. In particular, the hardware of sensor node was designed to provide high resolution and sensitivity, low noise, low power consumption, and capability to measure structural vibrations in an ultralow-power consumption mode to record sudden events. In addition, the software architecture of the smart sensor nodes was implemented to provide accurate time synchronisation and high-resolution event-triggered sensing. To test the various features of the wireless smart sensor network, a series of experimental and field tests was conducted on a small-scale steel bridge model and a full-scale in-service highway viaduct. The performance of the wireless smart sensor network was investigated in terms of sensitivity, event-triggered sampling mode, wireless communication, time synchronisation, and power consumption during these tests.

Phase 2: Development of a data management and data analysis toolbox: As mentioned in section 2.4, there is a need to design an efficient and user-friendly platform for managing and analysing large sets of SHM data to avoid the drawbacks associated with traditional file-based data management and analysis methods. Therefore, to enhance the performance of condition assessment of civil structures, it was decided to utilise MATLAB GUI Layout Toolbox environment to design a new management and analysis toolbox. The MATLAB-based toolbox includes data management and data analysis platforms, which are integrated into the wireless smart sensor network. The original feature of this toolbox is its compatibility with the developed wireless smart sensor network. The recorded data files are downloaded, managed and synchronised using the first tab of the toolbox. Then, the managed data files can be analysed using various data analysis techniques to extract useful information from raw measurements. Time-domain and frequency-domain system identification techniques have been implemented into the data analysis platform to extract modal parameters from vibration measurements. The results obtained using these techniques can be compared to each other to estimate the computational precision of dynamic characteristics of a structure. Extracting maximum useful information from raw measurements related to structural condition, avoiding human errors in processing large sets of monitoring data, and having an integrated platform for the developed sensor system are among the main goals of developing this toolbox.

Phase 3: Development of a vibration-based nonlinearity identification technique: As mentioned, there are still some requirements for further development of existing SHM systems that mostly investigate the behaviour of a structural system in its linear range. The system must identify early changes in a dynamic system prior to any significant damages. To this end, it was decided to develop a technique to identify nonlinearities in structural systems using the vibration measurements, which can be collected using the developed wireless sensor system. This technique combines vibration data sets with time series autoregressive modelling and

fuzzy clustering technique to identify the nonlinearity in a dynamic system. The technique is able to categorise the linear and nonlinear behaviours of a structure, when it is subjected to various levels of excitation source. To verify the performance of the method, a series of shaking table tests were conducted on a small-scale steel truss bridge model in the laboratory environment. The vibration data recorded using high performance accelerometers from the bridge model under different ground motions have been used for data analysis.

To sum up, the contributions of the research are pointed out as follows:

1. Development of a vibration-based Structural Health Monitoring system for condition assessment of large-scale civil infrastructures,
2. Design of a low-cost and high-performance wireless smart sensor network for measurement of ambient and earthquake-induced vibrations,
3. Development of an integrated MATLAB-based data management and data analysis toolbox compatible with the wireless smart sensor system,
4. Introducing a vibration-based nonlinearity identification technique for analysing earthquake-induced vibrations,
5. Conducting a series of shake table tests on a small-scale steel bridge model to evaluate different features of the wireless smart sensor network and accuracy of the new nonlinearity identification technique,
6. Instrumentation of one of the most important highway bridges in New Zealand, Newmarket Viaduct, with the developed wireless smart sensor system and condition assessment of this highway bridge using the ambient vibration data,
7. Vibration-based condition assessment of an in-service concrete bridge in Wellington, New Zealand, subjected to high-amplitude earthquakes.

2.7 Summary

In this chapter, a comprehensive literature review was conducted on different components of a vibration-based structural health monitoring system, including data sensing, data management and analysis, and damage identification. In the first section, the applications of structural health monitoring for full-scale bridge structures and the New Zealand's need for an advanced SHM system were investigated. In next section, the existing inspection techniques, including traditional methods and wired structural health monitoring systems, and their challenges for SHM of large-scale civil structures were provided. Following this section, the application of wireless sensor network for condition assessment of large-scale structures was investigated and the features of a wireless sensor network for SHM applications were discussed. In addition, a comparison was made on existing academic and commercial wireless smart sensor platforms developed for SHM applications. The need for management of large amount of SHM data was then presented for a reliable SHM system. In the last part of this chapter, an extensive literature review was conducted on damage identification, which is an important part of a SHM system. Parametric and non-parametric damage identification techniques and nonlinearity identification methods in structural dynamics were investigated and reviewed. At the end, the research questions were defined after the conducted literature review and the research gaps and corresponding contributions of this research were presented.

Chapter 3: Development of a Wireless Smart Sensor Network

3.1 Introduction

In this chapter, the development procedure of a high-fidelity wireless smart sensor network is presented, which was developed as a part of the integrated SHM system for condition assessment of large-scale civil structures. Three versions of the wireless accelerometer sensor board were designed to achieve a reliable and high-performance accelerometer wireless sensor board for vibration-based SHM applications. The main purpose of designing the new wireless sensor node was to lower the cost and power consumption compared to the wired sensor system and to achieve higher performance compared to existing wireless sensor system developed for SHM applications. Another important goal of the development was to control the hardware part of the system for different applications of structural health monitoring. Several experimental and field tests were conducted on small-scale and large-scale civil structures to evaluate the performance of the wireless sensor nodes in terms of sensitivity and resolution, time synchronisation, battery consumption, wireless communication, and event-triggered sampling mode, which will be presented in the following chapters.

3.2 Preliminary hardware design of the wireless smart sensor node

In the first phase of designing wireless smart sensor node for structural health monitoring applications, two versions were designed to address the needs for reliable SHM applications. The first version of wireless sensor node is a low-cost and low-power consumption sensor designed to measure high-amplitude earthquake-induced vibrations from large-scale structures. The second version of the wireless accelerometer node is a high performance and sensitive wireless accelerometer sensor node designed to record very low-amplitude ambient vibrations induced on large and stiff civil structures. The hardware of the two versions of wireless sensor nodes are presented in the following parts.

WSSN-Version 1: The hardware components and circuit design of the first version of wireless smart sensor nodes (WSSN-V1) is shown in Figure 3.1. The main components of the sensor platform are: (1) a pico-power microcontroller, (2) a XBee Radiofrequency (RF) module (3) an external memory for temporary data storage (EEPROM), (4) a Real-Time Clock (RTC), (5) a fully calibrated humidity and temperature sensor, and (6) a 3-axis digital-output accelerometer with an integrated 10-bit Analogue-to-Digital Converter (ADC).

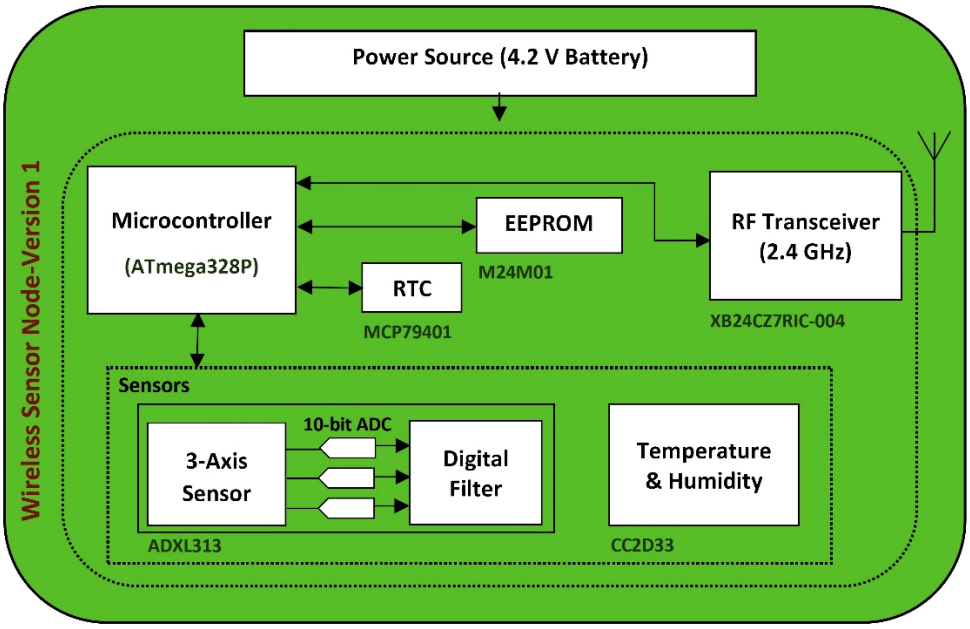

Figure 3.1. Circuit design of the first version of wireless smart sensor node.

A picoPower Atmel AVR 8-bit microcontroller, ATmega328/P [124], was selected for the sensor board design due to its low power consumption in active and sleep modes and user-selectable clock frequency ranging from 4MHz to 20MHz, which could make a great trade-off between the power consumption, performance and cost for SHM applications.

Based on the literature review, it was found that IEEE 802.15.4 is a very low power protocol for wireless sensor network and widely used for SHM applications. Therefore, XBEE S2C 802.15.4 Radiofrequency (RF) module [125] was used for wireless communication between wireless sensor nodes, which could support ZigBee and DigiMesh mesh networking protocols. The ZigBee protocol has been frequently used for WSN development for structural health

monitoring applications. The difference between the DigiMesh and ZigBee protocols is that for ZigBee topology a single coordinator is considered for the network and the router devices are always on. However, in DigiMesh topology each device is capable of routing, sleeping for power optimization and saving, and communicating via a mesh network. The advantages of DigiMesh over ZigBee are simpler setup, more flexibility to expand the network, offering better broadcasting support, and more robust mesh network. Therefore, DigiMesh topology was used in this study to simplify network setup and expand the wireless network reliability for large-scale instrumentation. According to this topology, all devices are same and no complex architecture is required to define various nodes on the network as end-nodes, routers, coordinators, border routers, which means all nodes are interchangeable and can route data [126]. This module is a low-cost and easy-to-employ module that could provide quick and seamless communication between nodes. Also, it could offer quick and robust communication in point-to-point, peer-to-peer, multipoint/star configurations, and wireless connectivity to a mesh network, which is the desired topology in this research for wireless communication between the sensor nodes. The XBee module and the configurations for DigiMesh and ZigBee wireless communication protocols are shown in Figure 3.2.

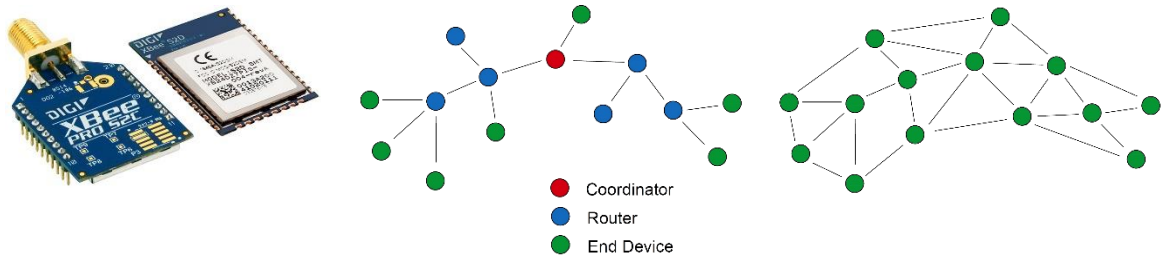

(a) **(b)** **(c)**

Figure 3.2. (a) XBee 802.15.4 RF module [125], (b) ZigBee topology, (c) DigiMesh topology.

Because the capacity of the microcontroller memory is not enough for high volume of vibration measurements, a 2-Mbit serial I^2C bus EEPROM (M24M01), from STMicroelectronics, was selected as external memory to temporarily store the recorded vibrations on board before

wireless transmission [127]. In addition, a low power I^2C Real Time Clock (MCP79401) with SRAM and protected EEPROM was used for providing time stamps for the sensor measurements [128]. It should be mentioned that although RTCs were used in the literature for the design of wireless sensor nodes to keep the sensor nodes synchronised, they cannot provide very well synchronised data sets desired for structural health monitoring applications. Therefore, in this research time synchronisation between wireless sensor nodes is provided using two pre-processing and post-processing synchronisation algorithms. The procedure of time synchronisation will be explained in detail in the following parts.

The first version of wireless sensor node has two sensing components for measuring the environmental parameters. Because the variation of environmental parameters, such as humidity and temperature, could affect the dynamic characteristics of structures and in general the accuracy of the vibration-based structural health monitoring, a fully calibrated humidity and temperature sensor (CC2d33) with low power consumption and high accuracy was selected to record temperature and humidity of the environment. The precision and accuracy of the sensor chip is ±2% RH and ±0.3 ℃ with 14-bit resolution. The most important component of the sensor board is the accelerometer chip for recording the structural vibrations. To tackle the problems associated with analogue-output accelerometers, a low power 3-axis digital-output accelerometer from Analog Devices (ADXL313) with an integrated ADC and an internal digital filter was selected to record structural vibrations from large-scale structures. This chip was selected due to its low cost and relatively high resolution, enough to collect high-amplitude vibrations induced by earthquakes. The typical noise density of the accelerometer is 150 μg/√Hz for X and Y axes and 250 μg/√Hz for Z axis, which could provide a reasonable accuracy for high-amplitude vibration measurements. This accelerometer can provide user selectable measurement range and the output resolution at each range are 10-bit resolution for ±0.5 g, 11-bit resolution for ±1 g, 12-bit resolution for ±2 g, and 13-bit resolution for ±4 g

ranges. For a data rate more than 100 Hz, the operating voltage range of the accelerometer is 2.0-3.6 V with supply current of 100-300 μA. Also, the accelerometer has a user-selectable bandwidth ranging from 6.25 to 3200 Hz. The accelerometer chip and its functional block diagram are shown in Figure 3.3.

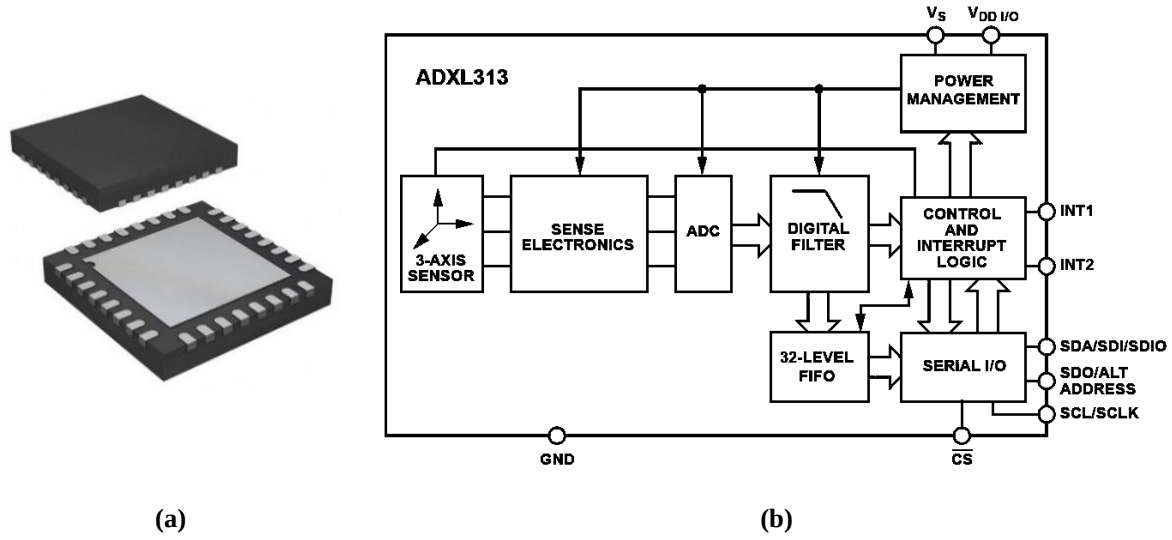

(a) **(b)**

Figure 3.3. ADXL313: (a) the sensor chip, and (b) the functional block diagram [129].

The advantages of WSSN-V1 are its low cost and low power consumption allowing to install dense array of sensors throughout large-scale structures to collect more data from different structural parts during earthquakes. It should be mentioned that the WSSN-V1 developed for earthquake-induced vibration measurements should continuously operate to be able to record the events. However, due to the fact this version of wireless sensor nodes operates with three AA industrial Alkaline Batteries and has limited lifetime, the design of the wireless sensor node needs to be modified to save the power. This modification has been done in designing the final version of wireless sensor node, which will be presented in the following sections. The top and bottom sides of the first version of the wireless sensor node with its components are depicted in Figure 3.4.

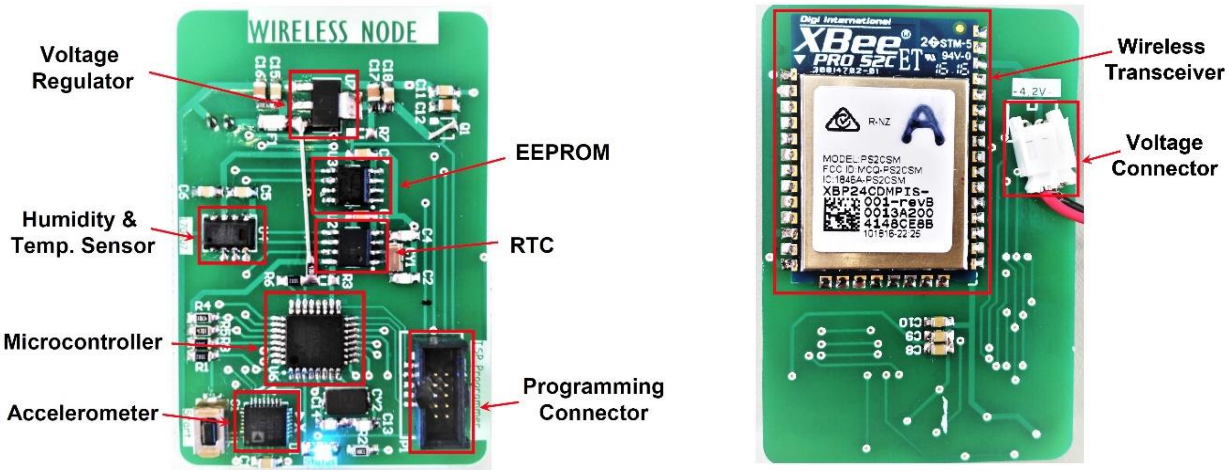

Figure 3.4. WSSN-V1: a) Top side, b) Bottom side.

In the second phase of the sensor system development, a high-performance and sensitive wireless sensor node was especially designed to record very low-amplitude ambient vibrations from large-scale civil infrastructures. The circuit design of the second version of wireless sensor node (WSSN-V2), including the components, is shown in Figure 3.5. As is obvious, most of the sensor components are same as the first version of wireless sensor node. However, in order to make the sensor node more sensitive for recording high signal-to-noise ratio (SNR) signals, some components of the previous version of the wireless accelerometer sensor board were replaced with new high-performance components. This version of wireless sensor node was set to time-triggered or periodic sampling mode, according to which the accelerometer nodes can wake up at a specific day and time and do sampling based on user-specified settings for sampling time and sampling frequency. WSSN-V2 could create large sets of vibration measurements, which need to be stored in a relatively big temporary storage memory before the wireless data transmission. To achieve this goal, a 64-Mbit (8-Mbyte) SPI external flash memory was integrated into the new board design. The architecture of this chip features a Page Programming Buffer that allows up to 256-bytes to be programmed in one operation, therefore it was selected as the temporal storage for the measurements. This low-power flash memory

offers flexibility and performance well beyond ordinary serial flash devices for systems with limited space, power and signal conections [130].

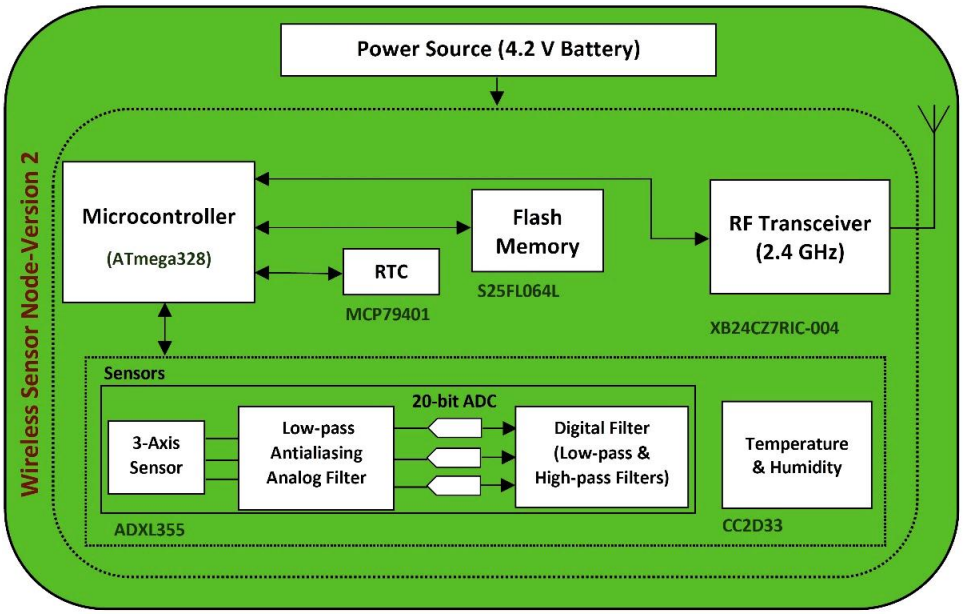

Figure 3.5. Circuit design of the second version of wireless smart sensor node.

In addition to the memory chip, the ADXL313 accelerometer was replaced by a very low-noise density and low-offset drift sensing component due to the fact that the ambient vibrations induced by wind, traffic and ambient factors throughout structures are low amplitude. The highly sensitive and low-power 3-axis digital-output accelerometer with selectable measurement range from Analog Devices, ADXL355, was selected to satisfy the requirements for ambient vibration measurement from very large and stiff civil structures. This sensing component can offer minimal offset drift over temperature and long-term stability enabling precision applications with minimal calibration. The functional block diagram of this accelerometer is shown in Figure 3.6.

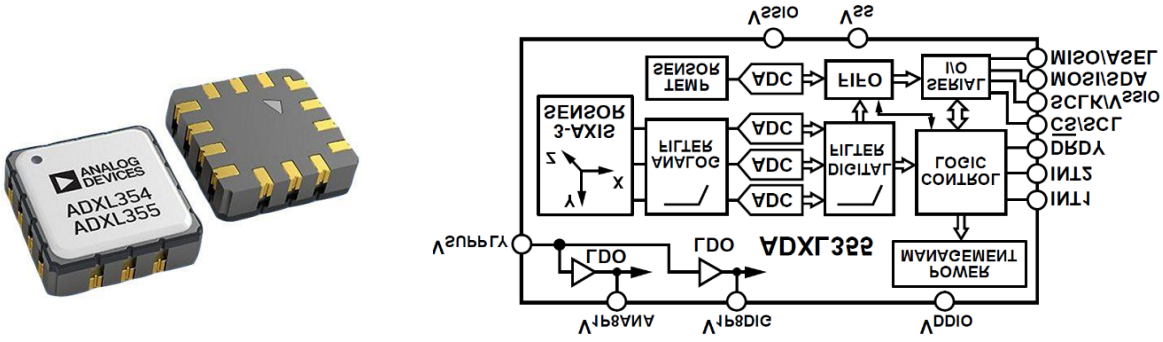

(a) **(b)**

Figure 3.6. ADXL355: (a) the sensor chip, and (b) the functional block diagram [131].

This accelerometer can support ±2.048 g, ±4.096 g, and ±8.192 g ranges with minimal offset drift over temperature and long-term stability enabling precision applications with minimal calibration. The accelerometer sensitivity is 256000 LSB/g, 18000 LSB/g and 64000 LSB/g for X-axis, Y-axis, and Z-axis, respectively. This low power chip has an ultralow noise density of 25 µg/√Hz in all axes ideal for very high-resolution vibration measurements. The operating voltage supply is 2.25-3.6 V with supply current of 300 µA in measurement mode and 21 µA in standby mode. As is obvious in block diagram of the ADXL355, it uses an analogue, low-pass, antialiasing filter with a fixed bandwidth of approximately 1.5 kHz to reduce out of the band noise to limit bandwidth for a high-resolution signal. In addition, it provides an internal 20-bit ADC to digitize the filtered analogue signal. An additional digital filtering (beyond the antialiasing filter), including a low-pass digital filter and a high-pass digital filter, presents excellent noise performance at different bandwidths. This filtering option includes low-pass digital decimation filter and a bypassable high-pass filter that provide output data rates between 3.9 Hz to 4 kHz. The top and bottom sides of the second version of the sensor node are depicted in Figure 3.7.

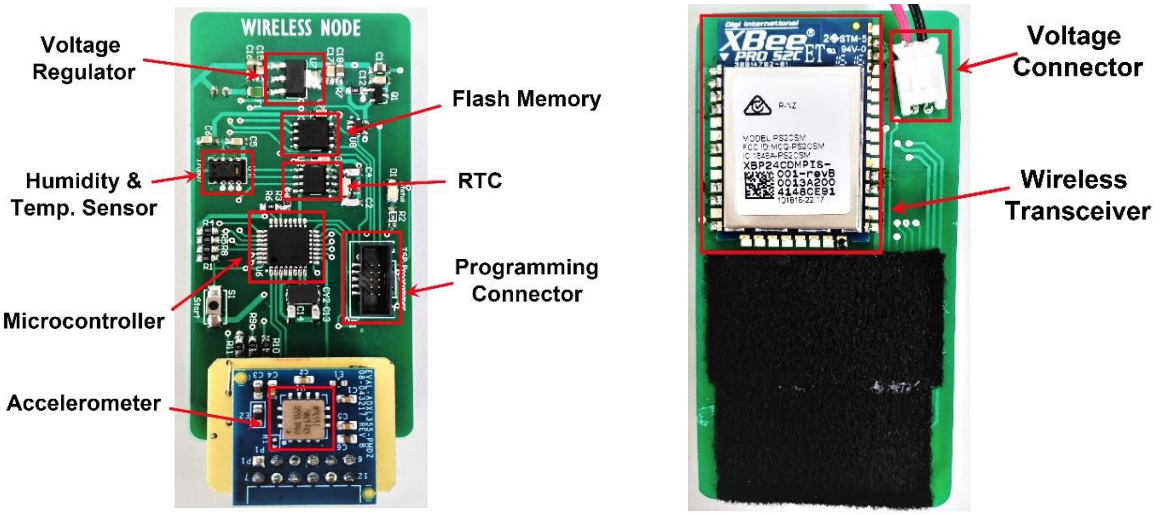

Figure 3.7 WSSN-V2: a) Top side, b) Bottom side.

3.3 Preliminary ambient vibration tests on full-scale structures

Some field tests were carried out in order to show the performance of two versions of wireless smart sensor nodes to measure vibration from large-scale structures. To this end, several experimental setups were performed on a footbridge and two office buildings using the two developed versions of wireless sensor nodes (WSSN-V1 and WSSN-V2) and an expensive wired accelerometer as the reference system. The first setup was performed on a footbridge located in Auckland, called Wellesley footbridge, and in another setup, the WS Building and WG Buildings of Auckland University of Technology (AUT) were instrumented using the sensors to show the sensitivity and resolution of WSSN-V1 and WSSN-V2 for measuring vibration from large-scale civil infrastructures. The wireless sensor nodes attached with their battery packs and the gateway node are shown in Figure 3.8. Also, the wired sensor system used for the tests are depicted in Figure 3.9.

The wired sensor system includes National Instrument CDAQ-9184 [132] with 4 SLOT Ethernet CompactDAQ Chassis as analogue-to-digital converter, a CompactDAQ Chassis attached to ADC chip to control data transmission, timing and synchronisation, and high-

performance one-axis analogue-output accelerometer from Crossbow GP Series [133]. It should be mentioned that the total costs of the wired sensor system, including the sensing device, acquisition system and cables for data transmission, is around 4,000 NZD for one channel of accelerometer, while the costs of the wireless sensor system, including the sensing devices, acquisition and transmission systems, and manufacturing costs are around 170 NZD and 250 NZD for WSSN-V1 and WSSN-V2, respectively.

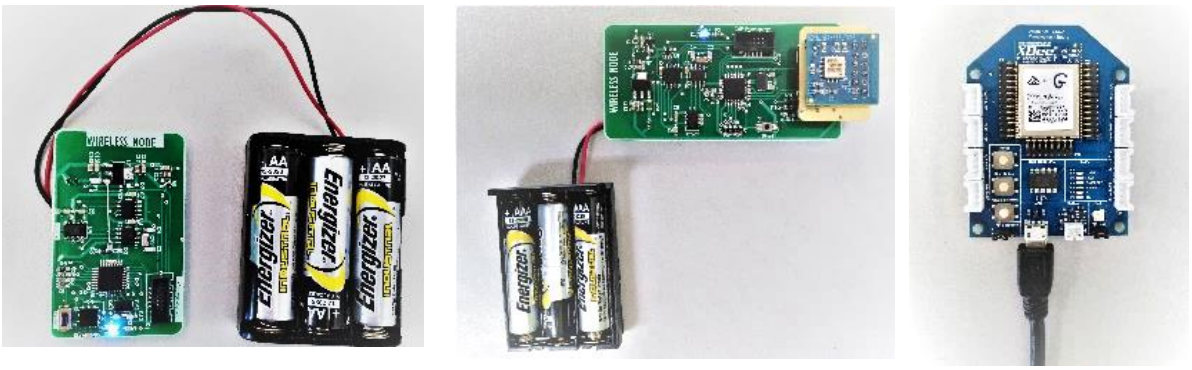

(a) **(b)** **(c)**

Figure 3.8. (a) WSSN-V1 with battery pack, (b) WSSN-V2 with battery pack, (c) gateway node.

(a) **(b)** **(c)**

Figure 3.9. a) National Instrument DAQ system, b) GP Series wired accelerometer, c) wired sensor system.

3.3.1 Vibration testing on a footbridge

The first field setup was performed on the Wellesley footbridge. The test was carried out on the main span of the bridge with the length of 15.0 m. During the test, WSSN-V1, WSSN-V2 and the wired accelerometer were installed on the mid-span of the bridge to measure the ambient vibrations induced by traffic in vertical direction. In another setup, free vibration test

was carried out by jumping on bridge in several intervals to compare the acceleration amplitudes and free vibration structural response recorded by the wired and wireless sensors. Figure 3.10 depicts the footbridge and the test setup during the ambient vibration test.

(a) **(b)**

Figure 3.10. (a) Wellesley footbridge, and (b) test setup for the bridge test.

After preliminary data manipulation and trend removal, the Power Spectral Density (PSD) values of vertical acceleration data recorded on the bridge by wired sensor system, WSSN-V1 and WSSN-V2 are shown in Figures 3.11 and 3.12 for ambient and free vibration tests, respectively. As is clear from the figures, in both vibration tests the wireless sensor nodes could measure the first two structural peaks with magnitudes of around 3.2 Hz and 7.2 Hz similar to the reference wired accelerometer. Another noteworthy result is that the natural frequencies obtained by wireless nodes are quite constant in both ambient and free vibration tests indicating their performance to measure structural modal parameters due to different excitation sources.

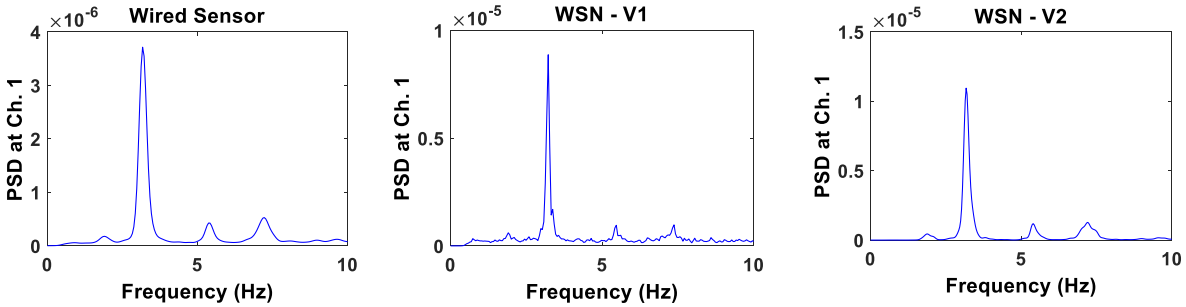

f_{s1} = 3.174 Hz **f_{s1} = 3.223 Hz** **f_{s1} = 3.174 Hz**

f_{s2} = 7.227 Hz **f_{s2} = 7.373 Hz** **f_{s2} = 7.202 Hz**

Figure 3.11. PSD values of vertical acceleration recorded on the bridge during ambient vibration test.

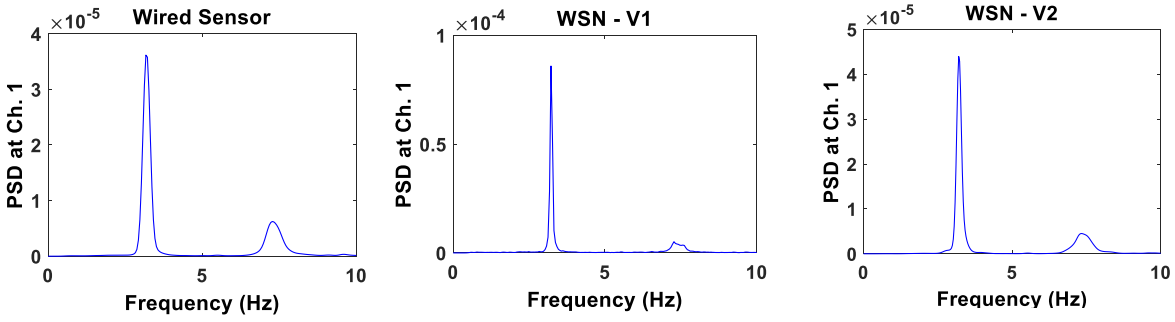

f_{s1} = 3.174 Hz f_{s2} = 7.275 Hz

f_{s1} = 3.223 Hz f_{s2} = 7.275 Hz

f_{s1} = 3.204 Hz f_{s2} = 7.324 Hz

Figure 3.12. PSD values of vertical acceleration recorded on the bridge during free vibration test.

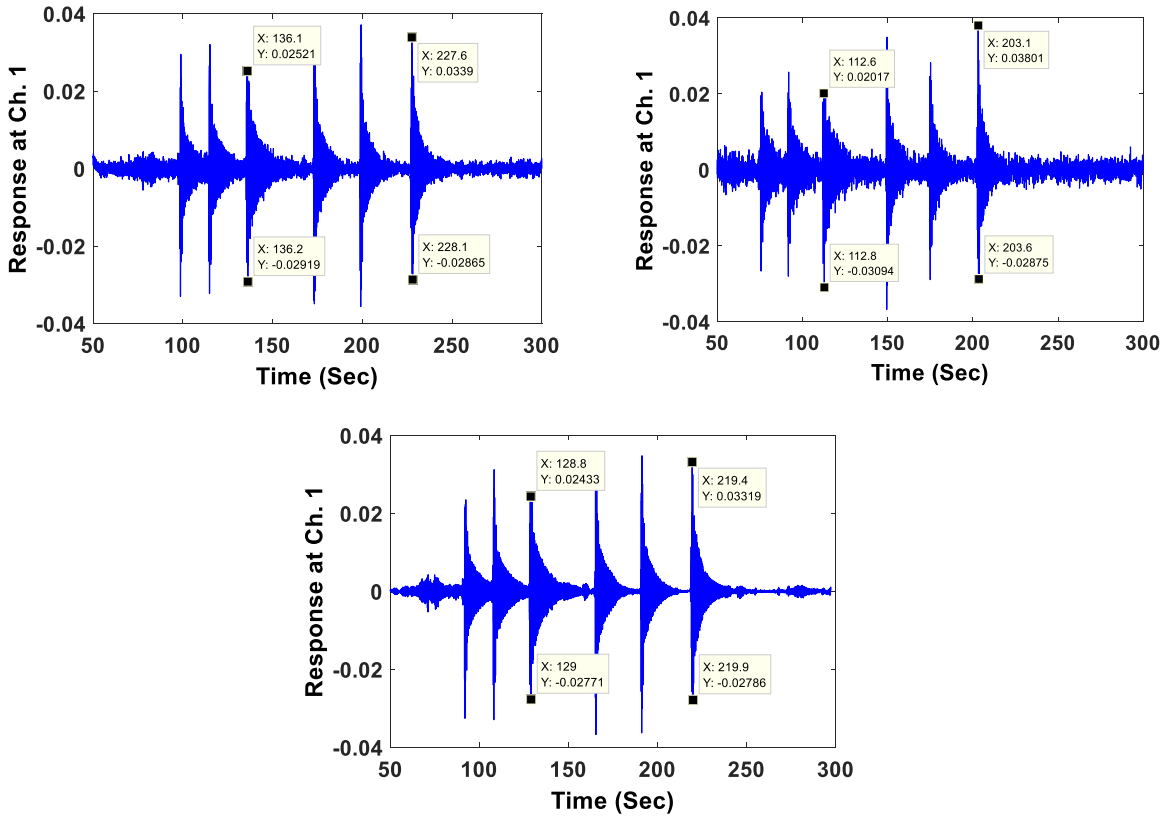

Figure 3.13. Vertical time-series acceleration recorded on the bridge during free vibration test.

Figure 3.13 shows acceleration time histories recorded from the bridge by three sensor systems during free vibration test. The acceleration amplitudes for three jumps are demonstrated in the figures to compare the amplitudes recorded by the reference system and wireless sensor nodes. As is obvious, the acceleration amplitudes recorded in this setup using the wired and wireless sensor systems are very comparable showing the performance of the wireless sensor nodes for

structural vibration measurement. Moreover, the free vibration structural responses recorded on the bridge due to the first jump are zoomed and depicted in Figure 3.14. The results show that the second version of wireless sensor nodes can provide very high Signal-to-Noise (SNR) ratio, hence resulting in high resolution for recording low-amplitude ambient vibration signals compared to the reference wired accelerometer.

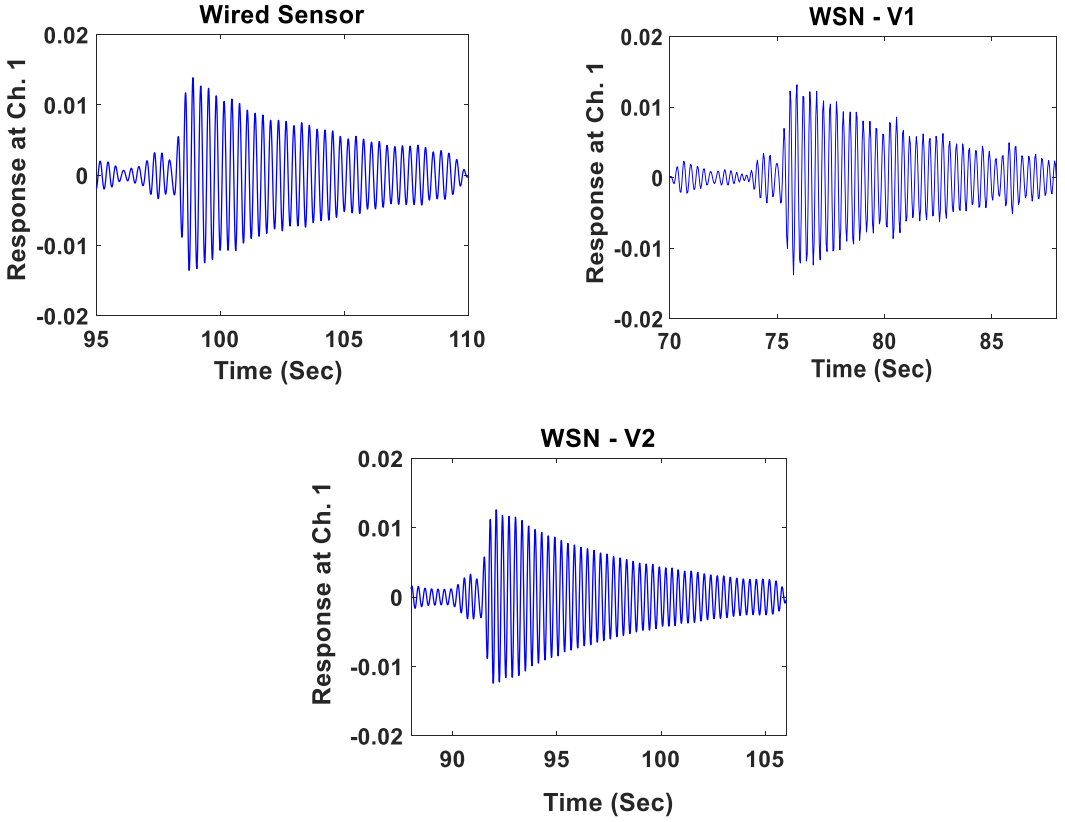

Figure 3.14. Free vibration structural response recorded due to the first jump on the bridge.

3.3.2 Vibration testing on two office buildings

For this setup, the 12-storey WG Building as a high-rise building and the 6-storey WS Building as a stiffer building were considered as target structures. In the first setup, three sensor systems were installed on floor 11 of the WG Building between 12:00-13:00 PM, the time with peak operational uses of the building and traffic on the street. The acceleration time-histories recorded during this test using the three accelerometer sensors are shown in Figure 3.15.

Figure 3.15. Longitudinal acceleration time histories recorded from floor 11 of the WG Building.

Table 3.1. Natural frequencies of the WG building obtained using various SI techniques.

Sensors	*PP*	*FDD*	*EFDD*	*SSI*
Wired	1.75	1.75	1.75	1.76
WSSN-V1	---	---	---	---
WSSN-V2	1.70	1.70	1.70	1.70

As is clear from the acceleration time histories recorded, the noise level of WSSN-V2 is very small in comparison to the WSSN-V1 and the high-performance wired accelerometer. Also, the noise level of WSSN-V1 is similar to the wired accelerometer sensor. The vibration datasets were analysed using different time-domain and frequency-domain system identification techniques, including pick peaking (PP), Frequency Domain Decomposition (FDD), Enhanced Frequency Domain Decomposition (EFDD), and Stochastic Subspace Identification (SSI). Table 3.1 presents the first longitudinal natural frequency of the WG Building. As is clear from the results, the wired accelerometer sensor and the second version of wireless smart sensor node could measure the first longitudinal structural mode with a magnitude of 1.75 Hz and 1.70 Hz, respectively. In addition, the first version of wireless sensor node (WSSN-V1) could not precisely measure the structural peak from the recorded vibration data. In the second setup, floor 6 of the WS building was also instrumented using the wired and wireless sensor systems. The acceleration time histories measured from WS building using the wireless and wired accelerometer sensors are shown in Figure 3.16.

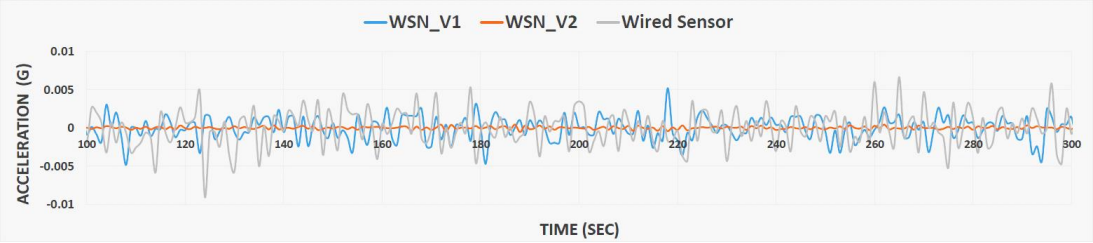

Figure 3.16. Transverse acceleration time histories recorded from floor 6 of the WS Building.

Table 3.2. Natural frequencies of the WS building obtained using various SI techniques.

Sensors	*PP*	*FDD*	*EFDD*	*SSI*
Wired	2.53	2.53	2.53	---
WSSN-V1	---	---	---	---
WSSN-V2	2.44	2.44	2.44	2.43

It is clear that the vibration data recorded using WSSN-V2 has a higher signal-to-noise ratio compared to the WSSN-V1 and the wired accelerometer sensor. Table 3.2 presents the first longitudinal natural frequency of the WS Building using the wireless and wired sensor systems. As is clear from the table, the wired accelerometer sensor was able to measure a structural peak of 2.53 Hz as the first longitudinal natural frequency using the frequency-domain SI techniques. WSSN-V2 also measured the first longitudinal natural frequency of the WS Building with a magnitude of 2.44 Hz. The results showed that the WSSN-V1 could not capture the first longitudinal structural peak of the WS building. It should be mentioned that the small variations between natural frequency values measured using wired and wireless accelerometer sensors from the buildings can be attributed to mathematical errors and different levels of measurement noises in the acceleration time-histories. In overall, the results of these tests show the high sensitivity of second version of wireless smart sensor node in measuring low-amplitude ambient vibrations from large-scale structures.

In order to show the accuracy and consistency of the results obtained, another vibration data set were recorded using WSSN-V1 and WSSN-V2 from the buildings at a different time interval to measure the ambient vibrations induced by wind loading. To this end, the buildings were tested by WSSN-V1 and WSSN-V2 between 22:00-23:00 PM on Saturday night when the operational activities in the buildings were minimum (no people in the building and traffic on the nearby street) and the level of wind loading was relatively high. The ambient vibration data measured using the two versions of wireless smart sensor nodes was analysed using the time-domain and frequency-domain system identification techniques. The results obtained for the first longitudinal natural frequency of the two buildings are presented in Table 3.3.

Table 3.3. Natural frequencies of the two buildings obtained from various SI techniques.

Structure	**WSSN-V1**				**WSSN-V2**			
	PP	***FDD***	***EFDD***	***SSI***	***PP***	***FDD***	***EFDD***	***SSI***
WG Building	---	---	---	---	1.70	1.70	1.70	1.70
WS Building	---	2.53	2.53	---	2.56	2.56	2.56	2.56

As is obvious from the analysis results, the first version of wireless sensor node was not able to precisely measure the first longitudinal natural frequency of the WG and WS buildings using the employed SI techniques. However, the WSSN-V2 was able to accurately capture the first longitudinal structural peak using both time-domain and frequency-domain SI techniques. It should be mentioned that the small variation in natural frequency values measured during both tests can be attributed to mathematical errors or different measurement noises. In total, the results obtained from the preliminary ambient vibration tests showed that the second version of the wireless sensor node is highly sensitive and precise to measure low-amplitude structural vibrations and its accuracy and resolution is comparable with the expensive high-performance wired accelerometer sensor.

3.4 Final hardware design of the wireless smart sensor node

After testing the performance of the wireless sensor nodes in terms of resolution and sensitivity for vibration measurement, the third version of wireless sensor node is designed and developed. This version of wireless accelerometer sensor node has the capability to record both ambient and earthquake-induced vibrations using time-triggered and event-triggered sampling modes. In another word, the features of the first two developed wireless smart sensor nodes were combined into a new wireless sensor board to make a new versatile wireless accelerometer node for vibration-based SHM applications.

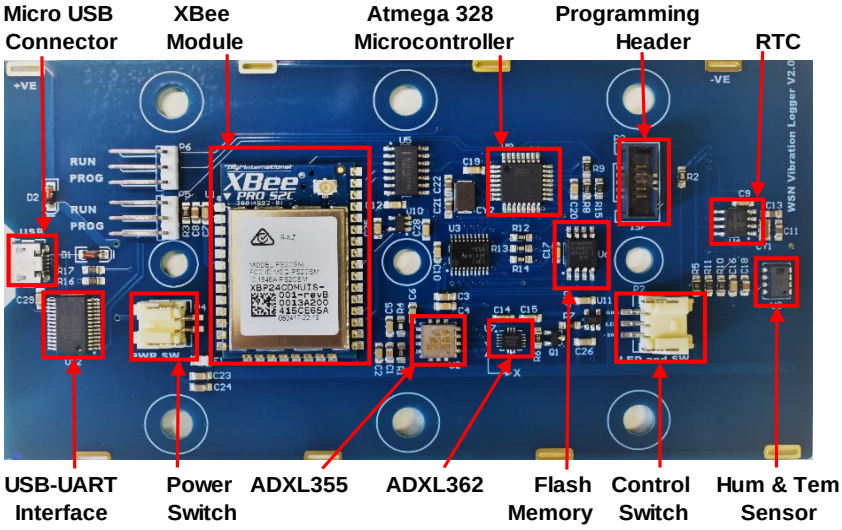

(a)

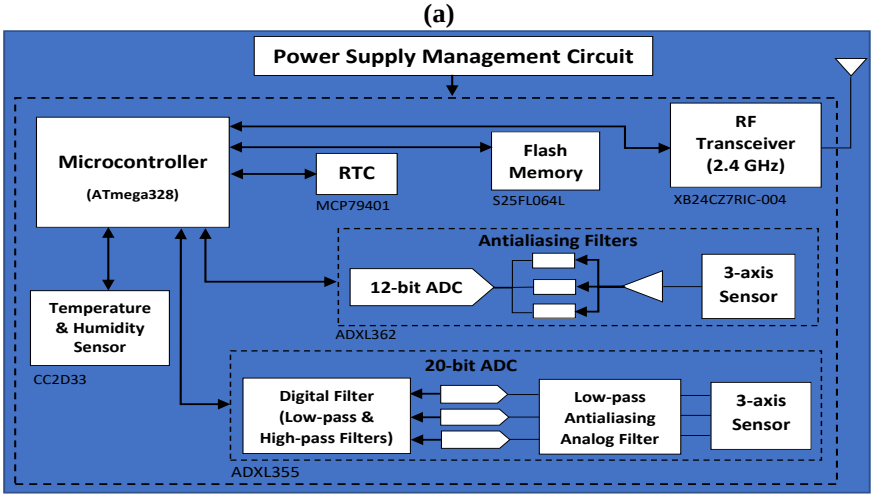

(b)

Figure 3.17. PCB design of the high-performance accelerometer sensor board: (a) top side, and (b) schematic design of the sensor board.

The first purpose of this development was to decrease the cost and power consumption of the sensor boards for instrumentation of large-scale structures by having all the features on a single board and the second purpose was to implement a power efficient event-triggered sampling mode for reliable earthquake-induced vibration measurements. The PCB and schematic design of the third version of wireless sensor node (WSSN-V3) with its components are shown in Figure 3.17. As is obvious from the WSSN-V3 design, most of the sensor board components are similar to the components used for the design of WSSN-V2. The only component that was added to the board design was a MEMS accelerometer for sudden event detection and sampling of earthquake-induced vibrations from structures. As mentioned, for a comprehensive vibration-based structural health monitoring application, it is crucially important to collect and analyse the vibrations induced by sudden events in addition to the ordinary low-amplitude ambient vibrations. However, there are some major challenges for the use of wireless sensor system for condition assessment of civil structures subjected to sudden events. The first challenge is the need of continuous operation of the sensor platform to record any events, which could deplete the power source of the sensor quickly like the first version of the developed wireless sensor node. The second challenge is that the event should be sampled with a high-resolution sensing component for an accurate estimation of structural condition after the event. In addition, it is important to preserve the important part of the data induced by the event for analysis, so the data induced at the incidence of the event should not be lost.

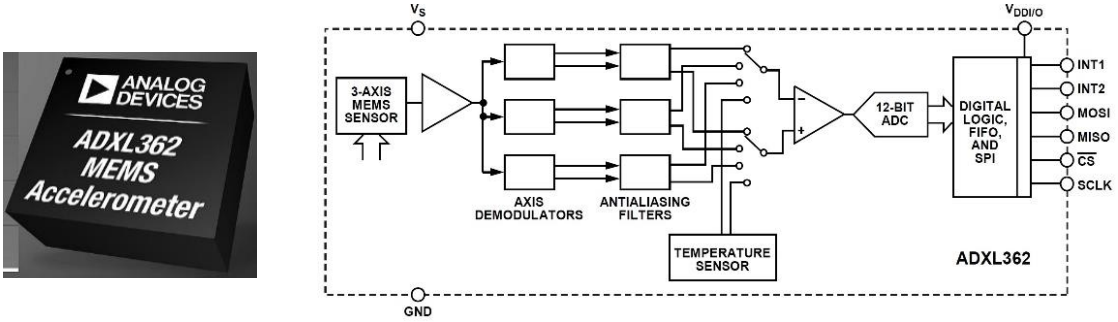

(a) **(b)**

Figure 3.18. ADXL362: (a) sensor chip, and (b) the functional block diagrams [134].

To achieve these goals, a micro power digital-output MEMS accelerometer from Analog Device [134], ADXL362, with a large First In, First Out (FIFO) buffer was selected as triggering element for the sensor board. The ADXL362 and its functional block diagram are shown in Figure 3.18. This digital-output accelerometer provides 12-bit output resolution; measurement range of ±2 g, ±4 g, and ±8 g, and sampling rate up to 400 Hz. It consumes only 13 μA in ultralow-noise mode and 0.27 μA in motion triggered wake-up mode at 3.3 V. This ultra-low power accelerometer can run continuously without drastically effecting the battery life of the sensor node. In addition, it has built-in logic to detect activities once the level of acceleration is above a user-defined threshold. Another feature of the ADXL362 is a deep 512-sample FIFO buffer. This large size buffer allows the accelerometer to record and store up all data leading up to an activity detection event for more than 13 seconds, which is this case, the important part of the event-triggered signal, can be preserved. Due to the specifications of the ADXL362, it was selected as the trigger component to wake up the whole sensor board in the presence of any events. The ADXL362 accelerometer was configured to continuously record accelerations on each axis. When acceleration above a predefined threshold level is detected, the ADXL362 activates an interrupt pin. The interrupt pin is tied directly to the microcontroller, so that when an acceleration event occurs the microcontroller comes out of sleep mode and powers on the high-performance ADXL355 to record a high-quality signal of the event. As soon as the ADXL362 has been configured, the acceleration data starts being logged into the flash memory, hence the event-triggered vibration signal can be captured. The recorded vibration signal is stored into the flash memory until next periodic sampling time when the gateway node sends the wake-up commands to the sensor nodes. Following this command and after the first periodic sampling, the event-triggered vibration signals are transferred to the base station. The final version of wireless sensor node enclosed with a customised weatherproof enclosure and the battery pack is shown in Figure 3.19.

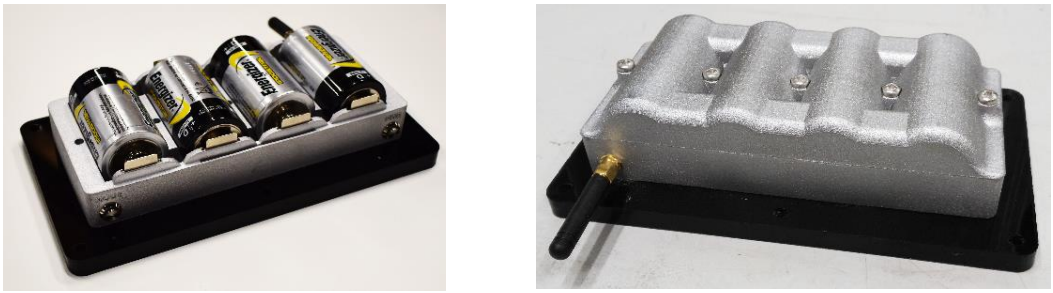

Figure 3.19. The WSSN-V3 enclosed with a customised enclosure and the battery pack.

Table 3.4. Power consumption of the components of WSSN-V3 in various operational states at 3.3 V.

Components	**Sleep mode (μA)**	**Full operation (mA)**
8-bit Processor @ 1MHz	0.1	0.2
XBee RF module	< 1	28 (receiving)
		33 (transmitting)
Flash memory	-	10 (reading)
		40 (writing)
Real-Time Clock	< 0.2	1.2×10^{-3}
Humidity & Temperature	-	0.75
ADXL355	-	0.2
ADXL362	0.01	0.013
Total Power consumption	*~3-4*	*~40*

As mentioned, the main goal of the WSSN-V3 development was to make a trade-off between the cost, power consumption, performance and sensitivity for structural health monitoring applications. Table 3.4 shows the power consumption of the sensor node components in sleep mode and full operational modes. The total power consumption of the wireless sensor node in sleep mode is between 3 to 4 μA. As is clear from the table, the AXDL355 accelerometer, temperature and humidity sensor, and the flash memory are completely powered off in sleep mode and their current is zero. It should be mentioned that the 2 to 3 μA of the power consumption comes from other components on the sensor board, such as voltage regulators. In full operation mode, the power consumption of the WSSN-V3 is close to 40 mA that is considered low power for a WSSN-based structural health monitoring system.

As shown in Figure 3.19, four D-Cell batteries with 12,000 mAh capacity power up the final version of the wireless sensor nodes that could provide a supply of 6.0 V at a full charge. If each sensor node uses 90% capacity of its power source before it is discharged below a certain voltage required by the node, the sensor node can continuously record at a service life of about 200 hours or 8 days. However, using the time-triggered sampling mode, the service life of a wireless sensor node increases to 400 days or more than one year for a sampling time of 30 min per day at frequency of 62.5 Hz. However, it should be mentioned the lifetime of a wireless sensor node decreases once it operates in the wireless network with other sensor nodes to communicate and transfer the recorded data to the base station unit. Therefore, the precise lifetime of the wireless sensor node depends on the settings of the network.

Table 3.5. Unit price of the components and total costs of the three versions of the wireless sensor nodes.

Components	**Manufacturer**	**Unit Price (NZD)**
8-bit Processor	Atmel Inc.	5
XBee RF module	Digi International Inc.	25
Real-Time Clock	Microchip Inc.	3
EEPROM	STMicro. Inc.	5
Humidity & Temperature	Amphenol Inc.	8
Accelerometer ADXL313	Analog Devices Inc.	10
PCB and other components	-	100
Total cost of WSSN-V1:		**~ 170 NZ$**
Accelerometer ADXL355	Analog Devices Inc.	70
Flash memory	Cypress Inc.	5
Total cost of WSSN-V2:		**~ 250 NZ$**
Accelerometer ADXL362	Analog Devices Inc.	19
Total cost of WSSN-V3:		**~ 270 NZ$**

The specifications of the components used for the design of the three versions of wireless smart sensor nodes including their manufacturer name and unit price are given in Table 3.5. It should be noted that the total cost of the sensor boards includes costs related to the sensor components and the sensor enclosure. As is clear from the table, the cost of the WSSN-V3 is a bit higher that the first two versions of wireless sensor nodes. However, the final version of wireless accelerometer sensor can be considered as a versatile sensing system to record any types of vibration from large-scale structures, which can save the costs for large-scale instrumentations.

3.5 Wireless sensor board comparison

As mentioned, most of the developed wireless smart sensor nodes were developed using analogue-output MEMS accelerometers. Such designs require expensive analogue circuit components. While, digital sensing architectures simplify design integration and eliminate analogue noise challenges. To show the high performance of the MEMS accelerometer used for the wireless senor node design, its specifications are compared with some of the high-performance digital-output wireless sensor node recently developed for SHM applications.

Table 3.6. Specifications of digital-output accelerometers used for SHM application.

Specifications	**Nagayama [50] (2007)**	**Bocca [57] (2011)**	**Zhu [135] (2018)**	**Navabian [136] (2018)**
Accelerometer	LIS3L02DQ	LIS3LV02DQ	M-A351	ADXL355
Noise Density ($\mu g.Hz^{-0.5}$)	103	103	0.5	25
Range (g)	± 2.0	± 2.0	± 5.0	± 2.048
Bandwidth (Hz)	0-640	0-640	0-100	0-1000
(ADC) (bit)	16	12	24	20
Power Consumption (Active mode) (mA)	1	0.65	20	0.2
Power Consumption (Sleep mode) (μA)	15	1	50	21

Table 3.6 shows the specifications of three recent developed digital-output wireless sensor nodes and the new developed wireless smart sensor node. As is obvious from the table, the sensitivity and noise density of ADXL355 used for wireless smart sensor development in this research is better than LIS3L02DQ and LIS3LV02DQ used by Nagayame [137] and Bocca [57], respectively. In terms of power consumption, ADXL355 performs better in measurement mode than these two MEMS accelerometers. The power consumption of ADXL355 in sleep mode is higher than these two accelerometers, however based on the sensor board design, the main components of wireless smart sensor node do not consume power in sleep mode. In addition, although the overall performance of M-A351 used by Zhu [135] in terms of noise density and resolution is better than ADXL355, this accelerometer requires high power in active mode that is a drawback for SHM applications. It can be concluded that ADXL355 is a good choice for development of wireless smart sensor node in this study, as it can provide a great trade-off between resolution and power consumption.

Table 3.7. Comparison between various commercial wireless accelerometer sensors.

Wireless sensors	Cost (NZD)	Weight (g)	Dimension (mm)
Sensquake Larze [138]	3816	850	120×80×80
Monnit ALTA [139]	1258	105	94×58.84×35
AX-3D BeanAir [140]	1012	220	65×59×35
SenSpot [141]	N/A	120	50×50×34
V-Mon 4000 [142]	N/A	250	117×66×40
WSSN-V1	170	100	60×38×10
WSSN-V2	250	100	78×38×10
WSSN-V3	710 (Sale price)	950	165×70×35

Table 3.7 also presents a comparison between the final version of wireless smart sensor node (WSSN-V3) and some of the commercial wireless accelerometer sensors in terms of cost, weight, and dimension. Sensquake Larze [138] is a highly sensitive triaxial MEMS

accelerometer and velocimeter with noise density of 5 μg.Hz$^{-0.5}$ at 10 Hz, an adjustable sampling frequency of 15 Hz to 3 kHz, and measurement range of ±2 g and ±6 g for ambient vibration tests and monitoring. Monnit ALTA [139] is a high-performance triaxial vibration meter to measure acceleration, velocity, displacement, and peak acceleration for vibration monitoring and building and bridge seismic activity monitoring. In addition, AX-3D BeanAir [140] is an ultra-low WIFI vibration sensor with built-in data logger. This wireless vibration sensor has a 24-bit delta-sigma ADC and a high-performance MEMS accelerometer with noise density of 45 μg.Hz$^{-0.5}$ at ±2 g. SenSpot [141] is a triaxial wireless vibration/accelerometer sensor designed for a scalable structural health monitoring. This high sensitive wireless accelerometer has measurement range of ±2 g, noise density of 25 μg.Hz$^{-0.5}$, and high accuracy of 1 mg resolution. V-Mon 4000 [142] is another high-performance wireless vibration sensor with measurement range of ±2 g to ±16 g, sampling rate up to 10 kHz, and resolution of 1 mg at ±2 g. As is obvious, the sale price of the final version of wireless sensor node is comparable with the commercial wireless accelerometer sensors. The sale price of the wireless smart sensor node includes the components, manufacturing, and labour costs. Therefore, it can prove that the hardware architecture considered for the final version of wireless accelerometer sensor meets the requirements for a low-cost wireless smart sensor node. In addition, this comparison shows that the weight and dimension of the WSSN-V3 can be modified and improved to be comparable with the existing wireless accelerometer sensor nodes in the market. It is noteworthy that the dimension and weight of the first and second versions of wireless smart sensor nodes do not include the sensor enclosure.

In overall, the comparison results presented in this part of the thesis show that there is a great trade-off between different features of the wireless smart sensor node, such as resolution and sensitivity, cost, and power consumption, that was one of the main goals of the sensor board development in this study.

3.6 Time synchronisation protocol

As mentioned, time synchronisation between the sensor nodes is crucially important for an accurate vibration-based damage identification in large-scale civil structures. In the developed wireless sensor network, two techniques have been implemented to provide an accurate time synchronisation between the wireless sensor nodes. The first technique is pre-processing technique with the use of a synch pulse coming from the gateway node that can wake up the whole sensor nodes at the same time. According to this technique, the wireless sensor nodes do not need to use their internal Real Time Clock (RTC) for time synchronisation. This pulse helps the wireless sensor network to start logging at a same time for each periodic recording. Therefore, time synchronisation before each periodic sampling could solve the time synchronisation error for long-term structural health monitoring. The second technique that is considered in the development of the wireless sensor system is a post-processing time synchronisation method. Based on the ADXL355 feature, the accelerometer should sample 100 samples at a frequency rate of 65 Hz resulting in 1.35 S of sampling. However, the idle sampling time of each accelerometer varies due to the fluctuations of their internal clocks. As shown in Eq. (3.1), the difference between the idle sampling time (T_{idle}) and the actual sampling time (T_{actual}) is considered as the time offset of each accelerometer chip (T_{offset}).

$$T_{offset} = T_{idle} - T_{actual} \tag{3.1}$$

The time offset is calculated using on board analysis and the value is shown on the header of each data files in text format. This time offset is used to calculate the compensated time for providing an accurate time synchronisation between various wireless sensor nodes. The compensated time (T_{com}) for each sensor board is different and calculated using Eq. (3.2):

$$T_{com} = \left(\frac{n_s}{f_s} \right) \times \left(1 + \frac{T_{offset}}{100} \right) \tag{3.2}$$

where n_s and f_s are the number of samples and sampling frequency, respectively. After calculating the time offset values for each sensor board, they will be used to calculate a new time series data. This process of synchronisation is performed using the data management platform developed in MATLAB to provide a synchronised data files for data analysis.

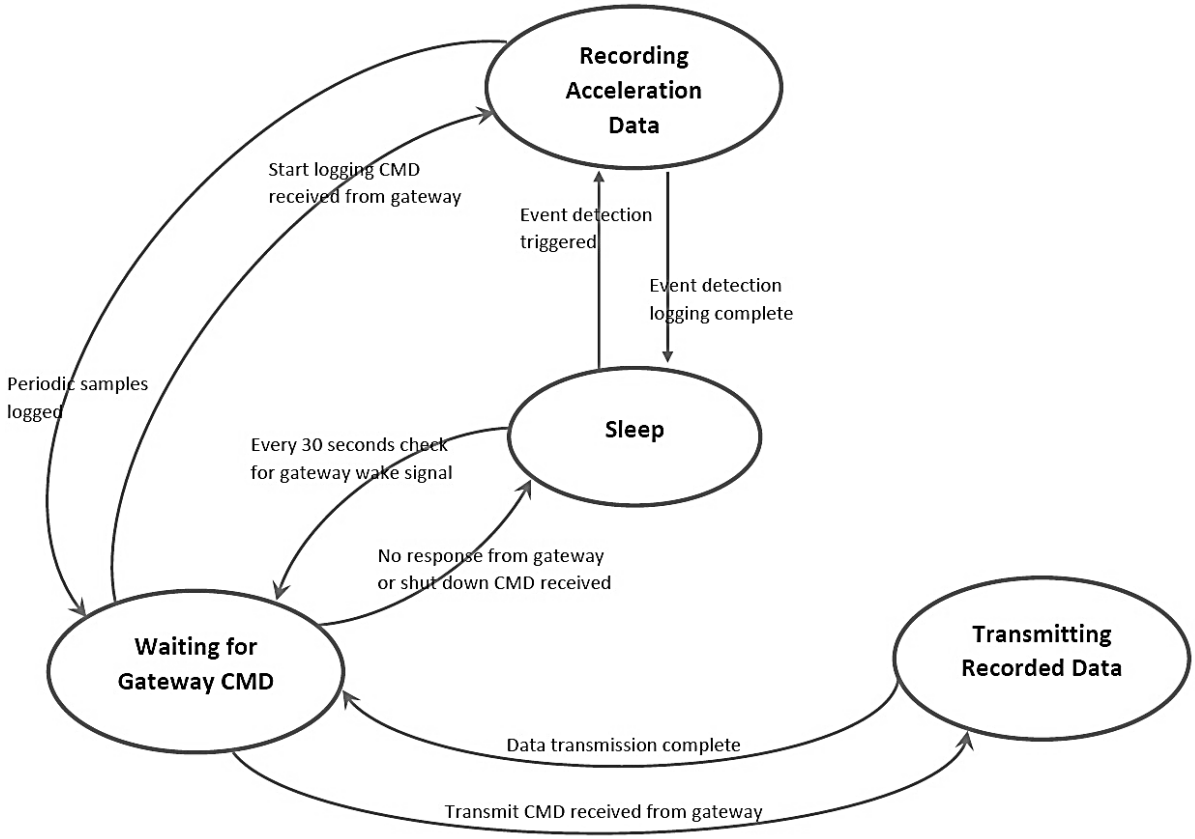

Figure 3.20. Main state machine of the wireless smart sensor network.

3.7 Software architecture of the wireless sensor network

In this part of the paper, the software architecture and configuration of the developed wireless smart sensor network will be presented. It includes the workflow and configuration of sensors on how to wake up, start sampling and transfer the measurements to the base station unit. The workflow of the wireless sensor network is presented in Figure 3.20 and explained in detail in this section. It includes four main states; Sleep state, Waiting for gateway commands state, Recording state, and Transmission state. Each of these states and their relationships will be explained in detail in the following.

1. Sleep mode: After turning on the physical switch of a sensor node, it will go to sleep or low-power shutdown mode and wait to receive a command from the gateway node. The sensor will check for gateway wake signal every 30 seconds to start the sampling. If it does not receive responses from the gateway, it will go back to sleep mode. The node will only exit the sleep mode if either of the following conditions are met: 1) the RTC interrupt occurs, which could occur periodically every 30 seconds, and 2) event detection is enabled and an event exceeds the trigger threshold. In first case, if the RTC interrupt occurs, the state will change to the "waiting for gateway CMD" state and a time out value of 500 ms will be set. In the case of occurrence of an event like an earthquake, the state will change to "Recording acceleration data" state and a time out value of 70 seconds.

2. Waiting for gateway Commands (CMD): In this state, the node handles the incoming commands and responses from the gateway. A node can receive seven different CMDs from the gateway node as follows:

- Wake-up CMD: this command is periodically sent based on the user's configuration of the gateway settings. When the Wake-up CMD is received, the node will read the on-board data, such as time, temperature, humidity and battery percentage and then store this information in the first section of the on-board flash memory. The node then waits for the start command from the gateway.
- Start CMD: The Start CMD is sent from gateway to all the nodes to synchronise the network in every time of recording. After receiving this command, the nodes will start the data recording process. The synch pulse from gateway to the sensor nodes could provide minimum synchronisation error between the nodes and keep the network synchronized for long-term SHM applications. It should be mentioned that the synchronisation error will increase as the number of network hops increases.

- Check for active nodes CMD: This command is sent from the gateway to the network of sensor nodes when the gateway is ready to receive the data from one of the nodes. If this CMD is received with one of the nodes, then the node will respond with another CMD that tells the gateway how many samples the gateway should expect (for error checking).
- Gateway ready for transmit CMD: This CMD is received from the gateway to signal the active node to start transmitting the samples. Only one node can transmit at a time and the first node to respond to the "Check for active nodes" CMD is the node that is selected.
- Transmit successful CMD: This CMD from the gateway to the active node indicates that the number of received samples is the same as the expected samples, which was indicated in the response to the "Check for active nodes" CMD for error checking. This command helps to avoid any loss of data and information recorded by the sensor nodes.
- Transmit unsuccessful: This command shows that the number of received samples by the gateway node was not the same as the expected samples as indicated in the response to the "Check for active modes" CMD. After receiving this command, the node will retry 10 times to transmit the logged data when instructed by the gateway.
- Shutdown CMD: this command is sent by the gateway when the transmission process is complete for all the nodes in the network. This is determined to be when the network goes quite for at least 5 seconds.

3. Recording acceleration data: At this stage, the node will start recording the data received from the ADXL355 accelerometer once the nodes have been instructed by the gateway to start logging or threshold event has been detected following an event. It will continue recording the data and storing it in the flash memory until the number of recorded samples reaches the desired record length, which is set by the user, or the time out value is exceeded from a specific value. The time out value for recording sessions is dependent on the record time set by the user during the initial configurations of the network.

4. Transmitting recorded data: In "Transmitting recorded data" state, the node will begin transmitting the data from flash memory to gateway node. Once the transmission is complete and all the data is transmitted, the node will return to the "Waiting for the gateway CMDs" state, which was mentioned above. If the transmission time out value is exceeded, then the node will return to "Sleep" mode.

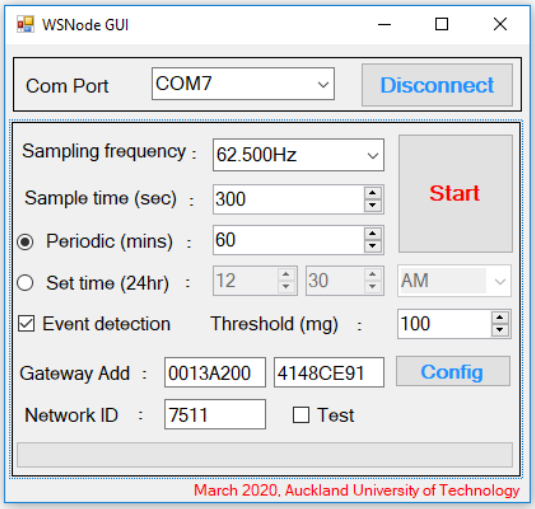

Figure 3.21. The Graphical User Interface for WSSN.

The software of the wireless smart sensor nodes has been developed and built using Atmel Studio 7, which is an Integrated Development Environment (IDE) for developing and debugging all Atmel applications. Due to the fact that an Atmel microcontroller, ATmega328/P, has been selected for the sensor board design, this easy-to-use environment has been utilised to write, build and debug the wireless sensor network software. Figure 3.21 presents the Graphical User Interface (GUI) developed for the wireless smart sensor network. This GUI acts as a connection between the wireless sensor network and the monitoring centre. The first step for connection to the wireless sensor network is to select the right communication port (COM#) and press the 'Connect' button. Then, the users should set initial parameters based on their application goals. These parameters are Sampling frequency in Hz, Sampling time in seconds, selecting different sampling modes (periodic or event detection), and paring the wireless sensors to a specific gateway node using the gateway address.

Table 3.8. Features of final version of wireless smart sensor node.

High-performance accelerometer	
Parameter	Value
Measurement range	±2.048, ±4.096, ±8.192 (g)
Axis	X, Y, Z
ADC resolution	20 (bit)
Sensitivity	256,000 (LSB/g @ ±2.048 g)
Scale factor	3.9 (μg/LSB)
Bandwidth	1.5 (kHz)
Triggered switch	No

Triggered accelerometer	
Parameter	Value
Measurement range	±2, ±4, ±8 (g)
Axis	X, Y, Z
ADC resolution	12 (bit)
Sensitivity	1,000 (LSB/g @ ±2 g)
Scale factor	1 (mg/LSB)
Bandwidth	12.5-400 (Hz)
Triggered switch	Yes

Digital conversion	
Parameter	*Value*
Analogue filter	Low-pass antialiasing filter (1.5 kHz)
Digital filter	Low-pass digital decimation & Bypass high-pass filter (3.9 Hz, 4 kHz)

Self-noise density estimates	
Parameter	*Value*
Noise density (X-axis, Y-axis, Z-axis)	25 (μg/Hz^{-2})
Velocity random walk	9 (μm/s/Hz^{-2} (X-axis, Y-axis)) 13 (μm/s/Hz^{-2} (Z-axis))

Communication	
Parameter	*Value*
Protocol	XBee 802.15.4 (2.4 GHz radio)
Network topology	DigiMesh and ZigBee configurations
USB port for data transmission	Yes

Battery specifications	
Parameter	*Value*
Chemistry	Alkaline D-Cell battery (12,000 mAh)
Battery lifetime	Continuous sampling rate: 200 hr Trigger mode: up to several months
Operating temperature	- 20 ℃ to 60 ℃

Features	
Parameter	*Value*
RTC (Real-time-clock)	Yes
Periodic sampling	Yes
Event-triggered sampling	Yes
Time synchronisation	Yes
Scalable Mesh network	Yes

LEDs & connectors	
Parameter	*Value*
Power indicator	1
Data acquisition LED	1
Data transmission LED	1
3 SMA connector	1
Micro-USB port	1

Temperature sensor	
Parameter	*Value*
Temperature range	- 40 to 125 (℃)
Accuracy	±0.3 (℃)
Resolution	14 (bit)
Temperature drift	< 0.05 (℃/yr)

Humidity sensor	
Parameter	*Value*
Humidity range	0 ~ 100 (%RH)
Accuracy	±2.0 (%RH)
Resolution	14 (bit)
Humidity drift	< 0.5 (%RH /yr)

Storage	
Parameter	*Value*
Type of storage	Flash memory
Storage size	64-Mbit (8-Mbyte)

Physical properties	
Parameter	*Value*
Weight	950 (g)
Dimension	165×70×35 (mm)

Based on the Periodic sampling mode, the wireless sensor nodes are programmed to periodically log and transfer acceleration data from structures. The periodic time between two continuous sampling can be set in minutes using this GUI. The wireless sensor network can also be programmed to record the structural responses at a specific time during 24 hours of a day. Another important sampling mode is the Event-triggered sampling that is activated when the Event detection box is selected. Users can also set the vibration threshold in *mg* to detect and record different sudden events with different amplitudes. In the last part, the all the wireless sensor nodes in the network can be paired and configured to operate with a specific gateway node by setting the Gateway Address. After setting all these parameters, the wireless smart sensor nodes start to operate by pushing the 'Start' button. By doing this, all the initial parameters are transferred to the wireless sensor nodes through the gateway node. A clear picture of all features of the wireless smart sensor node is presented in Table 3.8.

3.8 Summary

In this chapter, the development procedure of a wireless smart sensor network was presented to meet the requirements for measuring low-amplitude ambient vibration and sudden event monitoring of civil structures. The wireless smart sensor board can record both ambient and evet-induced vibrations using two time-triggered and event-triggered sampling modes. The hardware and software specifications of the wireless sensor nodes provide high quality and synchronised vibration measurements from civil structures.

In the first part of the chapter, the preliminary hardware design of the wireless smart sensor node was presented following with some preliminary ambient vibration tests on large-scale structures. The results of these test showed the high resolution of the developed wireless sensor system for SHM applications. In the next part of the chapter, the final hardware design of the sensor boards was explained with a focus on event detection feature of the wireless smart sensor nodes. The final version of wireless sensor platform consists of a high-sensitive sensing

component for high-fidelity vibration measurements and a reliable event detection switch through a trigger accelerometer to detect and record sudden events. Different specifications of the MEMS accelerometer chip used for the sensor design were compared with some of the high performance digital-output MEMS accelerometer sensors recently utilised for WSN development. Then, the time synchronisation protocol of the wireless smart sensor nodes in the network was presented. In the final part of the chapter, the software architecture of the wireless smart sensor network was explained to provide information on workflow of the wireless network.

Chapter 4: Data Management and Data Analysis Toolbox for SHM Data

4.1 Introduction

As mentioned in previous chapters, the aim of this research is to develop a state-of-the-art SHM system for civil engineering structures. In chapter 3, the development process of a new wireless smart sensor network was presented as the first component of the system. In this chapter, an integrated MATLAB-based computational platform is introduced for data management and data analysis of SHM data. This toolbox is compatible and connected to the wireless smart sensor system to shape a full package of structural health monitoring system. This toolbox has been developed in GUI Layout Toolbox of MATLAB, as it can provide powerful programming tools for creating sophisticated graphical user interfaces for managing and analysing large sets of SHM data recorded from civil structures. One of the main goals of the data management and analysis platform was to develop a monitoring environment than can decrease the utilisation of bulky monitoring instruments to reduce disturbance to the traffic flow during the inspection process. In addition, achieving reliable analysis results and avoiding human errors in processing large sets of SHM data were other goals of the toolbox development.

The developed system consists of two independent toolkits: data management toolkit (DMT) designed for managing and processing large sets of SHM data and data analysis toolkit (DAT) designed for modal identification. These toolkits have been connected to each other to provide an easy-to-use environment for condition assessment of structures. In general, the intention of this toolbox is to provide a user-friendly platform to:

- Manage large sets of time series measurements recorded using the wireless smart sensor network,
- Perform an accurate time synchronisation between different sensor nodes in the wireless network,

- Create new data files with a compatible format with data analysis toolkit,
- Download, visualise and process monitoring data that are continuously recorded from different types of civil structures,
- Trim, down sample, and filter the monitoring data using lowpass, bandpass, and highpass filtering options,
- Evaluate and visualise modal parameters of structures, including natural frequencies, mode shapes and modal damping ratios, using different time domain and frequency domain system identification techniques,
- Compare the analysis results obtained by different time-domain and frequency-domain system identification techniques,
- Save the analysis results as figures and new Excel and Text files.

In the following parts, more details about different parts of the MATLAB-based toolbox are presented. It should be mentioned that this toolbox has been used for data management and analysis of target structures during this research. In last part of this chapter, a new vibration-based nonlinearity identification technique is introduced based on time series Autoregressive modelling and fuzzy clustering algorithm. The acceleration time histories recorded from a steel bridge model during a series of shaking table tests will be utilised to assess the performance of the new technique. The analysis results obtained for the new nonlinearity identification technique will be presented in the following chapter.

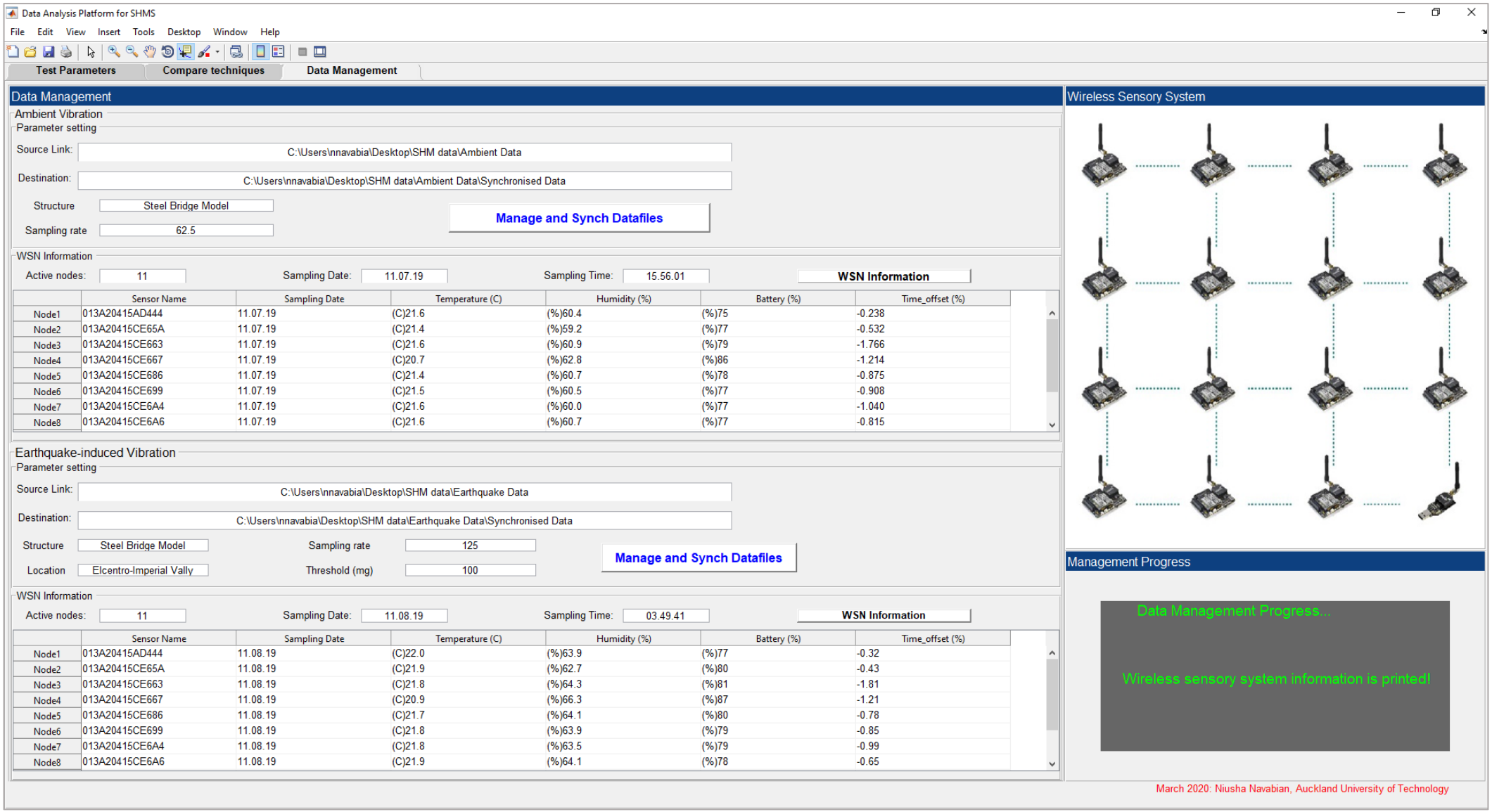

Figure 4.1. Data Management Toolkit.

4.2 Data Management Toolkit (DMT)

The DMT has been designed to manage large sets of structural health monitoring data without any user interaction. This toolkit is illustrated in Figure 4.1. Users can download, manage and combine the acceleration time histories recorded using different channels of wireless smart sensor nodes that are active in the network using the DMT. This toolkit has the capability to communicate with the wireless sensor system, download the data, change the format of raw measurement, synchronise the data files, and save the measurements in a new format. It could also offer functions for providing information related to the wireless sensor network and the sensors that are active in the network.

This toolkit has been divided to two separate sections, including 'Ambient Vibration' and 'Earthquake-induced Vibration'. In 'Ambient Vibration' section, the ambient vibration data sets can be automatically downloaded by providing the source link of the data files wirelessly transferred from the sensor network to the monitoring PC and the destination link, where users would like to save the new format of data. The name of the structure can be specified by users to be included in the header of the new data files. The sampling frequency of vibration measurements should be determined in 'parameter setting' section to be utilised for creating new time vector and time synchronisation purposes. After providing this information, the data files are managed and synchronised by pushing the 'Manage and Synch Datafiles' button. The data from different wireless sensor nodes are synchronised using the post-processing technique introduced in the previous chapter. Then, new data files compatible with the data analysis platform are automatically created and saved in the destination folder. It should be mentioned that the users are able to see the status of data management through the 'management progress' box located in the bottom of right corner of the toolkit.

In addition, a detailed information about the wireless smart sensor network and the active nodes in the network can be presented by pushing 'WSSN Information' button. This information

includes the number of active nodes, sensor identification name (sensor ID), sampling time and date, environmental temperature and humidity recorded by each active sensor node in the network, and the time offset of each wireless sensor node.

In 'Earthquake-induced Vibration' section, the earthquake-induced vibration data files are managed and synchronised. In this section, the Source link, Destination, Structure's name, Location of the earthquake, Sampling frequency, and the vibration threshold set for event-triggered sampling mode should be specified to be considered for data management and processing. Same as the ambient vibration, the earthquake-included vibrations are managed and synchronised by pushing 'Manage and Synch Datafiles' button. The information about the wireless smart sensor nodes, which have been triggered and sampled the earthquake-induced vibration, can be extracted in this section as well. The synchronised and managed earthquake signals can be analysed using various time and frequency domain methods implemented in DAT toolkit. More details about this toolkit are provided in the following part.

4.3 Data Analysis Toolkit (DAT)

The DAT toolkit has been designed to process and analyse the acceleration time histories measured using the wireless smart sensor network and managed using the DMT toolkit. This toolkit has two different panels, including 'Test Parameters' and 'Compare Techniques'.

The first panel is presented in Figure 4.2. The new format of vibration data files can be downloaded to this panel using 'Open Input File' pushbutton. Then, the data are analysed using the Vibration-based Data Analysis Platform. User can use preliminary data manipulation and analysis techniques or more complicated and intensive algorithms to run modal analysis and extract useful information from the raw measurements, such as natural frequencies, mode shapes, and modal damping ratios. These parameters will be then utilised for modal-based damage identification purposes. Both frequency domain and time domain system identification (SI) methods have been implemented that can be used for experimental (input-output data),

operational (output-only data) modal analysis of structures. The analysis results obtained from different techniques are shown in the ‘Compare Techniques’ panel. Users are able to plot and visualise the analysis results and compare the results of different analysis techniques as shown in Figure 4.3. It should be mentioned that Figures 4.2 and 4.3 present the time domain and frequency domain results obtained for an ambient vibration data set recorded from a highway Viaduct. The analysis results can be saved as figures, Excel and Text files by users. In the following, more details about the analysis panels will be provided.

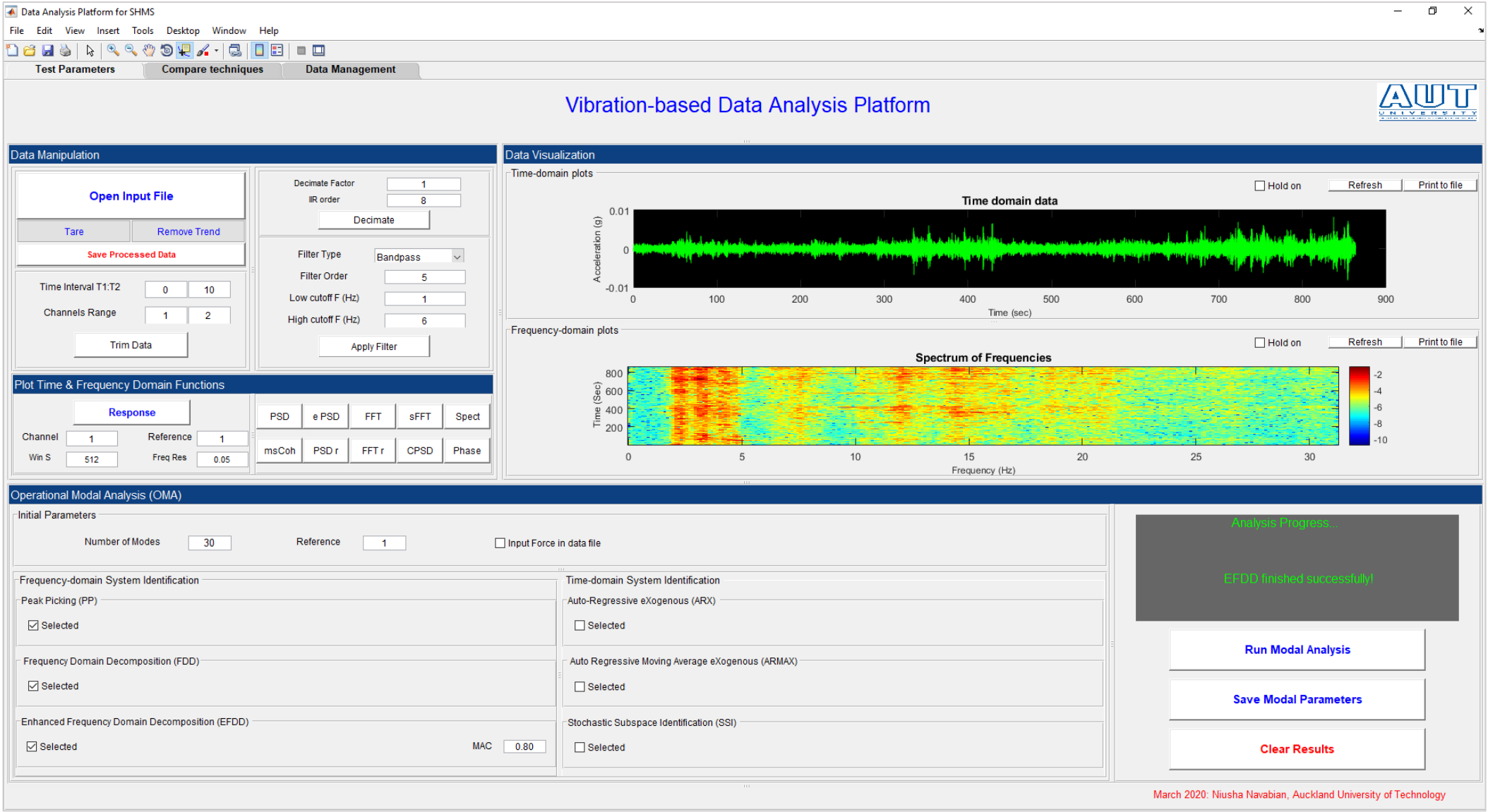

Figure 4.2. First panel of the DAT.

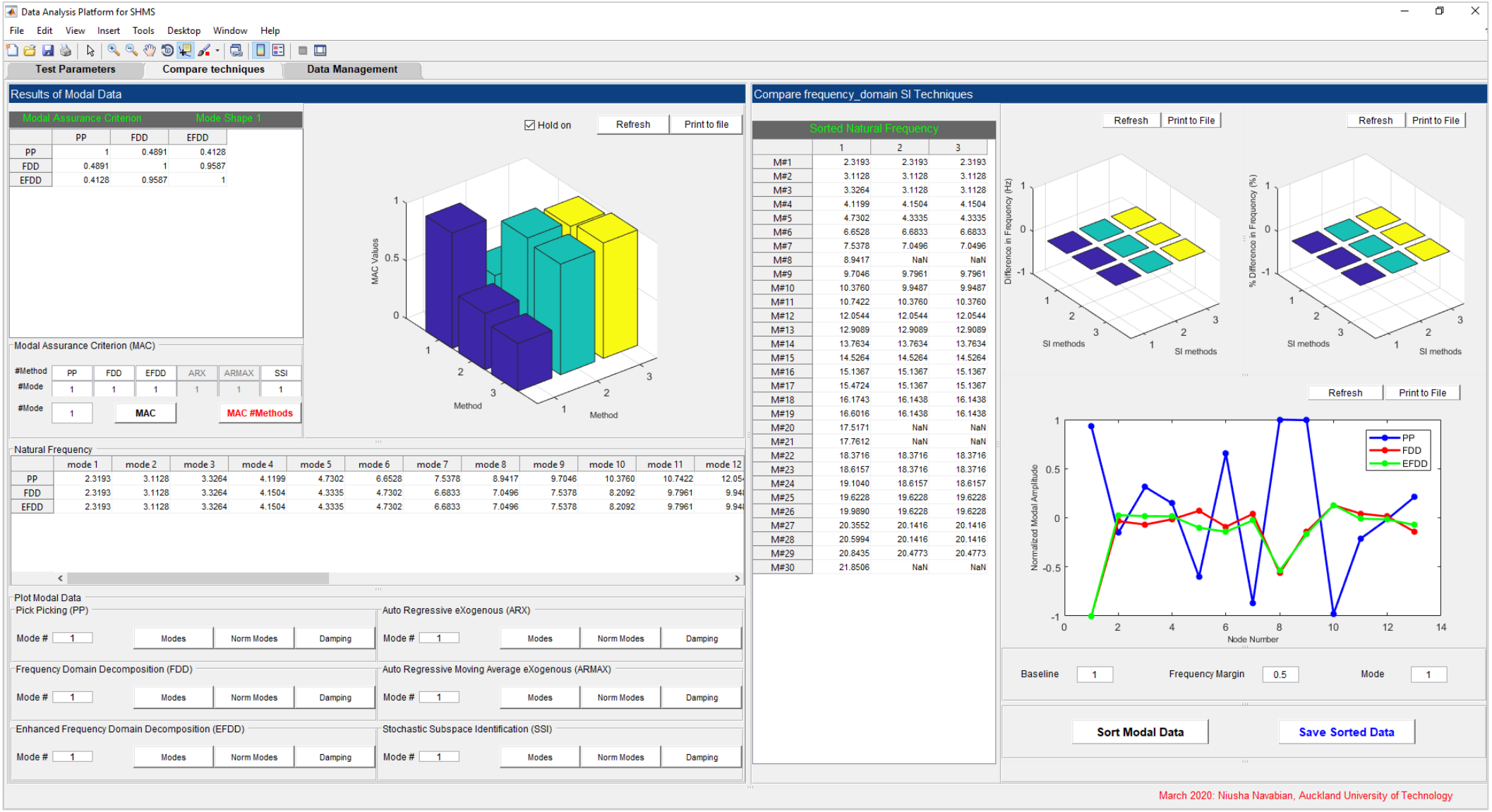

Figure 4.3. Second panel of the DAT.

4.3.1 Preliminary data analysis

As mentioned, the ‘Test Parameter’ panel includes preliminary data analysis and more complicated techniques for modal parameter estimation. After downloading a data file, preliminary data manipulation techniques can be performed through ‘Data Manipulation’ section on acceleration time histories to investigate various parameters on the analysis results. The preliminary data manipulation includes removing trend from data, down-sampling and decimation of data, data filtering, trimming specific channels of data into user-defined intervals, and saving the processed data in new files. It should be mentioned that there are three filtering options including, low-pass, high-pass, and bandpass filtering. For these filtering options, Filter order, low Cut-off frequency, and high Cut-off frequency should be set by users based on their analysis goals.

In addition, some preliminary data analysis techniques in both time and frequency domains can be performed on the vibration data through ‘Time and Frequency Domain Functions’ section. They include Power Spectral Density (PSD), Evolutionary Power Spectral Density (EPSD), Fast Fourier Transform (FFT), Sparse Fast Fourier Transform (SFFT), Spectrogram, Magnitude Squared Coherence (MSCoh), Cross Power Spectral Density (CPSD) of the time series signal and the Phase difference of two acceleration time series. The frequency window and resolution can be set in this section to provide users more flexibility to analyse time series signals. All the processed and analysed signals of various measurement channels can be visualised in ‘Data Visualisation’ section by two plotting areas. These figures showing various analysis results can be printed and saved as MATLAB Figures. It should be mentioned that the status of the toolbox can be checked using the ‘Analysis Progress’ box located in bottom of right corner of the toolkit.

4.3.2 System identification techniques

Several System Identification (SI) techniques have been implemented in the DAT to extract modal parameters of structures, such as natural frequencies, modal damping ratios, and mode shapes. These techniques are frequency domain techniques, such as Peak Picking (PP), Frequency Domain Decomposition (FDD), and Enhanced Frequency Domain Decomposition (EFDD), and time domain techniques, such as Autoregressive eXogenous (ARX), Autoregressive Moving Average eXogenous (ARMAX), and Stochastic Subspace Identification (SSI). The modal parameters are then utilised for condition assessment and damage identification of the structure. The users can select any of these methods for analysing the raw vibration measurements. The number of modes and the reference channel should be specified for the modal analysis. Then, by pressing the 'Run Modal Analysis', the selected time series data will be analysed. The obtained results can be saved to Excel format files or be cleared from the memory by users. The extracted modal parameters can be visualised in the second panel of the DAT, called 'Compare Techniques'. This panel is illustrated in Figure 4.3. The main purpose of this panel is to present and compare the analysis results obtained using various SI techniques to provide more accurate estimation of dynamic model of a system. In the first section of this panel, the results of modal analysis are presented and visualised. They include natural frequencies, mode shapes and their normalised counterparts, and modal damping ratios. In second part of this panel, the comparison results between various SI techniques can be obtained. The frequency difference in Hz, the frequency difference in percent, the difference between normalised modal amplitudes, and the difference between the sorted frequencies are among these comparisons. In addition, the Modal Assurance Criterion (MAC) values of different SI techniques can be obtained and plotted to evaluate the differences between estimated mode shapes. The mathematical background of SI techniques will be presented in the following sections.

Frequency-domain techniques: In total, three well-known output-only frequency domain SI techniques are used and developed in the data analysis toolbox. These methods are Peak-Picking (PP), Frequency Domain Decomposition (FDD), and Enhanced Frequency Domain Decomposition (EFDD) that are introduced in the following.

1. Peak-Picking (PP):

This SI method is among the simplest and accurate approach to estimate modal characteristics of a structures from experimental measurements [143]. This method is based on the fact that the Frequency Response Functions (FRFs) go through extreme values around natural frequencies. Natural frequencies are calculated by determining the peaks in auto spectra or PSD plots of recorded structural responses. To evaluate the PSD values of a signal, one should find the discrete-time Fourier transform of the signal and scale the squared of the result. Considering a discrete time series signal $x(k)$ with a length of *N*, its Fourier transform is calculated as:

$$X(f) = \sum_{k=0}^{N-1} x(k)\, e^{-j\,2\pi k f\ /\ N} \tag{4.1}$$

where *f* is natural frequency, $X(f)$ is the Fourier transform of $x(t)$, and *j* is the imaginary unit. The inverse discrete Fourier transform is determined as follows:

$$X(k) = \frac{1}{N} \sum_{k=0}^{N-1} X(f)\, e^{j\,2\pi k f\ /\ N} \tag{4.2}$$

The periodogram estimation of the PSD values of the time series signal is defined using its discrete Fourier transform using the following equation:

$$P_{xx}(f) = \frac{X(f)\, X^{*}(f)}{N F_s} = \frac{|X(f)|^2}{N F_s} \tag{4.3}$$

where '*' presents the complex conjugate and F_s is the sampling frequency. In this study, a method proposed by Welch [144] has been used to estimate the PSDs of times series signals. According to this method, the time histories of structural responses are divided into several

overlapping segments. Then, these segments are converted to frequency domain using a discrete Fourier transform with windowing process to decrease the leakage. The Auto PSDs and cross PSDs are calculated by considering a reference node signal for each time segment using the Fourier transforms and averaging over the data segments. The peak frequencies from the PSD functions are then considered as natural frequencies. Mode shapes of time series data are calculated by normalizing the auto PSDs at a specific measurement point and a specific natural frequency using the cross PSDs of the reference point at same natural frequency.

2. Frequency Domain Decomposition (FDD):

This technique is an extension of the classical frequency domain approach that is called Basic Frequency Domain (BFD) or the Peak-Picking technique. The classical SI techniques are able to provide reasonable estimations of natural frequencies and mode shapes if the structural modes are well excited and separated. In addition, these techniques have some limitation in case of frequency resolution of the spectral density estimate. Therefore, damping estimation is usually impossible or uncertain using the classical SI methods. However, Frequency Domain Decomposition (FFD) method eliminates these disadvantages associated with the classical approaches [96]. In this section, the theoretical background of this techniques are presented.

Considering $x(t)$ and $y(t)$ as the unknown inputs and the measured outputs of a system, their relationship can be expressed as follows [96, 143]:

$$G_{yy}(j\omega) = \overline{H}(j\omega)\, G_{xx}(j\omega)\, H(j\omega)^T \tag{4.4}$$

where $G_{xx}(j\omega)$ is the $r \times r$ PSD matrix of the input, $G_{yy}(j\omega)$ is the $m \times m$ PSD matrix of the responses, m is the number of responses, r is the number of inputs, $H(j\omega)$ is the $m \times r$ Frequency Response Function (FRF) matrix. Superscript T shows complex conjugate and "_" presents the transpose. The FRF matrix can be estimated using the following equation:

$$H(j\omega)=\sum_{k=1}^{n}\frac{R_k}{j\omega-\lambda_k}+\frac{\overline{R}_k}{j\omega-\overline{\lambda}_k} \tag{4.5}$$

where *n* is the number of modes. By considering ϕ_k and γ_k as the mode shape vector and the modal participation vector, respectively, the residue is calculated as follows:

$$R_k = \phi_k \ \gamma_k^T \tag{4.6}$$

Assuming the input excitation is white noise, Eq. (4.4) can be rewritten as following equation:

$$G_{yy}(j\omega)=\sum_{k=1}^{n}\sum_{s=1}^{n}\left[\frac{R_k}{j\omega-\lambda_k}+\frac{\overline{R}_k}{j\omega-\overline{\lambda}_k}\right]C\left[\frac{R_s}{j\omega-\lambda_s}+\frac{\overline{R}_s}{j\omega-\overline{\lambda}_s}\right]^H \tag{4.7}$$

where superscript *H* defines complex conjugate and transpose. After multiplying the two partial function factors, the output PSD values are decreased to a pole-residue form as below:

$$G_{yy}(j\omega)=\sum_{k=1}^{n}\left(\frac{A_k}{j\omega-\lambda_k}+\frac{\overline{A}_k}{j\omega-\overline{\lambda}_k}+\frac{B_k}{-j\omega-\lambda_k}+\frac{\overline{B}_k}{-j\omega-\overline{\lambda}_k}\right) \tag{4.8}$$

where A_k is the k^{th} residue matrix of the output PSD and is given by Eq. (4.9). Also, the contribution to the residue from the k^{th} mode is presented by Eq. (4.10):

$$A_k = R_k C\left(\sum_{s=1}^{n}\frac{\overline{R}_s^T}{-\lambda_k-\overline{\lambda}_s}+\frac{R_s^T}{-\lambda_k-\lambda_s}\right) \tag{4.9}$$

$$A_k = \frac{R_k C \overline{R}_k^T}{2\alpha_k} \tag{4.10}$$

where α_k is minus the real part of the pole $\lambda_k = -\alpha_k + j\omega_k$. As is clear, this term is dominating in the case of light damping. Therefore, the residue is proportional to the mode shape vector and is estimated using Eq. (4.11):

$$A_k \propto R_k C \overline{R}_k^T = \phi_k \gamma_k^T C \gamma_k \phi_k^T = d_k \phi_k \phi_k^T \tag{4.11}$$

where d_k is a scalar constant. It is noteworthy that only a limited number of modes, usually one or two modes, contributes at a specific frequency. By considering $sub(\omega)$ as this set of modes and a damped structure, spectral density of structural response is given by following equation:

$$G_{yy}(j\omega) = \sum_{k \in Sub(\omega)} \left(\frac{d_k \phi_k \phi_k^T}{j\omega - \lambda_k} + \frac{\bar{d}_k \bar{\varphi}_k \bar{\varphi}_k^T}{j\omega - \bar{\lambda}_k} \right) \tag{4.12}$$

where φ_k is the k^{th} vector of mode shapes. In order to estimate the modal parameters, first the power spectral density matrix should be estimated. In next step, the output PSD values $G_{yy}(j\omega)$ are decomposed by taking the Singular Value Decomposition (SVD) of the matrix as follows:

$$\hat{G}_{yy}(j\omega_i) = U_i S_i U_i^H \tag{4.13}$$

where U_i is a unitary matrix including the singular vectors u_{ij}. Also, S_i is a diagonal matrix including the scalar singular values s_{ij}. In the case of dominating one mode, assuming k^{th}, the first singular vector u_{i1} is an estimate of the mode shape:

$$\hat{\phi} = u_{i1} \tag{4.14}$$

3. Enhanced Frequency Domain Decomposition (EFDD):

The EFDD technique introduced in 2007 by Jacobsen et al. [145] is an extension of the FDD method described in the previous section. According to FDD method, the structural modes are easily selected by locating the peaks of the SVD plots of the PSD matrix of structural outputs. Due to the fact that this technique is based on FFT analysis, the accuracy of the natural frequency and mode shape can be affected by the FFT resolution. Also, modal damping ratios cannot be accurately estimated using this technique. However, EFDD enhances the accuracy of the modal parameter estimation. The PSD matrix of system responses $G_{yy}(j\omega)$ can be rewritten as follows, by performing SVD of the response PSD matrix at discrete frequencies:

$$G_{yy}(j\omega_i) = T_i \sum_i T_i^T \tag{4.15}$$

where T_i is a unitary matrix including the singular vectors t_{ij} and $\sum_i$ is a diagonal matrix including singular values σ_{ij} . Assuming only the k^{th} mode is dominant, the auto/cross PSD matrix can be defined as follows:

$$G_{yy}(j\omega_k) \cong \sigma_{k1}\, t_{k1}\, t_{k1}^T \tag{4.16}$$

Finally, the first singular vector at the k^{th} structural mode is considered as the k^{th} mode shape:

$$\varphi_k \cong t_{k1} \tag{4.17}$$

It should be mentioned that in FDD technique, modal frequencies are determined from the peaks of singular values and frequency plots, and the mode shapes are identified using the corresponding singular vectors. However, in EFDD technique, the auto/cross PSD of a structural peak is transferred to the time domain and the singular vectors present mode shapes. Using this technique, the modal damping can be evaluated using logarithmic decrement of the autocorrelation function.

Time-domain techniques: In this part, two famous time domain system identification techniques that have been implemented in the MATLAB toolbox are presented. These techniques are Stochastic Subspace Identification (SSI) and Autoregressive with eXogenous Inputs (ARX). It should be mentioned that Autoregressive Moving Average with eXogenous Inputs (ARMAX) has been also implemented for the toolbox development, which will be explained in the next part.

1. *Stochastic Subspace Identification (SSI):*

This method determines a stochastic state space model from the experimental measurements without estimating the spectra of the time series data [146, 147]. In general, two algorithms, including SSI-COV and SSI-DATA can be used for estimation of unknown characteristics of the system, such as natural frequencies, mode shapes, and modal damping ratios. According to

the SSI-DATA algorithm, a Hankel matrix is formed first from the experimental data. Then, oblique projections of the partitioned Hankel matrices are formed from which state-space matrices are calculated using Singular Value Decomposition (SVD) of the matrix. It is noteworthy first that a discrete time state space model at any *k* step is obtained using the following equations:

$$x_{k+1} = A\,x_k + B\,u_k + \omega_k \tag{4.18}$$

$$y_k = C\,x_k + D\,u_k + v_k \tag{4.19}$$

where x_k, u_k and y_k are state, input and output at time *k*, respectively. Also, *A*, *B*, *C*, and *D* present the system, input, output, and feedthrough matrices, which are estimated using system identification techniques. ω_k and v_k are the process and measurement noises. The linear discrete time state space equation of motion is presented as:

$$H(k) = \left[C^T \quad (CA)^T \ \ldots\ (CA^{p-1})^T\right]^T A^{k-1}\left[Ax(0) \quad A^2x(0) \ \ldots\ A^r x(0)\right] \tag{4.20}$$

By considering *k*=1 and *k*=2 and solving the above equation, the system and output matrices can be obtained using the following equations:

$$A = \sum^{1/2} T^T\, H(1) V \sum^{1/2} \tag{4.21}$$

$$C = \left[I \quad 0 \quad \ldots \quad 0\right] T \sum^{1/2} \tag{4.22}$$

Modal parameters of a continuous time series system, such as natural frequencies, mode shapes, and damping ratios, can be estimated using eigenvalues and eigenvectors of matrix *A:*

$$f_i = \left|\lambda_i\right| / 2\pi \tag{4.23}$$

$$\xi_i = -\frac{\mathrm{Re}(\lambda_i)}{2\pi f_i} \tag{4.24}$$

$$\Phi_i = C\,\psi_i \tag{4.25}$$

where f_i is the i^{th} modal frequency, ξ_i is the i^{th} damping ratio, and Φ_i is the i^{th} mode shape of the system. The obtained Hankel matrix for an input time series is given using Eq. (4.26):

$$U_{0/2i-1} = \begin{bmatrix} u_0 & u_1 & \dots & u_{j-1} \\ u_1 & u_2 & \dots & u_j \\ \dots & \dots & \dots & \dots \\ u_{i-1} & u_i & \dots & u_{i+j-2} \\ u_i & u_{i+1} & \dots & u_{i+j-1} \\ \dots & \dots & \dots & \dots \\ u_{2i-1} & u_{2i} & \dots & u_{2i+j-2} \end{bmatrix} = \begin{bmatrix} U_p \\ U_f \end{bmatrix} \tag{4.26}$$

where U_p and U_f are the past and future parts of the Hankel matrix. It is noteworthy that the value of the index i separating the past parts from the future parts should be greater than the maximum value considered for the system order. In addition, index j should be selected a value that as a result $2i + j - 2$ is less than the length of time series input and output data. The Hankel matrix of the system output Y can be obtained same as the system input. In total, the past input and output of the system can be combined in a matrix as follows:

$$W_p = \begin{bmatrix} U_p & Y_p \end{bmatrix} \tag{4.27}$$

In this technique, the next step is to calculate the oblique projection Ob_i of the time series input and output, which can be estimated using the following equation:

$$Ob_i = Y_{f/U_f} W_p = Y_f \begin{bmatrix} W_p^T & U_f^T \end{bmatrix} W_p \begin{bmatrix} W_p W_p^T & W_p U_f^T \\ U_f W_p^T & U_f U_f^T \end{bmatrix}^+_{first\ r\ columns} \tag{4.28}$$

In this equation, superscript '+' presents the Moore-Penrose matrix inverse. Also, r is the number of columns in W_p. It should be mentioned that the oblique projection can be obtained by the observability Γ_i and state sequence X_i using Eq. (4.29). Also, the observability matrix and the state sequence are computed using the SVD of oblique projection as given in Eq. (4.30):

$$Ob_i = \Gamma_i X_i = \left[C^T \quad (CA)^T \quad \ldots \quad (CA^{i-1})^T \right]^T \left[x_i \quad x_{i+1} \quad \ldots \quad x_{i+j-1} \right] \tag{4.29}$$

$$Ob_i = T \sum V^T \tag{4.30}$$

where T and V present unitary matrices of singular vectors, and $\sum$ is the diagonal matrix of singular values. The observability matrix and state sequence are calculated using the two following equations:

$$\Gamma_i = T \sum^{1/2} \tag{4.31}$$

$$X_i = \sum^{1/2} V^T \tag{4.32}$$

The A and C matrices introduced in Equations (4.21) and (4.22) are obtained using the observability matrix. Matrix A can be calculated using the following equation:

$$A = \Gamma_i^{+} \overline{\Gamma}_i \tag{4.33}$$

where $\overline{\Gamma}_i$ is given by the observatory matrix by removing the first rows corresponding to the number of outputs. Also, Γ_i^{+} is the pseudo-inverse of the observability matrix. Matrix C is also defined by considering the first rows of the observability matrix corresponding to the number of system outputs. Using A and C matrices, the natural frequencies, mode shapes and modal damping ratios, can be obtained. The natural frequencies and modal damping ratios can be adapted from the imaginary and real parts of the eigenvalues of A_c, which is the continuous time equivalent of matrix A. This matrix can be obtained using the following equation:

$$A_c = \frac{\ln(A)}{\Delta t} \tag{4.34}$$

In this equation, Δt is time step. The modal characteristics of system can be obtained using Eqs. (4.23) - (4.25). The following equation is utilised to obtain the real part of mode shapes [148]:

$$\Phi_{real} = \mathrm{Re}(\Phi_{comp}) + \mathrm{Im}(\Phi_{comp}) \mathrm{Re}(\Phi_{comp})^{+} \mathrm{Im}(\Phi_{comp}) \tag{4.35}$$

where subscripts *real* and *comp* present the real and complex parts of modes, respectively. In addition, *Im* defines the imaginary part. For using the SSI technique to estimate the modal parameters of structures, the order of system should be predicted. One of the most common way for the order prediction is the use of stabilisation diagrams [146, 147]. The modes that are consistently distributed across the system orders are considered as stable structural modes.

2. Autoregressive eXogenous (ARX) models:

ARX model is one of the well-known and polular methods for modal parameter estimation. This model is a simple technique to obtain the relation between input and output time series signals for various cases, inlcuding Single Input-Single Output (SISO) or Multiple Input-Multiple Output (MIMO), through which the system dynamic properties can be presented.

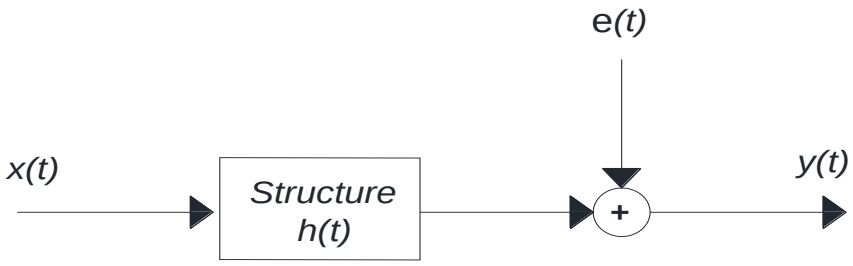

Figure 4.4. Block diagram of the ARX model.

Input-output representation of a linear dynamic system subjected to input excitation $x(t)$ at sample index t is presented in Figure 4.4. In this figure, $y(t)$, $h(t)$ and $e(t)$ describe the response of the system, the discrete-time impulse response function describing the relation between the input and output signals, and the system disturbance, respectively. This simple model performs effeciently when noise level of the system is low. In the case of high noise, the order of the model should be increaseed to compensate for the noise influence. The following linear difference equations can describe the ARX model:

$$y(t)+A_1 y(t-1)+...+A_{n_a} y(t-n_a)=B_0 x(t)+B_1 x(t-1)+...+b_{n_b} x(t-n_b)+e(t) \quad (4.36)$$

$$y(t)+\sum_{k=1}^{na} a_k y(t-k)=\sum_{k=1}^{nb} b_k x(t-nk-k+1)+e(t) \quad (4.37)$$

The general ARX model can be rewritten in the following polynomial equation:

$$A(q)y(t) = B(q)x(t) + e(t) \tag{4.38}$$

where,

$$A(q) = I + A_1 q^{-1} + A_2 q^{-2} + ... + A_{n_a} q^{-n_a} \tag{4.39}$$

$$B(q) = B_0 + B_1 q^{-1} + B_2 q^{-2} + ... + B_{n_b} q^{-n_b} \tag{4.40}$$

The model presented in Eq. (4.38) includes the Autoregressive part $A(q)y(t)$ and the exogenous input part $B(q)x(t)$. $A(q)$ and $B(q)$ are the coefficients to be estimated in the delay operator q^{-1}. n_a, n_b, and n_k are the model orders of the ARX model, and $e(t)$ is the residuals of the estimation process up to time *t*. By considering the following parameter matrix, the general ARX model can be rewritten as a linear regression:

$$\theta = [A_1 \quad A_2 \ ... \ A_{n_a} \quad B_0 \quad B_1 \ ... \ B_{n_b}]^T \tag{4.41}$$

$$y(t) = \theta^T \phi(t) + e(t) \tag{4.42}$$

The modal parameters can be directly evaluated using the least square method by minimising the norm of $e(t)$:

$$\Phi = \arg\min\left(\frac{1}{N}\sum_{t=k}^{k+N-1}\left\|e(t)\right\|^2\right) = \arg\min\left(\frac{1}{N}\sum_{t=k}^{k+N-1}\left\|y(t) - \theta^T\phi(t)\right\|^2\right) \tag{4.43}$$

where *N* is consecutive values of the responses from $y(k)$ to $y(k+N-1)$. The constructed ARX model is utilised to fit the experimental data after obtaining the measured force and acceleration signals on all measurement points. The ARX model makes a regressive connection between input vector $x(t)$ and output vector $y(t)$ through a residual vector $e(t)$. The modal characteristics of the system, matrices *A* and *B*, are calculated using the least square method. After modal parameter estimation, the state matrix can be defined as the autoregressive parameters:

$$A_{(na\times nb)}=\begin{bmatrix} -A_1 & -A_2 & -A_3 & \dots & -A_p \\ I & 0 & 0 & \dots & 0 \\ 0 & I & 0 & \dots & 0 \\ \dots & \dots & \dots & \dots & \dots \\ 0 & 0 & 0 & I & 0 \end{bmatrix} \tag{4.44}$$

The continuous eigenvalues, natural frequencies, and modal damping ratios of the system can be respectively estimated for each pole using the following equations:

$$[V\ ,\lambda]=eig\ (A) \tag{4.45}$$

$$f_i=\frac{\sqrt{\mathrm{Re}^2(\lambda_i)+\mathrm{Im}^2(\lambda_i)}}{2\pi} \tag{4.46}$$

$$\xi_i=-\frac{\mathrm{Re}(\lambda_i)}{2\pi f_i} \tag{4.47}$$

Table 4.1. Comparison between different system identification techniques [149, 150].

Methods	Advantages	Limitations
PP	– Fast processing time – Time efficient for on-site computation – Simple and easy-to-use algorithm	– Subjective task when peaks are unclear – Estimation of operational deflection shapes instead of mode shapes – Very sensitive to noise level – Unreliable damping estimation
FDD	– Fast identification process – Needs less time-series data compared to SSI method	– Sensitive to FFT analysis and frequency resolution – Unreliable damping estimation – Requirement of high-resolution output
EFDD	– More accurate in estimation of modal parameters compared to FFD – Not affected by FFT analysis	– Requires noise-free output from structure
SSI	– More reliable mode selection using stabilization method – Effective method for stabilization diagram construction – Higher quality compared to classical method – No need to convert time-series data to correlations or spectra	– Computationally intensive – Requires large set of time-series data – Requires high-quality input data
ARX	– Accurate estimation of modal parameters when data is high-quality – No need to convert time-series data to correlations or spectra	– Limitations to express the noise term of a dynamic system – Subjective to accuracy of model order estimation – Requires noise-free input-output time-series data
ARMAX	– Can express the disturbance of a dynamic system – No need to covert time-series data to correlations or spectra	– Subjective to accuracy of model order estimation – Requires noise-free input-output time-series data

A comparison between different system identification techniques implemented in the toolbox is presented in Table 4.1. The aim of this comparison is to provide the readers with a relaible guide to choose an appropriate method based on their application needs.

4.4 New vibration-based nonlinearity identification technique

In this part of the thesis, the new vibration-based nonlinearity identification technique is presented for analysing earthquake-induced vibration data. This method is based on linear time series modelling and testing the validity of basic principles of these linear models. The vibration-based nonlinearity identification technique utilises the time series Autoregressive Moving Average with Exogenous Inputs (ARMAX) modelling, probability theory, and Fuzzy C-Means (FCM) clustering algorithm to categorise the linear and nonlinear dynamic behaviours of a dynamic system. The concept of this method was extracted from the fact that residual error of a linear ARMAX model follows a normal distribution. In the following, the detailed description and mathemathics of this method will be provided.

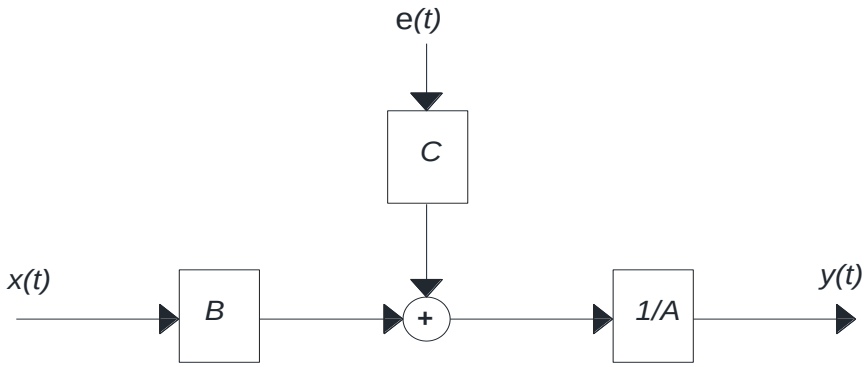

Figure 4.5. Block diagram of the ARMAX model.

As mentioned, there are different types of methods to model the behaviour of linear time-invariant and dependent systems. Autoregressive model is a type of random process to model the time series. Autoregressive with eXogenous Inputs (ARX) model, which is one form of autoregressive models, was introduced in previous part. One of the disadvantages of ARX modelling to simulate dynamic behaviour of a system is its limitation to express the noise term

due to the fact that it can represent the system disturbance as a discrete error. An ARMAX model is a more complete and flexible form of a ARX model that has an additional term as Moving Average (MA) (polynomial *C(q)*) to describe the disturbance dynamics of the system [151, 152]. The block diagram of the ARMAX model is presented in Figure 4.5 and the following equation describes the ARMAX model:

$$y(t)+\sum_{k=1}^{na} a_k\, y(t-k)=\sum_{k=1}^{nb} b_k\, x(t-nk-k+1)+\sum_{k=1}^{nc} c_k\, e(t-k)+e(t) \tag{4.48}$$

where a_k, b_k and c_k are the unknown coefficients of the model to be estimated and *na*, *nb*, *nc* and *nk* are the orders of the ARMAX model. Term $e(t-k)$ is the white-noise disturbance value. Using the backshift operator (q), the above equation can be expressed as follow:

$$A(q)\ y(t)=B(q)\ x(t)+C(q)\ e(t) \tag{4.49}$$

where $A(q)$, $B(q)$ *and* $C(q)$ designate the AR, X and MA polynomials of the model in the delay operator q^{-1}, which can be respectively defined by:

$$A(q)=I+A_1q^{-1}+...+A_{na}q^{-na} \tag{4.50}$$

$$B(q)=B_0+B_1q^{-1}+...+B_{nb}q^{-nb} \tag{4.51}$$

$$C(q)=I+C_1q^{-1}+...+C_{nc}q^{-nc} \tag{4.52}$$

In this study, in order to categorise the linear and nonlinear behaviour of the system, different ARMAX models are constructed from various amplitudes of earthquake-induced signals. Then, the residual errors can be estimated by the predicted output $\bar{y}(t)$ from ARMAX models, which is ideally a Gaussian process for a stationary signal [153], and the measurement output $y(t)$. These residual errors (E) are presented by the following equations for two groups of earthquake-induced signals.

$$E_L=y_L(t)\ -\ \bar{y}_L(t) \tag{4.53}$$

$$E_{un}=\ y_{un}(t)-\bar{y}_{un}(t) \tag{4.54}$$

where the subscript *L* represents a reference status that assumes the structure behaves linearly. Also, subscript *un* shows an unknown status of the structure to be categorised using the identification process. In this study, a vibration data set induced using a low-amplitude earthquake excitation has been assumed to represent the linear model of the structure as the reference model. The behaviour of the structure under other amplitudes of excitation is investigated in comparison to this reference model. The predicted responses extracted from the reference ARMAX model and the ARMAX models represented unknown status of the structure, can be expressed according to Eqs. (4.55) and (4.56):

$$\bar{y}_L = -\sum_{k=1}^{na} a_k\, y_L(t-k) + \sum_{k=1}^{nb} b_k\, x_L(t-nk-k+1) + \sum_{k=1}^{nc} c_k\, e(t-k) \tag{4.55}$$

$$\bar{y}_{un} = -\sum_{k=1}^{na} a_k\, y_{un}(t-k) + \sum_{k=1}^{nb} b_k\, x_{un}(t-nk-k+1) + \sum_{k=1}^{nc} c_k\, e(t-k) \tag{4.56}$$

As a general understanding, once the amplitude of excitation increases, the performance of the target structure alters from its reference state. Residual errors extracted from ARMAX time series models provide very significant information repressing this change. In this study, ARMAX models are constructed using various vibration data sets and their residual errors are compared to their counterparts extracted from a reference ARMAX model. This difference will increase, as the amplitude of excitation increases, and the structure starts to behave nonlinearly from a specific threshold. This is because the linear time series ARMAX models are able to simulate only the linear models of the structure and they cannot represent the nonlinear features of the structural responses. In this study, the difference between the residuals of ARMAX models of a reference state and unknown states are statistically measured. It was decided to use an appropriate statistical test and clustering technique in this study to evaluate and categorise the structural behaviour under various excitation sources.

In the first step, the difference between residual errors generated from the reference linear model and other unknown models are visually investigated. Empirical cumulative distribution

function (ECDF) of time series residuals are employed in order to control the similarity between the various data sets. The ECDFs of residuals are respectively presented by $\hat{G}(E_L)$ and $\hat{G}(E_{un})$ for the reference linear model and other unknown models and can be estimated using the following equations:

$$\hat{G}(E_L) = \frac{1}{n}\sum_{i=1}^{n} I\left(\left(E_L\right)_i \leq (E_L)\right) \tag{4.57}$$

$$\hat{G}(E_{un}) = \frac{1}{n}\sum_{i=1}^{n} I\left(\left(E_{un}\right)_i \leq (E_{un})\right) \tag{4.58}$$

Using the mentioned equations, the empirical cumulative distribution functions of each time series residuals are plotted to show the differences between residual errors of ARMAX models from the reference and unknown time series.

In order to statistically measure this difference between residual errors, a statistical test has been employed in this study. Kolmogorov-Smirnov (KS) test is utilised to investigate whether two probability distributions alter or not based on the empirical distribution function properties. This statistical test is a nonparametric test according to which there is no need to have prior assumption regarding the distribution pattern of the time series residuals. In the literature, it was shown that the KS test shows sensitivity to place and shape differences of the ECDF of two time-series signals. Also, this test is more reactive to the points located at middle of the distribution rather than its tails. In addition, the KS test can provide more advantages compared to the traditional statistical features, such as mean, variance, skewness, and kurtosis [154, 155]. Because of these benefits, KS statistical test is considered as one of the most powerful statistical signal processing tools for time domain analysis applications.

This statistical method uses the comparison between two time-series data sets and inquires a hypothesis that the data sets come from the same probability distribution. Using this test, a statistical distance between the ECDFs of two samples can be measured. The null distribution

of this statics is estimated based on the hypothesis that the time series are produced using a similar distribution for a specific significance level. Using this method, the difference between two time-series data can be quantified. In this study, the proposed nonlinearity identification algorithm employs the two-sample KS test to examine the similarity and measure the distance between the residual errors of the reference linear and unknown (linear or nonlinear) time series samples.

First, an ARMAX model is fitted to the reference data set and the residual error is estimated representing the linear reference distribution as E_L. In this study, it was assumed that the behaviour of the structure is linear under a very low amplitude excitation and the ARMAX modelling can reliably simulate the dynamic behaviour of the structure. Then, the residual errors are estimated for unknown states representing the unknown distribution as E_{un}, when the structure is subjected to higher levels of excitation.

The KS test utilises a null hypothesis, according to which the ECDF of the residual from unknown state is similar to the ECDF of the reference distribution. According to this statistical test, the KS test statistical distance judges if the null hypothesis *H* is to be rejected for a specific confidence interval. The null hypothesis *H* is presented as follows:

$$H = null \quad hypothesis = \begin{cases} 1 & E_L \neq E_{un} \\ 0 & E_L \equiv E_{un} \end{cases} \tag{4.59}$$

By considering, $\hat{G}(E_L)$ and $\hat{G}(E_{un})$ as the ECDFs of residuals for the reference linear model and other unknown models, the KS test statistical distance NI_{KS}^{*} that presents the difference between two distributions is estimated using the following equation:

$$SD_{KS}^{*} = Statistical \quad dis\,tance = \max_{-\infty<t<\infty} \left| \hat{G}^{T_1}(E_L) - \hat{G}^{T_2}(E_{un}) \right| \tag{4.60}$$

In this equation, T_1 and T_2 are the lengths of the two time-series signals to be tested. By Considering:

$$T = \frac{T_1 T_2}{T_1 + T_2} \tag{4.61}$$

The null hypothesis *H* of the two distributions that are equal is rejected at significance level α , in case that $SD_{ks} = \sqrt{T} SD_{ks}^*$ is greater than the corresponding critical value.

As stated in [156], both residual errors and model coefficients of autoregressive models contain very important information related to any alterations in a structural system. The information associated with these two features has some similarity and overlaps, but they are not equal and combining these two features can provide more comprehensive essential information related to linear and nonlinear behaviours of a structural system. Therefore, considering the residual errors and model coefficients, the nonlinearity indicator is expressed as follows:

$$NI = Nonlinearity \quad Indicator = \left[SD_{KS}^* \times \left| f_L^{\,2} - f_{un}^{\,2} \right| \right] \times 100 \tag{4.62}$$

where f_L and f_{un} are the natural frequency extracted from reference linear and unknown ARMAX models, respectively. And SD_{ks}^* is the KS test statistical distance between two ECDFs of residual errors in the reference linear state and unknown state.

The nonlinearity indicator has been described, but still there is a need to define a threshold to categorise the linear and nonlinear behaviour of the target structure. In this study, it was decided to utilise Fuzzy C-Means clustering algorithm (FCM) to identify nonlinear behaviour of the structure from its vibration measurements. This algorithm was first presented in [157] and was recently used to solve SHM problems [158]. The FCM algorithm provides a fuzzy decision with the help of the membership of an index in a cluster and allows each data point to belong to multiple clusters with varying degrees of membership. This unsupervised classification algorithm minimises the specific objective function $F(D, m)$ as presented in Eq. (4.63).

$$\min F(D, m) = \sum_{i=1}^{D} \sum_{j=1}^{N} \lambda_{ij}^{m} \, d_{ij}^{\,2} \tag{4.63}$$

$$d_{ij}^{2} = \left(x_i - center_j\right)^T \left(x_i - center_j\right) \tag{4.64}$$

where *D* is the number of data points and *N* is the number of clusters. *m* is the fuzzy partition matrix exponent for controlling the degree of fuzzy overlap, with $m \geq 1$. Fuzzy overlap refers to how fuzzy the boundaries between clusters are, that is the number of data points that have significant membership in more than one cluster. x_i is the i^{th} object of data sets to be clustered, which is set to be NI values in this study. $center_j$ is the centre of the j^{th} cluster that is calculated using Eq. (4.65). λ_{ij}^{m} defines the degree of membership of x_i in the j^{th} cluster, which is updated using Eq. (4.66) in each iteration time. For a given data point, x_i, the sum of the membership values for all clusters is one.

$$center_j = \frac{\sum_{i=1}^{D} \lambda_{ij}^{m} x_i}{\sum_{i=1}^{D} \lambda_{ij}^{m}} \tag{4.65}$$

$$\lambda_{ij} = \frac{1}{\sum_{k=1}^{N} \left(\frac{\left\| x_i - center_j \right\|}{\left\| x_i - center_k \right\|} \right)^{\frac{2}{m-1}}} \tag{4.66}$$

To sum up, the FCM algorithm categorises the nonlinearity indicator values in five steps during clustering. First, the algorithm starts randomly select cluster membership values. Then, the cluster centres are calculated for each cluster. It should be mentioned that number of clusters is considered two in this study. In the third stage, the degree of membership for each data points is updated according to Eq. (4.66). Then, the algorithm calculates the objective function. Steps 2 to 4 are repeated until the objective function improves by less than a specified minimum threshold or until after a specified maximum number of iterations. At the end of optimisation process, the algorithm can categorise linear and nonlinear behaviours of the target structure using the degree of membership. This identification method can identify very early changes in a dynamic system immediately after earthquakes and before occurrence of structural damages.

To verify the validity of the method, a series of shaking table tests have been conducted on six spans of a small-scale steel truss bridge model. The vibration responses of the structure subjected to different amplitudes of real ground motions were used for data analysis and the test results will be provided in the next chapter.

4.5 Summary

In the first part this chapter, a computational platform was developed in MATLAB environment to enhance the performance of data management and analysis for SHM applications compared to the traditional file-based approaches. This toolbox is compatible and connected to the developed wireless smart sensor network to provide a full-package of vibration-based SHM system. Specifically, the analysis platform has been designed for structural modal identification, dynamic monitoring, easy development of graphical interface, and providing powerful tools for data processing. The developed system consists of two independent toolkits: the data management toolkit (DMT) designed for managing and processing large sets of SHM data and the data analysis toolkit (DAT) designed for structural modal identification. These toolkits have been connected to each other to provide an easy-to-use environment for condition assessment of structures. Various time domain and frequency domain system identification techniques were implemented into the toolbox to extract modal parameters from vibration measurements. The MATLAB toolbox was utilised for data management and extraction of dynamic characteristics of target civil structures throughout this research.

In the second part of this chapter, a new vibration-based nonlinearity identification technique was introduced based on residual errors and coefficients of autoregressive time series models. The proposed algorithm was developed to identify and categorise any nonlinear behaviour in civil structures, especially after earthquakes. The vibration-based nonlinearity identification technique utilises the time series Autoregressive Moving Average with Exogenous Inputs

(ARMAX) models, probability theory, and Fuzzy C-Means (FCM) clustering tehniuqe to categorise the linear and nonlinear dynamic behaviours of structural systems. The concept of this method was extracted from the fact that residual error of a linear ARMAX model follows a normal distribution. The validity of the proposed nonlinearity identification algorithm will be investigated using a series of shaking table tests on a small-scale steel bridge model.

Chapter 5: Experimental Verifications using a Series of Shake Table Tests

5.1 Introduction

A series of shaking table tests was conducted at Auckland University of Technology (AUT) structures test laboratory on a small-scale steel bridge model. This chapter presents the setup details of these tests, including description of the bridge model, instrumentation and data collection, and types of the excitation sources subjected to the bridge model. The main goals of these series of vibration tests are given as below.

1. The first goal of the shaking table testing was to validate the performance of new wireless smart sensor network developed as the first component of the integrated SHM system. The sensor system performance was investigated in terms of sensitivity and resolution, event-triggered sampling mode, and accuracy of time synchronisation protocols implemented in software architecture of the wireless network. To do so, the bridge model was instrumented using wireless smart sensor nodes and reference highly sensitive wired accelerometer sensors and subjected to various types of excitation source.
2. The second goal of the shake table testing was to validate the accuracy of vibration-based nonlinearity identification technique developed for condition assessment of bridge structures. In order to simulate nonlinear behavior in the bridge mode, rubber-based supports were utilised and the bridge model was subjected to various levels of excitation to control the level of nonlinearity.

5.2 Experimental test setup

A series of shaking table tests were performed on a steel truss bridge model to compare the sensitivity of the developed wireless sensors with high-performance wired accelerometers and to evaluate the event-triggered sampling mode and time synchronisation, when the bridge is

subjected to real ground motions. The tests were conducted at the Structural Laboratory of the Auckland University of Technology (AUT). A uniaxial shaking table, one of the biggest in New Zealand, was utilised to simulate different types and amplitudes of excitation forces to the bridge model. In this part of the chapter, the setup details of experimental tests conducted on the shake table are presented. They include descriptions of the steel truss bridge model, location and orientation of wireless and wired accelerometer sensors on the bridge model, details of shaking table and data acquisition system used for the tests.

5.2.1 Description of the steel bridge model

A six-span steel truss bridge model, made of MERO space frame joining system (Tube-Node system), was used as the testbed structure for these series of shaking table tests. The structural system consists of tubular steel members connected together with spherical forged steel ball joints. The tubes are connected to ball joints by means of a cone welded to the end of the tube through which a high tensile bolt is screwed into the ball by means of a sleeve. The dowel pin is used to constrain the bolt to the sleeve to facilitate turning of the bolt. The window on the sleeve permits the inspection of the amount of penetration of the bolt inside the ball joints. Each span of the bridge structure consists of horizontal and vertical steel tubes with the length of 60.5 cm and diagonal steel tubes with the length of 85.5 cm. The outer diameter of all the steel tubes is 2.0 cm with a thickness of 0.25 cm. In total, the six-span bridge structure has 42 of the horizontal and vertical elements, 22 of the diagonal elements, and 24 of the ball joints. ST37 steel with modulus of elasticity of 21×10^{11} N/mm^2 and weight per unit volume of 7850 kg/m^3 and Poisson ratio of 0.3 is used for the steel bridge model. Different views of the bridge model with the member dimensions are shown in Figure 5.1.

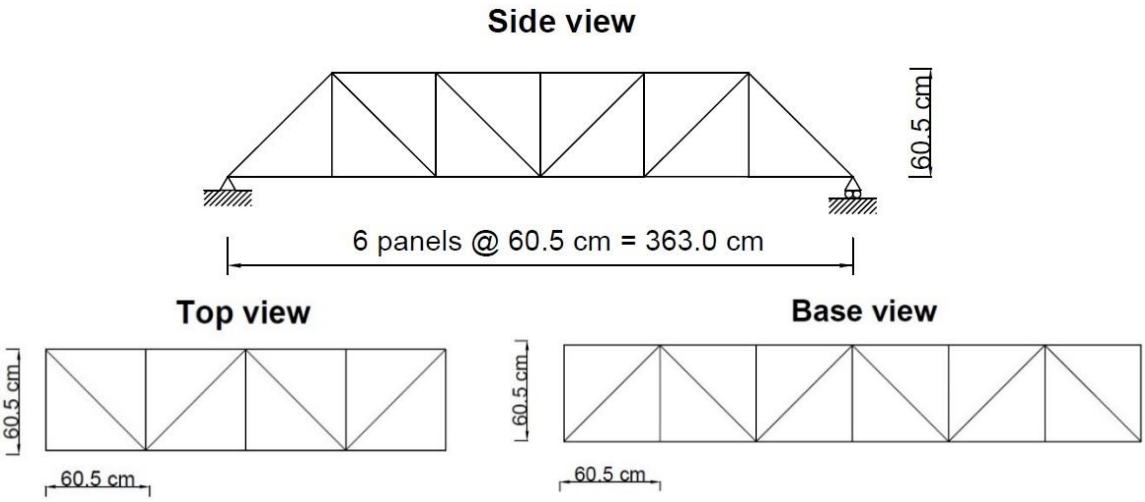

Figure 5.1 The six-span planar truss bridge model, side view, top view and the base view.

The full assembled structural model mounted on the shaking table are also depicted in Figure 5.2. In this figure, the steel ball joints and the pinned and roller ends used as the structural supports are also shown. As can be seen from the photos, the bridge model was placed on two pinned supports at one end and two roller supports at another end. The supports were mounted on timber base plates with the thickness of 7 mm. Then, the base plates were fixed to the shaking table using several strong bolts. As is obvious, the bridge model was aligned in diagonal direction of the shake table to simulate the real behaviour of bridge structures, when subjected to earthquake excitation. In addition, to provide high inertia mass for the bridge model during dynamic testing, five steel plates with dimension of 75.4 cm × 30 cm ×0.6 cm and with approximate weight of 10 kg were attached to top chord of the bridge in transverse direction of the structure. As shown in the figure, the bridge model was instrumented using wireless smart sensor nodes and reference wired accelerometer sensors. More details regarding the instrumentation and acquisition systems used for the dynamic testing will be provided in the following sections.

(a)

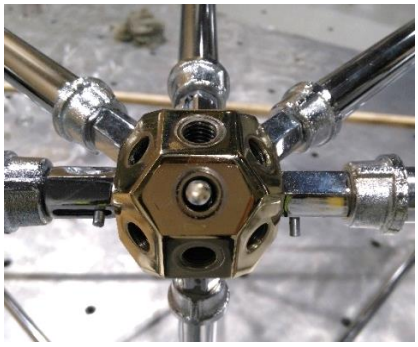

(b)

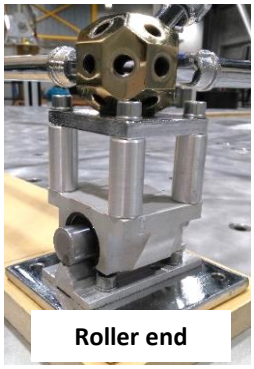

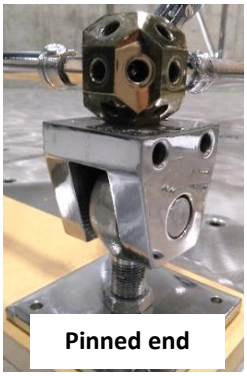

(c)

Figure 5.2. (a) The bridge model on the shaking table instrumented by wireless and wired accelerometers, (b) Steel ball joints, (c) roller and pinned Structural supports.

5.2.2 Instrumentation and data collection

As mentioned, the bridge model was instrumented using both wireless and wired accelerometer sensors. In total, eleven wireless smart sensor nodes were utilised for the vibration measurement during this series of dynamic testing. One wireless smart sensor node (WSSN0) was attached to the shake table to measure the ground motion excitations simulated using different types and amplitudes of excitation. Other wireless smart sensor nodes (WSSN1-WSSN10) were attached on top chord of the bridge to measure the structural responses due to various excitation sources.

In addition to the wireless sensor nodes, wired accelerometer sensors were also installed on the bridge model as the reference measuring system. A high-performance uniaxial wired accelerometer sensor, model 4610A manufactured by TE Connectivity [159], was selected as the reference system. This sensor is an ultra-low-noise accelerometer with a nominal sensitivity of 1011 mV/g, frequency range of 20-200 HZ, measurement ranges of ±2 g to ±100 g, and noise level of 2 μg/rms over 0-400 Hz. This high-performance accelerometer was designed for low-frequency static and dynamic vibration measurements. Figure 5.3 depicts the new developed wireless smart sensor node and the high-performance wired accelerometer sensor attached to the steel ball joints.

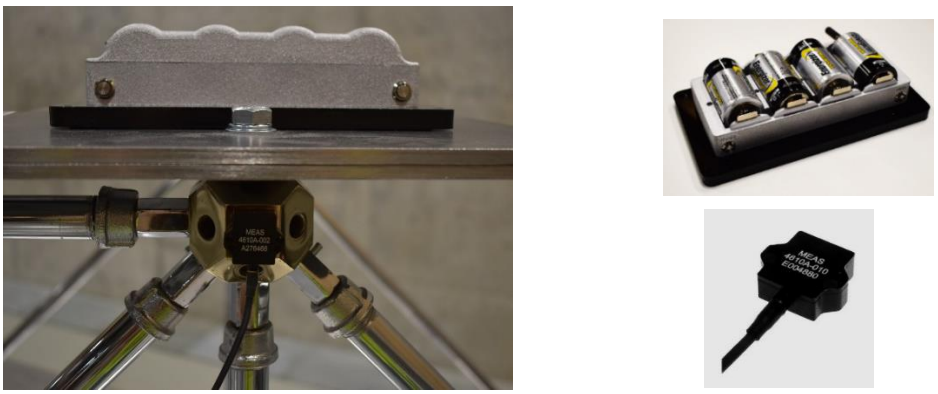

Figure 5.3. The wireless smart sensor node and the high-performance wired accelerometer.

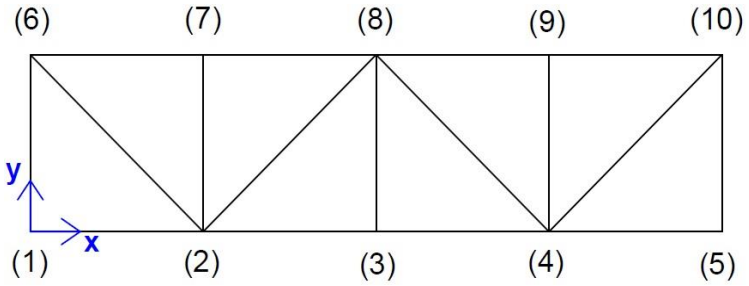

Figure 5.4. The locations of sensors on top chord of bridge (plan view).

Similar to the wireless accelerometer sensor nodes, one wired accelerometer (ACC0) was located on the shake table to measure the various ground motions simulated by the shake table. In addition, the ten wired accelerometers (ACC1-ACC10) were attached to the steel joints at top chord of the bridge to measure the structural responses. In order to provide more accurate

comparison between the measurements, both the wireless and wired accelerometer sensors were perfectly attached to the structure in approximately same locations. The locations and orientation of the wireless and wired accelerometer sensors are shown in Figure 5.4.

Table 5.1. Characteristics of the channels utilised throughout the testing.

Channel	Type	Sensitivity	Measurement point
0	Wired/Wireless	1011 mV/g / 256,000 LSB/g	Ground motion
1	Wired/Wireless	1011 mV/g / 256,000 LSB/g	Structural response @ joint 1
2	Wired/Wireless	1011 mV/g / 256,000 LSB/g	Structural response @ joint 2
3	Wired/Wireless	1011 mV/g / 256,000 LSB/g	Structural response @ joint 3
4	Wired/Wireless	1011 mV/g / 256,000 LSB/g	Structural response @ joint 4
5	Wired/Wireless	1011 mV/g / 256,000 LSB/g	Structural response @ joint 5
6	Wired/Wireless	1011 mV/g / 256,000 LSB/g	Structural response @ joint 6
7	Wired/Wireless	1011 mV/g / 256,000 LSB/g	Structural response @ joint 7
8	Wired/Wireless	1011 mV/g / 256,000 LSB/g	Structural response @ joint 8
9	Wired/Wireless	1011 mV/g / 256,000 LSB/g	Structural response @ joint 9
10	Wired/Wireless	1011 mV/g / 256,000 LSB/g	Structural response @ joint 10

It should be mentioned that the wired accelerometer sensors could record the structural vibrations only in transverse direction of the structure. The wireless smart sensor nodes could measure the bridge model responses in three directions (Transverse, longitudinal, and vertical directions). It means that X axis of the wireless sensor nodes is along with the longitudinal direction of bridge mode, Y axis is along with the transverse direction, and Z axis is along with the vertical direction. It should be mentioned that the wireless and wired accelerometer sensor nodes attached to the shake table for ground motion measurements are respectively presented as WSSN0 and ACC0. This numbering is used during this thesis for data analysis. Table 5.1 shows the characteristics of wireless and wired sensor nodes used for vibration measurement.

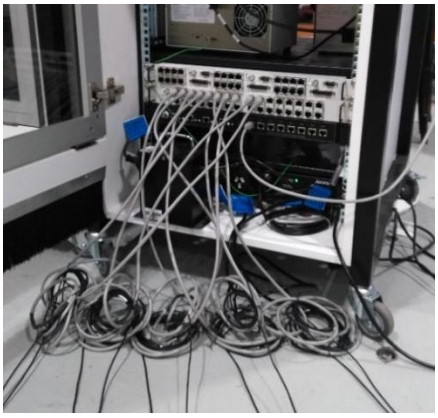

(a) **(b)**

Figure 5.5. (a) The XBee-Pro module for data transmission for wireless sensor system, and (b) data acquisition and transmission for the wired sensor system.

Figure 5.5 shows the data acquisition and transmission used for wireless and wired sensor systems during the vibration testing. Figure 5.5(a) shows the XBee-Pro S2C 802.15.4 Radio-Frequency module that was used for wireless sensor system. As mentioned in chapter 3, this module can provide wireless connectivity to end-points devices (wireless sensor nodes) in both ZigBee and DigiMesh topologies. The vibration data sets measured using wireless smart sensor nodes were wirelessly transferred to the monitoring PC using this module. It is also responsible for sending various commands to the wireless sensor nodes to set the network for different operational modes. More details about this module can be found in chapter 3. The recorded vibration data sets using different channels of wireless sensor nodes were transferred and saved as text files in a specific folder of the monitoring PC. For wired sensor system, the National Instrument Data Acquisition system (NI-DAQ) (Figure 5.5(b)) was utilised to convert the analogue signals recorded by the accelerometer sensors to digital counterparts. As is obvious from the figure, all the wired accelerometer sensors were attached to the DAQ using long cables. A software developed in LabVIEW program was used to read the acceleration time-series from NI-DAQ and save them as a text file.

5.3 Performance of the wireless smart sensor network

In this part of the thesis, the vibration measurements recorded using both wireless and wired accelerometer sensors are used to validate the performance of the developed wireless smart sensor network. The performance of the wireless sensor network is investigated in terms of sensitivity and event-triggered sampling mode of the smart accelerometer sensor nodes and time synchronisation protocols considered for the wireless network. To do so, the analysis results are provided after presentation of the excitation sources subjected to the bridge model.

Table 5.2. Characteristics of the excitation sources used for dynamic testing.

Name	Type	Amplitude
Test 1	Sine Sweep Excitation	0.2 mm
Test 2	El Centro Earthquake	8.5 mm
Test 3	El Centro Earthquake	21 mm
Test 4	El Centro Earthquake	43 mm
Test 5	El Centro Earthquake	85 mm
Test 6	Chi-Chi Earthquake	6.0 mm
Test 7	Chi-Chi Earthquake	100 mm
Test 8	Chi-Chi Earthquake	190

5.3.1 Excitation sources

As mentioned, a uniaxial shake table was used for these series of dynamic tests to simulate various types of ground motions as excitation sources. This shake table, considered as one of the largest in New Zealand, has 14 and 10 grinds in longitudinal and transverse directions, each with a dimension of 25 cm × 25 cm. The shaking table has a dimension of 4 m × 3 m with a maximum displacement of ±200 mm in longitudinal direction. The software is able to set and control the high capacity device to simulate different types of excitation sources, such as real and artificial ground motions, white noise signals, sine sweep signals, and etc. In this study,

two types of excitation sources, including the past recorded earthquake signals and sine sweep waves with different frequency ranges and amplitudes were simulated and subjected to the bridge model. The characteristics of these input signals are given in Table 5.2.

5.3.2 Sensitivity and resolution

In this section, the analysis results obtained regarding the resolution and sensitivity of the new wireless smart sensor nodes are presented. To show the performance of wireless smart sensor nodes, various tests with different excitation sources and measuring channels were conducted on the bridge model and the results of some of these tests are presented here. First, the bridge model was subjected to a sine sweep signal with peak amplitude of 0.2 mm and frequency range of 6-6.4 Hz.

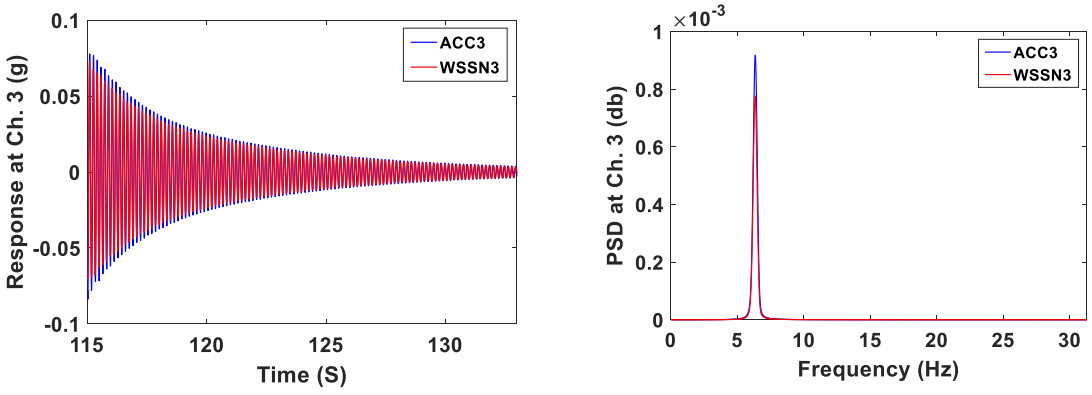

(a) **(b)**

Figure 5.6. (a) a time window of acceleration time histories, and (b) PSD values, measured using wireless and wired accelerometer sensors in transverse direction during Test 1.

A time window of acceleration time histories and the corresponding Power Spectral Density (PSD) measured using channel 3 of the wireless smart sensor node (WSSN3) and the wired accelerometer sensor (ACC3), which were located in mid-span of the bridge, are presented in Figure 5.6. As is clear from the result, there is a perfect match between the time domain and frequency domain results measured using the developed wireless sensor node and the reference wired accelerometer. The vibration data sets measured using both wired and wireless sensor

systems match very well showing the high sensitivity of the wireless smart accelerometer sensor node in measuring low amplitude vibrations.

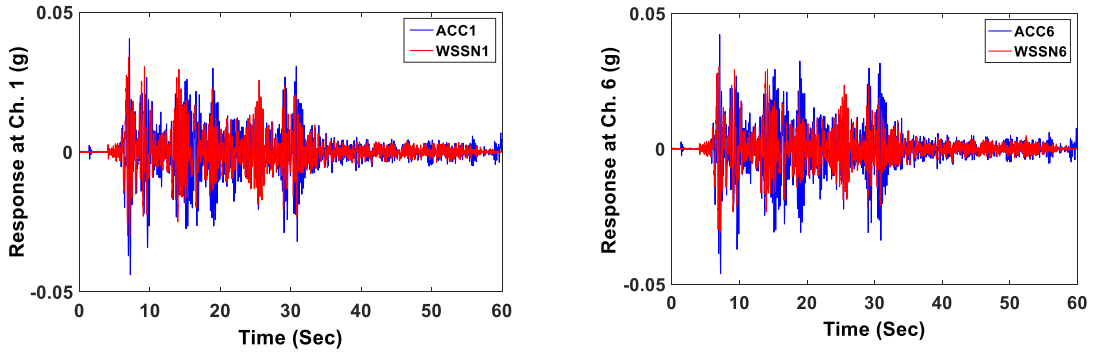

(a) Channel 1 **(b) Channel 6**

Figure 5.7. Acceleration time histories recorded in X direction (longitudinal) by wireless and wired accelerometers during Test 2.

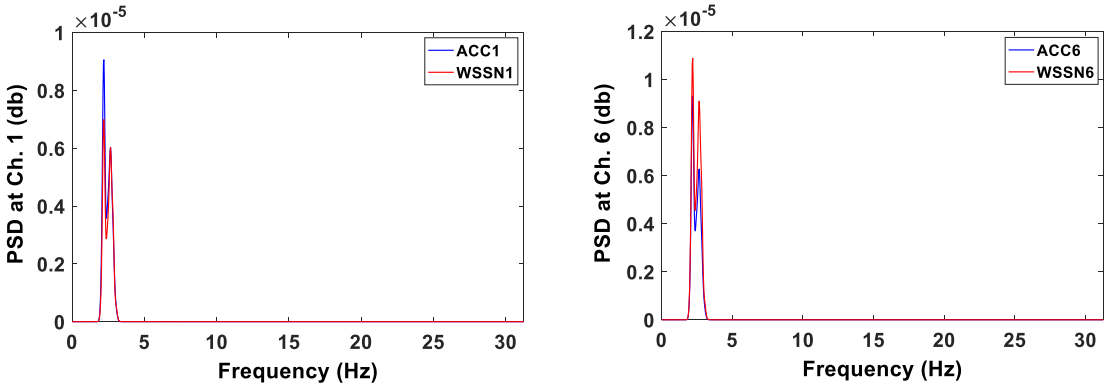

(a) Channel 1 **(b) Channel 6**

Figure 5.8. Natural frequencies measured in longitudinal direction (X direction) by wireless and wired accelerometers during Test 2.

As the uniaxial wired accelerometer sensor can measure the structural vibration only in transverse direction of the bridge model, two more wired accelerometer sensors were installed on joints 1 and 6 of the bridge in X direction to measure the structural responses in longitudinal direction of the structure. It should be mentioned that the wireless smart sensor nodes are able to measure both the longitudinal and transverse structural responses using X and Y axes. Figure 5.7 presents the acceleration time histories measured using channel 1 and channel 6 of the wireless and wired accelerometers in longitudinal direction (X direction) of the bridge model during Test 2. The bridge model was subjected to the El Centro Earthquake with a low

amplitude of 8.5 mm and duration of one minute. Figure 5.8 also shows the corresponding PSD values of the acceleration time series presented in Figure 5.7. As can be seen from the results, the amplitude of acceleration time series measured using the two channels match fairly. It should be mentioned that the small differences that can be observed in these figures is because the measurements from wired and wireless sensors are not perfectly synchronised as they were sampled using different acquisition systems. In addition, the frequency domain parameters extracted from the acceleration time histories shows a perfect match and both the PSD values measured from WSSN1 and WSSN6 are equal.

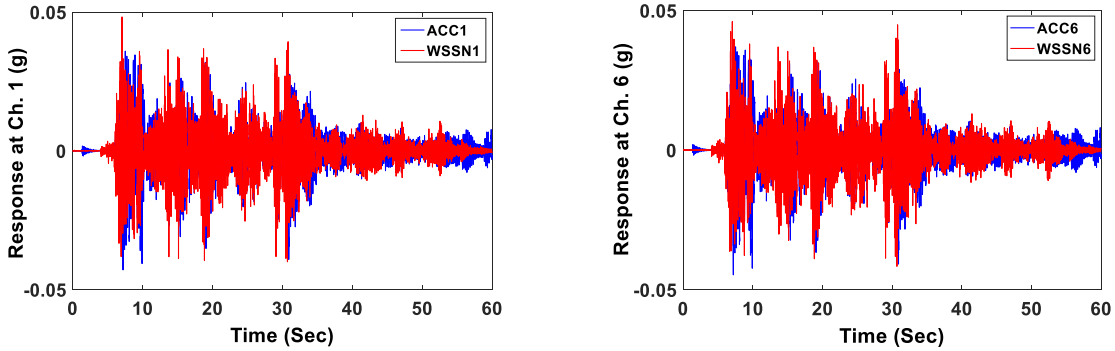

(a) Channel 1 **(b) Channel 6**

Figure 5.9. Acceleration time histories recorded in Y direction (Transverse) by wireless and wired accelerometers during Test 2.

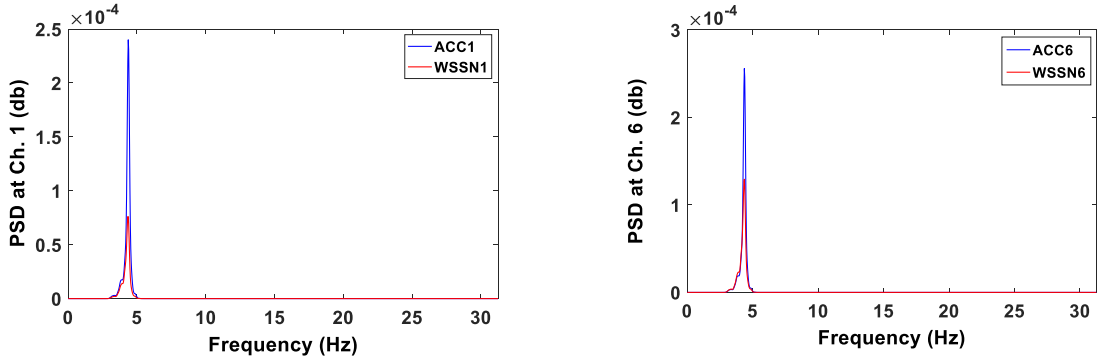

(a) Channel 1 **(b) Channel 6**

Figure 5.10. Natural frequencies measured in Transverse direction (Y direction) by wireless and wired accelerometers during Test 2.

The acceleration time histories and the corresponding PSD values recorded in transverse direction of the bridge model during Test 2 also depicted in Figures 5.9 and 5.10, respectively. The vibration data sets presented in these figures were measured using channel 1 and 6 of the

wired and wireless accelerometer sensors. It can also be observed that there is a good match between the time domain and frequency domain results obtained during Test 2.

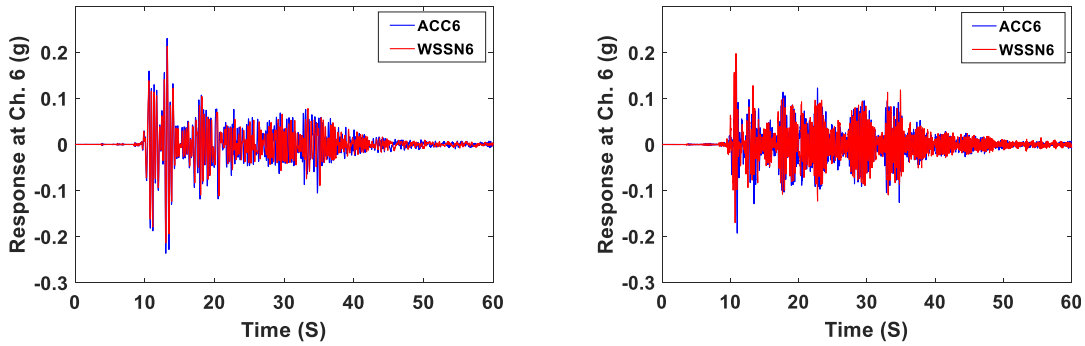

(a) X direction (longitudinal) **(b) Y direction (Transverse)**

Figure 5.11. Acceleration time histories recorded by wireless and wired accelerometers in longitudinal and transverse directions during Test 4.

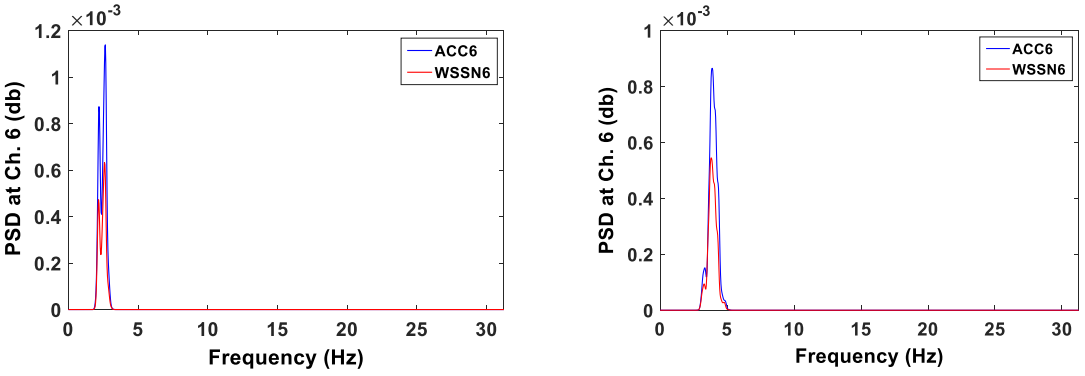

(a) X direction (longitudinal) **(b) Y direction (Transverse)**

Figure 5.12. Natural frequencies recorded by wireless and wired accelerometers in longitudinal and transverse directions during Test 4.

In another attempt, the bridge model was excited to a moderate amplitude earthquake. To do so, El Centro Earthquake with an amplitude of 43 mm and duration of one minute was subjected to the system. The acceleration time histories and the corresponding natural frequencies measured using channel 1 in both transverse and longitudinal directions of the structures are shown in Figures 5.11 and 5.12, respectively. As can be seen, there is a near to perfect match between acceleration and natural frequencies obtained using wireless smart sensor node and the reference wired accelerometer in both directions of the bridge model.

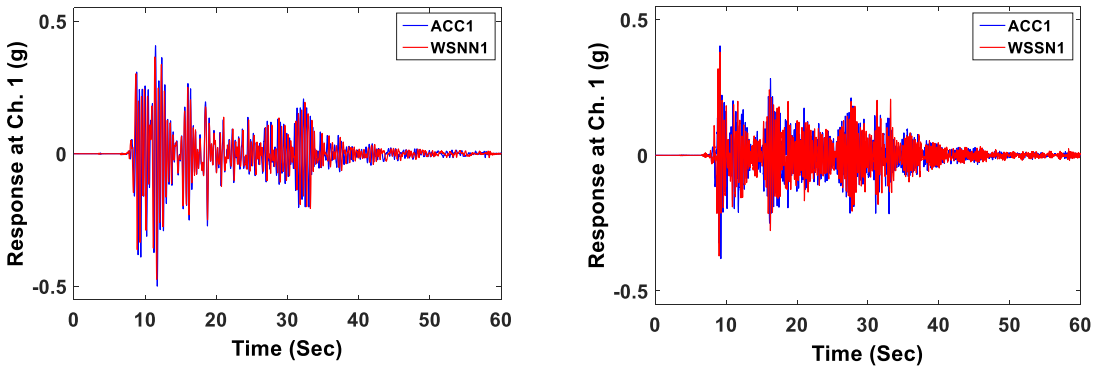

(a) X direction (longitudinal) **(b) Y direction (Transverse)**

Figure 5.13. Acceleration time histories recorded by wireless and wired accelerometers in longitudinal and transverse directions during Test 5.

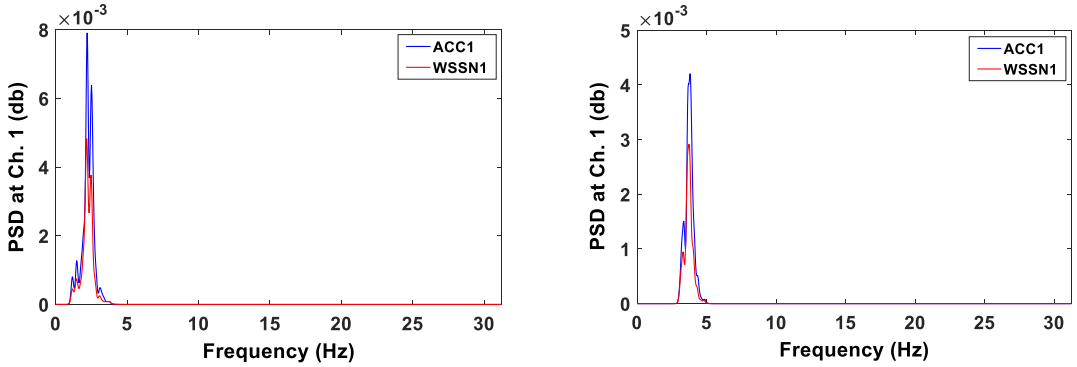

(a) X direction (longitudinal) **(b) Y direction (Transverse)**

Figure 5.14. Natural frequencies measured by wireless and wired accelerometers in longitudinal and transverse directions during Test 5.

The bridge model was also subjected to a high amplitude ground motion representing El Centro Earthquake. The bridge was subjected to El Centro Earthquake with a high peak amplitude of 85 mm. Figure 5.13 presents the acceleration time histories recorded by WSSN1 and ACC1 in both longitudinal and transverse directions. By comparing the amplitudes of acceleration time histories recorded by both wireless and wired accelerometers, it can be concluded that the wireless accelerometer sensor node measured the structural responses in both directions of the bridge with a high accuracy comparing to the reference wired accelerometers. Figure 14 also presents the PSD values of recorded acceleration time histories showing a very good match between the results obtained using wireless and wired accelerometers.

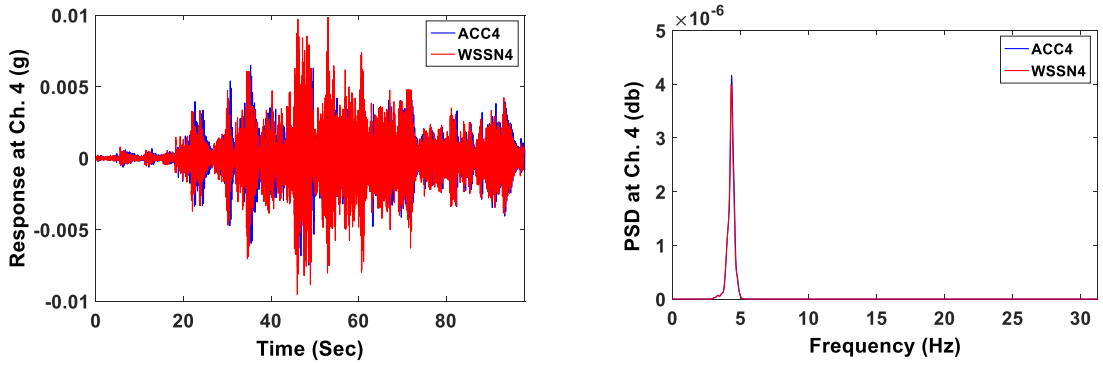

Figure 5.15. Acceleration time histories and natural frequencies measured by channel 4 in transverse direction during Test 6.

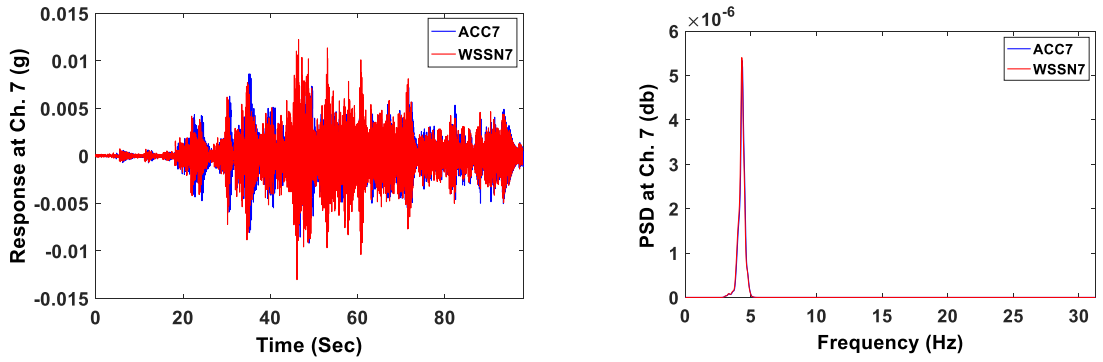

Figure 5.16. Acceleration time histories and natural frequencies measured by channel 7 in transverse direction during Test 6.

To investigate on consistency of the analysis results, the bridge was subjected to the Chi-Chi Earthquake. Different amplitudes of this earthquake were considered, including a low amplitude of 6 mm (Test 6), a moderate amplitude of 100 mm (Test 7), and a high amplitude of 190 mm (Test 8). Figures 5.15 and 5.16 presented the acceleration time histories and the corresponding PSD values measured in transverse direction of the bridge model by channels 4 and 7 during Test 6, respectively. It can be observed from the time and frequency domains analysis results that the wireless smart sensor nodes were able to record the low amplitude earthquake-induced vibrations during Test 6 as accurate as the wired accelerometers did.

Figures 5.17 and 5.18 also presented the results obtained for the first transverse natural frequency of the bridge model. These results were obtained during the moderate and high amplitudes of the Chi-Chi Earthquake excitations, i.e. Test 7 and Test 8, using channels 4 and 7 of the wireless and wired accelerometer sensors. The perfect match and consistency of the

first transverse natural frequency obtained from different channels of wireless smart sensor nodes that shows their high sensitivity compared to the reference sensor system.

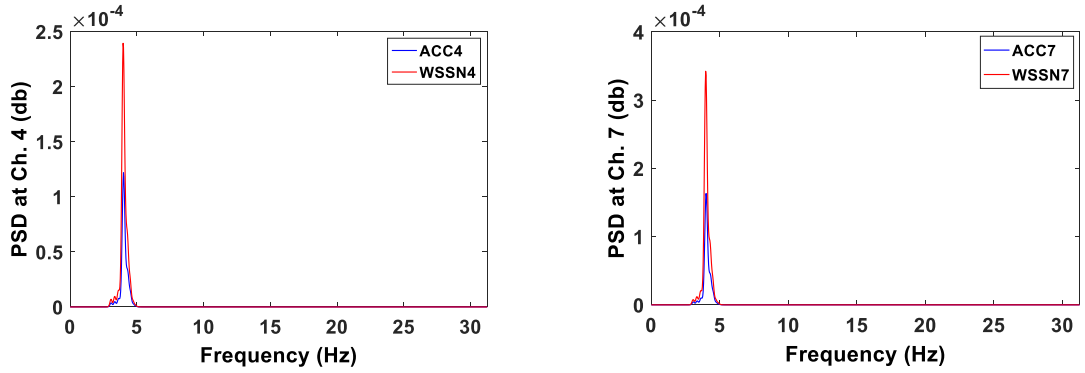

(a) Channel 4 **(b) Channel 7**

Figure 5.17. Natural frequencies measured in transverse direction during Test 7.

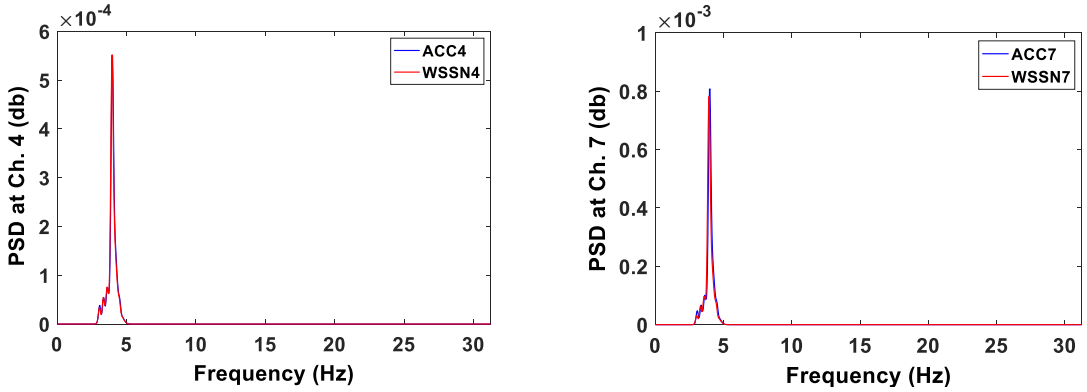

(a) Channel 4 **(b) Channel 7**

Figure 5.18. Natural frequencies measured in transverse direction during Test 8.

In total, the results presented in this section from the dynamic tests showed that the newly developed wireless smart accelerometer sensor nodes can measure structural vibrations induced by different types and amplitudes of excitation sources with a high resolution and sensitivity. It is noteworthy that the sampling frequency was set to 62.5 Hz for both wired and wireless accelerometer sensors during all the dynamic tests.

5.3.3 Event detection feature

In this section, in order to evaluate the event detection feature of the wireless smart accelerometer sensor, the results obtained from another series of dynamic tests are presented. To this end, the wireless smart sensor nodes were set to event-triggered sampling mode using

the GUI introduced in chapter 3. According to this mode, the wireless accelerometer sensors can record the event-induced vibrations with sampling frequency of 125 Hz for 60 seconds. For an accurate comparison between the wired and wireless sensor systems, the wired accelerometer sensors were also set to sample the structural vibrations at 125 Hz. Although the bridge model was subjected to various levels of excitation sources to investigate the accuracy of this sampling mode, the results of two dynamic tests are presented here. El Centro with a high amplitude of 85 mm was subjected to the bridge model as the sudden event to trigger the wireless smart sensor nodes. The vibration threshold for this test was set to 100 mg. It means that in the case of occurrence of any event that has greater amplitude than 100 mg, the ADXL362 accelerometer wakes up the sensor board to start sampling the event using the high performance ADXL355 accelerometer chip integrated into the sensor board.

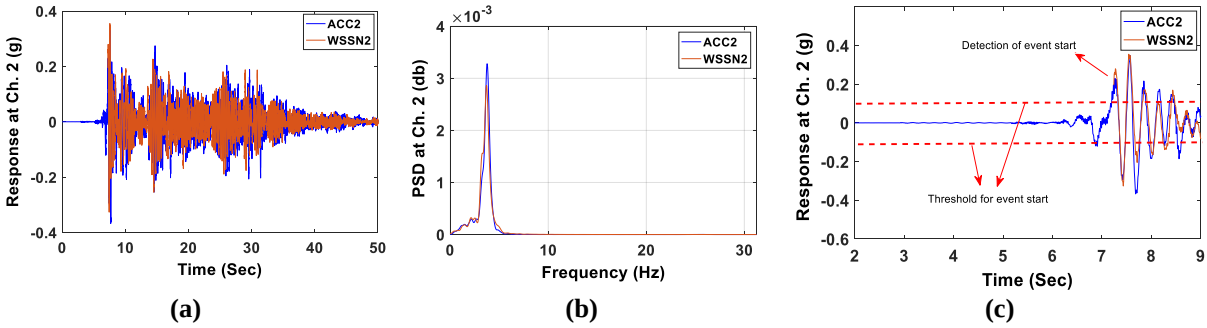

Figure 5.19. (a) Acceleration time histories, (b) PSD values, and (c) acceleration time histories for the event start measured using channel 2 during Test 5.

Figure 5.19 shows the acceleration time histories of the earthquake-induced vibration and the corresponding PSD values measured using channel 2 of the wired and wireless accelerometer sensors. As is obvious from the figure, after the first peak greater than 100 mg, the WSSN2 was awakened to log the structural responses. The acceleration time histories and corresponding PSD values obtained using the wireless node and the reference wired accelerometer matched well showing the ability of the wireless sensor to detect and record the event with a high precision. In order to present the consistency of the results, the results obtained by another channel of wireless sensor nodes is presented in Figure 5.20.

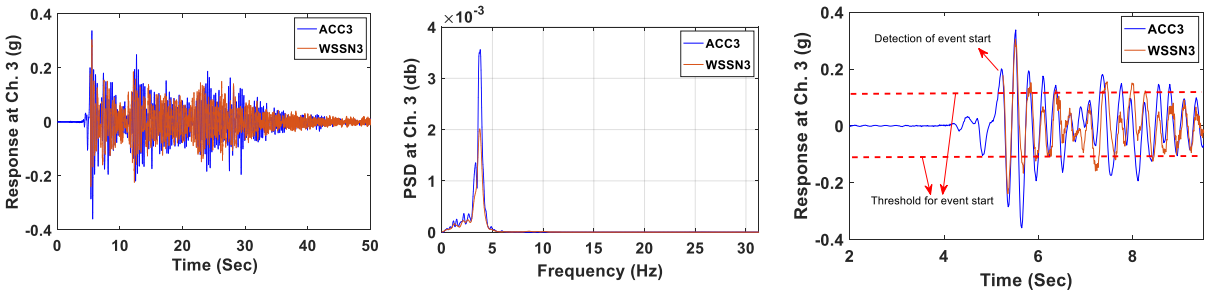

(a) **(b)** **(c)**

Figure 5.20. (a) Acceleration time histories, (b) PSD values, and (c) acceleration time histories for the event start measured using channels 3 during Test 5.

This figure depicts the time and frequency domain results obtained using channel 3 of the wired and wireless accelerometer sensors located in middle of the bridge span. As is clear, WSSN3 was able to detect and record the earthquake-induced vibration when the structural vibration exceeds 100 mg. In total, the results presented in this section shows that the event detection sampling mode of the developed wireless smart sensor node performs accurately for measuring various amplitudes of excitation sources.

All the wireless sensor nodes installed on the bridge structure were awakened as the vibration levels on the structural joints, where the wireless sensor nodes were installed, exceeded the predefined threshold during the two tests. It should be mentioned that with the current software setting of the wireless sensor nodes, the first few samples of the event cannot be logged and are missed. However, in the future development of the wireless smart sensor nodes, the first peak of the event-induced vibration will be added to the time series signal. It is noteworthy that all the data analysis carried out on the vibration data sets was performed using the new MATLAB-based toolbox.

5.3.4 Time synchronisation

The accuracy of time synchronisation protocols presented in Chapter 3 in development of wireless smart sensor nodes is investigated here using the vibration data sets measured during the dynamic tests. To do so, the vibration data recorded by various channels of wireless smart

sensor nodes are utilised. Figures 5.21 and 5.22 present the acceleration time histories measured by various channels of wireless sensor nodes in transverse and longitudinal directions. These vibration data sets were recorded during Tests 4 and 8 and then synchronised using the developed MATLAB-based toolbox. It was observed that the measurements recorded by different channels of wireless sensor nodes were well synchronised and the sensors maintained phase among themselves with a maximum synchronisation error of 1 millisecond. It can be concluded that they can be reliably used for damage identification techniques based on modal parameters. These results also confirm that the synch pulse as the pre-processing technique and the post-processing time synchronisation techniques could accurately synchronise different channels of the wireless sensor nodes.

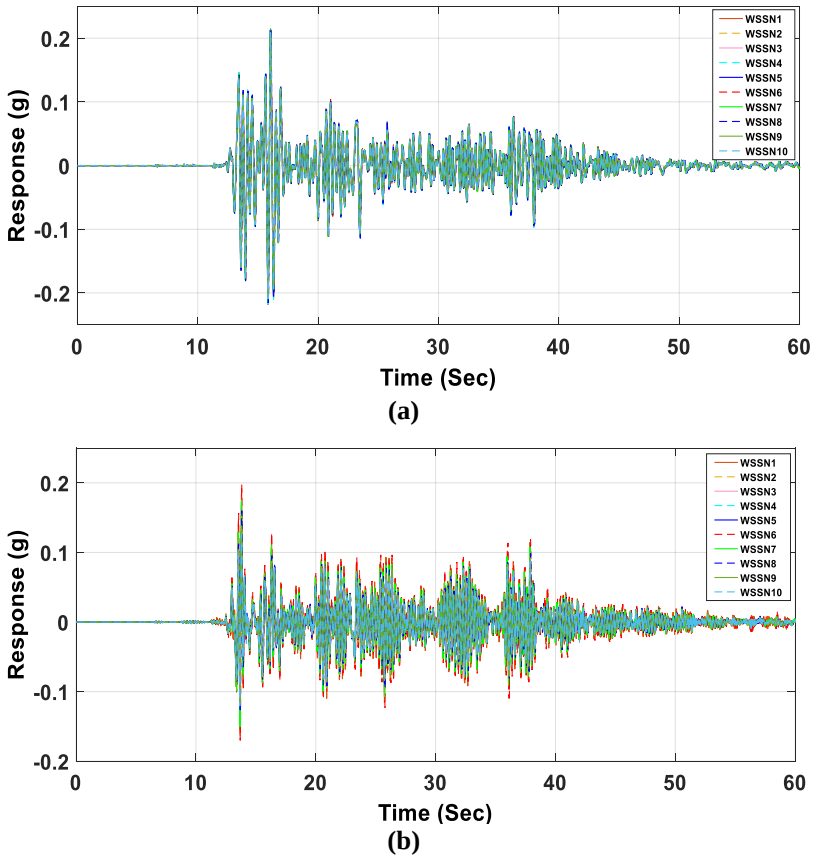

Figure 5.21. Acceleration time histories measured using ten wireless sensor nodes in (a) Longitudinal direction, and (b) Transverse direction of the bridge model during Test 4.

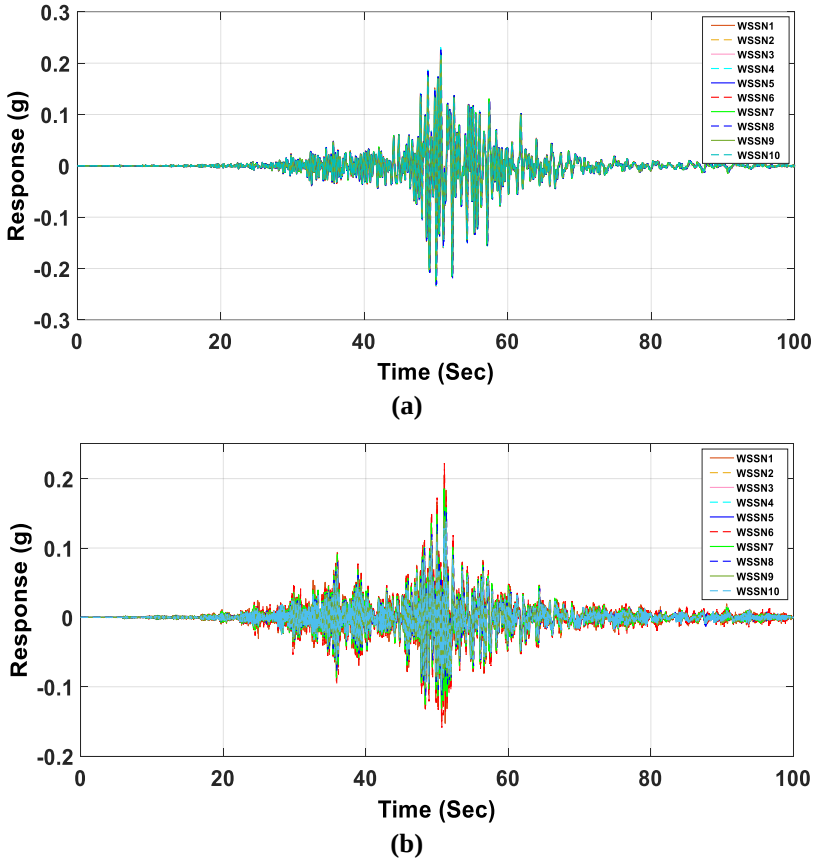

Figure 5.22. Acceleration time histories measured using ten wireless sensor nodes in (a) Longitudinal direction, and (b) Transverse direction of the bridge model during Test 8.

5.4 Vibration-based nonlinearity identification test results

In this part, another series of shaking table test on the small-scale bridge model are presented. The purpose of these dynamic tests was to validate the accuracy of the proposed vibration-based nonlinearity identification technique introduced in the previous chapter. First, some descriptions are provided regarding the test instrumentation and setup. Then, the analysis results obtained using the new nonlinearity identification algorithm are presented.

5.4.1 Description of shaking table tests

As mentioned, the steel bridge model was supported using two roller and two pinned supports. In order to simulate nonlinear behaviour in the bridge structure, four rubber mounts were attached to each pinned support of the bridge model. The mounts, made of natural rubber, were

cylindrically shaped in diameter of 30 mm and height of 40 mm. Due to the characteristics of rubbers in shear, they were selected as the main source of nonlinearity for the bridge structure. Using these elements, different levels of nonlinearity can be simulated using various amplitudes of excitation source. To do so, the bridge model was excited using different amplitudes of ground motion to control the nonlinearity degree of rubber-based supports. Figure 5.23 (a) shows one of these rubber-based supports.

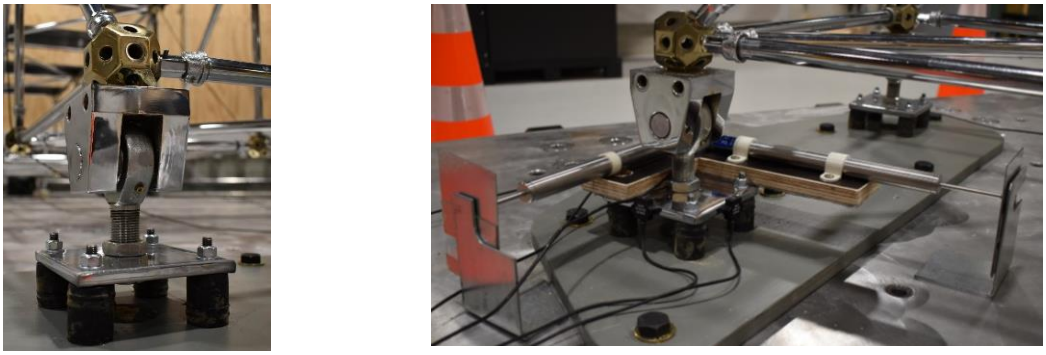

(a) (b)

Figure 5.23. Rubber-based pinned support, and (b) Instrumentation setup of the support.

Table 5.3. Characteristics of the sensors utilised throughout the dynamic tests.

Channel	Direction	Location
ACC 0	-	Shake table
ACC 1	Transverse	joint 1
ACC 2	Transverse	joint 2
ACC 3	Transverse	joint 3
ACC 4	Transverse	joint 4
ACC 5	Transverse	joint 5
ACC 6	Transverse	joint 6
ACC 7	Transverse	joint 7
ACC 8	Transverse	joint 8
ACC 9	Transverse	joint 9
ACC 10	Transverse	joint 10
ACC 11	Longitudinal	joint 6
ACC 12	Longitudinal	joint 1
ACC 13	Transverse	Rubber base
ACC 14	Longitudinal	Rubber base
LVDT 0	Transverse	Rubber base
LVDT 1	Longitudinal	Rubber base

It should be mentioned that same data acquisition system was utilised for these series of dynamic tests. The bridge model was instrumented using wired accelerometer sensors and LVDTs for this test setup in order to measure structural responses under different excitations. Table 5.3 shows characteristics of the wired accelerometers and LVDTs utilised for the tests. This table presents the name of channels, their measurement directions, and their locations on the bridge model. In total, 14 wired accelerometer sensors were attached to the steel joints to measure the structural responses. One wired accelerometer (ACC0) was located on the shake table to measure the ground motions simulated by the shake table. Ten wired accelerometers (ACC1-ACC10) were attached to the steel joints, joint 1 to joint 10, at top chord of the bridge to measure the structural responses in transverse direction. The location and orientation of these accelerometers have been shown in Figure 5.4. Due to the fact that the wired accelerometers can measure the structural responses in one direction (*y* direction), two more accelerometer sensors (ACC11-ACC12) were attached to joint 6 and joint 1 in longitudinal direction of the bridge. To monitor the nonlinearity degree of rubber-based supports, two accelerometer sensors (ACC13-ACC14) and two LVDTs (LVDT0-LVDT1) were installed on one of the supports in both transverse and longitudinal directions as shown in Figure 5.23 (b). The measurements from these sensors have been used to simulate the acceleration-displacement relationships of the rubber-based support under various excitation sources.

Table 5.4. Characteristics of the excitation sources used for dynamic testing.

Name	Type	Amplitude (mm)
Test 1	Sine Sweep Excitation	0.05, 0.1, 0.3, 0.7, 1, 2
Test 2	El Centro Earthquake	0.9, 13, 17, 35, 43, 52, 63, 70, 79, 83, 87, 98
Test 3	Chi-Chi Earthquake	6.5, 13, 26, 54, 100, 130, 190, 210
Test 4	Tabas Earthquake	4, 8, 16, 32, 64, 80, 120, 145, 160, 18, 190

As mentioned to simulate different degrees of nonlinearity in the structure, the bridge model was subjected to several ground motions with various amplitudes. The characteristics of the excitation sources used during the dynamic tests are given in Table 5.4, including their name, type, and amplitude.

5.4.2 Data analysis and results

In this part, the analysis results obtained using the new developed nonlinearity identification algorithm are presented using the vibration data measured from the bridge model. First, in order to show the nonlinear behaviour of the rubber-based supports during high amplitude of excitation, the acceleration-displacement graphs obtained from the instrumented rubber-based support are presented. To do so, the bridge model was excited using different amplitudes of two excitation sources, including sine sweep signal and El Centro earthquake.

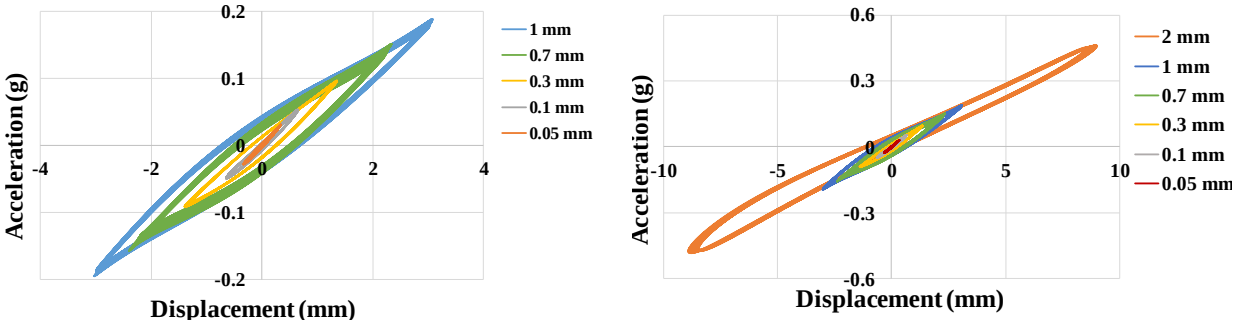

Figure 5.24. Acceleration-displacement graphs obtained from rubber-based support during Test 1.

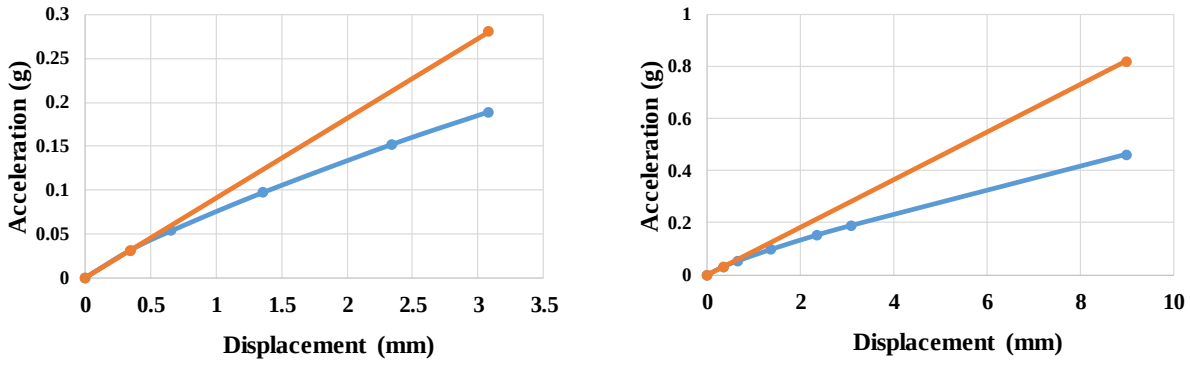

Figure 5.25. Backbone curves obtained from rubber-based support during Test 1.

Figure 5.24 shows the force-displacement graphs obtained from the rubber-based support during the sine sweep excitation in transverse direction of the bridge structure. The sine sweep

excitation was applied to the structure with different amplitudes started from a minimum of 0.05 mm to a maximum of 2.0 mm and frequency range of 6-6.4 Hz. Figure 5.25 also presents the corresponding backbone curves of the force-displacement hysteresis loops shown in Figure 5.24. As presented in these figures, the structure started to behave nonlinearly with the increase in excitation amplitude, as the slop of acceleration-displacement graphs starts to reduce gradually. It can be concluded from the results that the stiffness of the system starts to decrease after an amplitude of 0.1 mm.

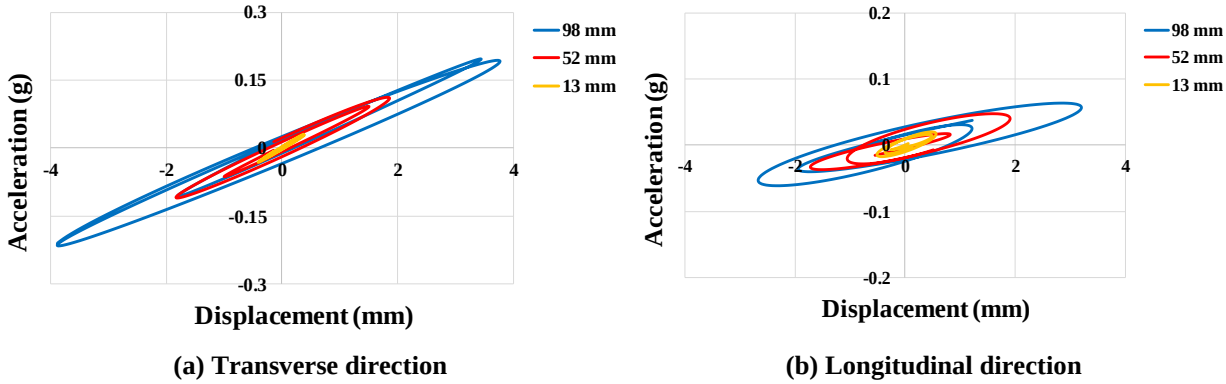

Figure 5.26. Acceleration-displacement graphs obtained from rubber-based support during Test 2.

Figure 5.26 also presents the acceleration-displacement graphs obtained from the rubber-based support during three different amplitudes of El Centro earthquake in both transverse and longitudinal directions. These results were extracted by considering just a few samples of data with maximum amplitudes. Similar to the sine sweep excitation, the bridge model showed nonlinear behaviour (reduction in stiffness) with the increase in excitation amplitudes. The reduction in slope of acceleration-displacement graphs is more obvious in longitudinal direction of the bridge model. It can be concluded that the rubber-based supports of the bridge model can represent the material nonlinearity type in the structural system. It should be mentioned that this category of nonlinearity is one of the most common nonlinearity types in real-world civil infrastructures, such as bridges. After confirming the presence of the

nonlinearity in the structural system using the rubber-based supports, the analysis results obtained using the nonlinearity identification algorithm are presented.

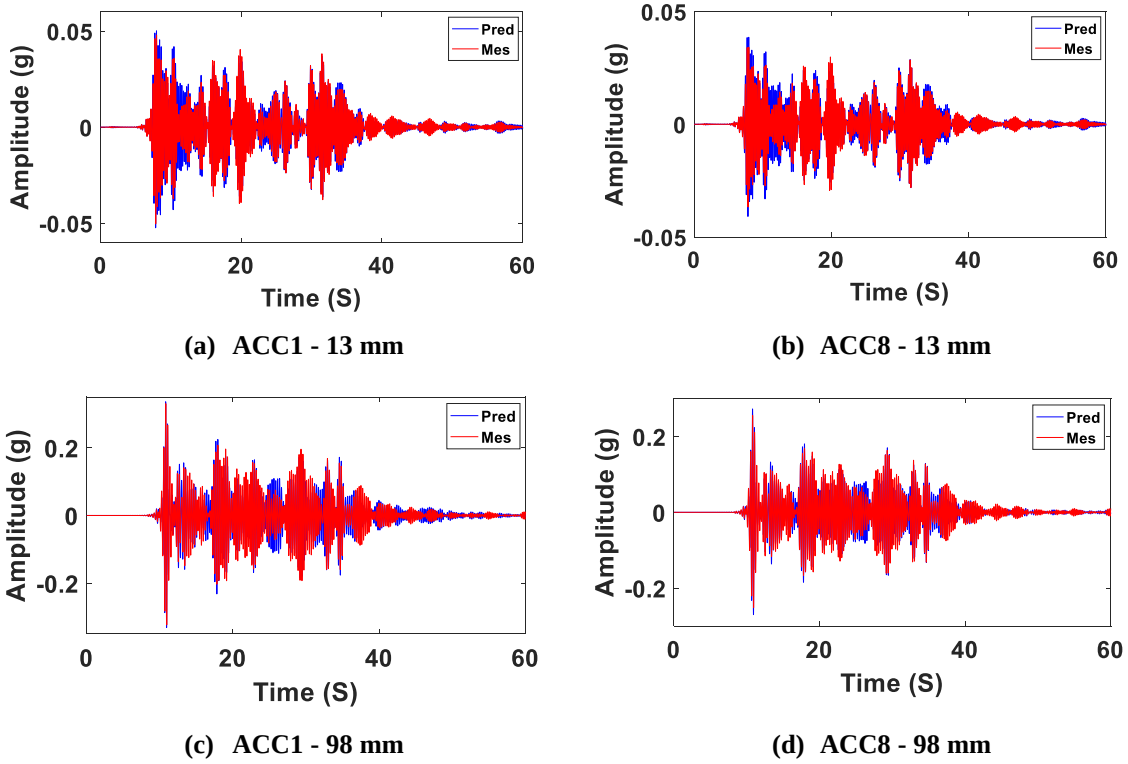

(a) ACC1 - 13 mm **(b) ACC8 - 13 mm**

(c) ACC1 - 98 mm **(d) ACC8 - 98 mm**

Figure 5.27. Measured and predicted responses recorded during Test 2 in transverse direction.

During the dynamic testing, the bridge model was subjected to three well-known ground motions; 1940 El Centro earthquake, 1999 Chi-Chi earthquake, and 1978 Tabas earthquake. A low amplitude of each earthquakes was applied to the bridge structure and assumed to represent its reference linear model. For example, it was assumed that the bridge model has a linear dynamic behaviour under the El Centro earthquake once an amplitude of 0.9 mm was applied to the model. So, this model was considered as a reference linear model to investigate the behaviour of the structure under this ground motion. Then, the bridge model was tested under other amplitudes from a minimum of 13 mm to a maximum of 98 mm. Different ARMAX models were constructed using the structural responses for different amplitudes. The ARMAX model constructed using the reference linear model was considered Linear model and the other ARMAX models from higher amplitudes of excitation were considered as Unknown models. It should be mentioned that the excitation input recorded using ACC0 located on the shake

table was used as the input of time series models. Figure 5.27 presents the structural responses measured from the bridge model using ACC1 and ACC8 during the amplitudes of 13 mm and 98 mm of El Centro earthquake. These figures also show the structural responses predicted from the corresponding ARMAX models. A fit ratio of 88.3% and 89.7% was obtained for channels 1 and 8 during the low amplitude of excitation (13 mm). Also, a fit ratio of 78.7% and 82.6% was obtained for channels 1 and 8 during the high amplitude of excitation (98 mm). It can be observed that the ARMAX modelling was able to predict the structural responses with satisfactory prediction and the numerical models are reliable to be used for nonlinearity identification process. The orders of polynomials n_a, n_b, n_c, and n_k for the vibration data sets were set to 4, 4, 1 and 1, respectively for data analysis to obtain the best representation of dynamic behaviour of the bridge model. In the next step, the residual errors were calculated for the reference model and the unknown models using Eqs. (4.53) and (4.54). The ECDFs of residual errors obtained from different amplitudes of El Centro earthquake using ACC1 and ACC8 are illustrated in Figure 5.28.

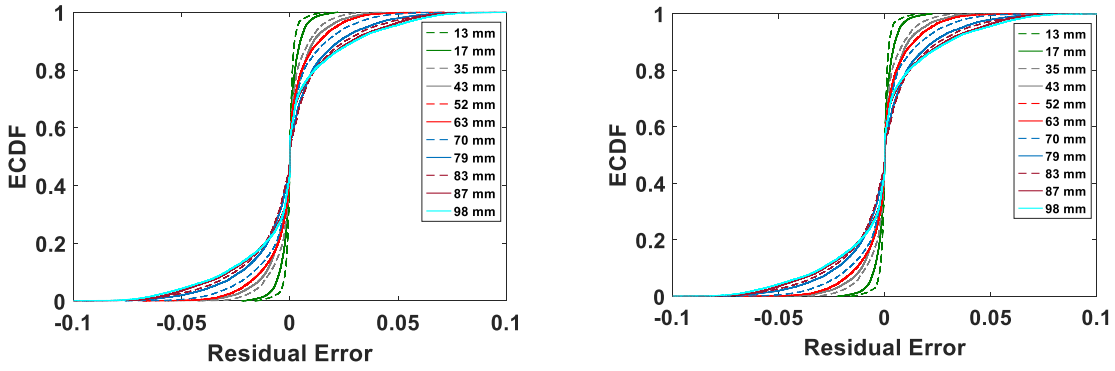

(a) ACC1 **(b) ACC8**

Figure 5.28. ECDFs due to various levels of El Centro Earthquake in transverse direction.

The empirical cumulative distribution function of each time series residuals graphically showed that the deviation of residual errors from the reference line increases as the amplitude of excitation increases. This shows the fact that the at higher levels of excitation, the residual errors extracted from linear ARMAX models do not follow a normal distribution. In the next

step, the nonlinearity indicators have been calculated for each data sets according to Eq. (4.62). To estimate this indicator, first the statistical distance between the ECDFs of residual errors of the reference ARMAX model and unknown ARMAX models was estimated using Eq. (4.60). It is noteworthy that the null hypothesis of the two residual time series has been tested at a significance level of 0.05 in this study. As stated, the nonlinearity indicator is based on combination between residual errors and coefficients of ARMAX models. In this study, it was decided to consider natural frequencies extracted from model coefficients as a sensitive dynamic parameter to any alterations in the structural system.

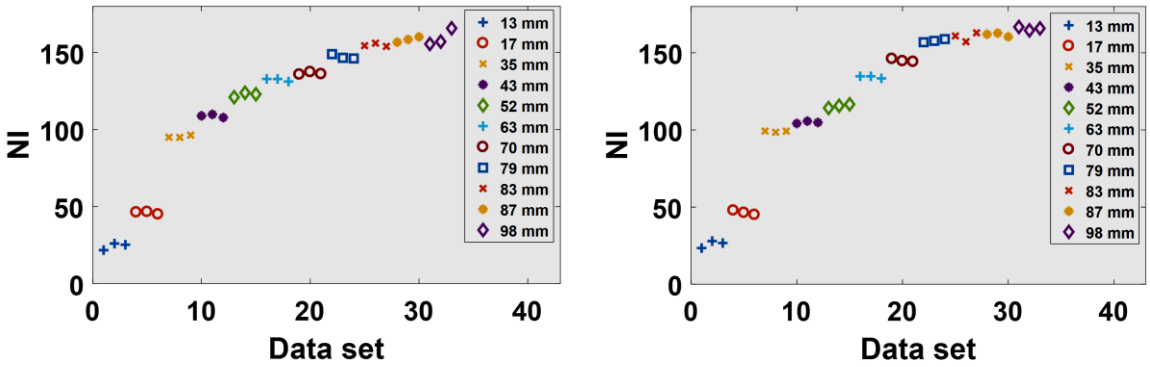

(a) ACC1 **(b) ACC8**

Figure 5.29. NI values obtained for different amplitudes of El Centro Earthquake.

Figure 5.29 presents the NI values obtained using channels 1 and 8 for various amplitudes of El Centro earthquake. It should be mentioned that there were 11 cases of excitation amplitudes subjected to the bridge model and the test under each amplitude was repeated three times. Therefore, the nonlinearity indicator was calculated and presented for 33 data sets. As can be seen from the figure, the NI values increase as the excitation amplitude increases. This shows the fact the dynamic behaviour of the rubber-based supports and the whole structural system changes when the bridge model is subjected to higher levels of excitation. Although this is a well-known fact that a dynamic system behaves differently under various amplitudes of excitation, it is crucially important to categorise the linear and nonlinear behaviours of the system and specify a range that the structure starts to behave nonlinearly.

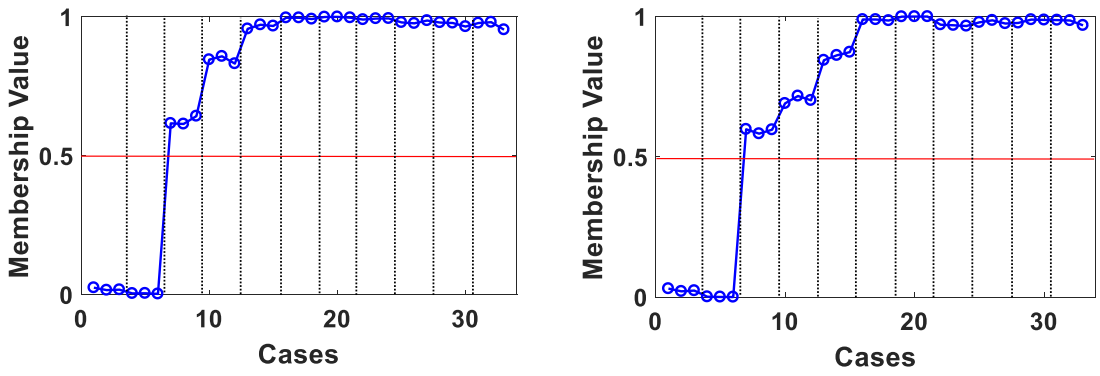

(a) ACC1 **(b) ACC8**

Figure 5.30. Membership due to NIs for different amplitudes of El Centro Earthquake.

In the last step, the obtained values of NIs for different amplitudes of El Centro Earthquake were categorised and classified using the FCM clustering algorithm. The number of clusters was set to 2 and the number of data points was considered 33 for all the measured time series data. Figure 5.30 presents the membership values due to NIs obtained for ACC1 and ACC8. As is obvious from the results, the NI values have been classified to two different clusters. The data points below the red line come from linear state of the structure with normal distribution of residual error and the data points above the red line present the nonlinear behaviour of the system without the normal distribution of residuals. Also, from the amplitude of 35 mm, the bridge model started to show nonlinear behaviour as the ECDFs of residual errors do not follow a normal distribution and the FCM algorithm could categorise it as a nonlinear behaviour. As expected, from this amplitude above, all the test cases showed nonlinear behaviour and classified as the nonlinear states of the structure. The same results were observed for other measurement channels; however, it has been decided not to include all the test results for conciseness. In the following, the nonlinearity identification results obtained for Chi-Chi earthquake and Tabas earthquake will be presented.

For Chi-Chi earthquake and Tabas earthquake, it was considered that the bridge model has a linear behaviour under an amplitude of 6.5 mm and 0.4 mm, respectively. Therefore, these models were utilised as the reference linear models to analyse the behaviour of the bridge

model under the earthquakes. The structural model was then excited by various amplitudes of these earthquake from a minimum of 13 mm to a maximum of 210 mm for Chi-Chi earthquake and from a minimum of 4 mm to a maximum of 190 mm for Tabas earthquake. Various ARMAX models were constructed for different amplitude cases.

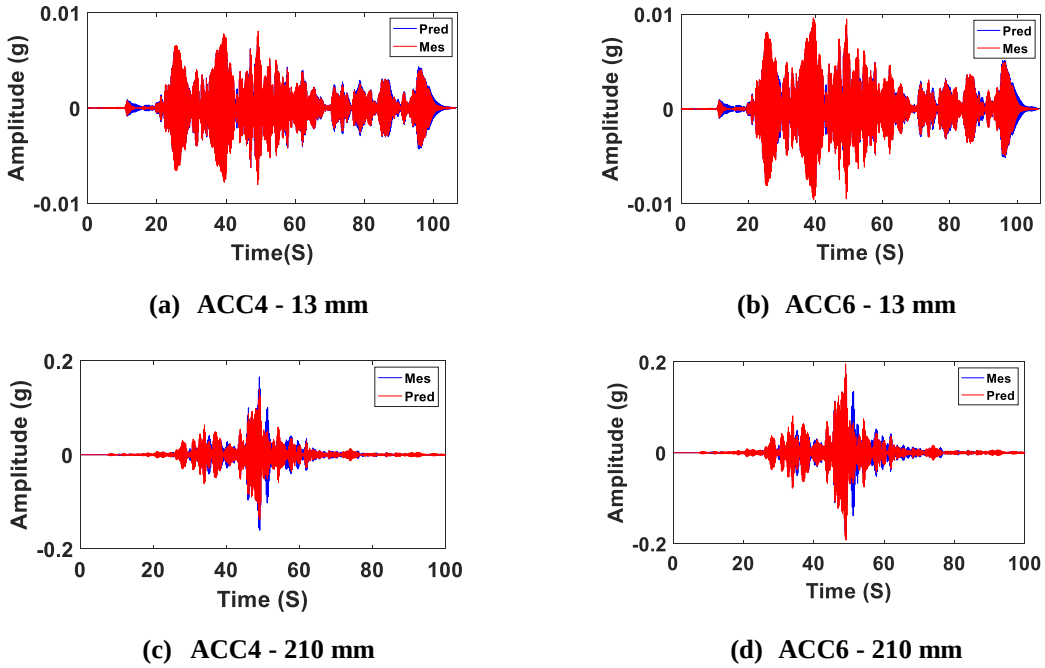

(a) ACC4 - 13 mm

(b) ACC6 - 13 mm

(c) ACC4 - 210 mm

(d) ACC6 - 210 mm

Figure 5.31. Measured and predicted responses recorded during Test 3 in transverse direction.

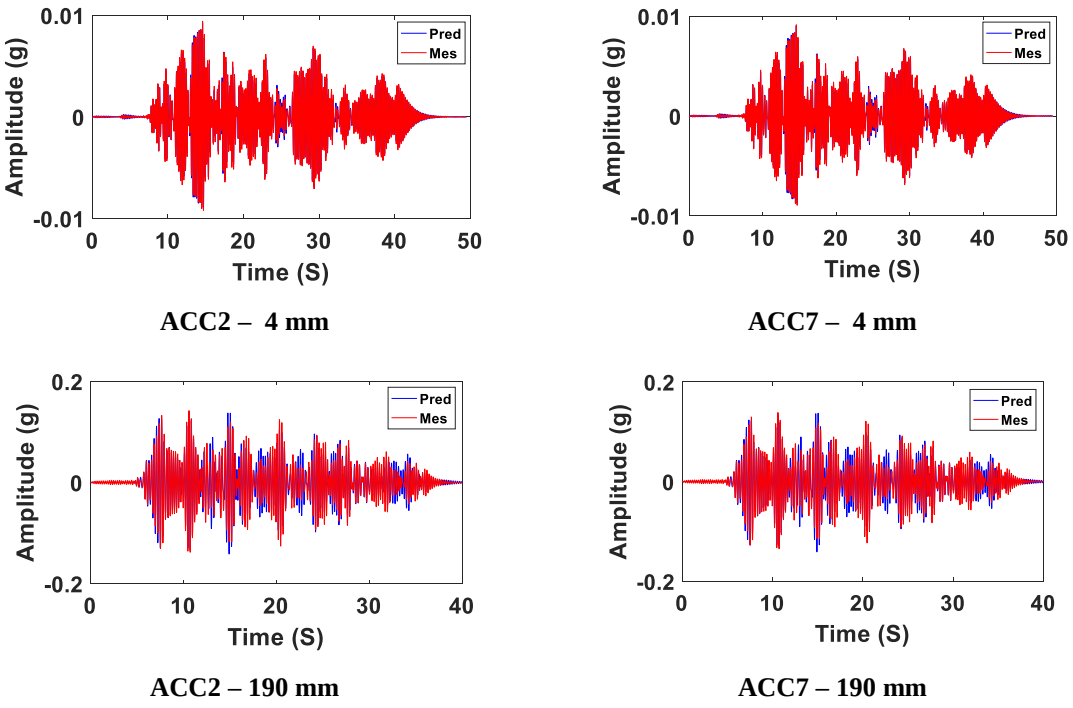

ACC2 – 4 mm

ACC7 – 4 mm

ACC2 – 190 mm

ACC7 – 190 mm

Figure 5.32. Measured and predicted responses recorded during Test 4 in transverse direction.

Figure 5.31 shows the structural responses measured from the model using ACC4 and ACC6 during amplitudes of 13 mm and 98 mm of the Chi-Chi earthquake and the structural responses predicted from the corresponding ARMAX models. Figure 5.32 also depicts the measured and predicted structural responses using ACC2 and ACC7 during amplitudes of 4 mm and 190 mm of the Tabas earthquake. A fit ratio of 95.3% and 96.4% was obtained for channels 4 and 6 during the low amplitude of excitation (13 mm). Also, a fit ratio of 86.2% and 88.9% was obtained for channels 4 and 5 during the high amplitude of excitation (210 mm). In addition, during the TABAS earthquake, a fit ratio of 98.8% and 98.9% was obtained for the amplitude of 4 mm and a fit ratio of 81.6% and 82.1% was estimated for the amplitude of 190 mm for channels 2 and 7, respectively. Therefore, considering the good fit ratios obtained for low and high amplitudes of earthquakes, the ARMAX models constructed from the measured vibration data sets can be reliably utilised for nonlinearity identification.

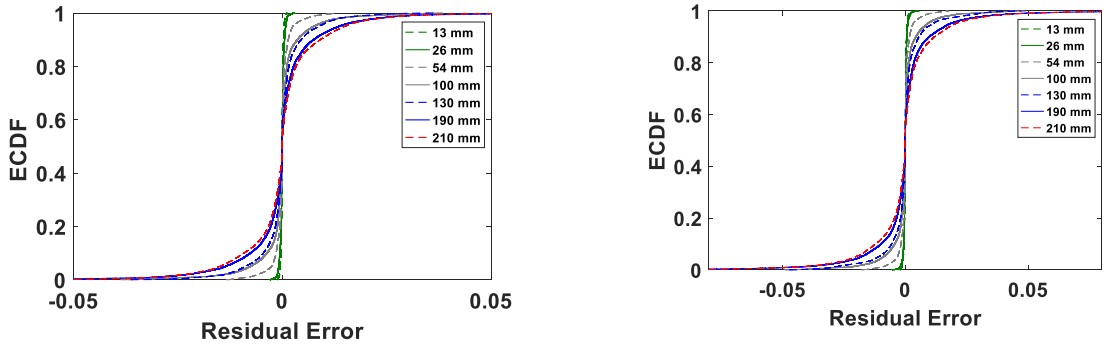

(a) ACC4 **(b) ACC6**

Figure 5.33. ECDFs due to various levels of Chi-Chi Earthquake in transverse direction.

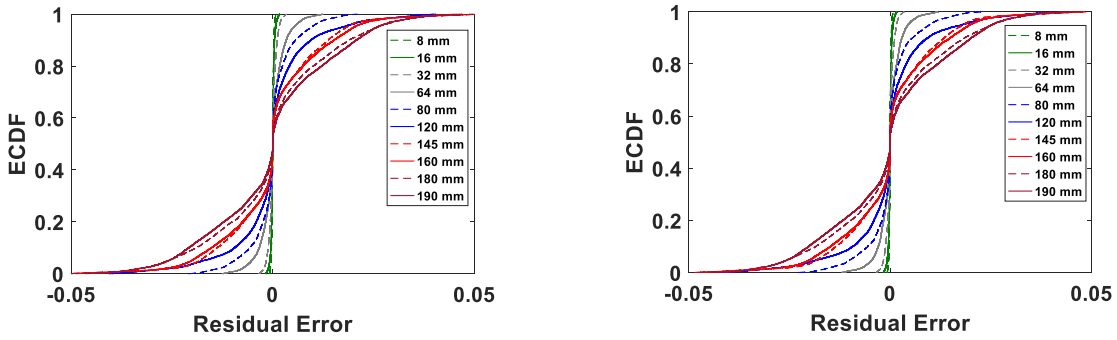

(a) ACC2 **(b) ACC7**

Figure 5.34. ECDFs due to various levels of Tabas Earthquake in transverse direction.

After calculating the residual errors, the ECDF values of residuals obtained from different amplitudes of Chi-Chi earthquake using ACC4 and ACC6 are shown in Figure 5.33(a) and (b), respectively. In addition, Figure 5.34(a) and (b) presents the ECDFs of residuals obtained from various amplitudes of Tabas earthquake using ACC2 and ACC7, respectively. As obvious, the ECDF plots corresponding to higher amplitudes of both ground motions showed more deviation from the reference line. This confirms the fact that the linear ARMAX model residuals do not follow a linear normal distribution as the amplitudes of excitation exceed from a specific range. This range varies for different ground motions with various frequency content.

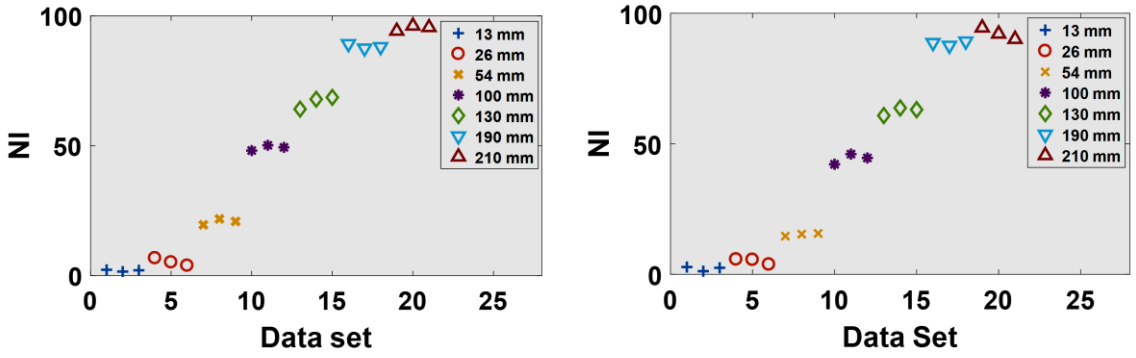

(a) ACC4 **(b) ACC6**

Figure 5.35. NI values obtained for different amplitudes of Chi-Chi Earthquake.

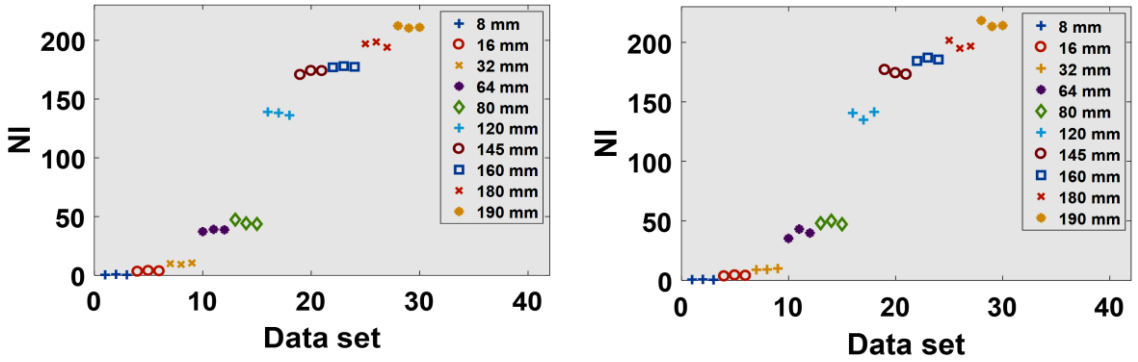

(a) ACC2 **(b) ACC7**

Figure 5.36. NI values obtained for different amplitudes of Tabas Earthquake.

The next step is to calculate the nonlinearity indicator based on the statistical distance between the ECDFs of residual errors and natural frequencies extracted from the reference ARMAX model and unknown ARMAX models. Figure 5.35 depicts the NI values obtained using channels 4 and 6 for different amplitudes of Chi-Chi earthquake. During this test, the bridge

model was subjected to 7 cases of excitation amplitudes each with three times of repetition. Therefore, the nonlinearity indicator was calculated and presented for 21 data sets. In addition, Figure 5.36 presents the NI values calculated for ACC2 and ACC7 using different amplitudes of Tabas earthquake for 30 sets of time series data. As is obvious from the results obtained, the nonlinearity indicator values increase as the excitation amplitudes of both earthquakes increase showing changes in dynamic behaviour of the system due to higher levels of excitations. This change has been gradually occurred during each amplitude of excitation that needs to be classified using the proposed clustering algorithm.

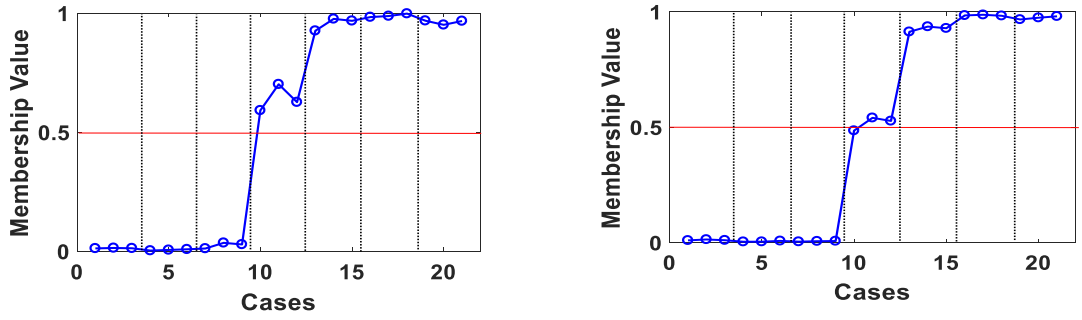

(a) ACC4 **(b) ACC6**

Figure 5.37. Membership due to NIs for different amplitudes of Chi-Chi Earthquake.

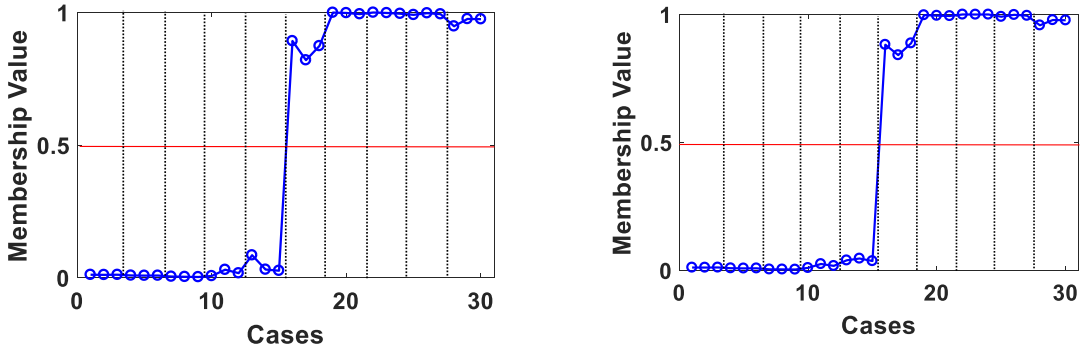

(a) ACC2 **(b) ACC7**

Figure 5.38. Membership due to NIs for different amplitudes of Tabas Earthquake.

Figure 5.37 shows the membership values due to NIs measured for ACC4 and ACC6 during Chi-Chi excitation. Also, the membership values due to NIs for different amplitudes of Tabas earthquake are respectively presented in Figure 5.38(a) and (b) for ACC2 and ACC7. It is noteworthy that the number of clusters was set to 2 for the clustering algorithm for both ground

motions. As can be seen from the results, the nonlinearity indicator values have been categorised to two groups for both earthquakes. The first group with data points below the red lines represents the linear dynamic behaviour of the bridge model associated with a normal distribution of residual errors extracted from the unknown ARMAX models. Also, the data points above the red line show nonlinear behaviour of the system when the amplitude of excitation exceed a specific limit. According to the results obtained here for Chi-Chi earthquake, the bridge model started to behave nonlinearly once the amplitude of excitation exceeds from 54 mm. In addition, the structure showed nonlinear behaviour once the amplitude of Tabas earthquake exceeds from 80 mm. From these amplitudes, the ECDFs of residual errors do not follow a normal and linear distribution, which have been classified using the proposed algorithm. Similar results were observed for other measurement channels installed on the bridge model due to these ground motions. In total, it can be concluded from the results that the proposed nonlinearity identification technique is able to identify and categorise nonlinear behaviour of a dynamic system with a high accuracy. This identification and classification algorithm can provide important information for an early damage identification as the presence of nonlinearity in a system can be considered as an indication of structural damage.

5.5 Summary and conclusion

This chapter presented the results of a series of shaking table tests on a small-scale steel bridge model. The purposes of these tests were to validate various features of the new wireless smart sensor network and the new vibration-based nonlinearity identification technique. In the first part, the experimental test setup information, including descriptions of the steel bridge model, instrumentation, and data collection system, were provided. Then, the results obtained regarding the performance of the wireless smart sensor network were presented. These results are summarised in the following:

1. The results of the shake table tests showed that the sensitivity and resolution of the developed wireless smart sensor nodes are comparable with expensive wired accelerometer sensors. The wireless sensors were able to record high-fidelity structural responses from the bridge model, when it was subjected to various types and amplitudes of excitation sources.
2. The results of the shake table test also showed that the wireless sensor nodes could continuously record structural responses in an ultralow-power mode and detect the occurrence of the sudden event induced by the shake table. Also, the wireless smart sensor nodes were able to record high-fidelity structural responses during the sudden event using high resolution accelerometer. Besides capturing sudden events from structures, this sampling mode helps to save the power source of the wireless smart sensor network for SHM applications.
3. The results showed that the wireless nodes maintained phase among themselves and were well synchronised during the dynamic testing. These results confirm the reliability of time synchronisation techniques introduced in this thesis.
4. The reliability of wireless communication provided by DigiMesh topology was investigated during the tests. The results showed that the vibration measurements were seamlessly transferred using this wireless topology that confirms the application of DigiMesh topology in the development of WSSN for SHM applications.

The results of shake table tests obtained using the vibration-based nonlinearity identification technique proved the validity of the method to analyse the earthquake-induced vibration data. The analysis results obtained for different ground motions showed that the technique was able to categorise the linear and nonlinear behaviours of the structure and identify nonlinearities by specifying a unique threshold for each subjected earthquake. This algorithm can be very helpful to assess the structural performance at early stage of damage occurrence after sudden events.

Chapter 6: Vibration-based Condition Assessment of a Full-scale concrete bridge in New Zealand

6.1 Introduction

In this chapter the dynamic behaviour of a full-scale in-service concrete bridge located in Wellington, New Zealand is investigated. The main purpose of this chapter is to show the importance of structural health monitoring of large-scale structures especially after earthquakes and to confirm the efficiency of vibration-based SHM for large-scale civil structures. This bridge was subjected to two large-amplitude earthquakes and several aftershocks. The ambient vibration and earthquake-induced vibration data sets collected using various wired accelerometer channels installed on the bridge were used to assess the dynamic behaviour of the structure after the subjected earthquakes. Two types of parametric and non-parametric time domain analysis methods were carried out on the monitoring data during one year of monitoring to obtain the vibration intensity parameters and dynamic characteristics of the bridge. A dynamic performance index was also utilised based on Autoregressive Moving Average with eXogenous excitation (ARMAX) models to evaluate the behaviour of the structure under different amplitudes of ground motions. A part of data analysis has been performed using the MATLAB toolbox introduced in chapter 2 [89] to show the competency of MATLAB environment in analysing large sets of SHM data.

In the following sections, a brief description of the bridge structure and the instrumentation layout installed on the bridge are provided. Then, the analysis results, including vibration intensities, averaged normalized Power Spectral Density (PSD), ARMAX parametric models, and the force-displacement relationships of the ambient and earthquake-induced time-series vibration data sets are presented to assess the condition of the structure during one year of monitoring period.

6.2 Thorndon Bridge description

The Thorndon Bridge, constructed between 1967 and 1972, is a twin 1.35 km long elevated concrete bridge along the original offshore of Wellington Harbour in Wellington, New Zealand. The bridge carries SH1 over the main trunk railway, the Inter Islander Ferry Terminal and also two significant access roads into Wellington city: Aotea Quay and Thorndon Quay [160]. This superstructure consists of simply supported precast concrete I girders spanning between pier caps. Two superstructure expansion joints were provided per span to enable the piers to respond independently to the seismic loads in a transverse direction. The northbound and southbound sections of the bridge are 11.5 m wide and carry three 3.5 m traffic lanes in addition to 0.5 m shoulders. Figure 6.1 depicts the general layout of the bridge and its location in Wellington, New Zealand.

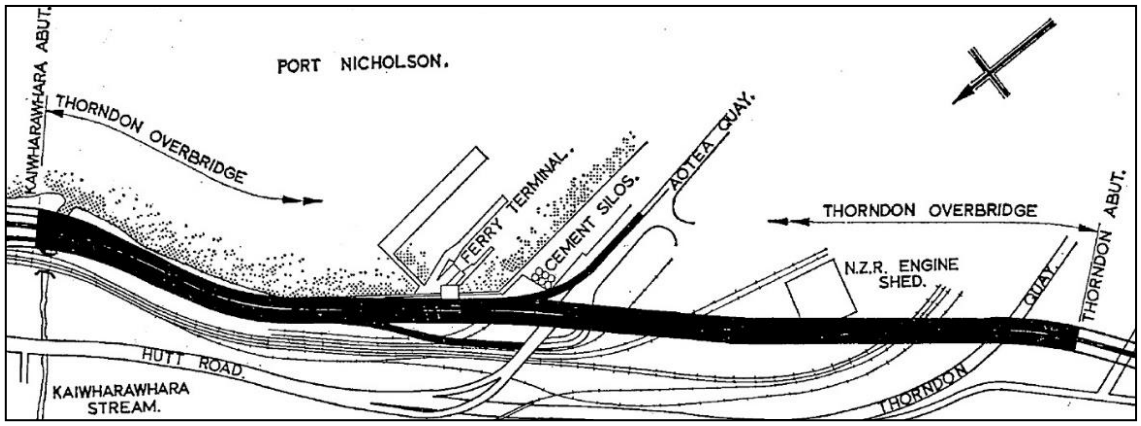

Figure 6.1. General layout of the Thorndon Bridge [160].

The Thorndon Bridge is located in a high seismicity area because the Wellington Fault, a significant earthquake source in the New Zealand, passes under the bridge. Therefore, it has recently been instrumented with strong motion accelerometers for long-term condition monitoring. This project is part of GeoNet Structures Instrumentation Programme (www.geonet.org.nz) to install multiple seismic instruments in various representative commercial and residential buildings and bridges located in areas with high seismic hazard throughout the New Zealand.

6.2.1 Instrument description

As is seen in Figure 6.2(a), there are two zones (North and South bounds) on the bridge with approximately 400 m distance between them, where accelerometers were instrumented. A total of 16 tri-axial accelerometers were instrumented on the bridge in these two zones. The line of the Wellington Fault is also shown in this picture, which exactly passes through Zone I of the bridge. Figure 6.2(b) shows the tri-axial accelerometer installed on the bridge to collect vibration data from the superstructure.

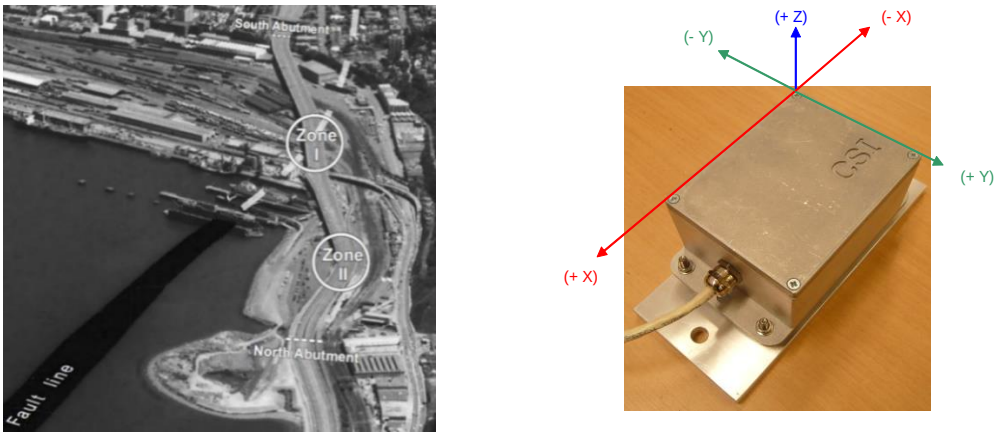

(a) **(b)**

Figure 6.2. (a) Instrumentation zones and the line of the Wellington Fault [160], (b) Strong motion tri-axial accelerometer.

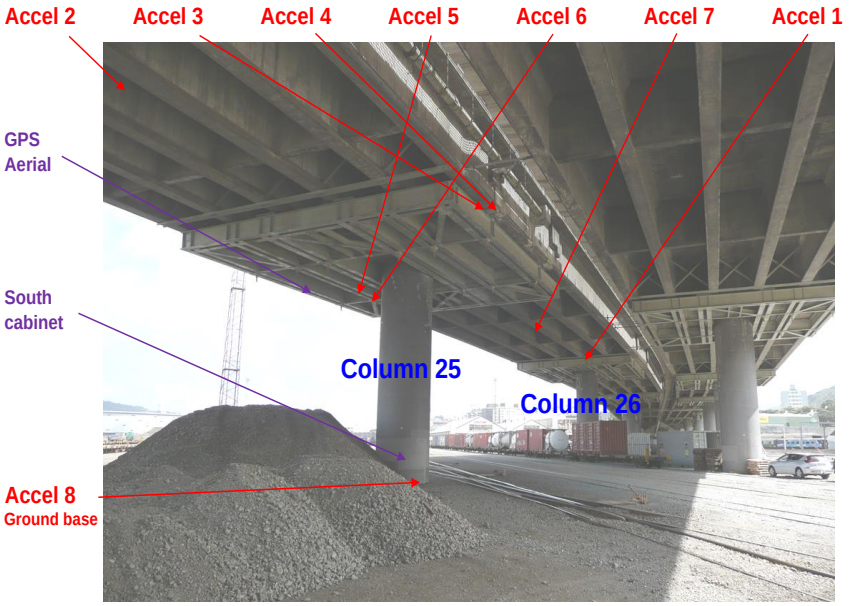

(a) Zone I

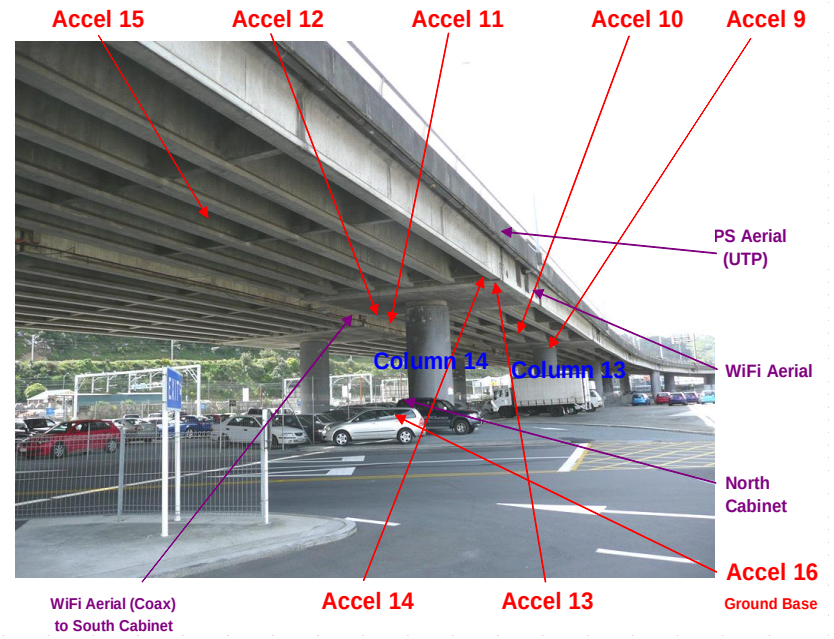

(b) Zone II

Figure 6.3. Sensor locations on the Thorndon Bridge.

Table 6.1. Details of sensor locations in Zone I and Zone II of the bridge.

Channel	Pier or Span	Description	Latitude (*m*)	Longitude (*m*)	Height (*m*)
1	Pier 25	Pier cap - centre	-41.26651768	174.7842129	-12.35
2	Span 24-25	Centre of span	-41.26654503	174.7840999	-10.35
3	Span 24-25	End of span - W side	-41.26655192	174.7840922	-10.35
4	Pier 26	Pier cap - E side	-41.26667898	174.7841426	-10.00
5	Pier 26	Pier cap - W side	-41.26668588	174.7841349	-10.00
6	Span 25-26	End of span - E side	-41.26677133	174.7839308	-12.70
7	Span 25-26	Centre of span	-41.26691316	174.7837731	-10.40
8	Pier 26	Ground level	-41.26660191	174.7841192	0.00
9	Pier 13	Pier cap - centre	-41.26338902	174.78738629	-6.90
10	Span 13-14	Centre of span	-41.26350349	174.78727889	-8.75
11	Span 13-14	End of span - W side	-41.26322082	174.78747097	-7.47
12	Pier 14	Pier cap - E side	-41.26330165	174.78739514	-7.40
13	Pier 14	Pier cap - W side	-41.26369325	174.78718130	-7.08
14	Span 14-15	End of span - E side	-41.26370134	174.78717371	-7.15
15	Span 14-15	Centre of span	-41.26377308	174.78702599	-9.00
16	Pier 14	Ground level	-41.26361797	174.78717150	0.00

The locations of accelerometers in Zone I and Zone II are illustrated in Figures 6.3(a) and (b), respectively. As it is illustrated in these figures, in each zone, seven accelerometers were installed on the superstructure on two adjacent piers and two adjacent spans and one accelerometer at ground level on concrete base slab of the control cabinet to measure the ground motions. Accelerometers 1 to 8 were located on piers 25 and 26, Spans 24-25 and 25-26 in Zone I and accelerometers 9 to16 on piers 13 and 14, Spans 13-14 and 14-15 in Zone II. Further details of the sensor locations are presented in Table 6.1.

6.2.2 Strong ground motions

Figures 6.4 and 6.5 illustrate the peak positive and negative accelerations recorded in transverse and vertical directions by accelerometer 6 installed on the pier of the bridge during the one-year monitoring period. As presented, the accelerometer recorded two strong ground motions in 2013 that were called the 2013 Seddon Earthquake and the Lake Grassmere Earthquake. The first ground motion with peaks of around -0.21 g to 0.20 g in transverse direction and -0.16 g to 0.13 g in vertical direction occurred in July 2013 in New Zealand's Cook Strait around 20 kilometers east of the town of Seddon in Marlborough. According to GeoNet, the earthquake struck at 5:09:32 pm at a depth of 13 km with a great magnitude of 6.5M. The quake caused some moderate damage in the wider Marlborough area and Wellington, the nation's capital city, 55 kilometers north of the epicenter and only minor injuries were reported. There were several aftershocks following the earthquake during 21 to 29 of July. The second earthquake with peaks of around -0.07g to 0.09g in transverse direction and -0.12g to 0.11g in vertical direction occurred at 2:30 pm on 16 August 2013, with a magnitude of 6.6M. The epicentre was located about 10 km south-east of Seddon, under Lake Grassmere, with a focal depth of 8 km. The earthquake caused significant land damage in the local area with landslips blocking roads. Buildings in Seddon were damaged, with some being declared uninhabitable. The earthquake was widely felt in North and South Islands of New Zealand.

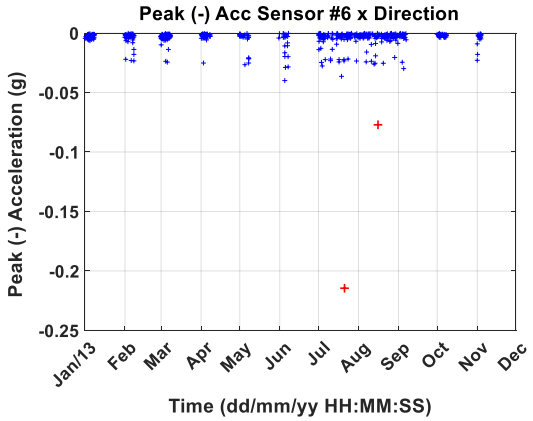

(a) Negative acceleration

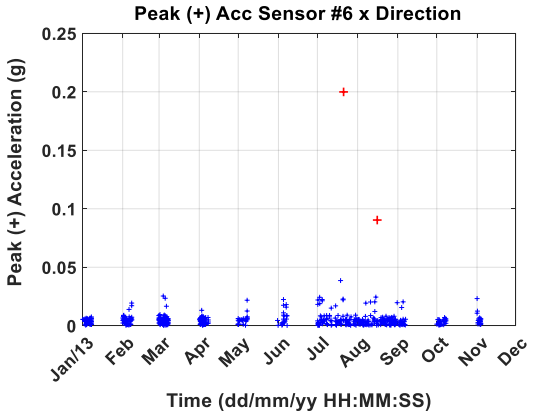

(b) Positive acceleration

Figure 6.4. Maximum accelerations recorded by ch.6 in *X* direction during one-year monitoring period.

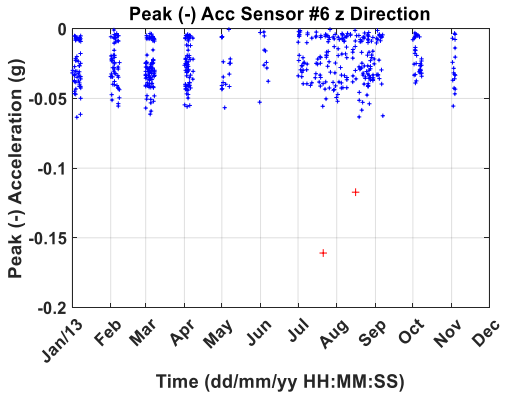

(a) Negative acceleration

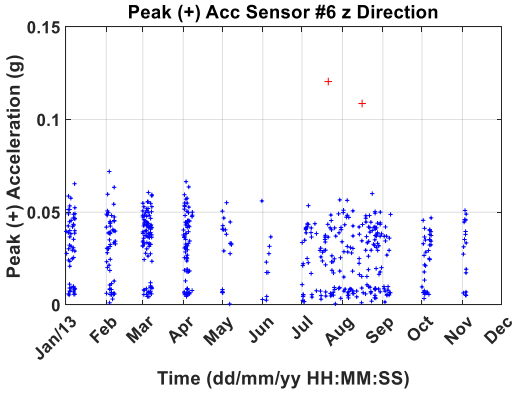

(b) Positive acceleration

Figure 6.5. Peak accelerations recorded by ch.6 in *Z* direction during one-year monitoring period.

In the next sections, first the histogram of vibration intensity parameters including peak accelerations, Root Mean Square (RMS) and Square Root of Sum of Squares (SRSS) of vibration measurements were automatically computed using the MATLAB toolbox providing a statistical treatment of the time-series response. A succession of Average Normalised Power Spectral Density (PSD) lines was then produced using the toolbox to form a spectrogram of hourly distribution of frequency components. In the next step, an automated procedure for modal parameter identification was implemented to extract dynamic characteristics of the bridge from successive hourly data sets. Moreover, a small window of recorded vibration data during the two large-amplitude earthquakes was analysed using the toolbox to provide a precise

examination of the bridge behaviour during the two strong ground motions. Subsequently, the results of the ARMAX parametric models were presented for different sets of vibration data with various amplitudes. Finally, the force-displacement relationships of the vibration measurements measured during the earthquakes were presented for further investigation on the dynamic behaviour of the bridge during the two earthquakes.

6.3 Non-parametric analysis methods

The intention of this section is to compare the dynamic behavior of the superstructure using Non-parametric analysis methods, including the vibration intensity and dynamic parameters of the superstructure. Vibration intensity parameters are good indicators of stress level of a structure subjected to dynamic loading because increasing this factor of individual structural members under similar operational loads can be considered as an indicator of fatigue-relevant damage mechanisms. In addition, the dynamic parameters of a structure, such as natural frequencies, are among reliable structural parameters that can be used for structural health monitoring of large-scale structures. The vibration data recorded from the bridge before and after the two major earthquakes, the Cook Strait earthquake and the Lake Grassmere earthquake, were utilised to assess the condition of the superstructure after and during the strong ground motions. Besides, the efficiency of the automated monitoring toolbox will be investigated for continuous structural monitoring applications.

6.3.1 Vibration intensity of the Thorndon Bridge

The ambient vibration data sets were continuously recorded from the bridge at a rate of 50 samples per second since August 2012. The raw vibration data sets were automatically divided into hourly intervals through the monitoring toolbox and then the peaks of accelerations, RMS, and SRSS values were calculated for every one-hour interval. Figures 6.6 (a) and (b) present the histograms of peak vertical acceleration values recorded by accelerometer 1 for two

monitoring periods: from January to June 2013 (before the major earthquakes) and from July to December 2013 (after the major earthquakes), respectively. The peak acceleration ranged from 0 to 0.15 m/s^2 and is centered around 0.05 m/s^2 for both monitoring periods. As is clear from the figures, there was no change in the peak acceleration distribution during the one-year monitoring period, before and after the two major earthquakes.

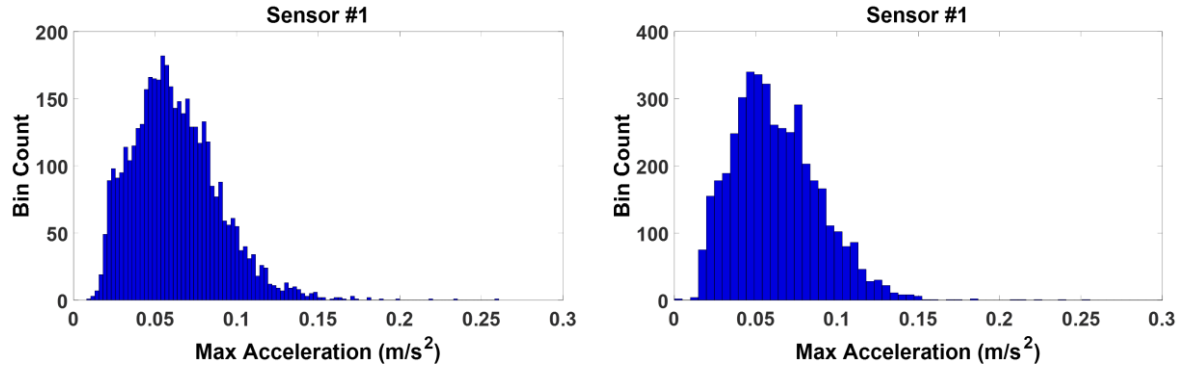

(a) From 1 January to 30 June **(b) From 1 July to 31 December**

Figure 6.6. Histograms of maximum vertical acceleration recorded by accelerometer 1.

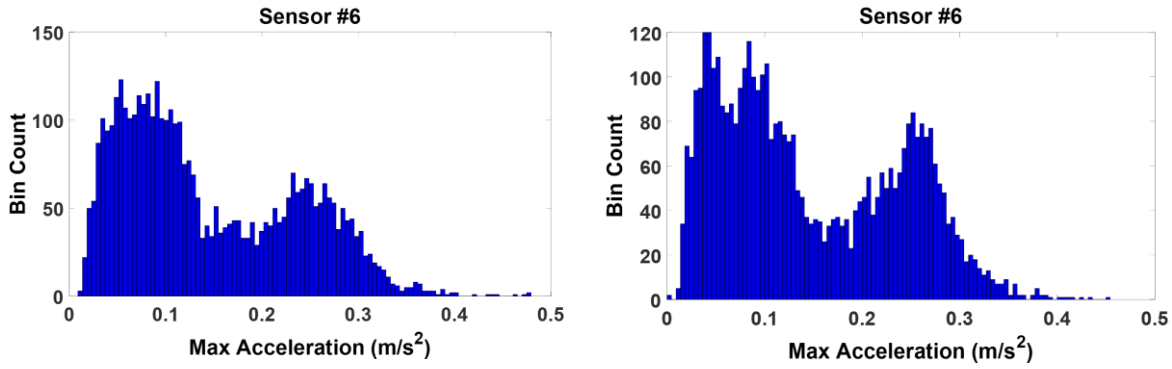

(a) From 1 January to 30 June **(b) From 1 July to 31 December**

Figure 6.7. Histograms of maximum vertical acceleration recorded by accelerometer 6.

Figures 6.7 (a) and (b) show the histograms of peak vertical acceleration values recorded by accelerometer 6 from January to June 2013 and from July to December 2013, respectively. The peak acceleration histogram comprises two distribution sections close to normal distribution of peak acceleration recorded by accelerometer 6. The peak acceleration in first section ranges from 0 to 0.15 m/s^2 and is centered on 0.08 m/s^2. This indicates very light traffic volume, likely

during night hours and outside the rush hours. In the second part of the histogram, the peak acceleration ranges from 0.15 to 0.4 m/s^2 with the center around 0.25 m/s^2. The peak acceleration values of the second part are higher than those of the first part indicating heavier traffic loads during rush hours. Similar to the results obtained for accelerometer 1, there is a same distribution of maximum acceleration for accelerometer 6 during two monitoring periods.

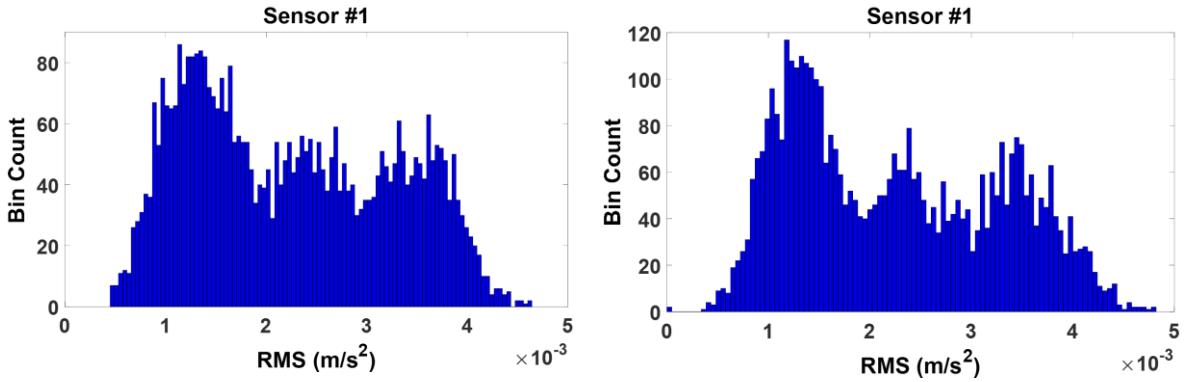

(a) From 1 January to 30 June **(b) From 1 July to 31 December**

Figure 6.8. Histograms of RMS of vertical acceleration recorded by accelerometer 1.

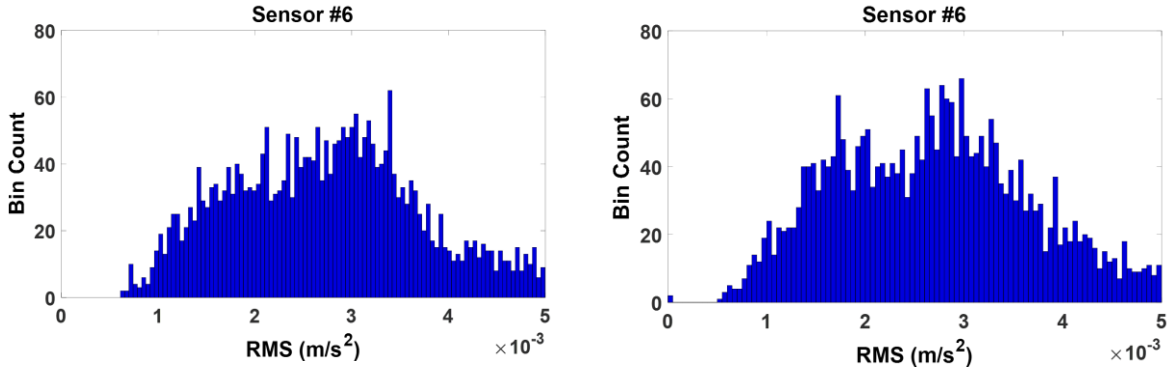

(a) From 1 January to 30 June **(b) From 1 July to 31 December**

Figure 6.9. Histograms of RMS of vertical acceleration recorded by accelerometer 6.

Histograms of Root Mean Square (RMS) values are also shown in Figures 6.8 and 6.9 for the vertical accelerations recorded by accelerometers 1 and 6, respectively. Similar to the peak acceleration values, the distribution and amplitudes of RMS values are identical in the two monitoring periods indicating no significant changes in this parameter of the bridge structure due to the two strong earthquakes.

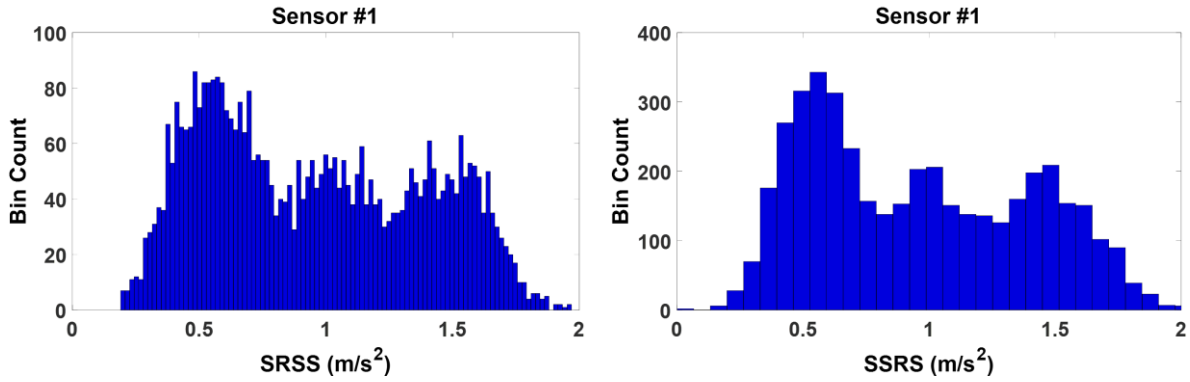

(a) From 1 January to 30 June **(b) From 1 July to 31 December**

Figure 6.10. Histograms of SRSS of vertical acceleration recorded by accelerometer 1.

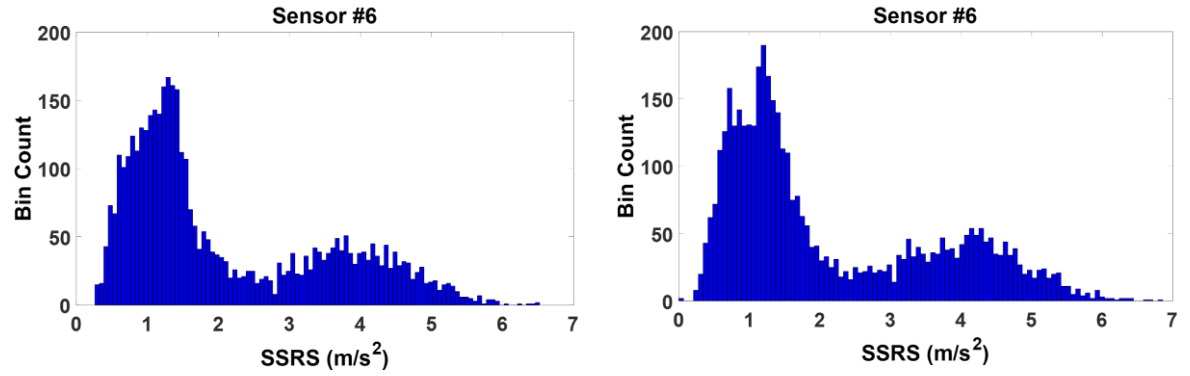

(a) From 1 January to 30 June **(b) From 1 July to 31 December**

Figure 6.11. Histograms of SRSS of vertical acceleration recorded by accelerometer 6.

The SRSS of continuously recorded ambient vibration data sets is also provided to assess different dynamic parameters of the structure. The histograms of SRSS values of the vertical accelerations recorded by accelerometers 1 and 6 are depicted in Figures 6.10 and 6.11, respectively for the two monitoring periods. As is obvious, there is a similar distribution of SRSS values before and after the strong earthquakes for the vibration data recorded by the two accelerometers. According to the analysis results obtained using the MATLAB-based computational toolbox, it can be concluded that the vibration intensities of the bridge have not changed due to the seismic loading of the two strong earthquakes. Moreover, the automated monitoring toolbox could precisely manage and assess large sets of vibration data continuously recorded from the bridge over the one-year monitoring period.

6.3.2 Dynamic characteristics of the Thorndon Bridge

In this part, the toolbox automatically performed time series analysis on recorded acceleration data to compute Average Normalised Power Spectral Density (PSD) spectra at different sensor locations. Spectrogram plots were obtained by plotting sequences of the Average Normalised Power Spectral Density of every one-hour data sets. From the spectrogram plots, the distribution of the frequency component was easily captured allowing observation of the time variation of natural frequencies as well as the identification of different intensity periods. The Average Normalised PSD distribution of acceleration data recorded in the *X* direction, the *Y* direction and the *Z* direction are separately shown in the following sections. It should be noted that the *X*, *Y*, and *Z* directions are respectively in transverse, longitudinal, and vertical directions of the bridge.

Acceleration data in the transverse (X) direction: Average Normalised Power Spectral Density distributions of acceleration data recorded in the transverse (*X*) direction obtained using the toolbox were displayed for the one-year monitoring period (Jan 2013 to Dec 2013) in Figures 6.12, 6.13 and 6.14, respectively. The acceleration data were recorded by accelerometers 2, 4, and 7 that were located in different locations on the bridge structure. As is shown, the natural frequency of the first transverse mode obtained using these sets of acceleration data was constant at about 1.36 Hz before the Cook Strait Earthquake and immediately after the strong ground motion, the frequency drops to 1.31 Hz. The drop of 0.05 Hz in natural frequency of the first transverse mode indicates a very minor but permanent alteration of the bridge dynamic characteristics due to the first major earthquake. As is obvious, there is no change in the natural frequencies after the second major earthquake occurred on 16 August 2013. It is noteworthy that the intensities of Average Normalised PSD distribution of transverse acceleration recorded by accelerometer 4 before the first major earthquake are higher than the intensities of PSD distribution after the earthquake (Figure 6.13). Some possible description for this alteration in

dynamic characteristics of the bridge could be the movement of the bridge deck or any changes in the footing boundary of the bridge. However, the authors cannot prove these potential sources of the change due to the lack of enough supporting evidence. More acceleration data and detailed information are needed to precisely investigate the cause of this change in bridge dynamic behavior.

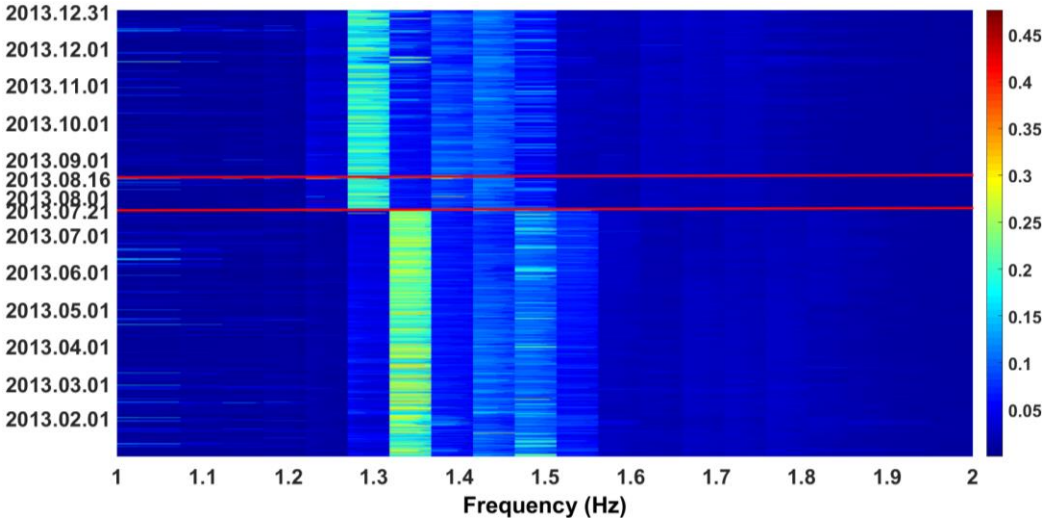

Figure 6.12. Average Normalized PSD of acceleration recorded by accelerometer 2 in *X* direction from 1 January to 31 December 2013.

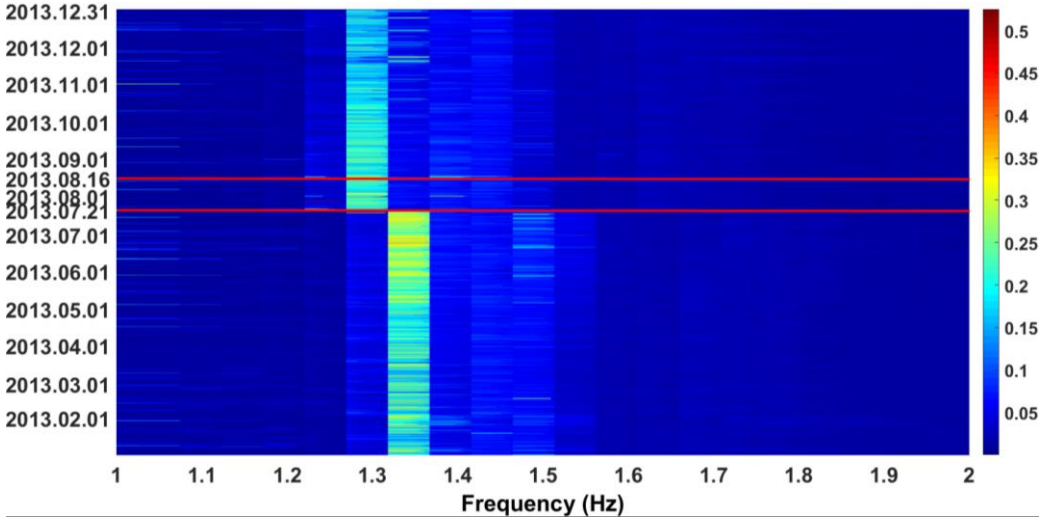

Figure 6.13. Average Normalized PSD of acceleration recorded by accelerometer 4 in *X* direction from 1 January to 31 December 2013.

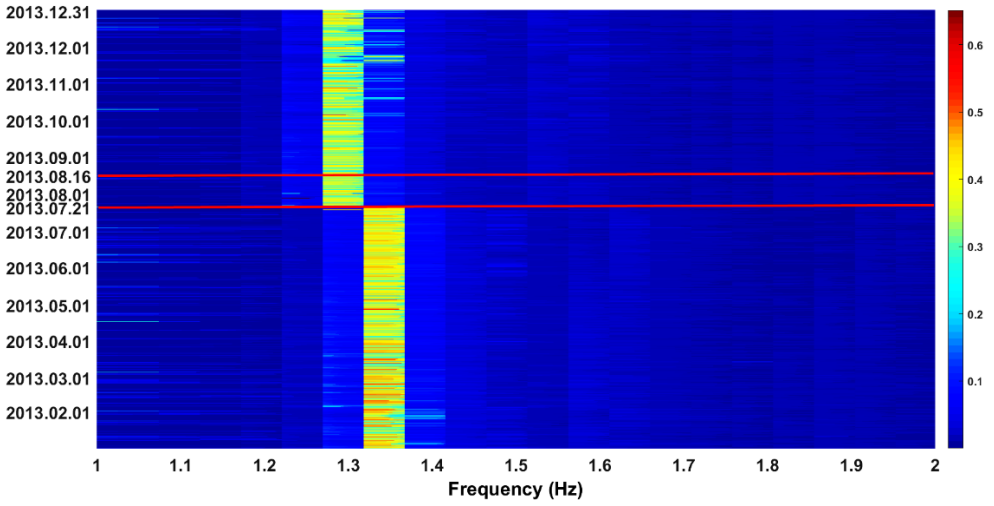

Figure 6.14. Average Normalized PSD of acceleration recorded by accelerometer 7 in *X* direction from 1 January to 31 December 2013.

Acceleration data in the longitudinal (Y) direction: The Average Normalised PSD distribution of acceleration recorded by accelerometer 6 in the longitudinal direction of the bridge is depicted in Figure 6.15 for one-year monitoring period. Due to the fact that the bridge behaved more stably under seismic loading along this direction, there is no clear drop in natural frequency of first longitudinal mode due to the two strong earthquakes. The result showed that the dynamic performance of the structure has remained almost unchanged along this direction.

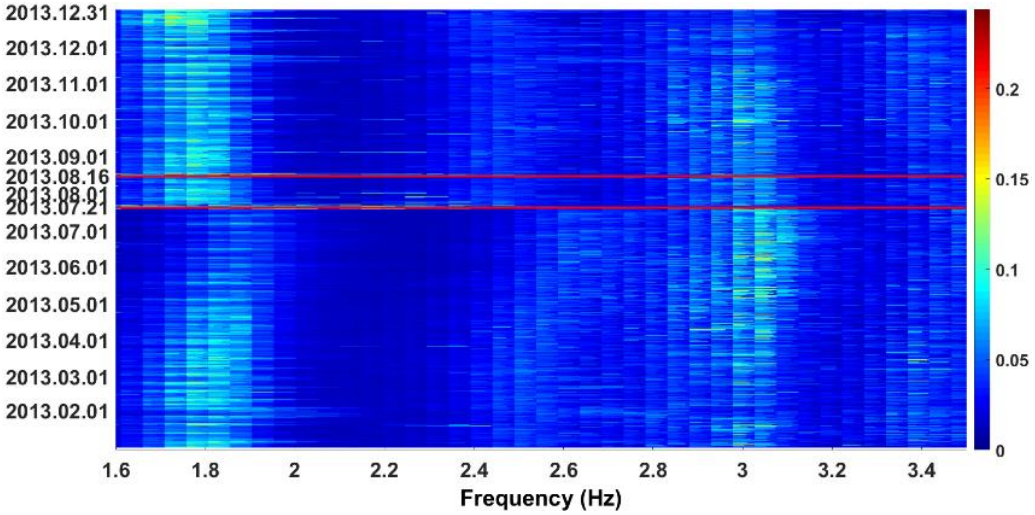

Figure 6.15. Average Normalized PSD of acceleration recorded by accelerometer 6 in *Y* direction from 1 January to 31 December 2013.

Acceleration data in the vertical (Z) direction: Figures 6.16-6.18 present the Average Normalised PSD distributions of vertical acceleration measured by accelerometers 2, 4 and 5 in the vertical direction. A similar permanent drop of 0.05 Hz in the natural frequency of the first vertical mode can be observed due to the first major earthquake occurring on 21 July 2013. However, there is no further drop or change in the natural frequency of the bridge in the vertical direction after the second major earthquake occurred on 16 August 2013. The shift in natural frequency of the first transverse and vertical modes indicates that the dynamic characteristics of the bridge slightly changed after the first strong ground motion, which needs more precise investigations about the type, location and severity of possible structural damage. It is noteworthy that the continuous analysis procedure using the automated toolkit was not computationally extensive and could be performed on a standard personal computer with 16 GB of RAM. The analysis run time depends on the size of data set that is downloaded by the user. For example, for a successive hourly data set recorded from the bridge, the analysis run time was approximately three to five minutes in this study. Therefore, total analysis run time was around three weeks for one year of monitoring data continuously recorded from the bridge.

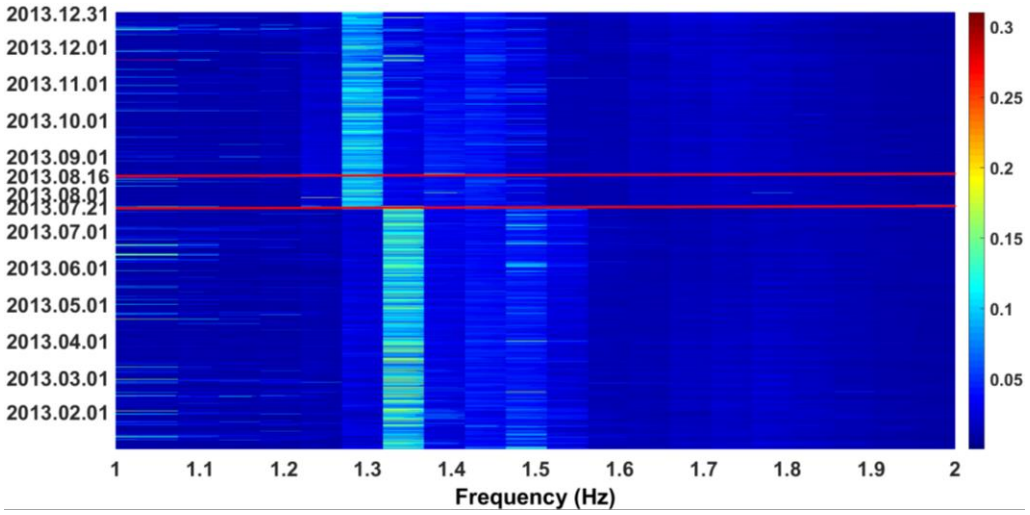

Figure 6.16. Average Normalized PSD of acceleration recorded by accelerometer 2 in *Z* direction from 1 January to 31 December 2013.

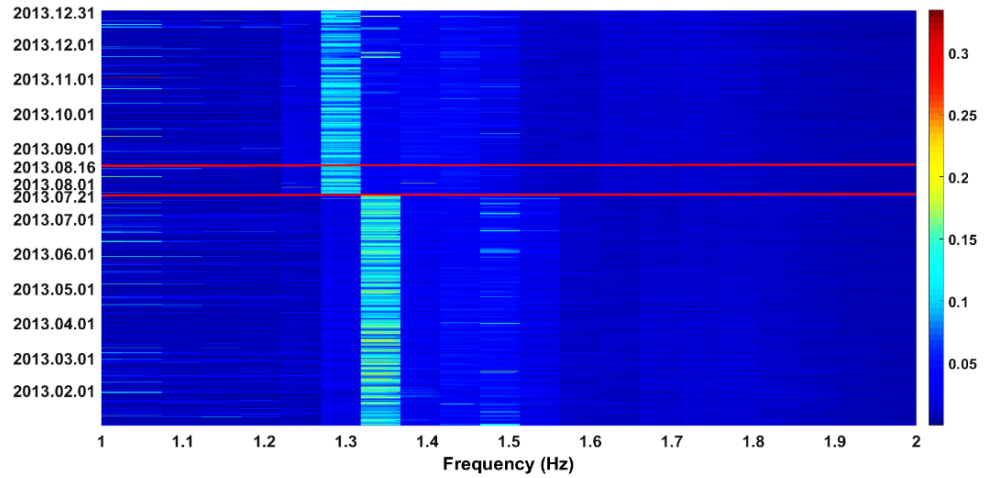

Figure 6.17. Average Normalized PSD of acceleration recorded by accelerometer 4 in Z direction from 1 January to 31 December 2013.

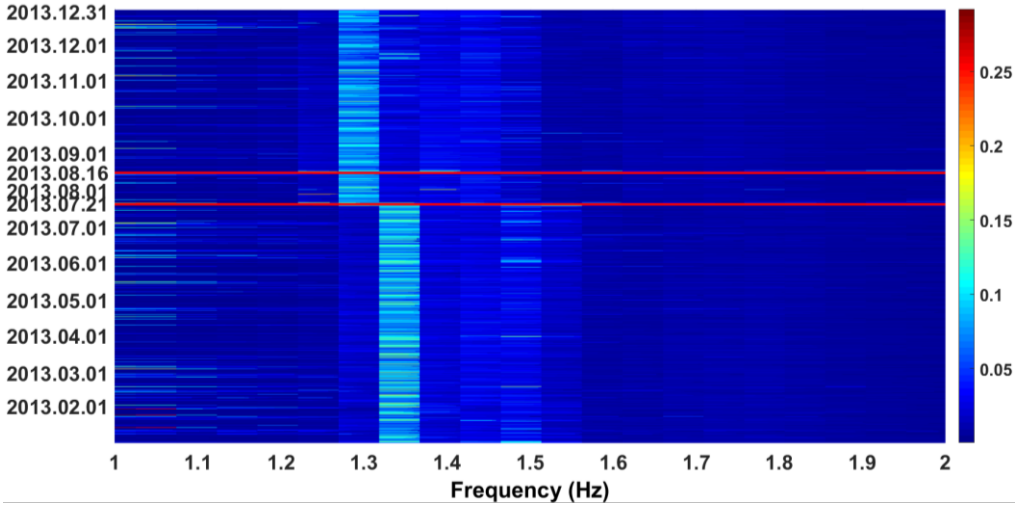

Figure 6.18. Average Normalized PSD of acceleration recorded by accelerometer 5 in *Z* direction from 1 January to 31 December 2013.

In order to present a precise examination of the bridge behaviour during strong earthquakes, a small window of vibration data collected during the two events was analysed using the automated monitoring toolbox. To this end, three sets of vibration data were considered, including a high-amplitude vibration induced by the Cook Strait Earthquake, a moderate-amplitude vibration induced by the Lake Grassmere Earthquake, and a low-amplitude vibration induced by an aftershock occurred after the second earthquake. The spectrogram of acceleration recorded by accelerometer 1 in the *X* direction during the first strong earthquake is shown in Figure 6.19. As is clear, the natural frequency of the bridge was constant at about

1.36 Hz before the first earthquake, and immediately after the strong ground motion, there was a significant drop in natural frequency to 0.97 Hz (the darkest point with magnitude of 0.97 Hz). This drop is due to the large amplitude of vibration subjected to the bridge during the 10 seconds of the strong earthquake. This large shift in the natural frequency could be an indicator that the structure did not follow linear behaviour during the strong earthquake as expected from a linear system. Moreover, the structure showed the same linear behaviour with constant frequency of around 1.36 Hz immediately after the earthquake.

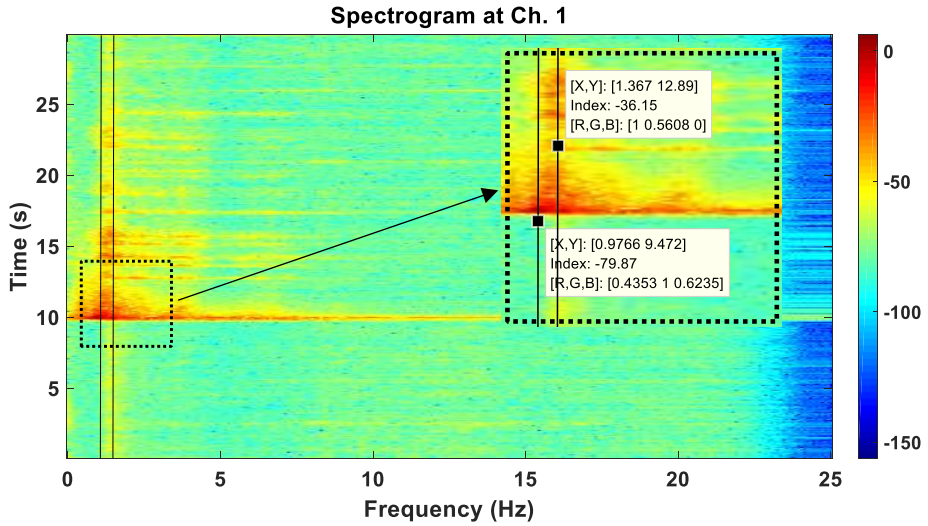

Figure 6.19. Spectrogram of acceleration recorded by accelerometer 1 in *X* direction during high-amplitude Earthquake.

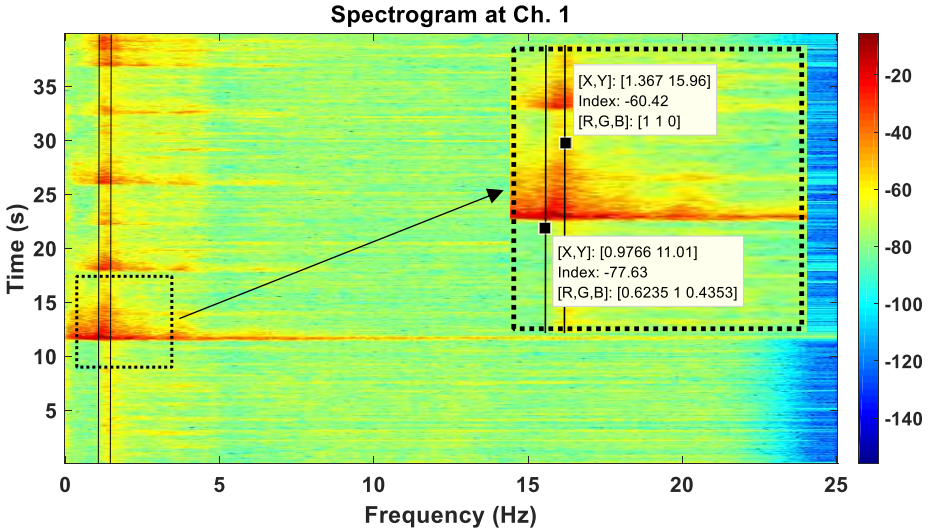

Figure 6.20. Spectrogram of acceleration recorded by accelerometer 1 in *X* direction during moderate-amplitude Earthquake.

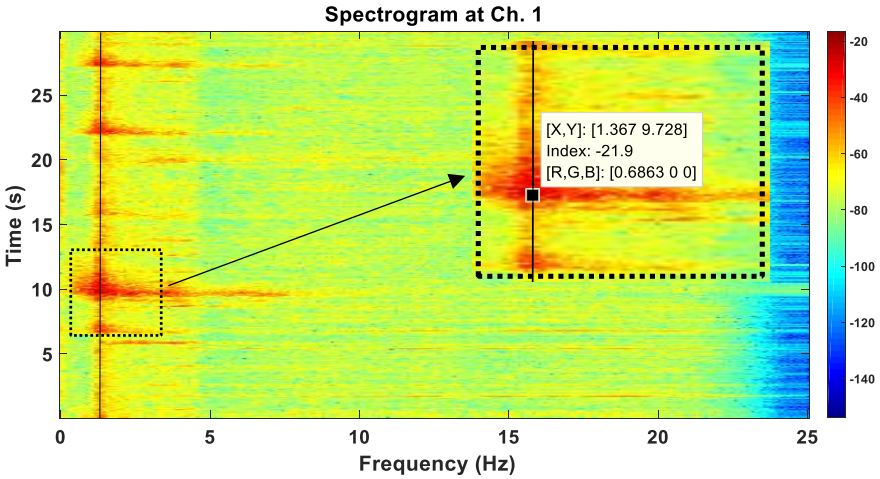

Figure 6.21. Spectrogram of acceleration recorded by accelerometer 1 in *X* direction during a low-amplitude aftershock.

The spectrogram of acceleration recorded by accelerometer 1 in the *X* direction during the moderate-amplitude earthquake (the second ground motion) is also shown in Figure 6.20. The result shows that the bridge was shaking at lower frequencies during the second strong ground motion. In addition, the same drop to 0.97 Hz in natural frequency was observed once the earthquake occurred. To further investigate the behaviour of the bridge, another vibration data set induced by a low-amplitude aftershock was also analysed. This aftershock occurred one hour after the Lake Grassmere earthquake on 16 August 2013. The spectrogram of the vibration data obtained for this data set is depicted in Figure 6.21. As is shown, there is no drop in the natural frequency of the bridge during the low-magnitude aftershock and the bridge behaved at a constant frequency of around 1.36 Hz. The possibility of bridge nonlinear behaviour during the strong earthquakes needs further investigations, which will be provided in the next parts.

To prove the consistency of the results obtained on the possibility of nonlinear behaviour of the superstructure during the earthquakes, the spectrograms of vibration data measured in different locations on the bridge are also presented in Figures 6.22 to 6.24. According to the dynamic characteristics of the bridge obtained using several data sets, it is clear that the structure behaves nonlinearly during the large-amplitude and the moderate-amplitude earthquakes and follows linear behaviour during the low-amplitude aftershock.

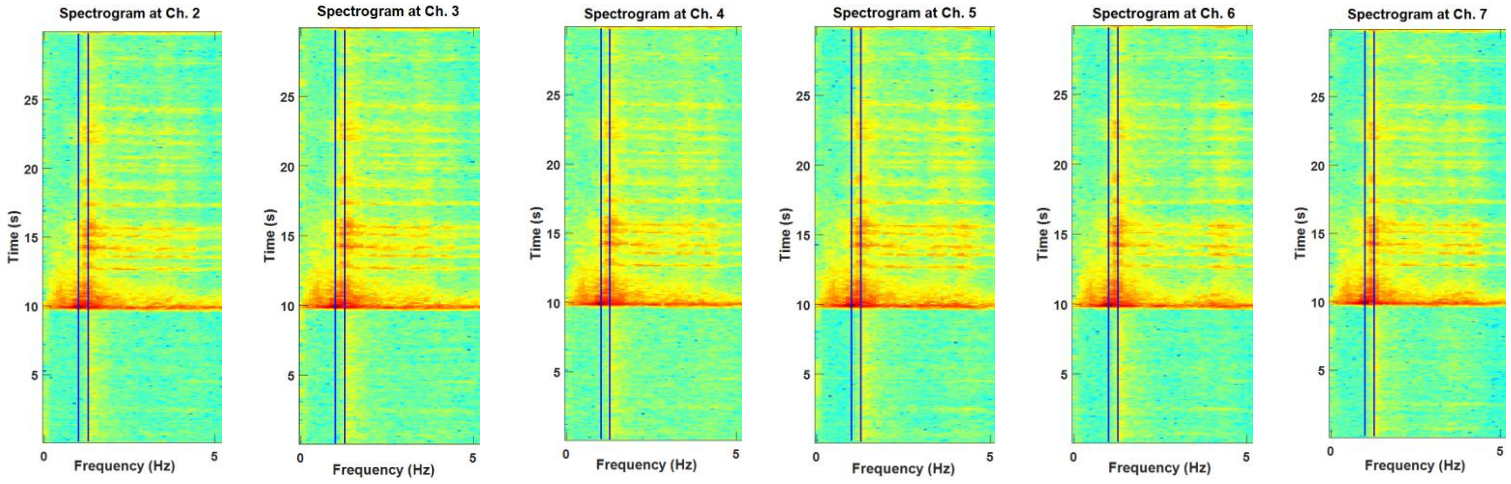

Figure 6.22. Spectrogram of acceleration recorded by accelerometers 2 to 7 in *X* direction during the Cook Strait Earthquake.

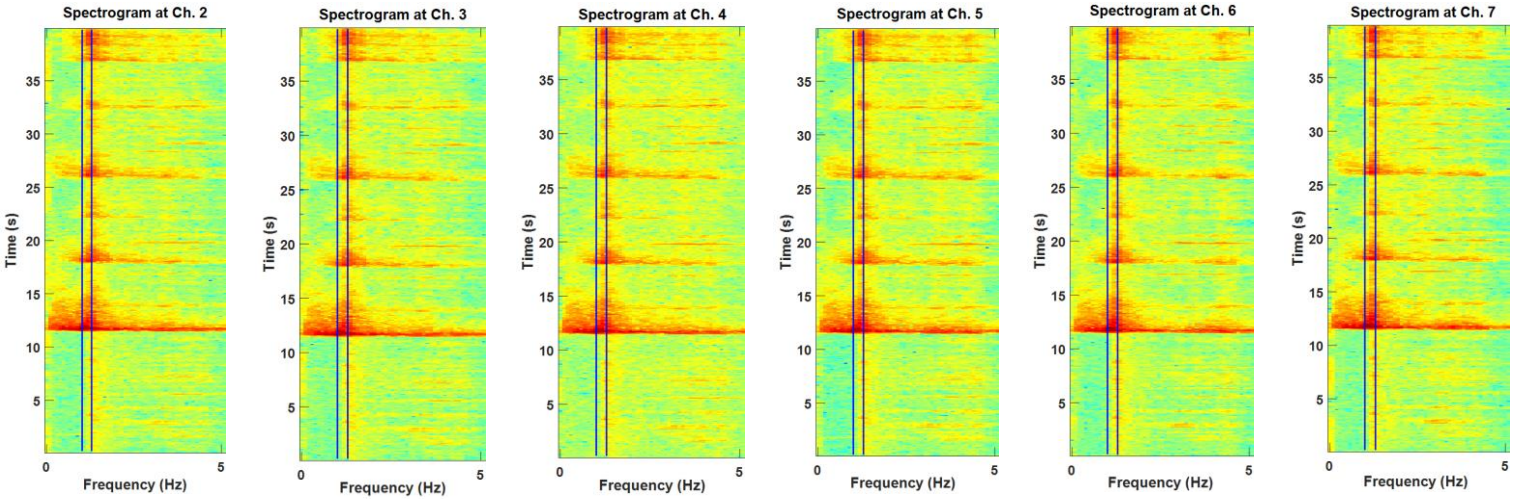

Figure 6.23. Spectrogram of acceleration recorded by accelerometers 2 to 7 in *X* direction during the Lake Grassmere Earthquake.

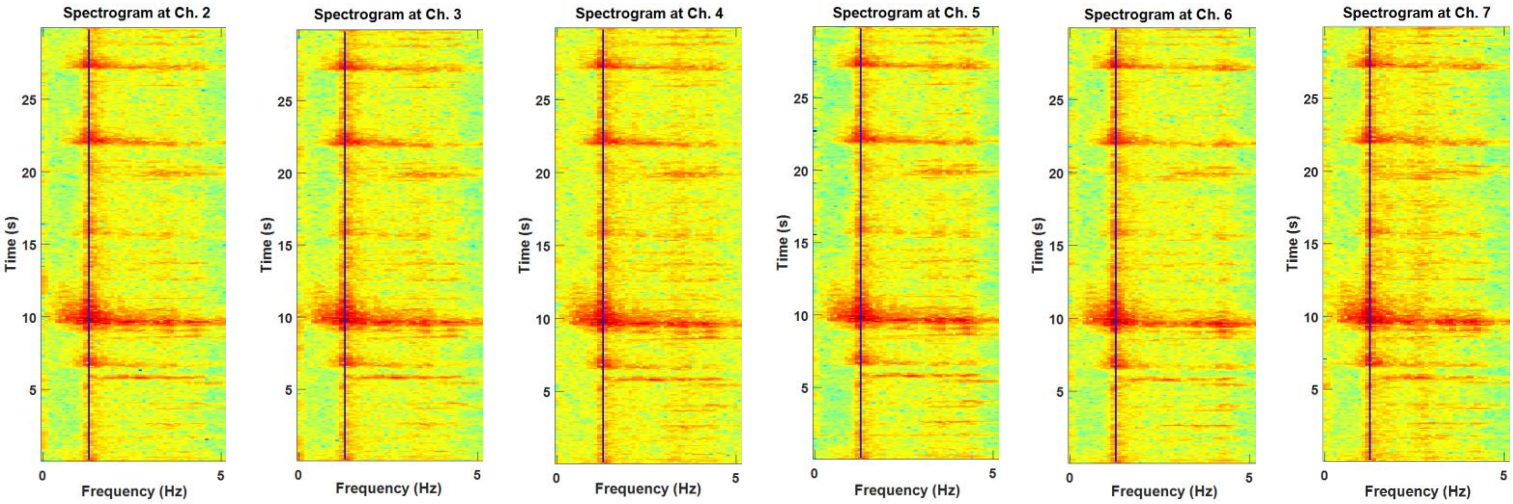

Figure 6.24. Spectrograms of acceleration recorded by accelerometers 2 to 7 in *X* direction during a low-amplitude aftershock.

It can be concluded that the superstructure started to behave nonlinearly once the amplitude of ground motion exceeds a specific range, which could cause serious and major structural damages. Therefore, it is crucially important for monitoring and maintenance purposes to estimate the range that the important civil infrastructures start to behave nonlinearly. It could lead the responsible people to take quick and accurate actions for damage assessment immediately after strong events, such as earthquakes.

Table 6.2. Details of the vibration data sets used for ARMAX models.

Dataset	Amplitude Range (g)	Input channel	Output channel	Date before earthquakes	Date after earthquakes
1	0.0232-0.0241	8	2	04/02/2013	07/10/2013
2	0.0096-0.0100	8	3	03/01/2013	27/08/2013
3	0.003-0.0032	8	7	07/03/2013	27/08/2013
4	0.003-0.0032	8	7	01/02/2013 07/03/2013	_
5	0.003-0.0032	8	7	_	27/08/2013 02/11/2013

6.4 parametric analysis methods

In this section, the integrity of the full-scale concrete bridge was evaluated using ARMAX parametric modelling, described in chapter 4. Three low magnitude earthquake-induced vibrations with different amplitudes, from 0.003g to 0.024 g, were considered to model the dynamic behavior of the structure for this part of analysis. The details of the data sets, including the input-output channels, recording date, and the magnitude of peak acceleration in *X* direction, were provided in Table 6.2. As is clear, for each range of amplitude, two data sets recorded before and after the two major earthquakes were considered. To model the structure using the ARMAX parametric modelling, both the excitation source and the corresponding structural responses need to be known. As mentioned, seven accelerometers were installed on

the deck and pier of the bridge and one accelerometer was installed on the ground level to record the ground motions. Here, the vibration recorded by accelerometer 8 at ground level was considered as input force and structural responses measured by accelerometers 2, 3, and 7 were considered as outputs of the structure. Only the acceleration data recorded in transverse direction of the bridge were considered for parametric modelling.

It is noteworthy that condition of the bridge under these low magnitude earthquakes was assumed to be undamaged. To obtain the best representation of dynamic behaviour of the bridge, orders of ARMAX model are determined by a trial-and-error process. The orders of polynomials n_a, n_b, n_c, and n_k for the data sets recorded before the earthquakes (undamaged condition) and the data sets measured after the earthquakes (unknown condition) were set 110, 90, 1 and 0, respectively. The frequency responses of dynamic models were obtained using the Bode plot. This plot can show the magnitude (in dB) and phase (in degree) of the system response as a function of frequency.

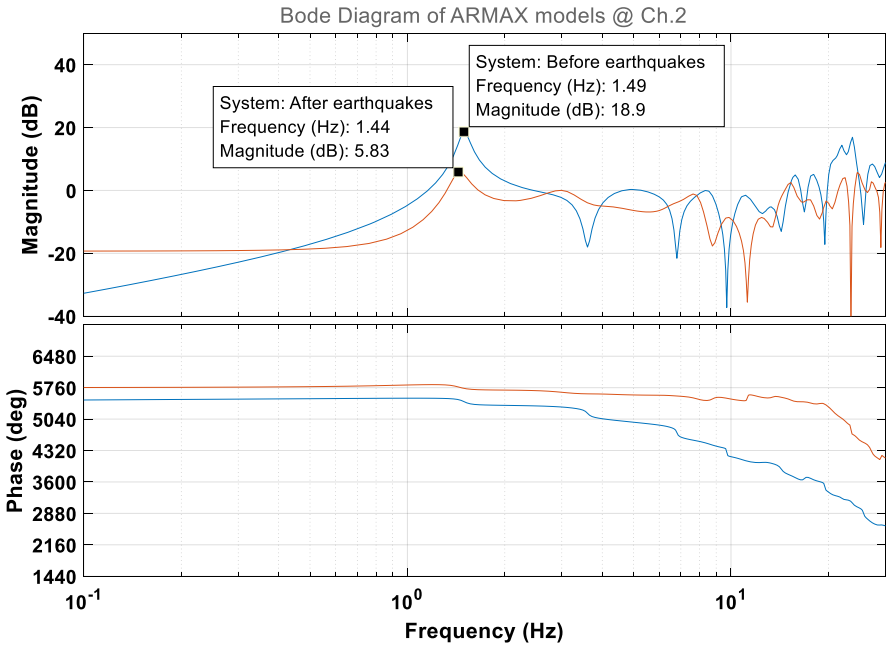

Figure 6.25. Bode plots of the dynamic models estimated by ARMAX using acceleration recorded by accelerometer 2 before and after the strong ground motions.

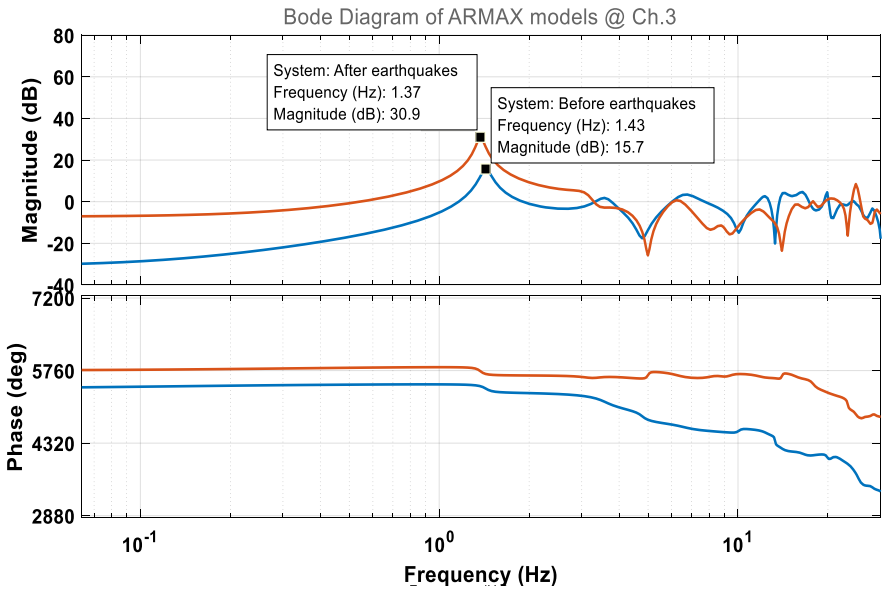

Figure 6.26. Bode plots of the dynamic models estimated by ARMAX using acceleration recorded by accelerometer 3 before and after the strong ground motions.

Figure 6.25 shows Bode plot of the dynamic model obtained using low magnitude earthquake-induced vibration data (range of 0.02g) recorded by accelerometer 2 on 4 February 2013 (before earthquakes) and 7 October 2013 (after earthquakes). As is clear, there is exactly 0.05 Hz shift in natural frequency of the first transverse mode after the strong ground motions. Subsequently, Figure 6.26 depicts an approximately similar change (0.06 Hz shift) in dynamic characteristics of the bridge using the vibration data recorded by accelerometer 3 (range of 0.01g). These data sets were respectively recorded on 3 January 2013 and 27 August 2013 before and after the large magnitude earthquakes. Another low-amplitude earthquake-induced data set with a range of 0.003 g was also analysed. The response of the bridge due to the input excitation was recorded by accelerometer 7 installed on the bridge deck on 7 March 2013 and 27 August 2013. The Bode plot of the dynamic model obtained using this data set is shown in Figure 6.27. As is clear, there is a shift of 0.2 Hz in natural frequency of the first transverse mode due to the strong earthquakes. The small variation between the estimated dynamic parameters of the bridge can be attributed to mathematical errors or different levels of measurement noise in the vibration data sets recorded at various locations on the bridge.

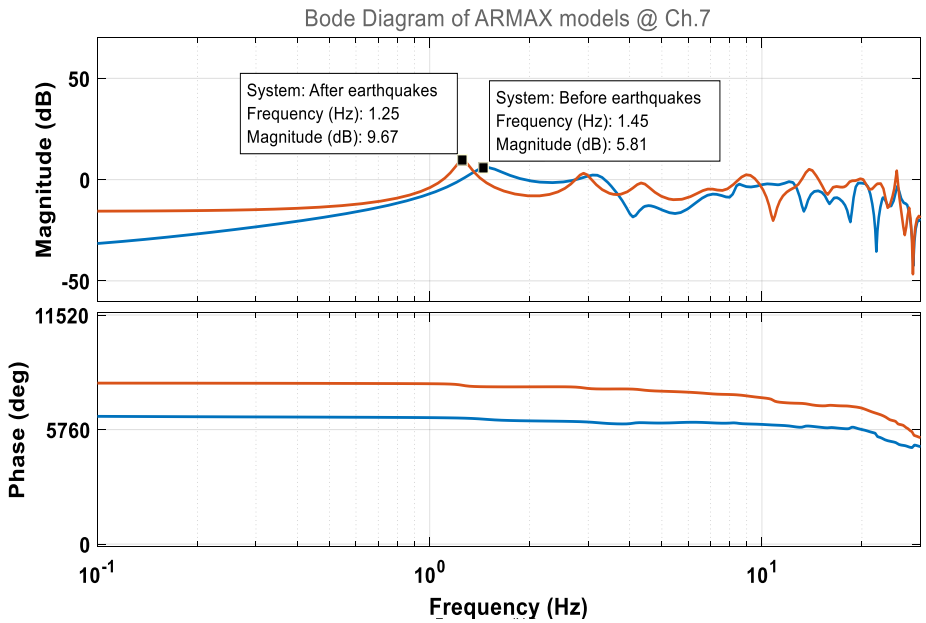

Figure 6.27. Bode plots of the dynamic models estimated by ARMAX using acceleration recorded by accelerometer 7 before and after the strong ground motions.

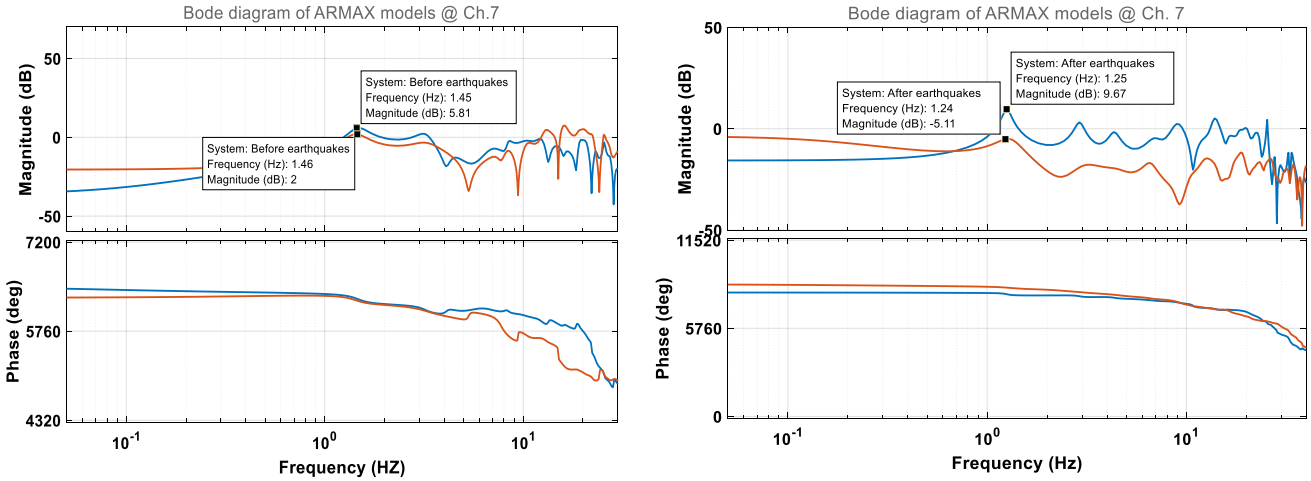

(a) Before earthquakes **(b) After earthquakes**

Figure 6.28. Bode plots of the dynamic models estimated by ARMAX modelling using acceleration recorded by accelerometer 7.

Figure 6.28(a) also shows the frequency response of the bridge dynamic models estimated using two vibration data set recorded by accelerometer 7 on 1 February 2013 and 7 March 2013 (before the two major earthquakes). Evidently, a constant natural frequency of around 1.45 Hz was estimated by two models obatained using the two vibration data sets. Moreover, the frequency response of the bridge estimated using another two low-magnitude earthquakes

recorded by accelerometer 7 after the two major earthquakes on 27 August 2013 and 2 November 2013 is presented in Figure 6.28(b) showing a constant frequency of around 1.25 Hz. The first transverse natural frequency of the bridge estimated by the developed ARMAX models are presented in Table 6.3 for the vibration data recorded from the structure before and after the two strong earthquakes. The results show the reliability of the parametric ARMAX modelling to estimate the dynamic behaviour of the large-scale structure using input and output vibration data sets with various amplitudes associated with measurement noises.

Table 6.3. Estimated first transverse natural frequncy of the bridge by ARMAX models.

Dataset	Amplitude Range (g)	Frequency (Hz) (Undamaged state)	Frequency (Hz) (Unknown state)	Error (Hz)
1	0.0232-0.0241	1.49	1.44	0.05
2	0.0096-0.0100	1.43	1.37	0.06
3	0.0030-0.0032	1.45	1.25	0.2
4	0.0030-0.0032	1.46 1.45	–	–
5	0.0030-0.0032	–	1.25 1.24	–

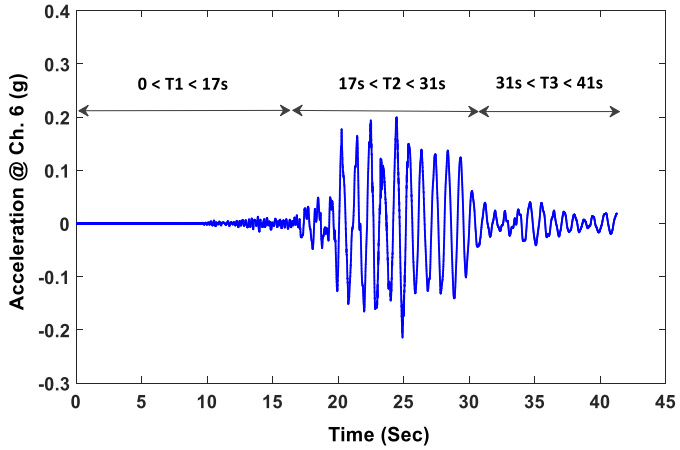

Figure 6.29. Acceleration response recorded by channel 6 due to the first strong earthquake.

In order to show the bridge behaviour during the first large-amplitude earthquake, the earthquake-induced vibration data set was analysed using the ARMAX model. As before, the vibration data recorded by accelerometer 8 was considered as input excitation subjected to the

structure and the vibration measured by accelerometer 6 was considered as the structural response. As can be seen in Figure 6.29, the earthquake-induced vibration recorded by accelerometer 6 was divided into three sections to investigate the influence of non-stationary vibration on the identified dynamic models. As indicated in this figure, the first section (T1) in the time interval, between 0 and 17 seconds, is ambient vibration, the second section T2, between 17 and 31 seconds, includes the most non-stationary vibration, while section T3, between 31 and 41 seconds, is considered the closest to the stationary signal.

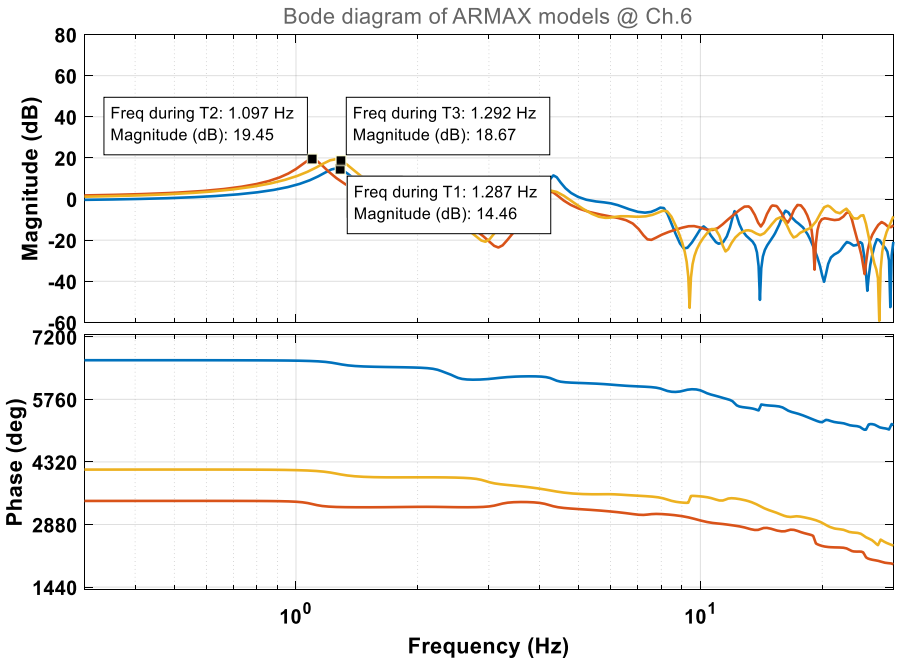

Figure 6.30. Bode plots of the ARMAX models using acceleration recorded by accelerometer 6 during large-amplitude earthquake.

The Bode plots of frequency response of the models are shown in Figure 6.30. It is clearly shown that during the large-amplitude earthquake, there is a significant drop to 1.09 Hz in natural frequency of the first transverse mode indicating that the bridge did not follow linear behaviour due to the large-amplitude earthquake and imminently after the strong shaking it behaved linearly at around 1.3 Hz. It is clearly shown that the data in the non-stationary intervals resulted from a natural event, such as a strong earthquake, could provide significant information about the behaviour and condition of structures during and after the event.

There are various approaches proposed for extracting damage sensitive features from SHM data using a time series analysis. As an example, Gul [161] proposed two damage identification methods based on the ARX model. The first method was based on the coefficients of the ARX model and the second method utilised the difference in ARX model fit ratios. here, a simple dynamic performance index is utilised based on the results of the ARMAX model. The index uses the response predicted from a linear ARMAX model to evaluate the dynamic behaviour of the system during the earthquakes. Considering y (t) as the response of the system, the dynamic performance index is defined by:

$$Index = \left\| \left| y(t)_{\exp} \right| - \left| y(t)_{num} \right| \right\| \tag{6.1}$$

where $y(t)_{exp}$ is the experimental structural responses measured from different locations on the structure and $y(t)_{num}$ is the numerical time series structural responses predicted from a baseline ARMAX model. The index presents the norm of difference between the experimental (unknown condition) and numerical structural responses (undamaged condition).

In this paper, a low magnitude earthquake-induced vibration data set collected from the bridge before the two strong earthquakes is considered as the baseline data set. The assumption here is that the bridge has a linear behaviour under this low-amplitude excitation before the two strong earthquakes. An ARMAX model is constructed using this data set as the reference linear model of the structure. After building the baseline linear ARMAX model, different input excitations are fed to the linear model to predict the output of the identified time series model using the past measured data. In this paper, the input excitations were recorded by accelerometer 8 located at the ground level. Due to the fact that ARMAX models can estimate a linear polynomial model of the system using the input/output data, the predicted responses of the system are linear structural responses as expected from a linear and undamaged system. Therefore, if the unknown condition of the system is linear, the difference between the predicted linear response and the measured response should be very small (close to zero). On

the other hand, for a system associated with possible nonlinearity and structural damage, different values of the index compared to threshold value of the structure are expected.

Table 6.4. Details of data sets used for dynamic performance index.

Dataset	Date of recording	Peak acceleration in X direction (g)
1	21/07/2013	0.168
2	16/08/2013	0.062
3	18/07/2013	0.029
4	20/07/2013	0.020
5	23/08/2013	0.016
6	22/07/2013	0.002

The results of the dynamic performance index based on the ARMAX models are presented in this part. In order to establish a threshold value for the index, low magnitude earthquake-induced vibrations with different levels of amplitude were used to establish a statically meaningful threshold level. The details of the data sets including the date of recording and the magnitude of peak acceleration recorded in the *X* direction are provided in Table 6.4. The first two data sets are the first two strong earthquakes and data sets 3 to 6 are low magnitude earthquakes recorded from the bridge before and after the two strong earthquakes. The assumption here is that the behaviour of the structure under these low-magnitude excitations is linear. It should be noted that the threshold value depends on several factors related to the characteristics of the structure, soil and ground excitation. This threshold level is a unique parameter for each civil structure and needs to be estimated from the undamaged data sets recorded from the structure.

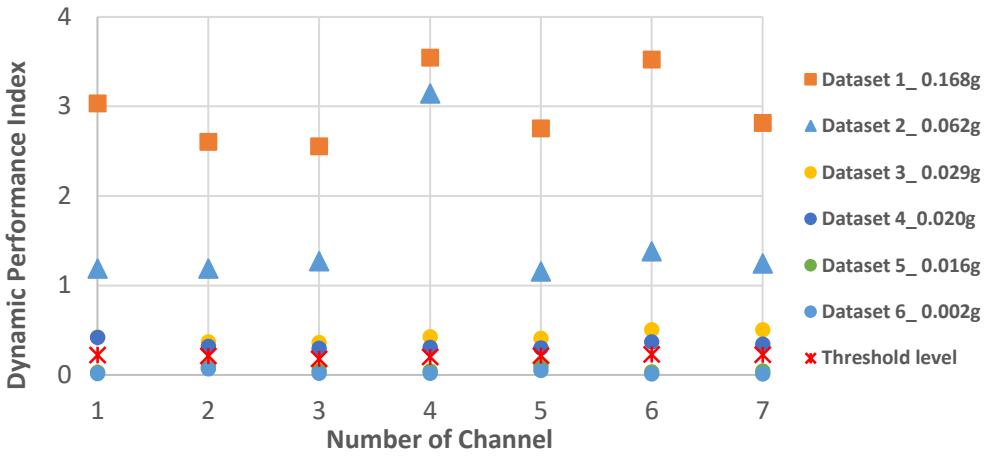

Figure 6.31. Dynamic performance index obtained for different data sets recorded from the bridge.

The index values obtained using the above-mentioned vibration data sets are presented in Figure 6.31 for different locations on the bridge. As is clear, the index values obtained from vibration data sets 3 to 6 are in a same range and close to zero. The mean value of the dynamic performance index obtained using the low magnitude earthquake-induced vibrations is considered as the threshold value to evaluate the dynamic performance of the bridge due to the strong earthquakes. The threshold value of the dynamic performance index was obtained 0.18 for the bridge. As is clear, the dynamic performance index obtained using the two strong earthquakes is higher than the threshold value. It is worth mentioning that the deviation of the performance index from the threshold value for the first earthquake was greater than for the second earthquake. This is because the first earthquake had a higher amplitude. This confirms that the bridge did not follow linear behaviour during the two strong earthquakes as expected from a linear system. In the next section, the force-displacement relationship of the acceleration data will be presented using the proposed toolbox.

6.5 Force-displacement graphs

By considering x as the displacement relative to the ground and $\ddot{x}_g$ as the ground acceleration, the equation of motion for a Single-Degree of Freedom (SDOF) system is given by:

$$M\ddot{x} + C\dot{x} + Kx = -M r\ddot{x}_g \tag{6.2}$$

where M, C, and K are the mass, damping, and stiffness matrix of the system, respectively and r is an $n \times 1$ unit vector ($r = [1 \ldots 1]^T$). Due to the fact that at peak accelerations the velocity values are equal to zero, the equation of motion can be simplified as follows:

$$M\ddot{x} + Kx = -M r\ddot{x}_g \tag{6.3}$$

$$Kx = -M(\ddot{x} + r\ddot{x}_g) \tag{6.4}$$

For a linear system, mass (M) and stiffness (K) are constant, therefore, according to Equation (6.4) the relationship between acceleration and displacement should be linear. However, this relationship is not linear for a system with nonlinearity. Using this simplification and considering the peaks of the acceleration data, the force-displacement relationships were obtained for further investigations on the dynamic behaviour of the bridge during the two strong earthquakes. To do so, the vibration data recorded during the two strong earthquakes and a low amplitude earthquake subjected to the bridge were analysed. It is noteworthy that for each data set, both experimental structural responses, recorded directly from the structure, and the numerical structural response, predicted linear response from the baseline ARMAX model, were analysed to compare the behaviour of the linear and unknown systems.

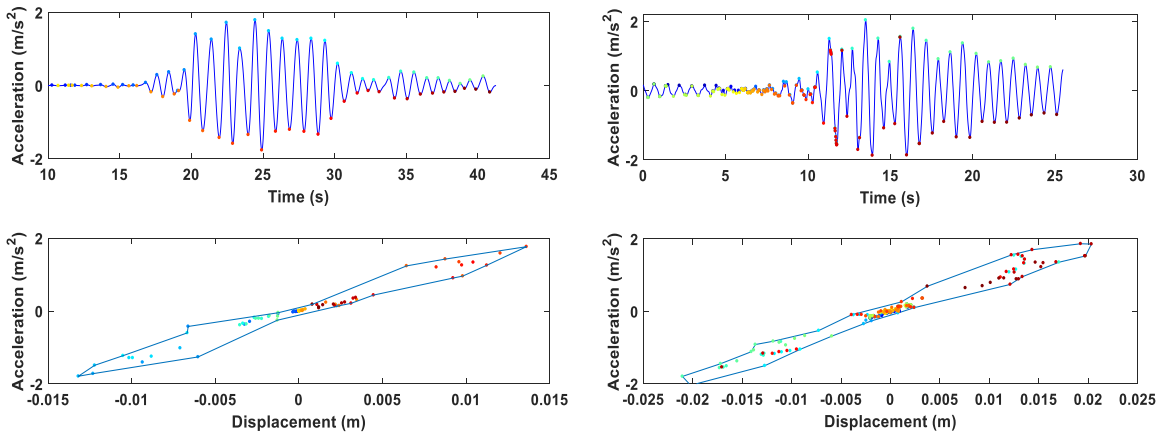

(a) Experimental data **(b) Predicted numerical data**

Figure 6.32. Force-displacement graphs for the first high amplitude earthquake recorded by accelerometer 6.

Figure 6.32 shows the force-displacement relationship for the experimental and numerical structural responses of the bridge due to the first strong earthquake recorded by accelerometer 6. Obviously, although the force-displacement graph for the linear numerical data showed a linear relationship, the force-displacement graph for the acceleration data measured from the full-scale structure (experimental data) showed a close to flag-shaped relationship during the large amplitude earthquake. This can be observed using the amplitude of the signal and the coloured points of the acceleration data during non-stationary intervals. In this figure, the structure behaves linearly during -1 to 1 m/s^2 and during the large amplitude shaking it exhibits close to nonlinear behaviour associated with possible reduction in stiffness (reduction in the slope of the force-displacement graph).

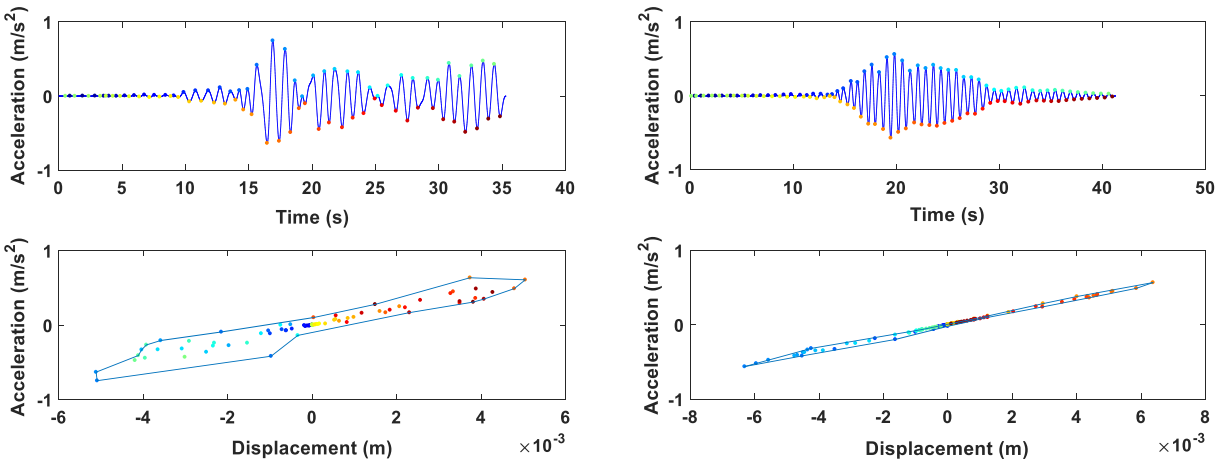

(a) Experimental data **(b) Predicted numerical data**

Figure 6.33. Force-displacement graphs for the second moderate amplitude earthquake recorded by accelerometer 6.

Figure 6.33 depicts the force-displacement relationship for the data recorded during the second strong earthquake. Evidently, the bridge behaviour was close to linear and started to show some nonlinearity during the large shaking of the earthquake. As is observed in Figure 6.34 for low magnitude earthquake, the force-displacement graphs showed linear relationships for both experimental and numerical structural responses. It is concluded that the near to flag-shaped force-displacement relationship during only the first strong earthquake can be considered an

indication for some nonlinearity in the bridge performance. Although the bridge dynamic characteristics were changed by the first strong earthquake (including the shift in natural frequency as a result of possible reduction in stiffness), the bridge followed linear behaviour immediately after the strong earthquake.

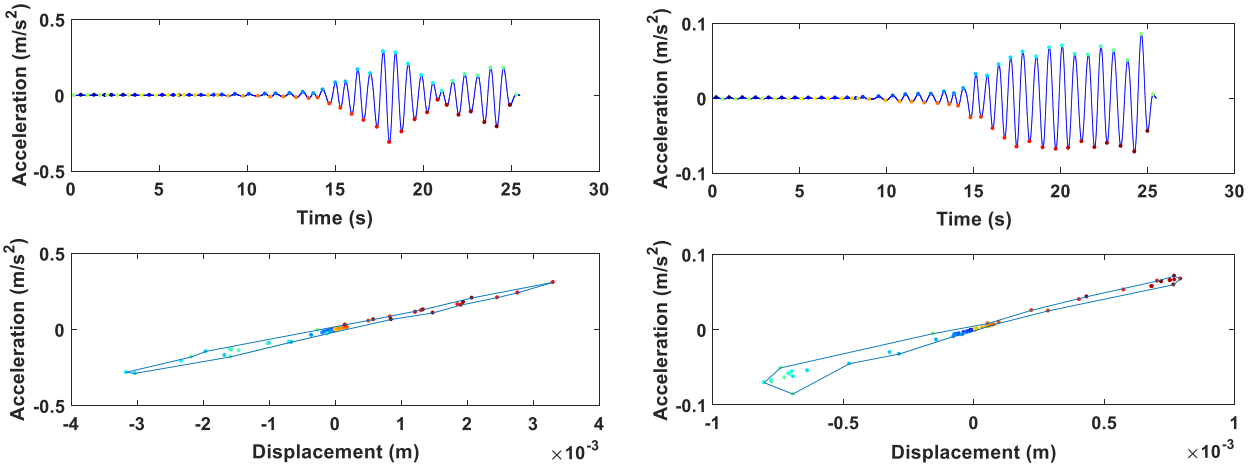

(a) Experimental data. **(b) Predicted numerical data.**

Figure 6.34. Force-displacement graphs for the low amplitude earthquake recorded by accelerometer 6.

Generally, the structure started to behave nonlinearly once the amplitude of the ground motion exceeds a specific range, which might cause minor to major structural damage. However, more investigations need to be done using more information and data sets to determine the type of nonlinearity and location and severity of any possible structural damage throughout the bridge due to the subjected earthquakes. The results presented in this chapter showed the capability of vibration-based data analysis and the reliability of MATLAB-based computational toolbox for structural health monitoring of large-scale civil structures.

6.6 Summary and Conclusion

A case study research paper presenting the results obtained on structural health monitoring of a large-scale bridge located in Wellington, New Zealand was presented in this chapter. This bridge was subjected to two large-amplitude earthquakes and several aftershocks. The structural performance was assessed using non-parametric and parametric analysis techniques

to obtain the vibration intensity parameters and dynamic characteristics of the structure. A dynamic performance index based on ARMAX modelling was used for further investigations on dynamic behaviour of the superstructure under different amplitudes of ground motions. All the analysis results obtained for the bridge structure were computed in MATLAB environment. These results have been summarised and presented in the following.

1. The analysis results of ambient and earthquake-induced vibrations recorded from the large-scale structure showed the efficiency and capability of the MATLAB-based toolbox in terms of management of large data sets and long-term monitoring of large-scale structures. It can be concluded that such monitoring environment provides engineers with accurate dynamic performance indicators to easily extract maximum useful information from raw vibration measurements.
2. The vibration intensity parameters, such as peak accelerations, Root Mean Square (RMS), and Square Root of Sum of Squares (SRSS), of measurements recorded in vertical direction of bridge were not changed by strong shaking of earthquakes and their following aftershocks. It can be concluded that such vibration-based parameters are less sensitive to minor structural damages compared to other dynamic parameters.
3. The time series analysis carried out on continuously recorded ambient vibration showed a minor but permanent drop of 0.05 Hz in natural frequencies of the first transverse and vertical modes after the first major earthquake. This drop indicated that the dynamic characteristics of the bridge were changed after the strong ground motion, which needs more precise investigations for the type, location and severity of any possible structural deterioration due the subjected earthquakes.
4. Based on the analyses carried out on the earthquake-induced vibrations, a significant drop in natural frequency of the first transverse mode was observed during the two strong earthquakes. In addition, the results of the dynamic performance index based on

ARMAX modelling showed that dynamic behaviour of the bridge during both earthquakes is different from the linear threshold value obtained by the baseline vibration data sets. A near to flag-shaped force-displacement relationship during the first strong earthquake indicated close to nonlinear behaviour of the bridge during the first large-amplitude earthquake. It can be concluded that the type and range of nonlinearity vary based on the amplitude of the excitation. It is crucially important to estimate this nonlinearity range for structures, especially those located in high seismic zones for taking quick and accurate actions immediately after strong seismic events.

5. Another conclusion, which can be driven from the analysis results, is the performance and efficiency of the parametric ARMAX modelling to estimate the dynamic behaviour of a full-scale structure. As it was shown, this modelling method could precisely model the dynamic behaviour of large-scale structures using low-amplitude vibrations associated with measurement noises.
6. By making comparisons between the performance of the output-only non-parametric and input-output parametric time-series methods for modelling the dynamic behaviour of a full-scale structure, it can be concluded that the simple output-only models can estimate the dynamic characteristics of the structure as efficiently as more complex input-output models can.
7. As a final conclusion, although there are some minor but permanent changes in dynamic characteristics of the bridge and possible nonlinearity in the bridge behaviour due to the subjected ground motions, the overall dynamic performance of the large-scale structure needs to be precisely investigated using more sets of data for the type, location and severity of any possible structural damage due to the subjected earthquakes.

Chapter 7: Full-scale Bridge Health Monitoring using the Developed WSSN-Based SHM System

7.1 Introduction

In this chapter, the results of a bridge health monitoring project using the developed wireless SHM system is presented. The testbed structure is the Newmarket Viaduct, which is one of the most distinctive engineering features' of New Zealand. One main goal of this instrumentation was to evaluate the performance of the developed wireless smart sensor network in an outdoor environment for condition assessment of large-scale civil infrastructures. In addition, assessment of dynamic performance of the superstructure after several years in operation was another goal of the bridge instrumentation.

In order to achieve these important goals, the bridge structure was instrumented during two phases of field testing. In the first phase, 20 wireless smart sensor nodes were installed on span 9 of the bridge on 30 November 2018. The wireless sensors were recorded ambient vibration for one month and during this monitoring period some issues in terms of battery source, wireless communication and data transmission were found. After updating the hardware and software of the sensor nodes, the same span of the bridge was re-instrumented using final version of the wireless accelerometer sensor nodes on 25 November 2019. The modal characteristics of the bridge, such as natural frequencies, obtained using the vibration measurements recorded during the ambient vibration tests were utilised for dynamic assessment of the structure after several years in operation. It should be mentioned that in this research, the modal parameters of the bridge structure obtained during previous ambient vibration tests were also utilised to evaluate the dynamic performance of the Newmarket viaduct.

7.2 Description of the Newmarket Viaduct

7.2.1 Original Newmarket Viaduct and its replacement

The original Newmarket Viaduct was constructed in 1966 as the first post-tensioned, balanced cantilever bridge built locally. The viaduct was a ground-breaking design for New Zealand and part of the country's largest road link. As mentioned in [162], no attention had been considered to compensate for the effects of differential temperature in the design of the structure, which could lead to weak resistance to traffic and seismic loads and extreme cracking issues over the lifetime of the structure. Therefore, after more than 40 years in operation, it was decided to replace the old structure with a new replacement due to several deficiencies in design and on-going pressures on capacity of the motorway network. The new structure was constructed and opened to traffic at the end of 2010. The new replacement of Newmarket Viaduct is a horizontally and vertically curved, post-tensioned concrete box bridge, comprising two parallel twin bridges. The Northbound and Southbound Bridges are supported on independent pylons and joined together via a cast in-situ concrete 'stich'. Several views of the new constructed Newmarket Viaduct are shown in Figure 7.1.

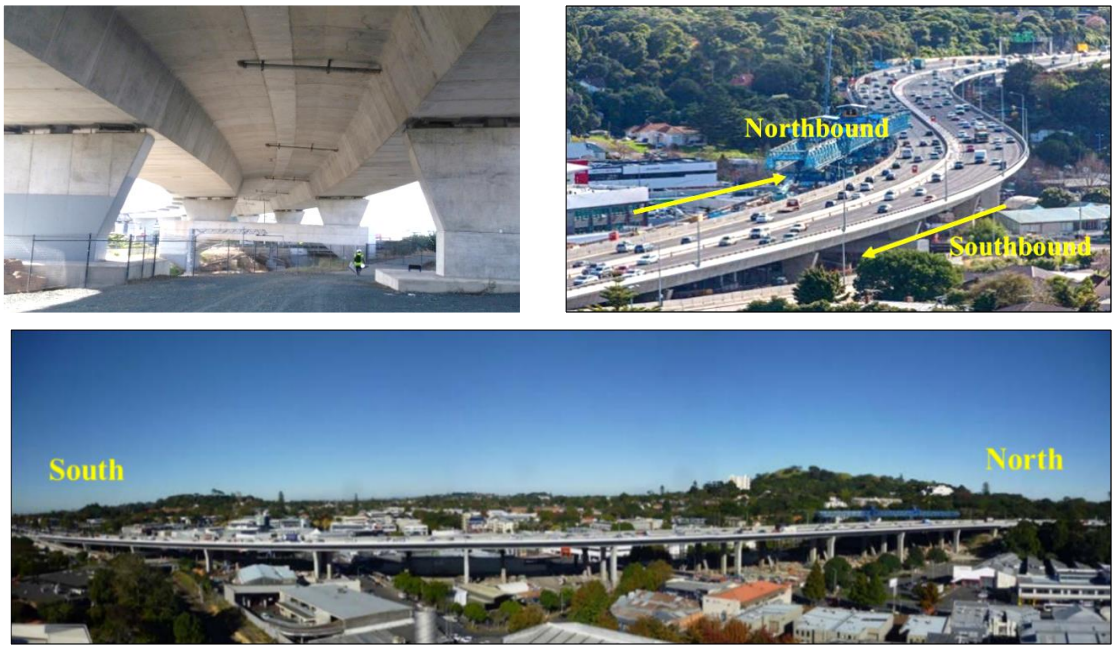

Figure 7.1. Several views of the Newmarket Viaduct.

Approximately 4200 t of reinforcing steel and 30000 m^3 of concrete have been consumed for the new construction. The new bridge with a total length of 690 m has twelve individual different spans ranging from 38.67 m to 62.01 m with an average length of approximately 60 m [163]. 20 concrete cylinder specimens with the dimension of 100 mm × 200 mm were used as concrete samples for laboratory tests to measure the material properties of the concrete used for the construction. Based on the investigations carried out on the samples, the 28-days compressive strength, the elastic modulus and the density of concrete were measured to be 60 MPa, 36 GPa and 2550 kg/m^3, respectively. The superstructure is located in an area with moderate seismicity and the closest fault to site is 30 km. The new constructed bridge was designed to endure the earthquakes with a 2500 year return period [164].

7.2.2 Structural elements

The Newmarket Viaduct is an S-shaped bridge in planar view, which has two horizontal curves with 760 m and 690 m radius and a very slight vertical curvature. The post-tensioned concrete box bridge was constructed with 468 precast concrete sections with roughly 3.0 m long using balanced cantilever construction [165]. According to this technique for bridge erection, two precast segments of the concrete girder are placed on their specific locations, which are symmetrical on both sides of the pier in the case of the Newmarket Viaduct, and retained on the place using post-tensioned tendons. Then, the next segment is added to the system using the same process. At the end of construction of each span, the concrete stich is casted in-situ at mid-span and the continuity tendons are stressed. After completion of this stage, the concrete girder is considered a continuous beam. As mentioned, the bridge is comprised of two parallel twin bridges that are a continuous single-cell box girder. The cross section of the concrete box girder with its dimensions according to the New Zealand Transport Agency (NZTA) drawings are shown in Figure 7.2.

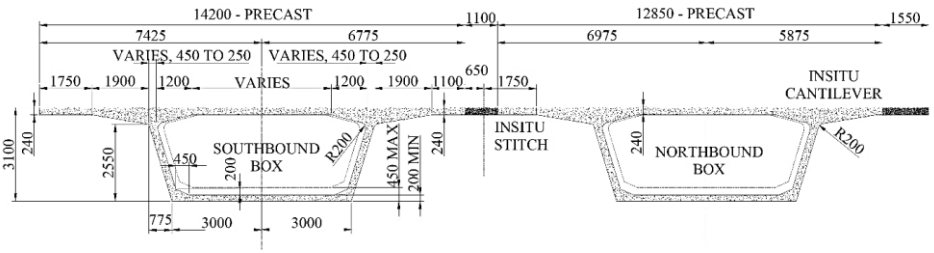

Figure 7.2. The bridge deck cross section based on the NZTA drawings (all dimensions are in mm).

(a) Pier diaphragm **(b) Intermediate diaphragm**

Figure 7.3. Location of the diaphragms inside the box girder [162].

As is obvious, the cross section takes 0.6 m wide right-hand shoulders, 1.2 m wide left-hand shoulders, and four 3.5 m wide southbound and northbound traffic lanes. Although the superstructure has a constant depth of 3.10 m and top slab thickness of 240 mm, the other dimensions shown in cross section change along the length of the bridge. Figure 7.3 depicts the pier diaphragm and intermediate diaphragm of the Newmarket Viaduct. The intermediate diaphragms, which are located at one and two-third points of each span, perform as deviator points for the external post-tensioning [162]. Both bridges were founded on independent piers and connected using the cast in-situ concrete 'stich' as shown in Figure 7.4.

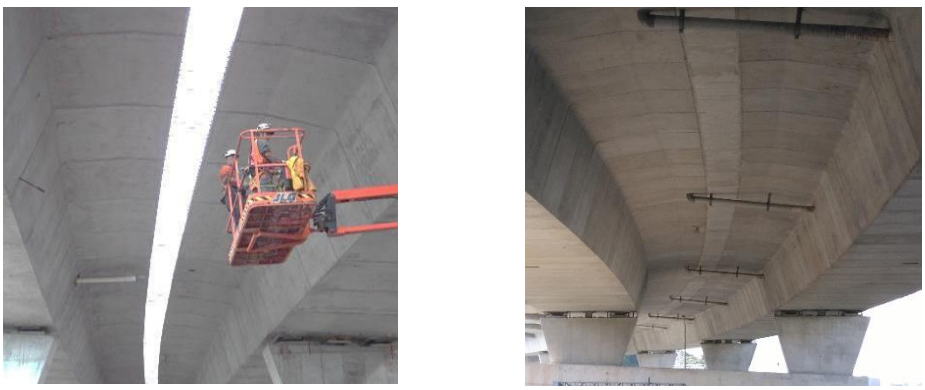

Figure 7.4. The Newmarket Viaduct before and after casting the in-situ concrete stich.

Twelve concrete piers with the height of between 2.88 m to 22.05 m were placed under each twin bridge to support the intermediate spans (Pier A (PA) to Pier M (PM)). The piers of the viaduct have a rectangular 3.50 m×1.50 m cross section in their lower and mid-height portions, but the height of the top portion changes between 2.45 m and 4.40 m. The bridge piers are supported on square rigid footings except piers PG, PH, PJ, PL, and PM, which are supported on piles. The dimension of the pier caps and footings are 7.0 m ×7.0 m ×2.0 m. Piers B and H are supported on two pinned bearings under each girder. Piers C-G are monolithic with the concrete girder and the abutment at the south end and piers A and J-M are supported on two sliding bi-directional elastomeric seismic devices under each girder, which could allow to have longitudinal displacement. Figure 7.5 shows two views of the seismic isolation bearing as support under some of the piers at the Newmarket Viaduct. In addition, the plan and elevation views of the Southbound and Northbound bridges based on the NZTA drawings are shown in Figure 7.6 to demonstrate a clear view of the Newmarket Viaduct. It should be mentioned that in this thesis, the longitudinal and transverse directions are defined with respect to the curved centre line of the bridge and the vertical direction is considered in the gravity direction.

Figure 7.5. Seismic isolation bearings at Newmarket Viaduct.

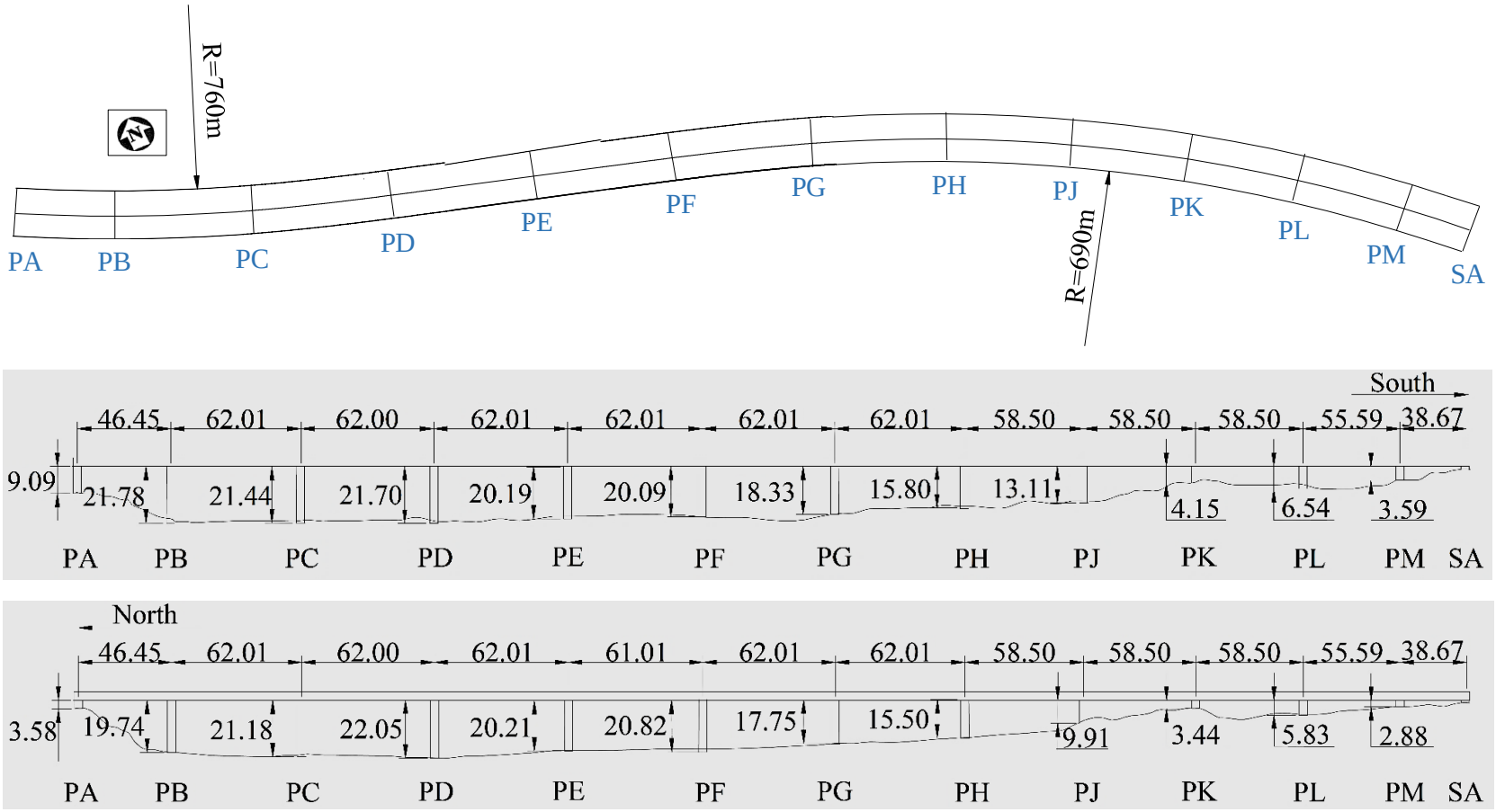

Figure 7.6. Plan and elevation views of the Southbound and Northbound Bridges based on the NZTA drawings (All dimensions are in mm).

7.3 Existing wired SHM system on the Newmarket Viaduct

The Newmarket Viaduct was instrumented using a wired SHM system designed by a research team from University of Auckland in 2009. Spans 8 and 9 of the bridge were instrumented using the developed wired SHM system. The system included 20 vibrating wire strain gauges that could also measure the temperature values, 42 embedded temperature sensors, four baseline systems for measuring deflections, and two external temperature and humidity sensors inside and outside the concrete box girder. In addition, six uniaxial accelerometers were installed on these spans to measure the vibration induced by traffic on the bridge in both vertical and transverse directions. The elevation view of sensor locations on Spans 8 and 9 are shown in Figure 7.7.

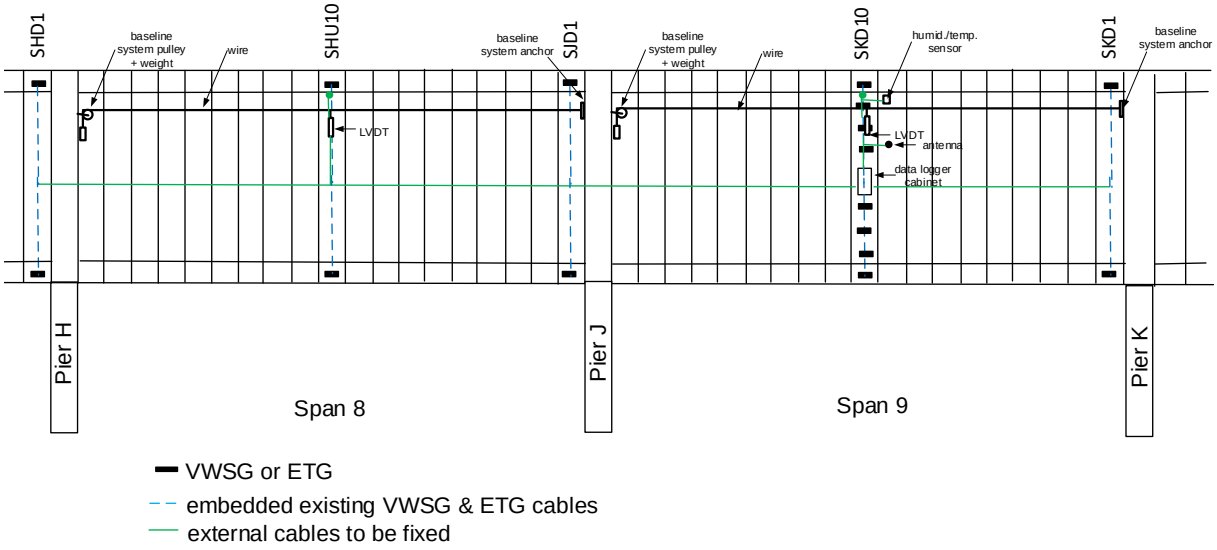

Figure 7.7. The elevation view of spans 8 and 9 of the Newmarket Viaduct [151].

Four strain gauges were embedded in concrete in some special locations having maximum moment values. These locations are in the middle of the both spans, near to their piers and at the ends of the spans. 42 temperature sensors were spread uniformly in both webs along their height in the middle of Span 9. As is clear in Figure 7.7, more sensors were located in the top and bottom slab and across the webs. Four baseline systems integrated into the wired SHM system include a displacement transducer (LVDT) and a taut wire that has been embedded

inside the girder along its right- and left-hand sides. The schematic location of the SHM system in cross section view of the bridge is shown in Figure 7.8. In this figure, the strain gauges are depicted by squares and the temperature sensors with dots.

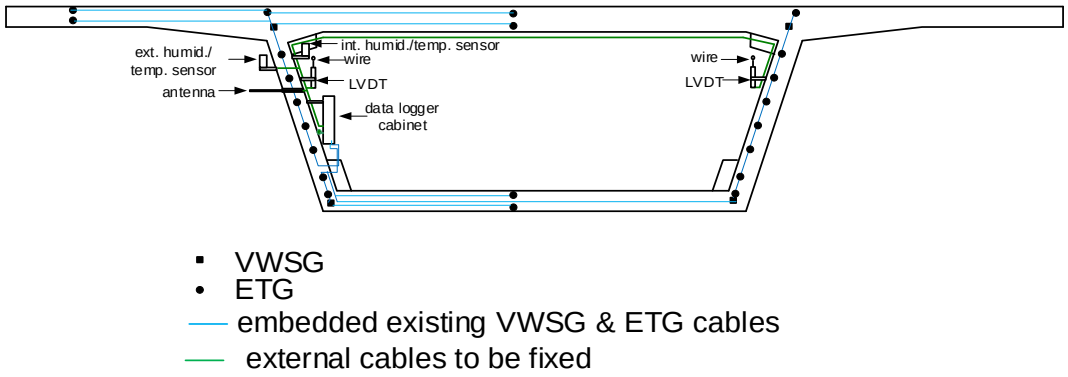

Figure 7.8. Location of the wired SHM system in cross section view of the bridge [151].

In the monitoring system, LVDTs were fixed to the concrete girder at middle of the span and its moveable end to the wire. The sensor can move once the concrete box girder deflects, however the wire remains in its location to provide a reference point for measuring the deflection of the girder. In addition, Vibrating Wire Strain Gauge (VWSG) was utilised as strain gauge for the SHM system. The VWSG performs based on the principle that a tensioned wire vibrates at a proportional frequency to the strain in the wire. A wire is tensioned between two mounting blocks, which can be attached to the structure. Any applied load to the structure can alter the distance between the blocks resulting in the alteration of tension value in the wire. In the next step, an electromagnet is utilised to pluck the wire to record the frequency of wire in tension. Then, by applying the calibration factors to the measured frequency, the strain values can be obtained. These types of strain gauges can be installed on the structure surface or embedded into concrete members. In this SHM system, the recorded data by the sensor system is logged by a data logger installed on the mid span and downloaded from University of Auckland (UoA) using a wireless modem over a cellular telephone network. The data logger with the connected wires from various types of sensors are shown in Figure 7.9.

Figure 7.9. Data logger of the wired SHM system.

7.4 Initial deployment of wireless SHM system on the Newmarket Viaduct

The developed wireless SHM system were installed on span 9 of the Newmarket Viaduct for an initial evaluation of the system performance in an outdoor environment for condition monitoring of large-scale civil infrastructures. Due to the fact that several ambient vibration tests were conducted on span 9 of the bridge during different phases of structure's lifetime, this span was selected to be instrumented. The field experiments were conducted on 30th of November 2018 for one month of monitoring under operational conditions, which did not interface with the flow of the traffic over the bridge. 20 wireless smart sensor nodes (version 2) were installed inside the box girder on both sides of the span. 14 sensor nodes (WSSN1-WSSN14) were installed on internal surface of the bridge deck and the remaining six wireless accelerometer sensors (WSSN15-WSSN20) were fastened on post-tensioning cables on both sides of the span. Figure 7.10 shows the locations of the sensor nodes inside the box girder in plan and cross section views and some of the installed wireless smart sensor nodes on the bridge deck and post-tensioning cables. In the following sections, first the hardware and software setups considered for first phase of instrumentation are presented. Then, the performance of the system is evaluated using preliminary data analysis. At the end, the issues of wireless sensor network found during the bridge instrumentation are discussed.

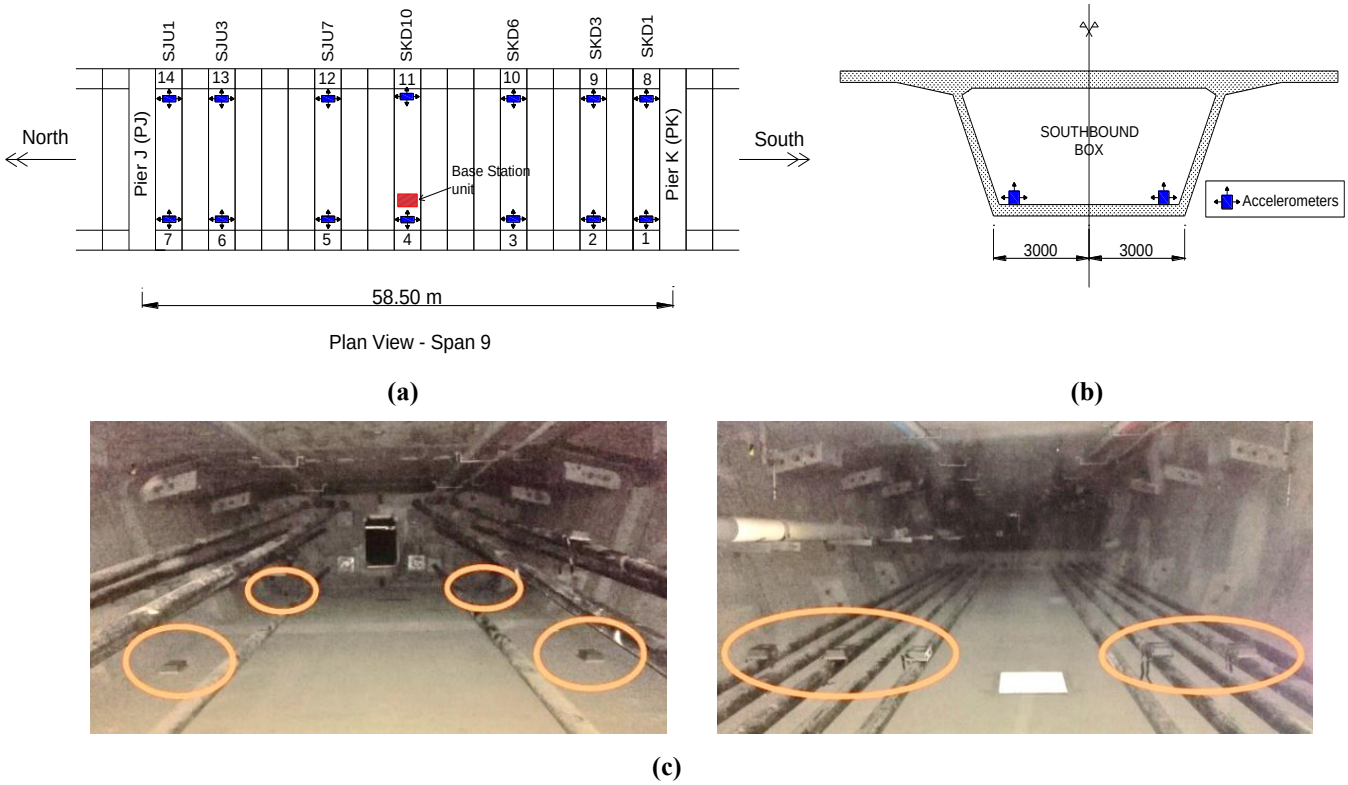

Figure 7.10. The locations of wireless sensor nodes in (a) plan view, and (b) girder cross section, and (c) some of the sensor nodes installed on the bridge deck and post-ternsioning cables (the figures are not scale).

7.4.1 Hardware & software setups

As mentioned, the second version of the wireless smart sensor nodes were utilised for the first phase of instrumentation. In order to avoid environmental effects on the sensor nodes, all the sensor units were enclosed with a weatherproof plastic enclosure. Then, the plastic enclosures were attached to timber plates to ease the installation process. In order to avoid damage to the bridge structure, it was decided to glue the timber plates to concrete surface of the bridge deck using Epoxy. It should be mentioned that the wireless smart sensor nodes were fastened around the post-tensioning cables using strong straps to measure the vibration induced by traffic on the post-tensioning cables. It was decided that the wireless smart sensor nodes sample the structural ambient vibration using time-triggered sampling mode. During this instrumentation, the wireless smart accelerometer nodes were powered using a special type of power bank attached to the USB port of the sensor nodes. It is noteworthy that most of the high capacity

power banks have been instructed using AutoOff mode, which means they stop providing supply to the device after about some time of little or no power draw depending on its threshold. Therefore, once they go to sleep mode following with a power draw, the power banks will be shut off and need to be powered with human interaction. In this study, a 12,000 mAh capacity battery pack from Voltaic System with Always-On mode feature was utilised to power the sensor nodes. Always-On mode is a feature that according to it, the battery output does not shut off after a set amount of time. Therefore, it can be used for a continuous sampling mode of the wireless sensor nodes.

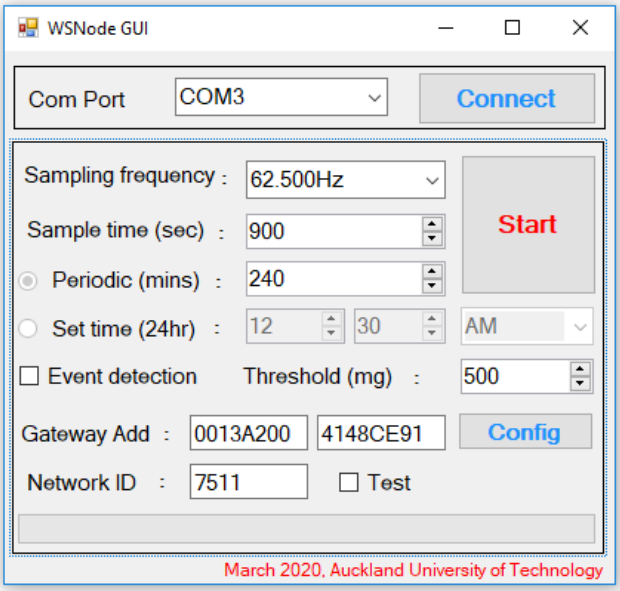

Figure 7.11. The setting of the GUI for phase one of bridge instrumentation.

The wireless smart sensor nodes were programmed and instructed using the GUI introduced in chapter 3. Figure 7.11 depicts the programmed GUI for this phase of bridge instrumentation. As can be seen, the sensor nodes were instructed to measure the ambient vibrations induced by traffic on the bridge for 15 minutes every 4 hours that results in six sampling per day. The sampling frequency was set to 62.5 Hz for this setup. One of the most important components of the wireless SHM system is the base station unit, which is considered as a key link between the wireless smart sensor system and the monitoring centre.

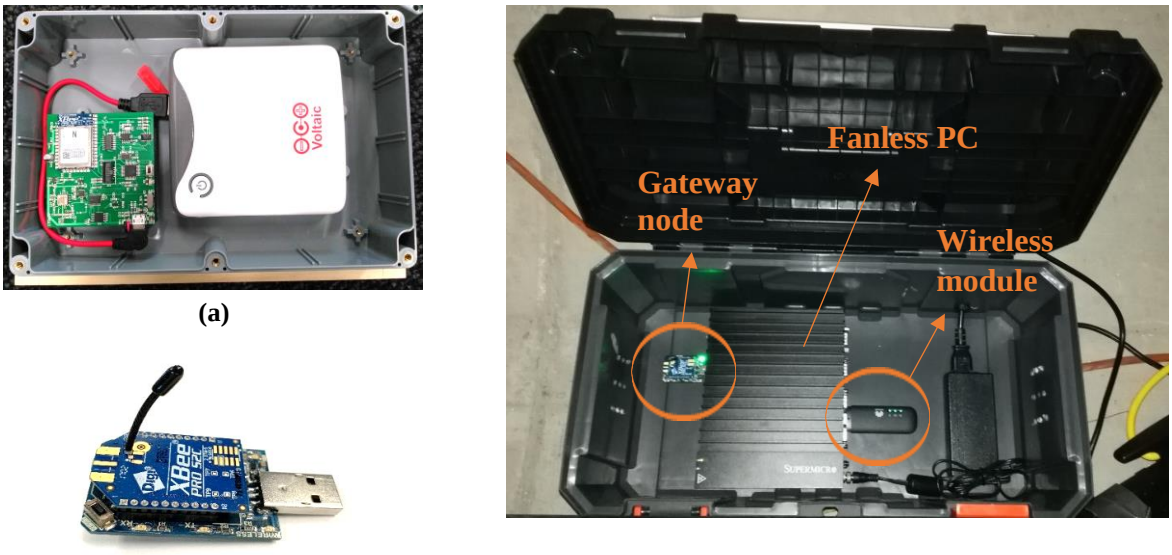

(a)

(b)

(c)

Figure 7.12. (a) WSSN-V2, (b) the gateway node, and (c) the base station unit.

In this research, the base station unit consists of a fanless industrial grade Mini PC, an USB Wi-Fi modem for remote access to the system, and an XBee module as the gateway node. All of these components were enclosed using a weatherproof enclosure to be protected from environmental effects in an outdoor environment. For the desktop computer, a fanless and noiseless Intel core i7-7500U Windows operating Microcomputer was selected for the system due to its high specifications. The small size PC has a processor speed of 2.7 GHz up to 3.5 GHz, 16 GB Ram, 256 GB Solid State Drive (SSD), 128 MB memory capacity, and 40 GB hard drive capacity suitable for running the wireless sensor system and the related data analysis platforms for SHM applications. An XBee Pro Series 2C module was also connected to the base station unit as the gateway node with the responsibility of managing the wireless sensor network and sending user-defined commands to the wireless smart sensor nodes for different tasks, such as waking up, starting sampling, transmitting and receiving the recorded data. For this setup, the base station unit was installed at the middle of the span roughly close to the bridge electrical system. One of the wireless sensor nodes attached to a power bank, the

gateway node, and the base station unit installed on the Newmarket Viaduct are shown in Figure 7.12.

7.4.2 Performance evaluation and preliminary data analysis

The wireless smart sensor network was intended to measure the dynamic responses of the bridge deck and post-tensioning cables due to traffic and wind loads subjected to the bridge structure. It should be mentioned that traffic loading is the dominant source of vibration for the Newmarket viaduct. The acceleration time series recorded by wireless smart sensor nodes located in the middle to the end of span (WSSN4-WSSN7) are shown in Figure 7.13.

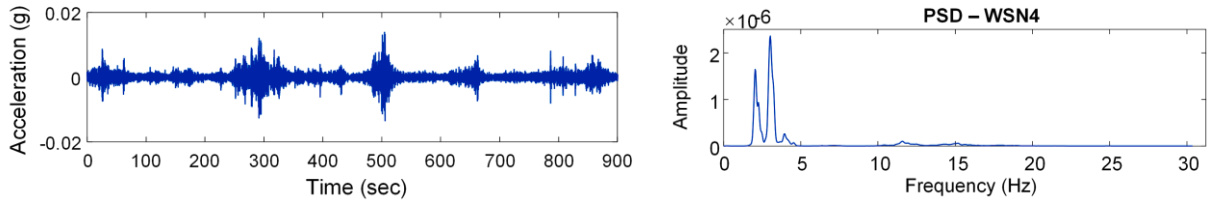

(a) WSSN4

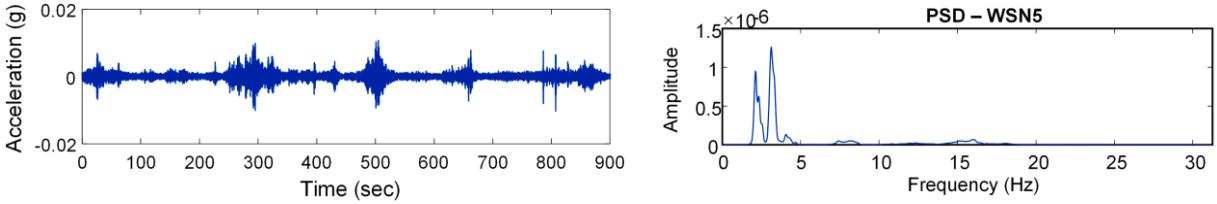

(b) WSSN5

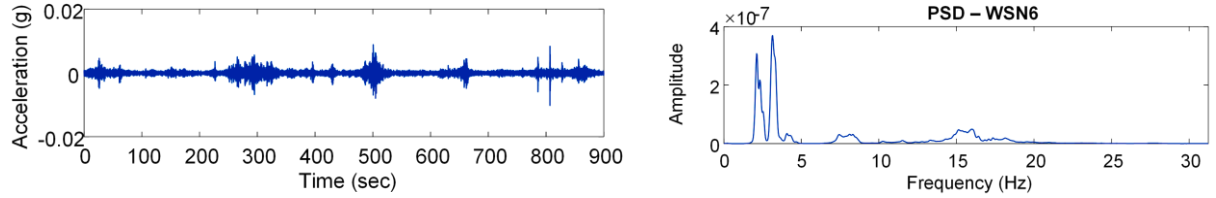

(c) WSSN6

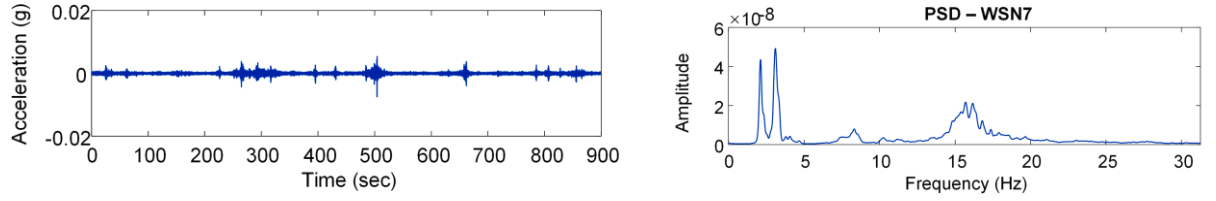

(d) WSSN7

Figure 7.13. Vertical acceleration time histories and the PSD values of the bridge deck recorded on November 30, 2018 at 9:00 PM.

These measurements were recorded in vertical direction of the bridge structure using WSSN4, WSSN5, WSSN6, and WSSN7. After preliminary data manipulation and the mean and trend removal, the Power Spectral Density (PSD) values were also plotted for each time-series signal. As mentioned, the vibration data sets were recorded at sampling frequency of 62.5 Hz for 15 minutes that resulted in 56,250 samples per channel. As is clear from these figures, although the amplitude of ambient vibration recorded from the bridge deck was about ±1 mg throughout the test duration, spikes of near to 15 mg were observed. These spikes were likely caused by travelling of heavy vehicles on the motorway. Very consistent and similar structural peaks were measured using different wireless smart sensor nodes, which correspond to the first few vertical modes of the bridge structure.

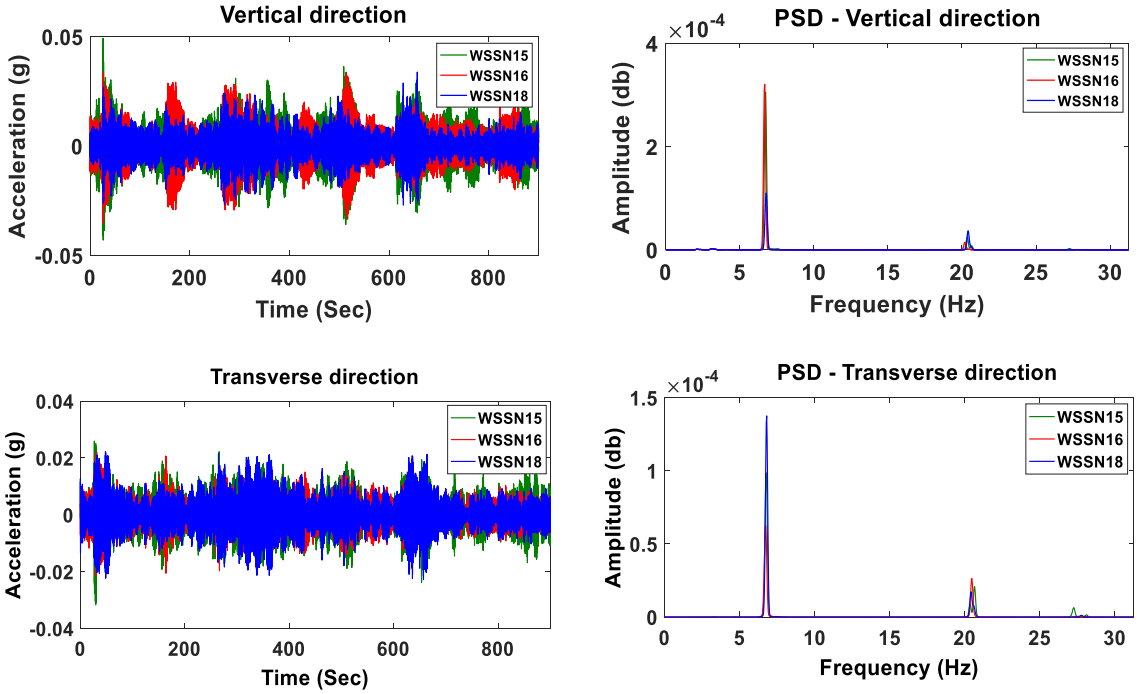

Figure 7.14. Vertical and transverse acceleration time histories and the PSD values of three post-tensioning cables recorded on November 30, 2018 at 9:00 PM.

Figure 7.14 depicts the acceleration time histories measured from three post-tensioning cables in vertical and transverse directions using three wireless accelerometer sensor nodes attached to the post-tensioning cables. Each figure includes the time series signals and the corresponding

PSD values measured by WSSN15, WSSN16, and WSSN18. As is clear from the figures, the measured acceleration data across the post-tensioning cables ranged from 7 mg to a peak of close to 50 mg for the vertical direction and a peak of close to 30 mg for transverse direction. Two precise and distinct spectral peaks were also observed in both directions measured by all the wireless smart sensor nodes showing the first two vertical and transverse natural frequencies of the post-tensioning cables. As expected, the natural frequencies of the post-tensioning cables are obtained identical in vertical and transverse directions. The ambient vibration data sets presented for the bridge deck and the post-tensioning cables were recorded on 30 November 2018 at 9:00 PM (first day of the bridge instrumentation). So far based on these results, it can be concluded that the wireless smart sensor nodes are capable to record clear and low-noise time histories of very low-amplitude vibrations induced by traffic and wind loading throughout the structure. This can confirm the fact that the wireless accelerometer sensor nodes can be utilised for ambient vibration measurements from large-scale structures to estimate their dynamic characteristics for damage identification purposes. The vibration recorded in longitudinal direction is ignored for analysis as they are not effective on dynamic condition of the structure. The vibration data sets were managed using DMT toolkit first and then analysed using the DAT toolkit to extract modal characteristics of the bridge structure.

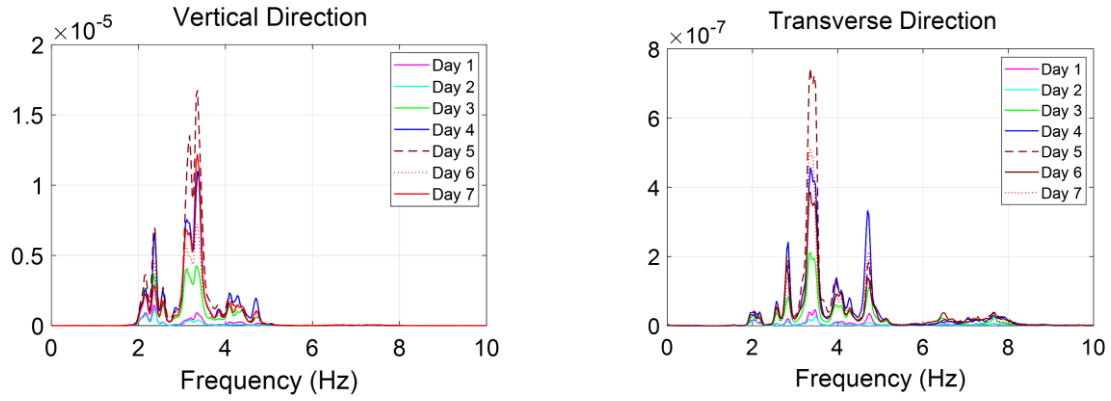

Figure 7.15. PSD values of acceleration recorded by WSSN11 in Transverse and vertical directions.

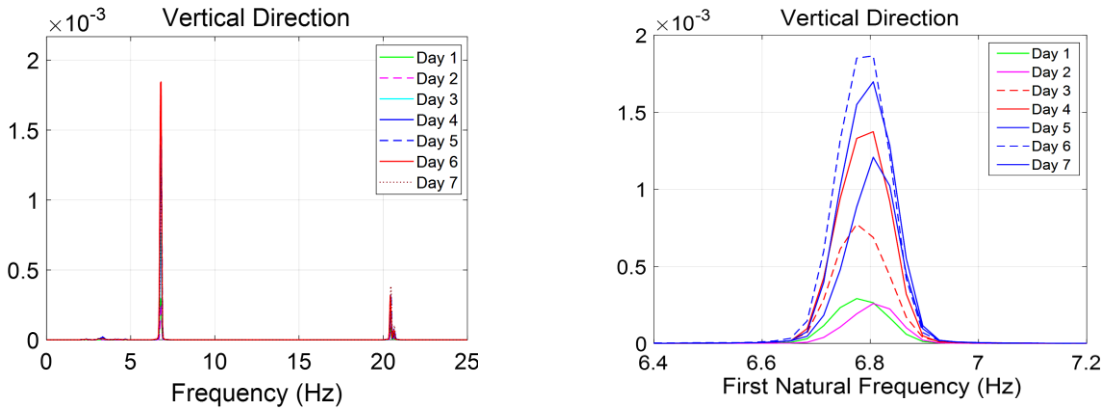

Figure 7.16. Power spectral densities of acceleration recorded by WSSN18 in vertical direction.

Figure 7.15 presents the PSD values of acceleration time histories measured by WSSN11, which was located at middle of the bridge span, in both vertical and transverse directions of the structure. In addition, Figure 7.16 illustrates the PSD values obtained from vibration data set measured using WSSN18 attached to one of the post-tensioning cables in vertical direction. The vibration data sets were recorded at 1:00 PM during one week of monitoring period that is from 1 December 2018 (on Saturday) to 7 December 2018 (on Friday).

As can be seen from the results, the PSD values obtained from the vibration data recorded from the bridge deck and the post-tensioning cable on weekend (December 1 & 2) are less that the values obtained during weekdays because of less traffic loads on the bridge motorway during the first two days of the monitoring period. The results showed a good consistency between the PSD values obtained from different sets of acceleration time histories recorded at different days of a week. In addition, the vibration data recorded during one week of monitoring period have been analysed using Enhanced Frequency Domain Decomposition (EFDD) technique to identify dynamic characteristics of the bridge. Figure 7.17 shows the variation of first two transverse natural frequencies and first four vertical natural frequencies of the bridge deck measured using WSSN4 during first week of monitoring. A good consistency in vertical and transverse natural frequencies was observed during the monitoring period. The small variations between the results can be due to the stationarity of signal and accuracy of computational algorithm.

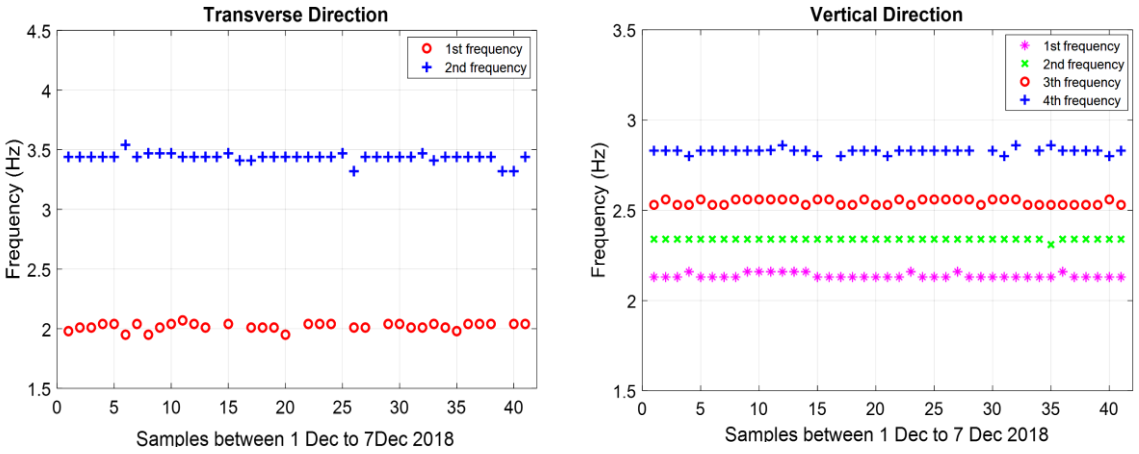

Figure 7.17. Variation of bridge modal frequencies during first week of monitoring period.

A common concern regarding the wireless sensor network is time synchronisation between different channels of sensor nodes distributed across a structure. In such network, each sensor node operates with its internal clock, which owns a unique offset specification. The developed wireless smart sensor network uses a synch pulse that is broadcast to all nodes in the network for a synchronised sampling. This command is transferred using an electromagnetic wave, so the wireless sensor nodes will have a nanosecond difference to receive this starting command. A post-processing time synchronisation technique was also performed on the vibration measurements in MATLAB environment using time offsets of each wireless sensor nodes. Figure 7.18 shows a time window of acceleration time histories measured by five wireless smart sensor nodes across the network during a traffic event on the bridge structure. The results confirm that the wireless sensor nodes maintained phase among themselves with a maximum synchronisation error of 1 millisecond and the data can be reliably used for a precise estimation of bridge modal characteristics, such as mode shapes. This also substantiates the techniques used for time synchronisation of the wireless network in this research.

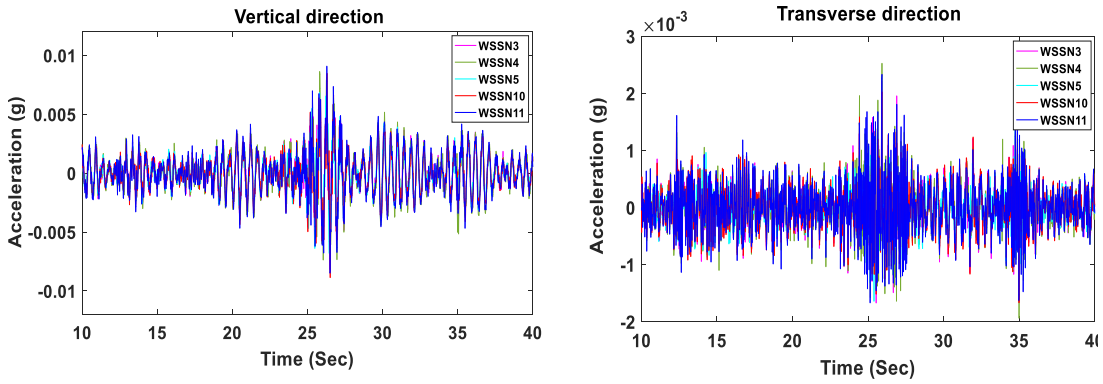

(a) Vertical direction **(b) Transverse direction**

Figure 7.18. Time window overly of acceleration time histories during a traffic event.

In this part, the effect of vibration amplitude on the frequency of the post-tensioning cables is investigated using the wireless sensor nodes. To do so, the vibration method using multiple modes developed in [166] is used. This method starts with the equation of motion of a cable with bending rigidity as follows:

$$m\frac{\partial^2 z}{\partial t^2}+EI\frac{\partial^4 z}{\partial t^4}-T\frac{\partial^2 z}{\partial x^2}=0 \tag{7.1}$$

where z is vertical displacement, x is longitudinal coordinate, m is the unit mass, EI is the bending stiffness of the cable and T is the cable tension in the direction of cable length. Then, by assuming that EI and T are constant along the cable length and hinged boundary conditions at both ends, the above equation can be represented by:

$$T=4ml^2\left(\frac{f_n}{n}\right)^2-\frac{EI\pi^2}{l^2}n^2 \tag{7.2}$$

where l is the length and f_n is the n^{th} natural frequency of the cable. The relation between $\left(\frac{f_n}{n}\right)^2$ and n^2 can be rearranged as:

$$\left(\frac{f_n}{n}\right)^2=\frac{EI\pi^2}{4ml^4}n^2+\frac{T}{4ml^2}=an^2+b \tag{7.3}$$

Due to the fact that a cable is a flexible structure, multiple natural frequencies can be easily measured using the vibration measurements. By obtaining linear regression between multiple

$\left(\frac{f_n}{n}\right)^2$ and n^2 and considering b and a as the y-intercept and slop of the linear regression, EI and T can be estimated as:

$$EI = \frac{4ml^4}{\pi^2}a \tag{7.4}$$

$$T = 4ml^2 b \tag{7.5}$$

In this part, two sets of low-amplitude and high-amplitude vibration data sets recorded at 5:00 AM and 9:00 PM on second day of monitoring are considered for analysis. Figure 7.19 shows the acceleration time-histories recorded from the post-tensioning cable by WSSN18. As is obvious, the data recorded at 9:00 PM has higher amplitude in comparison to the vibration recorded at 5:00 AM. The first three natural frequencies of the cable obtained using these data sets were calculated using PSD estimation.

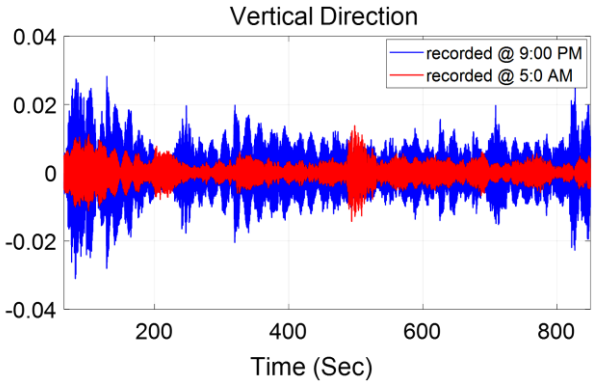

Figure 7.19. Time-history acceleration recorded at 5:00 AM and 9:00 PM by WSSN18.

A linear regression was carried out to find the relation between $\left(\frac{f_n}{n}\right)^2$ and n^2 for the two acceleration time histories. The linear regression results and corresponding equations are presented in Figure 7.20 and Table 7.1 for these acceleration time series.

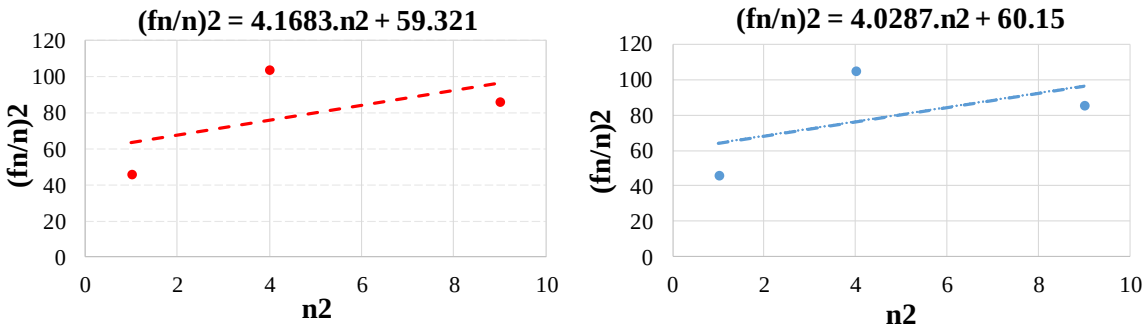

(a) Recorded @ 5:00 AM **(b) Recorded @ 9:00 PM**

Figure 7.20. Linear regression equations obtained using the first three natural frequencies.

Table 7.1. Natural frequencies measured during four stages of ambient vibration tests on the bridge.

DATASET	MODE #1	MODE #2	MODE #3	EQUATION
RECORDED @ 5:00 AM	6.77	20.42	27.86	$\left(\frac{f_n}{n}\right)^2 = 4.16n^2 + 59.32$
RECORDED @ 9:00 PM	6.80	20.48	27.77	$\left(\frac{f_n}{n}\right)^2 = 4.02n^2 + 60.15$

As can be seen, the first two natural frequencies of the cables, the most dominant ones, increased as the vibration amplitude increased by the traffic loading. Accordingly, term *b* obtained from the linear regression, which represents the cable tensile force, was higher for the data set with higher vibration amplitude. Therefore, as expected the natural frequencies of post-tensioning cable and corresponding tensile forces are proportional to the magnitude of vibration induced by traffic loading. Higher modes of vibration can result in more accurate regression between $\left(\frac{f_n}{n}\right)^2$ and n^2 for obtaining the tensile force in post-tensioning cables.

In total, the results presented in this part showed consistent and precise natural frequencies of bridge deck and post-tensioning cables obtained by various channels of wireless smart sensor nodes. The results of the field testing on the viaduct showed that the wireless sensor nodes maintained phase among themselves and were well synchronised. In addition, it was shown that the tension forces induced in post-tensioning cables by traffic on the highway can be estimated using the vibration data measured by the wireless smart sensor nodes.

7.4.3 Issues found during the first field testing

Based on the analysis carried out so far on the acceleration time histories recorded during first phase of the instrumentation, it was observed that the wireless accelerometer sensor nodes have a good performance to sample low-amplitude ambient vibrations from the large-scale structure and the post-tensioning cables. In addition, the preliminary analysis results could also prove the efficiency of the MATLAB-based data management and analysis platform for processing of SHM data measured from the bridge structure. However, it should be mentioned that some technical issues were found during the first phase of instrumentation in terms of battery source and wireless communication. These issues are pointed out in the following.

- **Battery source:** As mentioned the wireless sensor nodes were programmed to record acceleration time histories for 15 minutes every 4 hours. The power source for the wireless sensor nodes was a power bank with Always-on feature. After two weeks of monitoring period, it was remotely observed that some of the sensor nodes did not record and transfer the acceleration data to the base station unit. It was assumed that the power banks might not be compatible with the hardware and software design of the wireless smart sensor nodes that can cause some issues for data sampling and transmission. Therefore, it was decided to replace the power banks with a more reliable and compatible power source. As mentioned in chapter 3, the final version of wireless sensor nodes was powered up using four 1.5. V Alkaline D-Cell batteries with 12,000 mAh capacity to provide 6.0 V for the sensor nodes at a full charge. One unit of wireless sensor node can continuously record at a service life of about 200 hours or 8 days. However, it should be mentioned that the lifetime of one unit of wireless sensor node is significantly reduced once the sensor node operates in the wireless network with other wireless sensor nodes.

- **Wireless communication:** Another issue found during the first phase of instrumentation was related to the wireless communication between wireless sensor nodes and the gateway unit. During one month of monitoring period, it was observed that one or two wireless sensor nodes stopped to transfer the recorded data and exited from the wireless network after several trials for data transmission. Those sensor nodes were not able to wake up and start sampling data for the next periodic sampling times. After some investigations, it was concluded that the settings considered for wireless communication is causing this issue. In the final version of wireless sensor nodes, the setting of the XBee wireless network was improved to tackle this issue. Also, in order to extend the wireless communication and broadcasting range, an external antenna was integrated to the board design.
- **Corrupted data:** A minor but important issue that was found during the monitoring period was the observation of corrupted acceleration measurements in some data files. It was observed that the first few samples of some data files were corrupted presenting out-of-the-range acceleration values. Also, the data files did not have header for providing information related to time drift, temperature, humidity, and battery percentage. Due to the fact that such information is important for data management and analysis using the developed toolbox, this issue should have been fixed to provide reliable measurements of acceleration data. Based on the investigations carried out, it was discovered that this issue is a memory related issue, which was fixed by updating the software configurations in development of final version of wireless sensor nodes.

After fixing these issues and updating the hardware and software configurations of the accelerometer sensors, the final version of wireless smart sensor nodes was utilised for second phase of bridge instrumentation that is presented in the following section.

Figure 7.21. Second phase of the Newmarket viaduct instrumentation using final version of wireless smart sensor nodes.

7.5 Re-instrumentation of the Newmarket Viaduct

As planned, Newmarket viaduct was re-instrumented using the final version of wireless smart sensor network. To do so, Span 9 of the highway bridge was considered again for second phase of instrumentation. The field testing was carried out on 25 November 2019 under operational conditions. 20 units of final version of wireless smart sensor nodes were installed inside the box girder on both sides of the span. It was decided to install the sensor nodes roughly at the same locations corresponding to the first phase of instrumentation for comparison purposes. The locations of the wireless sensor nodes inside the box girder in plan and cross section views can be viewed in Figures 7.10 (a) and (b). As before, 14 sensor nodes (WSSN1-WSSN14) were installed on internal surface of the bridge deck and the remaining six wireless accelerometer sensors (WSSN15-WSSN20) were fastened on post-tensioning cables on both sides of the span. Figure 7.21 shows some of the photos taken during the second phase of bridge instrumentation.

In order to protect the sensor nodes from environmental effects, a customised weatherproof enclosure was designed for the wireless sensor boards and their battery packs. Two metal pushbuttons have been placed on external surface of the enclosures. The function of one of the pushbuttons is to power on and off the sensor nodes and the other is to represent the operational mode of the sensor nodes during data logging and data transmission. Same as the first phase of bridge instrumentation, it was decided to attach the sensor nodes on timber plates and glue them to the concrete surface of the bridge deck using Epoxy. In addition, six of the wireless smart sensor nodes were fastened around the post-tensioning cables using strong straps to measure vibration induced using traffic on post-tensioning cables.

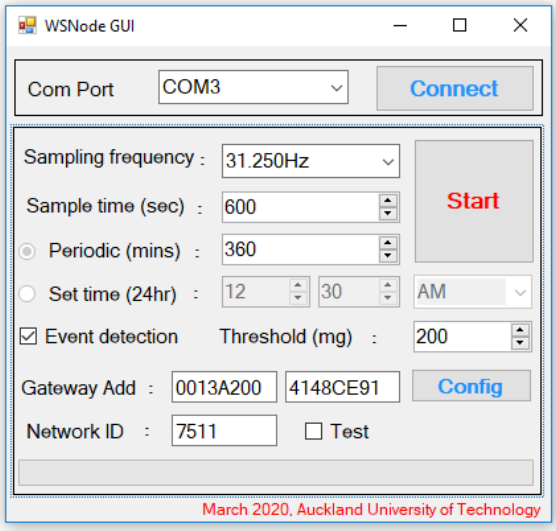

Figure 7.22. The setting of the GUI for phase two of bridge instrumentation.

Figure 7.22 shows the settings of the GUI considered for second phase of bridge instrumentation. As shown, the sensor nodes were programmed and instructed to record the traffic-induced ambient vibrations for 10 minutes every 6 hours for the first week of monitoring period. Then, the settings of the wireless sensor network were remotely changed to recorded 10 minutes of ambient vibration once per day. It should be mentioned that for this phase of bridge instrumentation, the sensor system was set to event-triggered sampling mode in addition to the periodic sampling mode. For the first trial, the vibration threshold for event detection

status was considered 200 mg. The sampling frequency was set to 31.25 Hz for this setup. It is noteworthy that same base station unit used for first field testing was utilised for re-instrumentation of the viaduct. In the following parts, the performance of the final version of wireless sensor nodes during the second phase of the Newmarket viaduct instrumentation will be evaluated and the dynamic condition of this superstructure will be assessed using the vibration measurements recorded using the wireless sensor system.

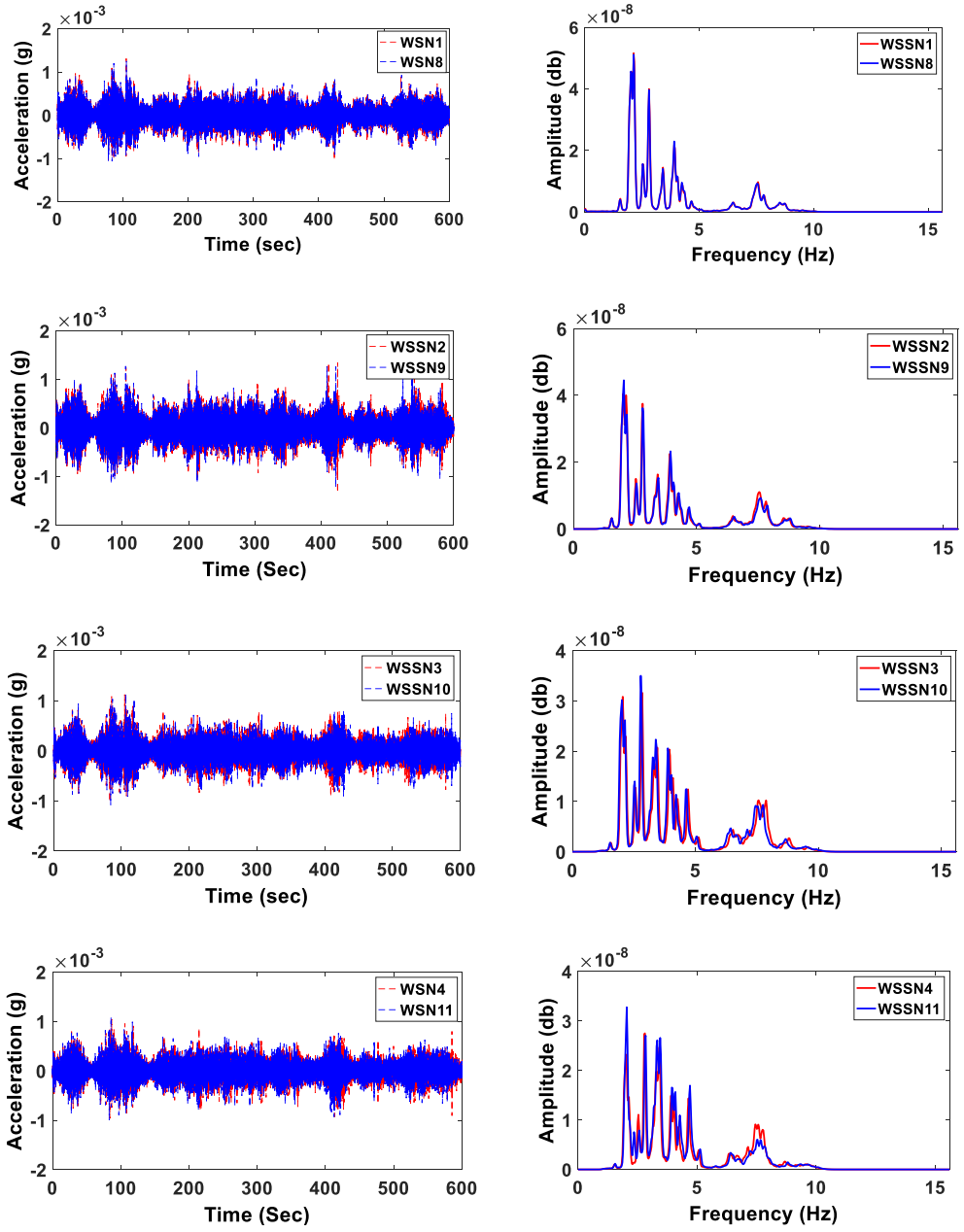

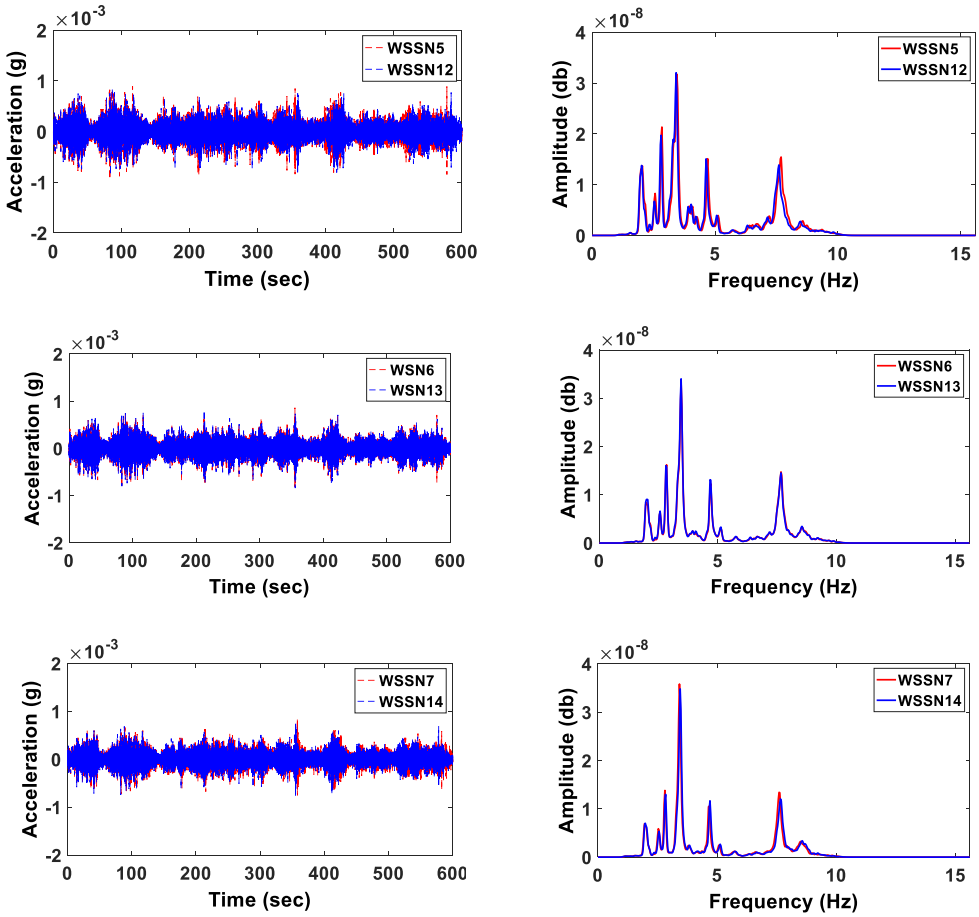

Figure 7.23. Transverse acceleration time histories and the corresponding PSD values of the bridge deck recorded by various wireless smart sensor nodes.

7.5.1 Dynamic characteristics of Newmarket viaduct

In this part, the results obtained during the second phase of bridge instrumentation are presented. These results include the dynamic characteristics of the Newmarket viaduct obtained from the vibration measurements and the performance evaluation results of final version of the wireless smart sensor system. Following this section, the condition of the bridge is investigated by comparison between the modal parameters obtained during various ambient vibration tests. Figure 7.23 shows the acceleration time histories and the corresponding PSD values measured in transverse direction of the bridge deck. The data were recorded on November 28, 2019 at 8:30 PM from the bridge using different channels of wireless sensor nodes located on both sides of the span. To compare the amplitude of vibration, the time domain and frequency

domain results obtained using each two wireless nodes facing each other in cross section (Figure 7.10(b)) were plotted in one figure. The traffic-induced time series vibration data and their corresponding natural frequencies measured using adjacent sensor nodes match perfectly. Also, it was observed that the structural peaks measured in transverse direction of the structure using various channels of wireless sensor nodes (WSSN1 to WSSN14) are identical.

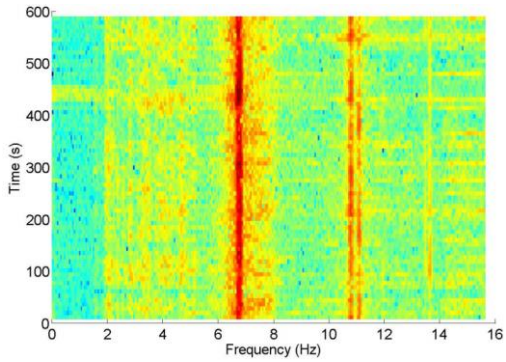

(a) Transverse direction – WSSN16

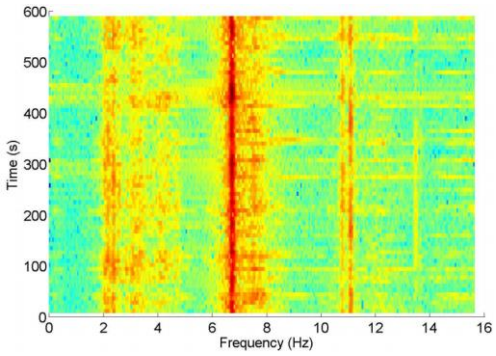

(b) Vertical direction – WSSN16

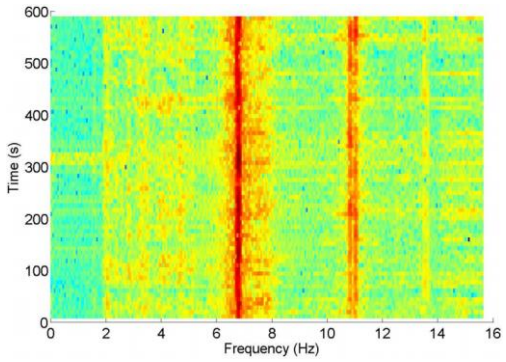

(a) Transverse direction – WSSN19

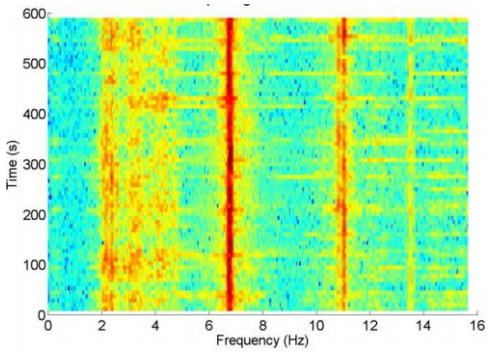

(b) Vertical direction - WSSN19

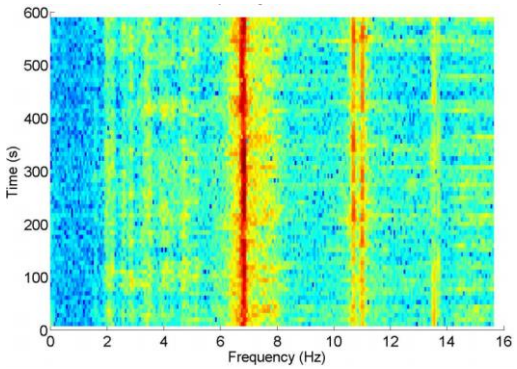

(a) Transverse direction – WSSN20

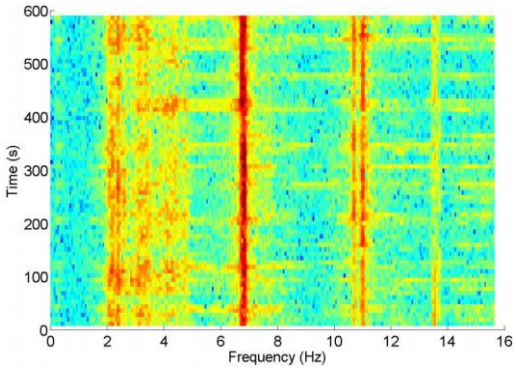

(b) Vertical direction - WSSN20

Figure 7.24. Spectrogram of acceleration time histories recorded from the post-tensioned cables on November 28, 2019 at 8:30 PM.

Figure 7.24 also shows the spectrogram of acceleration time histories that shows the variation of frequencies versus time. The vibration data used for analysis were measured using WSSN16, WSSN19, and WSSN20 in both vertical and transverse directions of three post-tensioning cables. It should be mentioned that WSSN16 and WSSN19 were attached to the post-tensioning cables that were parallel to the bridge deck surface, while the WSSN20 was attached to the end of the post-tensioning cable with an angle to the bridge deck surface.

As can be seen, the distribution of transverse and vertical natural frequencies of the three post-tensioning cables over time match very well. Also, as expected the PSD values of vertical and transverse modes of all three post-tensioning cables follow a similar pattern in time. In overall, the time and frequency domains results obtained from the bridge deck and post-tensioning cables show high performance of final version of wireless sensor nodes used for second phase of bridge instrumentation. It should be mentioned that data management and data analysis for the presented analysis results were performed using the developed MATLAB toolbox.

In the next part, the vibration data sets recorded during one month of monitoring period, from 13 December 2019 to 13 January 2020, were analysed using Enhanced Frequency Domain Decomposition (EFDD) technique. The purpose of these analysis series is to investigate the variation of natural frequencies, temperature and humidity measured using wireless sensor system during one month of monitoring period. Figures 7.25 and 7.26 present the results obtained for variations of first five natural frequencies measured in transverse and vertical directions of the bridge structure. The vibration data sets measured using WSSN11 and WSSN14, which were respectively located in the middle and end of the bridge span, were utilised here.

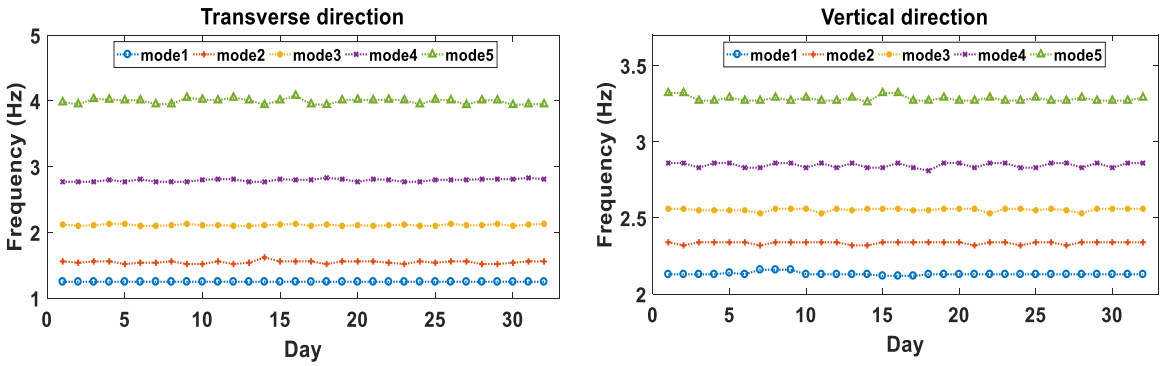

Figure 7.25. Variation of bridge modal frequencies obtained using WSSN11 during one month of monitoring period.

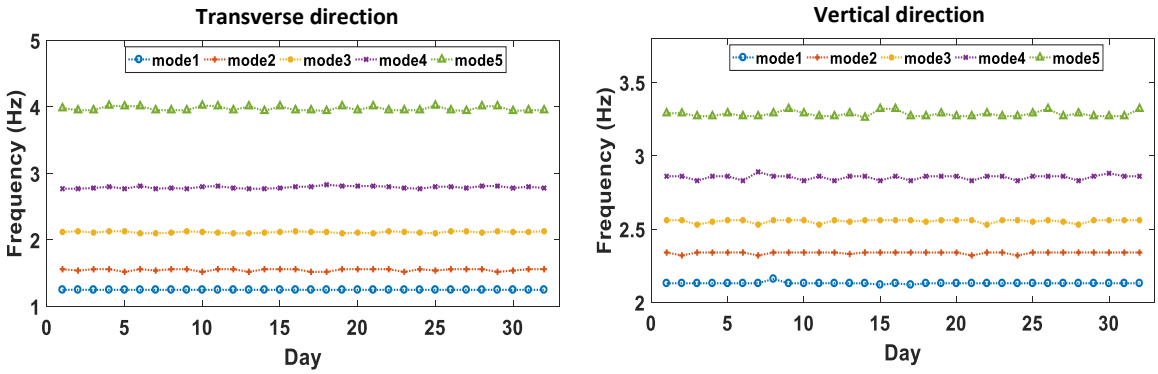

Figure 7.26. Variation of bridge modal frequencies obtained using WSSN14 during one month of monitoring period.

As is obvious from the results, all natural frequencies (from mode 1 to mode 5) measured in transverse and vertical directions have a smooth distribution and a good consistency over one month of monitoring period. However, it can be observed that the higher structural modes (modes 4 and 5) have more fluctuations in comparison to the lower modes due to effect of measurement noises. In overall, it can be concluded that the small variations between frequencies can be due to stationarity of low-amplitude ambient vibrations and accuracy of computational algorithm used for analysis.

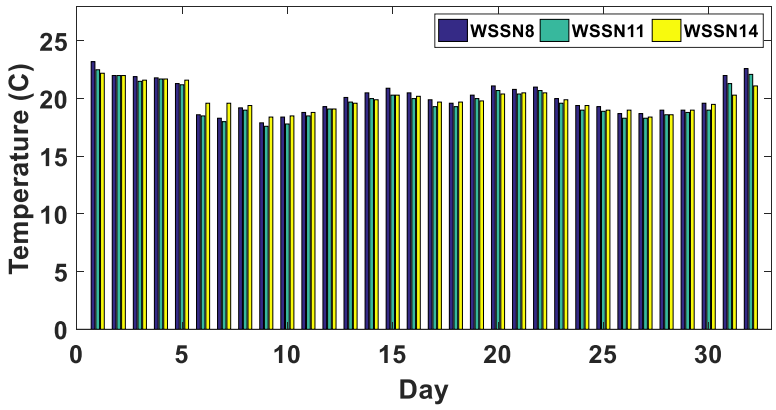

Figure 7.27. Variation of environmental temperature during one month of monitoring period.

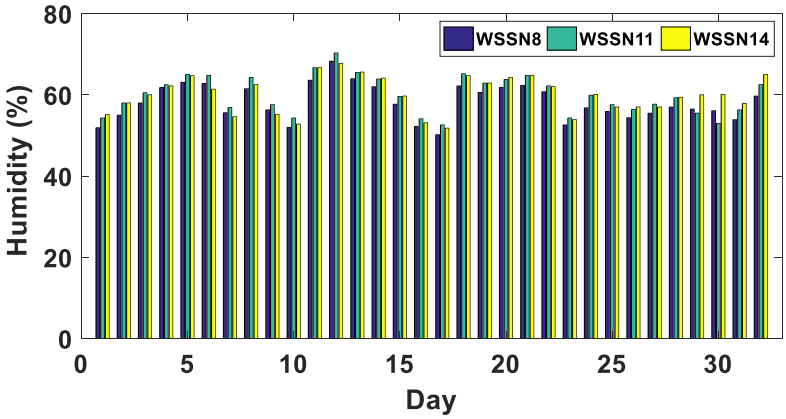

Figure 7.28. Variation of environmental humidity during one month of monitoring period.

Figures 7.27 and 7.28 also depict the variations of environmental temperature and humidity measured using three different wireless sensor nodes, WSSN8, WSSN11, and WSSN14, during one month of monitoring period. It can be observed that the temperature measured from inside the box girder ranged from a minimum of 17.6 ℃ to a maximum of 23.3 ℃ during this monitoring period. Also, humidity of internal environment of the bridge deck ranged from a minimum of 50.2 % to a maximum of 73.1 % during this monitoring period. It can be concluded from the results that there is a reasonable distribution of temperature and humidity measured using three channels of wireless smart sensor nodes that shows the accuracy and sensitivity of temperature and humidity sensor integrated to the sensor board design for environmental parameters' measurement. These parameters and their effects on dynamic characteristics of civil structures take an important role for an accurate condition assessment of structures.

Table 7.2. First five natural frequencies (Hz) of the bridge deck measured using various sensor nodes.

Mode	Reference node													
	1	**2**	**3**	**4**	**5**	**6**	**7**	**8**	**9**	**10**	**11**	**12**	**13**	**14**
	Vertical modes													
V1	2.03	2.03	2.03	2.03	2.04	2.03	2.03	2.03	2.03	2.03	2.02	2.03	2.03	2.03
V2	2.34	2.32	2.34	2.31	2.34	2.34	2.31	2.32	2.34	2.32	2.34	2.31	2.34	2.34
V3	2.56	2.53	2.53	2.53	2.56	2.56	2.55	2.53	2.53	2.53	2.56	2.53	2.53	2.56
V4	2.86	2.86	2.83	2.86	2.86	2.83	2.80	2.86	2.86	2.83	2.86	2.83	2.86	2.83
V5	3.32	3.32	3.27	3.27	3.29	3.27	3.27	3.29	3.27	3.29	3.27	3.27	3.29	3.26
	Transverse modes													
T1	1.25	1.22	1.22	1.25	1.25	1.25	1.25	1.25	1.25	1.22	1.25	1.25	1.25	1.25
T2	1.56	1.56	1.56	1.53	1.54	1.55	1.52	1.55	1.56	1.52	1.56	1.56	1.56	1.55
T3	2.13	2.13	2.13	2.10	2.13	2.13	2.13	2.13	2.13	2.10	2.10	2.10	2.11	2.10
T4	2.77	2.77	2.77	2.77	2.77	2.78	2.77	2.77	2.78	2.74	2.78	2.77	2.79	2.79
T5	3.90	3.90	4.03	4.02	4.08	4.08	3.90	3.90	4.05	4.02	4.08	4.05	4.08	3.90

V1 = Vertical mode 1, T1 = Transverse mode 1, Tor1 = Torsional mode 1

The first five vertical and transverse natural frequencies of the bridge structure obtained using various channels of wireless smart sensor nodes (WSSN1-WSSN14) are presented here. Table 7.2 provides the analysis results obtained using EFDD technique for a vibration data set measured on November 25, 2019 (the first day of bridge instrumentation) at 17:30 PM. In addition, the first two vertical and transverse natural frequencies of all post-tensioning cables obtained using WSSN15-WSSN20 are provided in Table 7.3. As can be seen from the analysis results, there is a perfect match between the transverse and vertical natural frequencies obtained using various wireless smart sensor nodes installed on bridge deck and post-tensioning cables, which is an indication of reliable performance of final version of wireless sensor system for recording low-amplitude ambient vibrations from the large-scale bridge structure.

Table 7.3. First two natural frequencies (Hz) of post-tensioning cables measured using different sensors.

Mode	Reference node					
	WSSN15	**WSSN16**	**WSSN17**	**WSSN18**	**WSSN19**	**WSSN20**
	Vertical modes					
V1	6.77	6.68	6.68	6.65	6.74	9.64
V2	20.42	20.41	20.40	20.39	20.40	22.80
	Transverse modes					
T1	6.77	6.77	6.74	6.74	6.77	9.64
T2	20.42	20.42	20.42	20.41	20.42	22.78

V1 = Vertical mode 1, T1 = Transverse mode 1

Based on the results obtained during the second phase of bridge instrumentation, it was observed that the final version of wireless smart sensor nodes has a reliable performance and high sensitivity to measure ambient vibrations from a full-scale structure. More specifically, the acceleration data files recorded and transferred using different channels of wireless sensor nodes were uncorrupted and out of any bugs to be analysed using the MATLAB toolbox. Also, the tests confirmed the durability of the four D-Cell batteries implemented for the final version of wireless smart sensor nodes during one month of monitoring period. These two issues that were found during the first phase of instrumentation have been completely fixed. In addition, although all the final version of wireless sensor nodes installed on the bridge span showed a satisfactory communication with the gateway unit during the one-month monitoring period, however, the current wireless communication protocol needs further development for long-term monitoring applications. In total, several experimental and field tests conducted so far can confirm a reliable and high performance of various features of the wireless smart sensor network for structural health monitoring projects.

7.5.2 Condition assessment of Newmarket viaduct

In the last part of this chapter, the dynamic performance of the bridge structure was investigated using the vibration data measured during the second phase of bridge instrumentation. To do so, the modal parameters of the structure, such as natural frequencies, obtained during both phases of bridge instrumentation were compared to the counterparts obtained during previous ambient vibration tests. It should be mentioned that three series of ambient vibration tests were conducted on the Newmarket viaduct during various construction phases [162]. Table 7.4 presents these ambient vibration tests conducted on the Newmarket viaduct from construction phase (2011) until current lifetime of the structure (2019).

Table 7.4. Different ambient vibration tests conducted on the Newmarket viaduct from 2011 to 2019.

Name	Test Type	Test Date	Structure
Test 1	Ambient vibration test	28-29 November 2011	Southbound Bridge
Test 2	Ambient vibration test	29-30 November 2012	Southbound & Northbound Bridges
Test 3	Ambient vibration test	2-3 December 2014	Southbound & Northbound Bridges
Test 4	Ambient vibration test	30 November 2018	Southbound Bridge
Test 5	Ambient vibration test	25 November 2019	Southbound Bridge

Test 1 was carried out only on the southbound bridge on 28th and 29th of November 2011 during construction works in preparation for casting the concrete 'stich'. It should be mentioned that during this test, only the Southbound bridge was open to traffic. Test 2 was carried out on both northbound and southbound bridges on 29th and 30th of November 2012 immediately after casting the concrete 'stich' and shortly before completion of the entire construction project. On 2nd and 3rd of December 2014, another series of ambient vibration testing (Test 3) was performed on northbound and southbound bridges to investigate the condition of the structure after two years of operation. Test 4 refers to the first phase of instrumentation on 31th of

November 2018 and Test 5 refers to the second phase of instrumentation on 25th of November 2019 using the wireless SHM system. The vibration data and corresponding natural frequencies measured during these ambient vibration tests are used in this part of the thesis to assess the overall dynamic condition of the Newmarket viaduct after several years in operation. In addition, to compare the mode shapes extracted from various system identification methods, Modal Assurance Criterion (MAC) values were also calculated. The Modal Assurance Criterion is generally used as a measure of correlation between two mode shapes. The MAC value corresponding to the i^{th} mode shape, ϕ_{ij} and ϕ_{ij}*, is defined by [168]:

$$MAC_i = \frac{\left[\sum_{j=1}^{n} \Phi_{ij} \Phi_{ij}^{*}\right]^2}{\sum_{j=1}^{n} \Phi_{ij}^2 \sum_{j=1}^{n} \phi_{ij}^{*2}} \tag{7.6}$$

where n is the number of elements in the mode shape vectors. A MAC value close to unity indicates perfect correlation between the two mode shapes and the value close to zero indicates mode shapes that are orthogonal.

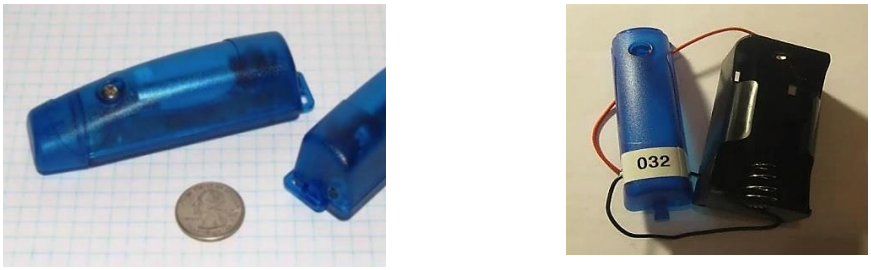

Figure 7.29. Accelerometer X6-1A equipped with a D-cell battery holder for ambient vibration tests.

All of these tests were performed under ambient excitation and traffic was utilised as the main source of excitation. Large numbers of standalone USB accelerometers, models X6-1a and X6-2, produced by the Gulf Coast Design Concepts (www.gcdataconcepts.com) were used to measure the vibration induced by traffic on the bridge during Test 1, Test 2, and Test 3 as shown in Figure 7.29. The heart of this accelerometer is a low-noise 3-axis digital-output MEMS accelerometer chip by STMicroelectronics. Although these accelerometer sensors are

able to record and store the vibration measurements in a large capacity SD card integrated to their board design, they cannot transfer the measurement using wireless communication [162]. Therefore, they can be only used for one-off ambient vibration testing. As mentioned in [162], a sampling frequency of 160 Hz was selected for vibration measurements during the first three field tests. As mentioned before, the sampling frequency of wireless smart sensor nodes was set to 62.5 Hz and 31.25 Hz during Tests 4 and 5, respectively. The test results obtained only for Span 9 of the bridge during all the above-mentioned tests are presented here. It should be mentioned that the location of accelerometer sensors inside the box girder are approximately identical during all these conducted tests. Table 7.5 presents the first five natural frequencies measured in vertical and transverse directions of the bridge deck during Test 1 obtained using Peak-Picking (PP), Enhanced Frequency Domain Decomposition (EFDD), and Stochastic Subspace Identification (SSI) techniques.

Table 7.5. Natural frequencies of bridge obtained during Test 1 [162].

Mode	Natural frequencies [HZ]			MAC with EFDD	
	PP	EFDD	SSI	PP	SSI
(1)	(2)	(3)	(4)	(5)	(6)
Vertical modes					
V1	2.11	2.12	2.12	0.72	0.94
V2	2.27	2.25	2.26	0.88	0.99
V3	2.42	2.44	2.43	0.90	1.00
V4	2.66	2.64	2.64	0.87	0.94
V5	289	2.89	2.90	-	0.95
Transverse modes					
T1	1.06	1.05	1.05	0.93	0.92
T2	139	1.39	1.40	0.74	0.84
T3	1.65	166	1.66	0.88	0.92
T4	2.12	2.11	2.11	0.91	0.92
T5	2.76	2.76	2.75	0.79	0.88

V1 = Vertical mode 1, T1 = Transverse mode 1

Table 7.6. Natural frequencies of bridge obtained during Test 2 [162].

Mode	Natural frequencies [HZ]		MAC with EFDD
	EFDD	SSI	SSI
(1)	(2)	(3)	(4)
Vertical modes			
V1	2.03	2.04	1.00
V2	2.15	2.15	0.95
V3	2.34	2.35	1.00
V4	2.55	2.55	0.96
V5	2.82	2.82	0.92
Transverse modes			
T1	1.25	1.25	0.98
T2	1.56	1.55	0.92
T3	2.15	2.17	0.89
T4	2.81	2.80	0.98
T5	3.94	3.91	0.98

V1 = Vertical mode 1, T1 = Transverse mode 1

Table 7.6 also presents the modal parameter results obtained during Test 2. For this test, the first five natural frequencies of the bridge deck obtained in vertical and transverse directions were estimated using EFDD and SSI techniques. The last column of this table also provides the MAC values between EFDD and SSI methods. Following these results, the first four transverse natural frequencies and first five vertical natural frequencies measured during Test 3 have been presented in Table 7.7. For comparison purposes, the counterparts measured during Test 1 and Test 2 are also given in this table.

As is obvious from the results, there is a very good match between the transverse and vertical natural frequencies obtained from different ambient vibration tests. More specifically, the consistency between vertical and transverse natural frequencies of the bridge structure obtained during Test 2 and Test 3 indicates the fact that there were no obvious changes in overall dynamic performance of the viaduct from 2012 to 2014 after two years in operation.

Table 7.7. Comparison between natural frequencies obtained during Test1, Test 2, and Test 3 [162].

Test	Transverse modes (Hz)				Vertical modes (Hz)				
	T1*	T2	T3	T4	V1	V2	V3	V4	V5
1	1.05	1.41	1.67	2.12	2.12	2.25	2.43	2.66	2.88
2	1.25	1.56	2.15	2.81	2.03	2.15	2.34	2.54	2.82
3	1.25	1.56	2.17	2.81	2.03	2.15	2.34	2.54	2.82

V1 = Vertical mode 1, T1 = Transverse mode 1

The modal parameters obtained during the first and second phase of bridge instrumentation using wireless smart sensor nodes are presented in Tables 7.8 and 7.9, respectively. The traffic-induced vibration data sets measured during Test 4 and Test 5 were analysed using PP, FDD, EFDD, and SSI methods to extract dynamic characteristics of the Newmarket viaduct.

Table 7.8. Natural frequencies of the bridge deck obtained during Test 4.

Mode	Natural frequencies [HZ]				MAC with EFDD		
	PP	FDD	EFDD	SSI	PP	FDD	SSI
(1)	**(2)**	**(3)**	**(4)**	**(5)**	**(6)**	**(7)**	**(8)**
Vertical modes							
V1	2.04	2.04	2.04	2.04	0.97	0.99	0.89
V2	2.34	2.34	2.34	2.31	0.81	0.90	0.76
V3	2.55	2.56	2.56	2.55	0.95	0.99	0.90
V4	2.86	2.86	2.86	2.81	0.75	0.91	0.83
V5	3.21	3.23	3.23	3.20	0.71	0.88	0.68
Transverse modes							
T1	1.25	1.25	1.25	1.28	0.95	0.99	0.81
T2	1.55	1.56	1.56	1.52	0.92	0.98	0.85
T3	2.13	2.13	2.13	2.11	0.79	0.94	0.75
T4	2.81	2.81	2.81	2.80	0.82	0.99	0.74
T5	3.96	3.96	3.96	3.93	0.85	0.95	0.70

V1 = Vertical mode 1, T1 = Transverse mode 1

Table 7.9. Natural frequencies of the bridge deck obtained during Test 5.

Mode	Natural frequencies [HZ]				MAC with EFDD		
	PP	FDD	EFDD	SSI	PP	FDD	SSI
(1)	(2)	(3)	(4)	(5)	(6)	(7)	(8)
Vertical modes							
V1	2.02	2.04	2.04	2.01	0.95	0.99	0.89
V2	2.34	2.34	2.34	2.35	0.70	0.89	0.91
V3	2.56	2.56	2.56	2.60	0.88	0.95	0.83
V4	2.86	2.83	2.83	2.85	0.92	0.98	0.85
V5	3.23	3.23	3.23	3.20	0.97	0.98	0.77
Transverse modes							
T1	1.28	1.25	1.25	1.25	0.90	0.99	0.75
T2	1.56	1.56	1.56	1.54	0.93	0.85	0.96
T3	2.12	2.13	2.13	2.12	0.75	0.92	0.90
T4	2.81	2.83	2.83	2.83	0.86	0.95	0.80
T5	3.96	4.05	4.05	3.96	0.70	0.83	0.83

V1 = Vertical mode 1, T1 = Transverse mode 1

In these tables, the first five natural frequencies obtained for vertical and transverse directions of the bridge deck and the MAC values with EFDD technique are provided. The vibration data sets measured using WSSN14 on 30 November 2018 at 21:00 PM during Test 4 and vibration data sets measured by WSSN14 on 29 December 2019 at 18:00 PM during Test 5 were used to extract modal parameters. As is obvious, there is a good match between modal parameters of the bridge structure measured using various system identification techniques in both time and frequency domain techniques showing the reliability of output-only SI techniques in estimation of dynamic characteristics of large-scale structure.

In addition, there is a very good match between the transverse and vertical natural frequencies obtained from different ambient vibration tests. The small difference between the results of T1 with other tests is due to the fact that Test 1 was carried out before the casting the concrete 'Stich' and the northbound and southbound bridges were separate from each other. Generally, the consistency observed in dynamic characteristics of the bridge shows there are no significant

changes in the overall dynamic performance of the structure after several years of operation and the bridge has a reliable performance under the traffic loading. It should be mentioned that for more precise investigation on dynamic performance of the Newmarket viaduct, more vibration data sets should be recorded throughout different locations of the structure.

7.6 Summary and conclusion

In this chapter, the results of a bridge health monitoring project using the developed wireless SHM system was presented. The testbed structure is the Newmarket Viaduct, which is one of the most distinctive engineering features' of New Zealand. One main goal of this instrumentation was to evaluate the performance of the developed wireless smart sensor network in an outdoor environment for condition assessment of large-scale civil infrastructures. The performance of the wireless sensor network was investigated in terms of sensitivity, wireless communication, time synchronisation, and battery consumption during the bridge instrumentation. In addition, assessment of overall dynamic performance of the superstructure after several years in operation was another goal of the bridge instrumentation. Two phases of bridge instrumentation using the wireless SHM system were presented in this chapter. First, the initial deployment of the wireless SHM system on the bridge was presented providing a detailed information on the system setup. Then the performance of wireless smart sensor nodes was evaluated using the vibration measurements and the technical issues, which were found during the test, were presented and discussed. After improving the hardware and software issues of the wireless sensor nodes, the bridge was re-instrumented using the final version of wireless accelerometer sensor nodes on 25 November 2019. The dynamic characteristics of the structure were measured and presented using the vibration data and the performance of final version of wireless smart sensor nodes was investigated. In the last part of the chapter, the modal characteristics of bridge obtained during both phases of bridge instrumentation were utilised for condition assessment of the structure after several years in operation. The modal

parameters of the bridge obtained during previous ambient vibration tests were utilised to evaluate the dynamic performance of the Newmarket viaduct. The following results were concluded from various sections of this chapter:

1. Consistent and precise structural peaks were obtained using the vibration data recorded by various wireless sensor nodes from the bridge deck in both vertical and transverse directions. The natural frequencies of vertical and transverse modes measured from all post-tensioning cables followed a similar pattern in time. In addition, the tension forces of the post-tensioning cables could be estimated using the vibration data measured by the wireless smart sensor nodes. In overall, the time and frequency domain results obtained from the bridge deck and post-tensioning cables showed that the wireless smart sensor nodes are capable to record low-noise time histories of low-amplitude vibrations induced by traffic throughout the structure.
2. The results of the field testing on the viaduct showed that the wireless sensor nodes maintained phase among themselves and were well synchronised. These results confirm the reliability of the time synchronisation techniques considered for WSN development in this research. It can be concluded that the wireless smart sensor network can be reliably utilised for dynamic characteristics estimation of structures.
3. A very good consistency was observed between the PSD values obtained for the first five vertical and transverse natural frequencies of the bridge during one month of monitoring period. In addition, there is a satisfactory distribution of temperature and humidity measured using three channels of wireless smart sensor nodes that shows the accuracy of temperature and humidity sensor integrated to the sensor board design.
4. During the tests, the reliability of wireless communication provided by DigiMesh topology was investigated in an outdoor environment. The results showed that vibration measurements were seamlessly transferred using this wireless topology that

confirms the application of DigiMesh topology in development of wireless smart sensor networks for SHM applications. However, the wireless communication protocol needs further developments for long-term SHM applications.

5. As can be seen from the analysis results, there is a good match between modal parameters of the bridge structure measured using various system identification techniques in both time and frequency domain techniques showing the reliability of output-only system identification techniques implemented into the MATLAB toolbox to estimate dynamic characteristics of large-scale structures.
6. The natural frequencies of the bridge extracted from vibration data recorded by wireless sensor nodes was comparable with the counterparts measured at different construction phases of the structure. The consistency of results showed that there are no obvious changes in overall dynamic performance of the structure after several years in operation and the bridge has still a reliable performance under the traffic loading.
7. The data management and analysis performed using the developed MATLAB toolbox on the vibration data sets recorded from the bridge structure showed a good performance of ADT and DMT toolkits for a synchronised managing and reliable analysis of vibration measurements.

In the next chapter of this dissertation, the key original findings during this research will be presented. Also, some of the possible future developments and applications for this research will be discussed.

Chapter 8: Conclusions and Future Studies

8.1 Conclusions

In this research, a full-package of vibration-based structural health monitoring system has been developed to enhance the damage identification process of large-scale civil structures. This system can provide asset owners and engineers with a reliable and easy-to-use platform for monitoring the integrity of civil infrastructures. This system consists of three important components, which are a new wireless smart sensor network, a MATLAB-based data management and data analysis platform compatible with hardware part, and a new vibration-based nonlinearity identification technique for early damage identification purposes. In the following, the development process of the SHM system is summarized and the corresponding original conclusions are provided.

In chapter 3, the hardware and software specifications of different versions of wireless smart sensor nodes were presented. In this chapter, various features of the wireless smart sensor system, including hardware design and software workflow of the wireless network, event-triggered sampling mode, time synchronisation protocols, and power source were presented and discussed. The developed sensor platform consists of a high-sensitive sensing component for high-fidelity vibration measurements and a reliable event detection switch through a trigger accelerometer to detect and record sudden events. The hardware of the smart sensor node was designed to provide high resolution and sensitivity, low noise, low power consumption, and capability to measure structural vibrations in ultralow-power consumption mode to record sudden events. Also, the software architecture of the smart sensor nodes was implemented to provide accurate time synchronisation and event-triggered sensing with high resolution. The specifications of the final version of wireless sensor nodes were compared with the most recent developed high-performance wireless accelerometer sensor nodes. The comparison results showed that there is a good trade-off between sensitivity, resolution, and power consumption

of new wireless accelerometer sensor nodes compared to existing wireless sensor nodes. A series of preliminary ambient vibration tests were conducted on a pedestrian bridge and two large-scale office buildings at early stage of development of the wireless sensor system. The analysis results obtained using the vibration data measured during these tests showed the high sensitivity of the digital-output wireless smart sensor nodes in recording low-amplitude ambient vibrations from large-scale structures in comparison to an expensive and high-performance wired accelerometer sensor.

In chapter 4, in order to enhance the performance of data management and analysis system for structural health monitoring compared to the traditional file-based approaches, a MATLAB-based toolbox was developed and introduced. The original feature of this toolbox is its compatibility with the developed wireless smart sensor network. The MATLAB-based toolbox includes data management and data analysis platforms, which are integrated into the developed wireless smart sensor network. Various time domain and frequency domain system identification techniques were implemented into the data analysis platform to extract modal parameters from vibration measurements. The results obtained using these techniques can be compared to each other to estimate the computational precision of the dynamic characteristics of target structures. The MATLAB toolbox was utilised for data management and extraction of dynamic characteristics of civil structures tested throughout this study. The recorded data files from the target structures in this research were downloaded, managed and synchronised using the first tab of the toolbox. Then, the managed and synchronised data files were analysed using various analysis techniques to extract modal parameters of structures. The analysis results of vibration measurements showed that the toolbox was able to efficiently manage and synchronise vibration data files from twenty wireless smart sensor nodes and analysed them using various system identification techniques. At the end of this chapter, a new vibration-based nonlinearity identification technique was proposed in order to identify early changes in

a dynamic system prior to any significant damages especially after earthquakes. This technique combines vibration data sets with time series autoregressive modelling and fuzzy clustering technique to identify the nonlinearity in a dynamic system. The technique can categorise the linear and nonlinear behaviours of a structure, when it is subjected to various levels of excitation source.

In chapter 5, the analysis results of a series of shaking table tests on a small-scale steel bridge model were presented. The purposes of these tests were to validate the various features of new developed wireless smart sensor network and the new vibration-based nonlinearity identification technique. Important results were obtained regarding the performance of the wireless smart sensor network, in terms of sensitivity and resolution, evet-triggered sampling mode, and time synchronisation.

The results of the shake table tests showed that the sensitivity and resolution of final version of wireless smart sensor nodes are comparable with expensive high-performance wired accelerometers. The wireless sensors were able to record high-fidelity structural responses from the bridge model, when it was subjected to various types and amplitudes of excitation source. Also, the wireless smart sensor nodes could record high-fidelity structural responses during sudden events using high sensing resolution accelerometer. Besides capturing sudden events from structures, this sampling mode helps to save the power source of the wireless smart sensor nodes for long-term SHM applications. The test results showed that the wireless sensor nodes maintained phase among themselves and were well synchronised, which can confirm the reliability of the time synchronisation techniques proposed for wireless sensor network in this research.

In addition, the results of these series of dynamic tests confirmed that the new vibration-based nonlinearity identification technique was able to identify nonlinear behaviour of structures once they are subjected to different levels of earthquake excitations. This algorithm was able to

categorise the linear and nonlinear behaviours of the bridge model and define a specific threshold under each excitation sources. This method proved this fact that vibration measurement from civil structure can provide very important information about structural performance. This identification process can be very helpful for engineers to assess structural performance at an early stage after sudden events, such as large-amplitude earthquakes.

In chapter 6, a case study research paper presenting the results obtained on structural health monitoring of a large-scale bridge located in Wellington, Thorndon Bridge, is presented to show the efficiency of vibration-based SHM systems for large-scale structures. This bridge was subjected to two large-amplitude earthquakes and several aftershocks. The vibration data sets recorded using wired accelerometer sensors were utilised to assess the bridge condition. The bridge performance was assessed using non-parametric analysis techniques and parametric analysis techniques to obtain the vibration intensity parameters and dynamic characteristics of the bridge. A dynamic performance index based on Autoregressive Moving Average with eXogenous excitation (ARMAX) modelling is utilised to assess the dynamic behaviour of the superstructure under different amplitudes of ground motions.

All the data analysis results obtained for this superstructure were computed in a MATLAB environment using vibration-based SHM techniques. The analysis results of ambient and earthquake-induced vibrations recorded from the large-scale structure showed the efficiency and capability of the MATLAB-based toolbox in terms of management of large data sets and long-term monitoring of large-scale structures. It can be concluded that the vibration-based monitoring environment can provide engineers with accurate dynamic performance indicators to easily extract maximum useful information from raw vibration measurements.

The vibration intensity parameters, such as peak accelerations, Root Mean Square, and Square Root of Sum of Squares, of vibration measurements recorded in vertical direction of the bridge were not changed by the strong shaking of the earthquakes and their following aftershocks. It

can be concluded that such vibration-based parameters are less sensitive to minor changes throughout the large-scale structure compared to other dynamic parameters.

The time-series analysis carried out on continuously recorded ambient vibration showed a minor but permanent drop of 0.05 Hz in natural frequencies of the first transverse and vertical modes after the first major earthquake. This drop indicated that the dynamic characteristics of the bridge were changed after the strong ground motion, which needs more precise investigations for the type, location and severity of any possible structural deterioration due the subjected earthquakes.

In addition, the results of the dynamic performance index based on the ARMAX model showed that the dynamic behaviour of the bridge during both earthquakes is different from the linear threshold value obtained by baseline vibration data sets. A near to flag-shaped force-displacement relationship during the first strong earthquake indicated close to nonlinear behaviour of the bridge during the first large-amplitude earthquake. It can be concluded that the type and range of nonlinearity vary based on the amplitude of the excitation. It is crucially important to estimate this nonlinearity range for structures, especially those located in high seismic zones to provide useful information for taking quick and accurate actions immediately after strong seismic events.

Another conclusion, which can be driven from the analysis results, is the performance and efficiency of the parametric ARMAX models to estimate the dynamic behaviour of a full-scale structure. As it was shown, this modelling method could precisely model the dynamic behaviour of large-scale structures using very low-amplitude vibrations associated with measurement noises. Also, by making comparisons between the performance of output-only non-parametric and input-output parametric time-series methods for modelling the dynamic behaviour of a full-scale structure, it can be concluded that the simple output-only models can

estimate the dynamic characteristics of the structure as efficiently as more complex input-output models can.

In Chapter 7, the results of a bridge health monitoring project using the developed vibration-based SHM system was presented. The Newmarket Viaduct located in Auckland, New Zealand was selected as the target structure. One main goal of this instrumentation was to evaluate the performance of the developed wireless smart sensor network in an outdoor environment for condition assessment of large-scale civil infrastructures. In addition, assessment of overall dynamic performance of the superstructure after several years in operation was another goal of the bridge instrumentation. The modal parameters of the bridge structure obtained using previous ambient vibration tests conducted during various construction phases of the bridge structure were utilised to evaluate the dynamic performance of the Newmarket viaduct.

Consistent and precise structural peaks were obtained using the vibration data recorded by various wireless sensor nodes from the bridge deck in both vertical and transverse directions. The natural frequencies of vertical and transverse modes measured from all post-tensioning cables follow a similar pattern in time. In addition, the tension forces of post-tensioning cables could be estimated using the vibration data measured by wireless sensor nodes. In overall, the time and frequency domains results obtained from the bridge deck and post-tensioning cables show the wireless smart sensor nodes are capable to record low-noise time histories of low-amplitude vibrations induced by traffic loading throughout the structure.

The results of the field testing on the viaduct showed that the wireless sensor nodes maintained phase among themselves and were well synchronised in an outdoor environment. These results confirm the reliability of the time synchronisation techniques introduced for WSN development. It can be concluded that the wireless sensor nodes can be reliably utilised for dynamic characteristics estimation of full-scale structures.

A very good consistency was observed between the PSD amplitudes obtained for the first five vertical and transverse natural frequencies of the bridge deck during one month of monitoring period. In addition, there is a satisfactory distribution of temperature and humidity measured using three channels of wireless smart sensor nodes that shows the accuracy of temperature and humidity sensor integrated to the sensor board design.

During the experiments, the reliability of wireless communication provided by DigiMesh topology was investigated in an outdoor environment. The results showed that the vibration measurements were seamlessly transferred using this wireless topology that confirms the application of DigiMesh topology in development of wireless smart sensor network for SHM applications. However, it should be mentioned that the wireless communication protocol needs further development for long-term monitoring applications.

In addition, it was observed that there is a good match between modal parameters of the bridge structure measured using various system identification techniques in both time and frequency domain techniques showing the reliability of output-only system identification techniques implemented into the MATLAB toolbox to estimate dynamic characteristics of large-scale structures.

The natural frequencies of the bridge structure extracted from vibration data recorded by wireless smart sensor nodes was compared with the counterparts measured at different construction stages of the viaduct. The consistency of the results showed that there are no obvious changes in overall dynamic performance of the superstructure after several years of operation and the bridge has still a reliable performance under the traffic loading.

Also, the data management and analysis performed using the developed MATLAB toolbox for the vibration data sets recorded from the bridge structure showed a good performance of ADT and DMT toolkits for a synchronised data managing and reliable analysis of vibration measurements for an accurate structural condition assessment.

To sum up, all the presented results obtained from several laboratory and field experiments conducted during this research showed the performance of the developed vibration-based SHM system in hardware and software parts for condition assessment of large-scale civil infrastructures.

8.2 Future studies

The work presented in this thesis reveals the importance of the vibration-based SHM system for condition assessment of large-scale civil structures. As a part of each development, some technical issues were faced related to the wireless sensor network. These issues, including the battery source, the accuracy of vibration measurements, and wireless communication, were found during the first phase of Newmarket Viaduct instrumentation. Most of these technical issues were fixed after updating the software architecture and modifying the hardware components of the wireless sensor node.

In overall, the different components of the developed vibration-based SHM system can be further developed to be applicable for various SHM projects. Here, some suggestions are presented for future studies to help other researchers to define the relevant research questions.

1. Adding different types of sensing components to the system in addition to accelerometer sensor to measure various physical parameters, such as displacement, velocity, strain, and tilt,
2. Implementing a SD card to the wireless smart sensor board for conducting more time-efficient one-off dynamic testing,
3. Combining the first few samples of the earthquake-induced signal stored in FIFO buffer of the ADXL362 and the vibration data recorded using the high-performance ADXL355,
4. Further development of the DigiMesh topology for reliable long-term monitoring projects,

5. Implementing on-board analysis for the wireless smart sensor nodes, such as system identification and vibration-based nonlinearity identification technique,
6. Developing vibration-based methods to find out the nonlinearity type and severity for early damage identification.
7. Implementing various vibration-based linear and nonlinear damage identification techniques into different tabs of the expandable MATLAB-based toolbox,
8. Connecting the toolbox to a permanent and reliable database to store the raw measurements and the analysis results of each monitored structure.

References

1. Spencer Jr, B., et al., *Next generation wireless smart sensors toward sustainable civil infrastructure.* Procedia Engineering, 2017. **171**: p. 5-13.
2. Enckell, M., *Structural health monitoring using modern sensor technology: long-term monitoring of the New Årsta Railway Bridge*. 2006, KTH.
3. Bergmeister, K. and U. Santa, *Global monitoring concepts for bridges.* Structural Concrete, 2001. **2**(1): p. 29-39.
4. Farrar, C.R., et al., *Variability of modal parameters measured on the Alamosa Canyon Bridge*. 1996, Los Alamos National Lab., NM (United States).
5. Farrar, C.R. and K. Worden, *An introduction to structural health monitoring.* Philosophical Transactions of the Royal Society of London A: Mathematical, Physical and Engineering Sciences, 2007. **365**(1851): p. 303-315.
6. Brownjohn, J.M., *Structural health monitoring of civil infrastructure.* Philosophical Transactions of the Royal Society of London A: Mathematical, Physical and Engineering Sciences, 2007. **365**(1851): p. 589-622.
7. Brownjohn, J., et al. *A structural health monitoring paradigm for civil infrastructure*. in *1st FIG International Symposium on Engineering Surveys for Construction Works and Structural Engineering, Nottingham, United Kingdom*. 2004.
8. Rytter, A., *Vibrational based inspection of civil engineering structures*. 1993, Dept. of Building Technology and Structural Engineering, Aalborg University.
9. Navabian, N. and S. Beskhyroun, *Investigation on dynamic behaviour of a full-scale reinforced concrete bridge subjected to strong earthquakes using an automated analysis platform.* Structure and Infrastructure Engineering, 2019: p. 1-20.
10. Adams, D.E. and C.R. Farrar, *Classifying linear and nonlinear structural damage using frequency domain ARX models.* Structural Health Monitoring, 2002. **1**(2): p. 185-201.
11. Omenzetter, P., S. Bush, and P. McCarten, *Guidelines for data collection and monitoring for asset management of New Zealand road bridges.* 2015.
12. Omenzetter, P., et al., *Prioritisation methodology for application of bridge monitoring systems for quick post-earthquake assessment.* Journal of Civil Structural Health Monitoring, 2014. **4**(4): p. 255-276.
13. Carder, D.S., *Observed vibrations of bridges.* Bulletin of the Seismological Society of America, 1937. **27**(4): p. 267-303.
14. Inaudi, D. *Overview of 40 bridge structural health monitoring projects*. in *International bridge conference, IBC*. 2010.
15. Farrar, C. and G. James III, *System identification from ambient vibration measurements on a bridge.* Journal of Sound and Vibration, 1997. **205**(1): p. 1-18.
16. Wong, K.Y., *Instrumentation and health monitoring of cable-supported bridges.* Structural control and health monitoring, 2004. **11**(2): p. 91-124.
17. Çelebi, M., *Real-time seismic monitoring of the New Cape Girardeau Bridge and preliminary analyses of recorded data: an overview.* Earthquake Spectra, 2006. **22**(3): p. 609-630.
18. Caicedo, J.M. and S.J. Dyke. *Determination of member stiffnesses for structural health monitoring*. in *Proceedings of the 3rd World Conference in Structural Control*. 2002. Italy: John Wiley and Sons.
19. Zhou, G.D., T.H. Yi, and B. Chen, *Innovative design of a health monitoring system and its implementation in a complicated long-span arch bridge.* Journal of Aerospace Engineering, 2017. **30**(2): p. B4016006.
20. Bas, S., et al., *Structural health monitoring system of the long-span bridges in Turkey.* Structure and Infrastructure Engineering, 2018. **14**(4): p. 425-444.
21. Zhang, C., et al., *Research on deflection monitoring for long span cantilever bridge based on optical fiber sensing.* Optical Fiber Technology, 2019. **53**: p. 102035.
22. Chen, Z., et al., *Deployment of a smart structural health monitoring system for long-span arch bridges: A review and a case study.* Sensors, 2017. **17**(9): p. 2151.
23. Djordjevic, B.B. *NDE in space*. in *Ultrasonics Symposium, 1990. Proceedings., IEEE 1990*. 1990. IEEE.

24. Dubin, E.E. and B.S. Yanev. *Managing the East River bridges in New York City*. in *6th Annual International Symposium on NDE for Health Monitoring and Diagnostics*. 2001. International Society for Optics and Photonics.
25. Moore, M., et al., *Reliability of visual inspection for highway bridges, volume I*. 2001, Turner-Fairbank Highway Research Center.
26. Teng, C., *Structural health monitoring of a bridge structure using wireless sensor network.* 2012.
27. Wang, Y., J.P. Lynch, and K.H. Law, *A wireless structural health monitoring system with multithreaded sensing devices: design and validation.* Structure and Infrastructure Engineering, 2007. **3**(2): p. 103-120.
28. Hamburger, R.O., *A policy guide to steel moment-frame construction*. 2000: Federal Emergency Management Agency.
29. Abudayyeh, O., *A sensor network system for the health monitoring of the Parkview bridge deck*. 2010, Michigan. Dept. of Transportation.
30. Magalhães, F., Á. Cunha, and E. Caetano, *Dynamic monitoring of a long span arch bridge.* Engineering Structures, 2008. **30**(11): p. 3034-3044.
31. Meyer, J., et al., *Wireless sensor networks for long-term structural health monitoring.* Smart Structures and Systems, 2010. **6**(3): p. 263-275.
32. Farrar, C., *Historical overview of structural health monitoring.* Lecture notes on structural health monitoring using statistical pattern recognition, 2001.
33. Celebi, M., *Seismic instrumentation of buildings (with emphasis on federal buildings)*. 2002, Citeseer.
34. Straser, E.G., *A modular, wireless damage monitoring system for structures.* 1999.
35. Kurata, M., et al. *Preliminary study of a wireless structural monitoring system for the new carquinez suspension bridge*. in *Proceedings of the Fifth World Conference on Structural Control and Monitoring*. 2010.
36. Pakzad, S.N., et al., *Design and implementation of scalable wireless sensor network for structural monitoring.* Journal of infrastructure systems, 2008. **14**(1): p. 89-101.
37. Lynch, J.P., et al., *Design and performance validation of a wireless sensing unit for structural monitoring applications.* Structural Engineering and Mechanics, 2004. **17**(3-4): p. 393-408.
38. Wang, G., et al., *Ship hull structure monitoring using fibre optic sensors.* Smart materials and structures, 2001. **10**(3): p. 472.
39. Zimmerman, D. *Looking into the crystal ball: The continued need for multiple viewpoints in damage detection*. in *Key Engineering Materials*. 1999. Trans Tech Publ.
40. Ihler, E., et al. *Integrated wireless piezoelectric sensors*. in *Proc. SPIE*. 2000.
41. Paek, J., et al. *A wireless sensor network for structural health monitoring: Performance and experience*. in *Embedded Networked Sensors, 2005. EmNetS-II. The Second IEEE Workshop on*. 2005. IEEE.
42. Strubbs, N., et al. *Verification of a methodology to nondestructively evaluate the structural properties of bridges*. in *Structural Health Monitoring Workshop, Stanford Univ., Palo Alto, Calif*. 1999.
43. Sohn, H. and C.R. Farrar. *Statistical process control and projection techniques for damage detection*. in *Proceedings of European COST F3 Conference on System Identification and Structural Health Monitoring (pp. 105–114*. 2000. Citeseer.
44. Lynch, J.P. and K.J. Loh, *A summary review of wireless sensors and sensor networks for structural health monitoring.* Shock and Vibration Digest, 2006. **38**(2): p. 91-130.
45. Gadre, D.V., *Programming and customizing the AVR microcontroller*. 2000: McGraw-Hill Professional.
46. Spencer, B., et al., *Next Generation Wireless Smart Sensors Toward Sustainable Civil Infrastructure.* Procedia Engineering, 2017. **171**: p. 5-13.
47. Jang, S. and B.F. Spencer Jr, *Structural health monitoring for bridge structures using smart sensors*. 2015, Newmark Structural Engineering Laboratory. University of Illinois at Urbana-Champaign.

48. Nagayama, T., J. Rice, and B. Spencer Jr. *Efficacy of Intel's Imote2 wireless sensor platform for structural health monitoring applications*. in *Proceedings of the Asia-Pacific Workshop on Structural Health Monitoring, Yokohama, Japan*. 2006.
49. Spencer, B.F., M.E. Ruiz-Sandoval, and N. Kurata, *Smart sensing technology: opportunities and challenges.* Structural Control and Health Monitoring, 2004. **11**(4): p. 349-368.
50. Nagayama, T., B. Spencer Jr, and J.A. Rice. *Structural health monitoring utilizing Intel's Imote2 wireless sensor platform*. in *The 14th International Symposium on: Smart Structures and Materials & Nondestructive Evaluation and Health Monitoring*. 2007. International Society for Optics and Photonics.
51. Cho, S., et al., *Smart wireless sensor technology for structural health monitoring of civil structures.* Steel Structures, 2008. **8**(4): p. 267-275.
52. Rice, J.A. and B. Spencer Jr. *Structural health monitoring sensor development for the Imote2 platform*. in *Proc. SPIE*. 2008.
53. Whelan, M.J. and K.D. Janoyan, *Design of a robust, high-rate wireless sensor network for static and dynamic structural monitoring.* Journal of Intelligent Material Systems and Structures, 2009. **20**(7): p. 849-863.
54. Swartz, R.A., et al., *Structural monitoring of wind turbines using wireless sensor networks.* Smart structures and systems, 2010. **6**(3): p. 183-196.
55. Park, J.-H., et al., *Autonomous smart sensor nodes for global and local damage detection of prestressed concrete bridges based on accelerations and impedance measurements.* Smart Structures and Systems, 2010. **6**(5-6): p. 711-730.
56. Jo, H., et al. *Development of high-sensitivity accelerometer board for structural health monitoring*. in *Proc. SPIE*. 2010.
57. Bocca, M., et al., *A synchronized wireless sensor network for experimental modal analysis in structural health monitoring.* Computer-Aided Civil and Infrastructure Engineering, 2011. **26**(7): p. 483-499.
58. Chae, M., et al., *Development of a wireless sensor network system for suspension bridge health monitoring.* Automation in Construction, 2012. **21**: p. 237-252.
59. Kohler, M.D., T.H. Heaton, and M.-H. Cheng. *The Community Seismic Network and Quake-Catcher Network: Enabling structural health monitoring through instrumentation by community participants*. 2013. International Society for Optical Engineering.
60. Sabato, A. and M.Q. Feng, *Feasibility of frequency-modulated wireless transmission for a multi-purpose MEMS-based accelerometer.* Sensors, 2014. **14**(9): p. 16563-16585.
61. Kohler, M.D., et al., *ShakeNet: A portable wireless sensor network for instrumenting large civil structures.* 2015.
62. Sabato, A., C. Niezrecki, and G. Fortino, *Wireless MEMS-based accelerometer sensor boards for structural vibration monitoring: a review.* IEEE Sensors Journal, 2017. **17**(2): p. 226-235.
63. Nagayama, T. and B.F. Spencer Jr, *Structural health monitoring using smart sensors*. 2007, Newmark Structural Engineering Laboratory. University of Illinois at Urbana-Champaign.
64. Pakzad, S.N., *Development and deployment of large scale wireless sensor network on a long-span bridge.* Smart Structures and Systems, 2010. **6**(5-6): p. 525-543.
65. Rice, J. and B. Spencer Jr, *Flexible smart sensor framework for autonomous full-scale structural health monitoring. NSEL report series, No. 18, University of Illinois at Urbana-Champaign.* hdl. handle. net, 2009. **2142**: p. 13635.
66. Jang, S., et al., *Structural health monitoring of a cable-stayed bridge using smart sensor technology: deployment and evaluation.* 2010.
67. Jo, H., et al., *Development and application of high-sensitivity wireless smart sensors for decentralized stochastic modal identification.* Journal of Engineering Mechanics, 2011. **138**(6): p. 683-694.
68. Spencer Jr, B.F. and S. Cho. *Wireless smart sensor technology for monitoring civil infrastructure: technological developments and full-scale applications*. in *Proceedings of the World Congress on Advances in Structural Engineering and Mechanics (ASEM'11)*. 2011.
69. Whelan, M.J., M.V. Gangone, and K.D. Janoyan, *Highway bridge assessment using an adaptive real-time wireless sensor network.* IEEE Sensors Journal, 2009. **9**(11): p. 1405-1413.

70. Gangone, M.V., M.J. Whelan, and K.D. Janoyan, *Wireless monitoring of a multispan bridge superstructure for diagnostic load testing and system identification.* Computer-Aided Civil and Infrastructure Engineering, 2011. **26**(7): p. 560-579.
71. Sabato, A., et al., *A novel wireless accelerometer board for measuring low-frequency and low-amplitude structural vibration.* IEEE Sensors Journal, 2016. **16**(9): p. 2942-2949.
72. Sabato, A. *Pedestrian bridge vibration monitoring using a wireless MEMS accelerometer board*. in *Computer Supported Cooperative Work in Design (CSCWD), 2015 IEEE 19th International Conference on*. 2015. IEEE.
73. Sabato, A. *A Novel, Wireless Acceleration Evaluator Used for Health Monitoring of Aging Structures and Bridges*. in *Proceedings of 10th International Workshop on Structural Health Monitoring (IWSHM 2015), Stanford, CA, USA*. 2015.
74. Rice, J.A. and B. Spencer Jr. *Structural health monitoring sensor development for the Imote2 platform*. in *Sensors and Smart Structures Technologies for Civil, Mechanical, and Aerospace Systems 2008*. 2008. International Society for Optics and Photonics.
75. Kim, S., et al. *Health monitoring of civil infrastructures using wireless sensor networks*. in *Proceedings of the 6th international conference on Information processing in sensor networks*. 2007. ACM.
76. Zhu, L., et al., *Development of a high-sensitivity wireless accelerometer for structural health monitoring.* Sensors, 2018. **18**(1): p. 262.
77. Sabato, A., C. Niezrecki, and G. Fortino, *Wireless MEMS-based accelerometer sensor boards for structural vibration monitoring: a review.* IEEE Sensors Journal, 2016. **17**(2): p. 226-235.
78. Sabato, A., et al., *A novel wireless accelerometer board for measuring low-frequency and low-amplitude structural vibration.* IEEE Sensors Journal, 2016. **16**(9): p. 2942-2949.
79. Garner, A.C. and W.K. Huff, *The wreck of Amtrak's Sunset Limited: News coverage of a mass transport disaster.* Disasters, 1997. **21**(1): p. 4-19.
80. Jeong, S., et al. *A data management infrastructure for bridge monitoring*. in *SPIE Smart Structures and Materials+ Nondestructive Evaluation and Health Monitoring*. 2015. International Society for Optics and Photonics.
81. Jeong, S., et al. *A distributed cloud-based cyberinfrastructure framework for integrated bridge monitoring*. in *Sensors and Smart Structures Technologies for Civil, Mechanical, and Aerospace Systems 2017*. 2017. International Society for Optics and Photonics.
82. Zhou, H., et al., *A structural health monitoring data management system for instrumented cable-supported bridges.* 2006.
83. Koo, K.Y., N.D. Battista, and J.M.W. Brownjohn. *SHM data management system using MySQL database with MATLAB and web interfaces*. in *5th International Conference on Structural Health Monitoring of Intelligent Infrastructure (SHMII-5), Cancún, México*. 2011.
84. Smarsly, K., K.H. Law, and D. Hartmann, *Multiagent-based collaborative framework for a self-managing structural health monitoring system.* Journal of computing in civil engineering, 2011. **26**(1): p. 76-89.
85. Smarsly, K., K.H. Law, and D. Hartmann, *Multiagent-based collaborative framework for a self-managing structural health monitoring system.* Journal of computing in civil engineering, 2012. **26**(1): p. 76-89.
86. Zaslavsky, A., C. Perera, and D. Georgakopoulos, *Sensing as a service and big data.* arXiv preprint arXiv:1301.0159, 2013.
87. Zárate, B.A., J.M. Caicedo, and P. Ziehl, *Development and implementation of a cyberinfrastructure framework for research in nondestructive evaluation using acoustic emission data.* Journal of Computing in Civil Engineering, 2013. **28**(3): p. 05014001.
88. Zhang, Y., et al., *SenStore: A scalable cyberinfrastructure platform for implementation of data-to-decision frameworks for infrastructure health management.* Journal of Computing in Civil Engineering, 2016. **30**(5): p. 04016012.
89. Beskhyroun, S. *Graphical interface toolbox for modal analysis*. in *Ninth Pacific Conference on Earthquake Engineering*. 2011.
90. Doebling, S.W., et al., *Damage identification and health monitoring of structural and mechanical systems from changes in their vibration characteristics: a literature review.* 1996.

91. Gul, M., *Investigation of damage detection methodologies for structural health monitoring.* 2009.
92. Silva, J.M., N.M. Maia, and J. Silva, *Theoretical and experimental modal analysis.* England: Research Studies Press Ltd, 1997.
93. Allemang, R.J. and D. Brown, *A unified matrix polynomial approach to modal identification.* Journal of sound and Vibration, 1998. **211**(3): p. 301-322.
94. Allemang, R.J., *Vibrations: Experimental modal analysis.* Structural Dynamics Research Laboratory, Department of Mechanical, Industrial and Nuclear Engineering, University of Cincinnati, 1999.
95. Peeters, B. and C. Ventura, *Comparative study of modal analysis techniques for bridge dynamic characteristics.* Mechanical Systems and Signal Processing, 2003. **17**(5): p. 965-988.
96. Brincker, R., L. Zhang, and P. Andersen. *Modal identification from ambient responses using frequency domain decomposition*. in *Proc. of the 18*'International Modal Analysis Conference (IMAC), San Antonio, Texas*. 2000.
97. Beskhyroun, S., et al., *Dynamic behaviour of a 13-story reinforced concrete building under ambient vibration, forced vibration, and earthquake excitation.* Journal of Building Engineering, 2019: p. 101066.
98. Brownjohn, J.M., *Ambient vibration studies for system identification of tall buildings.* Earthquake engineering & structural dynamics, 2003. **32**(1): p. 71-95.
99. Caicedo, J.M., S.J. Dyke, and E.A. Johnson, *Natural excitation technique and eigensystem realization algorithm for phase I of the IASC-ASCE benchmark problem: Simulated data.* Journal of Engineering Mechanics, 2004. **130**(1): p. 49-60.
100. Yang, J.N., et al., *Identification of natural frequencies and dampings of in situ tall buildings using ambient wind vibration data.* Journal of engineering mechanics, 2004. **130**(5): p. 570-577.
101. Catbas, F., M. Gul, and J. Burkett, *Damage assessment using flexibility and flexibility-based curvature for structural health monitoring.* Smart materials and structures, 2007. **17**(1): p. 015024.
102. Gul, M. and F.N. Catbas, *Ambient vibration data analysis for structural identification and global condition assessment.* Journal of Engineering Mechanics, 2008. **134**(8): p. 650-662.
103. Peeters, B. and G. De Roeck, *Stochastic system identification for operational modal analysis: a review.* J. Dyn. Sys., Meas., Control, 2001. **123**(4): p. 659-667.
104. Sohn, H., et al., *Structural health monitoring using statistical pattern recognition techniques.* Journal of dynamic systems, measurement, and control, 2001. **123**(4): p. 706-711.
105. Worden, K., G. Manson, and N.R. Fieller, *Damage detection using outlier analysis.* Journal of Sound and Vibration, 2000. **229**(3): p. 647-667.
106. Sohn, H. and C.R. Farrar, *Damage diagnosis using time series analysis of vibration signals.* Smart materials and structures, 2001. **10**(3): p. 446.
107. Omenzetter, P. and J.M.W. Brownjohn, *Application of time series analysis for bridge monitoring.* Smart Materials and Structures, 2006. **15**(1): p. 129.
108. Carden, E.P. and J.M. Brownjohn, *ARMA modelled time-series classification for structural health monitoring of civil infrastructure.* Mechanical systems and signal processing, 2008. **22**(2): p. 295-314.
109. Nayyerloo, M., *Real-time structural health monitoring of nonlinear hysteretic structures.* 2011.
110. Masri, S., A. Chassiakos, and T. Caughey, *Structure-unknown non-linear dynamic systems: identification through neural networks.* Smart Materials and structures, 1992. **1**(1): p. 45.
111. Masri, S., et al., *Application of neural networks for detection of changes in nonlinear systems.* Journal of Engineering Mechanics, 2000. **126**(7): p. 666-676.
112. Zang, C., M.I. Friswell, and M. Imregun, *Structural damage detection using independent component analysis.* Structural Health Monitoring, 2004. **3**(1): p. 69-83.
113. Kim, H. and H. Melhem, *Damage detection of structures by wavelet analysis.* Engineering structures, 2004. **26**(3): p. 347-362.
114. Sun, Z. and C. Chang, *Statistical wavelet-based method for structural health monitoring.* Journal of structural engineering, 2004. **130**(7): p. 1055-1062.

115. Hou, Z., M. Noori, and R.S. Amand, *Wavelet-based approach for structural damage detection.* Journal of Engineering mechanics, 2000. **126**(7): p. 677-683.
116. Hera, A. and Z. Hou, *Application of wavelet approach for ASCE structural health monitoring benchmark studies.* Journal of Engineering Mechanics, 2004. **130**(1): p. 96-104.
117. Bornn, L., C.R. Farrar, and G. Park, *Damage detection in initially nonlinear systems.* International Journal of Engineering Science, 2010. **48**(10): p. 909-920.
118. Trendafilova, I., et al. *Detection, localisation and identification of nonlinearities in structural dynamics*. in *PROCEEDINGS OF THE INTERNATIONAL SEMINAR ON MODAL ANALYSIS*. 2001. Citeseer.
119. Farrar, C.R., et al., *Nonlinear system identification for damage detection*. 2007, Los Alamos National Laboratory (LANL), Los Alamos, NM.
120. Worden, K., et al., *A review of applications of nonlinear dynamics to structural health monitoring.* Journal of Structural Control and Health Monitoring, 2007. **15**: p. 540-567.
121. Tomlinson, G. *Detection, identification and quantification of nonlinearity in modal analysis-a review*. in *Proceedings of the 4th International Modal Analysis Conference*. 1986.
122. Billings, S. and K. Tsang, *Spectral analysis for non-linear systems, Part I: Parametric non-linear spectral analysis.* Mechanical Systems and Signal Processing, 1989. **3**(4): p. 319-339.
123. Storer, D. and G. Tomlinson. *Higher order frequency response functions and their relation to practical structures*. in *9th International Modal Analysis Conference, Florence*. 1991.
124. *ATmega328P*. Atmel Corporation, 1600 Technology Drive, San Jose, CA 95110 USA, 2015.
125. *DIGI XBEE® S2C802.15.4 RF MODULES.* Digi International Inc., 2018.
126. *Wireless Mesh Networking: ZigBee Vs DigiMesh.* . Digi International Inc., 2018.
127. *M24M0, Electrically Erasable PROgrammable Memory.* STMicroelectronics, 2017.
128. *MCP7940X Real-Time Clock.* Microchip Technology Inc., 2009.
129. *ADXL354/355, MEMS Accelerometer.* Analog Devices, Inc., 2016.
130. *S25FL064L, FL-LSPI Flash Memory.* Cypress Semiconductor Corporation, 2019.
131. *ADXL354/355, MEMS Accelerometer.* Analog Devices, Inc., 2016.
132. *NI cDAQ™-9184, 4-Slot, Ethernet CompactDAQ Chassis.* national instruments (NI), 2017.
133. *CXL-GP Series, General Purpose Accelerometer*. MEMSIC, Inc, 2015.
134. *Digital-Output MEMS ADXL362 Accelerometer*. Analog Devices, Inc. , 2012.
135. Zhu, L., et al., *Development of a high-sensitivity wireless accelerometer for structural health monitoring.* Sensors, 2018. **18**(1): p. 262.
136. Navabian.N, B.S., *Low-cost and High-performance Wireless Sensor Nodes for Structural Health Monitoring Applications.* . 9th European Workshop on Structural Health Monitoring Conference (EWSHM2018), 2018.
137. Nagayama, T., B. Spencer Jr, and J.A. Rice. *Structural health monitoring utilizing Intel's Imote2 wireless sensor platform*. in *Sensors and Smart Structures Technologies for Civil, Mechanical, and Aerospace Systems 2007*. 2007. International Society for Optics and Photonics.
138. Sensequake. *Sensquake Larze Monitoring System*. 2018; Available from: https://www.sensequake.com/.
139. MONNIT. *Monnit ALTA Industrial Wireless Accelerometer - Advanced Vibration Meters* Available from: https://www.onetemp.co.nz/monnit.
140. BeanAir. *BeanAir BND-WILOW-AX-3D-2G Wireless Sensor*. Available from: https://www.beanair.com/.
141. SenSpot. *Wireless Vibration/Acceleration SenSpot™ Sensor, Resensys.*; Available from: https://www.resensys.com/senspot-vibration.html.
142. 4000, V.-M. *Wireless Vibration Sensor.*; Available from: https://inertia-technology.com/product/vibration-monitoring-vmon-4000/#gf_5.
143. Bendat, J.S. and A.G. Piersol, *Engineering applications of correlation and spectral analysis.* New York, Wiley-Interscience, 1980. 315 p., 1980.
144. Welch, P., *The use of fast Fourier transform for the estimation of power spectra: a method based on time averaging over short, modified periodograms.* IEEE Transactions on audio and electroacoustics, 1967. **15**(2): p. 70-73.

145. Jacobsen, N.-J., P. Andersen, and R. Brincker. *Using EFDD as a robust technique for deterministic excitation in operational modal analysis*. in *Proceedings of the 2nd international operational modal analysis conference*. 2007. Aalborg Universitet.
146. Van Overschee, P. and B. De Moor, *Subspace identification for linear systems: Theory—Implementation—Applications*. 2012: Springer Science & Business Media.
147. Katayama, T., *Subspace methods for system identification*. 2006: Springer Science & Business Media.
148. Friswell, M. and J.E. Mottershead, *Finite element model updating in structural dynamics*. Vol. 38. 2013: Springer Science & Business Media.
149. Andersen, P., et al. *Comparison of system identification methods using ambient bridge test data*. in *Proc. of the 17th international modal analysis conference, Kissimee, Florida*. 1999.
150. De Roeck, G., B. Peeters, and W.-X. Ren. *Benchmark study on system identification through ambient vibration measurements*. in *Proceedings of IMAC-XVIII, the 18th international modal analysis conference, San Antonio, Texas*. 2000.
151. Ljung, L., *System identification*, in *Signal analysis and prediction*. 1998, Springer. p. 163-173.
152. Söderström, T. and P. Stoica, *System identification.* 1989.
153. Lee, S., *A note on the residual empirical process in autoregressive models*. Statistics & probability letters, 1997. **32**(4): p. 405-411.
154. Wang, X. and V. Makis, *Autoregressive model-based gear shaft fault diagnosis using the Kolmogorov–Smirnov test.* Journal of Sound and Vibration, 2009. **327**(3-5): p. 413-423.
155. Kar, C. and A. Mohanty, *Application of KS test in ball bearing fault diagnosis.* Journal of sound and vibration, 2004. **269**(1-2): p. 439-454.
156. Mei, L., A. Mita, and J. Zhou, *An improved substructural damage detection approach of shear structure based on ARMAX model residual.* Structural Control and Health Monitoring, 2016. **23**(2): p. 218-236.
157. Bezdek, J.C., *Pattern recognition with fuzzy objective function algorithms*. 2013: Springer Science & Business Media.
158. da Silva, S., et al., *Structural damage detection by fuzzy clustering.* Mechanical Systems and Signal Processing, 2008. **22**(7): p. 1636-1649.
159. *MODEL 4610A ACCELEROMETER.* TE Connectivity Inc., 2017.
160. Wood, J. *Strong motion records from the Thorndon Overbridge in the 2013 Cook Strait and Lake Grassmere earth-quakes*. in *Proceedings of the annual conference of the New Zealand Society of Earthquake Engineering (NZSEE2014)*. 2014.
161. Gul, M., *Investigation of damage detection methodologies for structural health monitoring*. 2009: University of Central Florida.
162. Chen, X., *Assessment of the dynamics and performance of an in-service twelve-span twin bridge using in-situ testing and finite element modelling*. 2015, ResearchSpace@ Auckland.
163. Chen, X.H., P. Omenzetter, and S. Beskhyroun. *Dynamic testing and long term monitoring of a twelve span viaduct*. in *Key Engineering Materials*. 2013. Trans Tech Publ.
164. Billings, I. and S. Tucker. *Seismic assessment and retrofit concepts for the Newmarket Viaduct*. in *13 WCEE: 13 th World Conference on Earthquake Engineering Conference Proceedings*. 2004.
165. Mathivat, J. and C. Emberson, *The cantilever construction of prestressed concrete bridges*. 1984: Wiley Chichester et al.
166. Shimada, T., *Estimating method of cable tension from natural frequency of high mode.* Doboku Gakkai Ronbunshu, 1994. **1994**(501): p. 163-171.
167. Chen, X., P. Omenzetter, and S. Beskhyroun. *Comparison of output-only methods for modal identification of a twelve-span viaduct*. in *Proceedings of the 5th International Operational Modal Analysis Conference*. 2013.
168. Ewins, D., *Modal testing: theory, practice and application. 2000, Baldock*. Research Studies Press. XIII.